

University of Alberta
Department of Civil &
Environmental Engineering



Structural Engineering Report No. 220

**RATIONAL DESIGN OF PRESTRESSED
AND REINFORCED CONCRETE TANKS**

by
Abdelaziz A. Rashed
David M. Rogowsky
and
Alaa E. Elwi

December 1997

Recent Structural Engineering Reports

Department of Civil Engineering

University of Alberta

194. *Experimental Investigation of the Compressive Behavior of Gusset Plate Connections* by Michael C.H. Yam and J.J. Roger Cheng, September 1993.
195. *Some Behavioural Aspects of Composite Trusses* by Berhanu Woldegiorgis and D.J. Laurie Kennedy, January 1994.
196. *Flexural Behavior of High Strength Concrete Columns* by Hisham H.H. Ibrahim and James G. MacGregor, March 1994.
197. *Prediction of Wrinkling Behavior of Girth-Welded Line Pipe* by Luis T. Souza, Alaa E. Elwi, and David W. Murray, April 1994.
198. *Assessment of Concrete Strength in Existing Structures* by F. Michael Bartlett and James G. MacGregor, May 1994.
199. *The Flexural Creep Behavior of OSB Panels Under Various Climatic Conditions* by Naiwen Zhao, J.J. Roger Cheng, and Lars Bach, June 1994.
200. *High Performance Concrete Under High Sustained Compressive Stresses* by Said Iravani and James G. MacGregor, June 1994.
201. *Strength and Installation Characteristics of Tension-Control Bolts* by Scott T. Undershute and Geoffrey L. Kulak, August 1994.
202. *Deformational Behavior of Line Pipe* by Magdi Mohareb, Alaa E. Elwi, Geoffrey L. Kulak and David W. Murray, September 1994.
203. *Behavior of Girth-Welded Line Pipe* by Nader Yoosef-Ghodsi, Geoffrey L. Kulak and David W. Murray, September 1994.
204. *Numerical Investigation of Eccentrically Loaded Tied High Strength Concrete Columns* by Jueren Xie, Alaa E. Elwi, and James G. MacGregor, October 1994.
205. *Shear Strengthening of Concrete Girders Using Carbon Fibre Reinforced Plastic Sheets* by Efrosini H. Drimoussis and J.J. Roger Cheng, October 1994.

Structural Engineering Report No. 220

**RATIONAL DESIGN OF PRESTRESSED AND
REINFORCED CONCRETE TANKS**

by

Abdelaziz A. Rashed

David. M. Rogowsky

and

Alaa E. Elwi

Department of Civil and Environmental Engineering

The University of Alberta

Edmonton, Alberta Canada T6G 2G7

December 1997

Abstract

The structural design of environmental concrete structures such as water reservoirs and sewage treatment tanks is not covered explicitly in Canadian design standards. A variety of foreign sources are frequently used. While all these sources purport to produce safe, leak resistant and durable tanks, the various design standards require significantly different amounts of reinforcement and concrete. The most significant difference appears between the design of reinforced concrete and prestressed concrete tanks. The lack of agreement between the major sources implies that the profession has yet to converge upon a rational solution. The objective of this study is to rationalize the design procedures for reinforced and prestressed concrete tanks so that an applicable Canadian design standard be developed. The study investigates the concept of partial prestressing in liquid containment structures. This concept is currently used successfully in the design of other types of structures. Understanding the behaviour of partially prestressed tanks is the key for providing rational solutions ranging from reinforced concrete at one end of the design spectrum to fully prestressed concrete at the other.

The present study included experimental and analytical phases. In the experimental phase a total of eight full-scale specimens, representing segments from typical tank walls, were subjected to load and leakage tests. The test specimens covered a range of prestressed and non-prestressed reinforcement ratios and were subjected to various combinations of loads. Also, while the specimens were under load, leakage tests

were conducted to obtain leakage rates through the cracks. The results of both tests are described. The ability of a flexural compression zone to prevent leakage, and the ability of fine cracks to seal themselves (autohealing) are discussed. They appear to be important design parameters that are not explicitly recognized in current design standards.

In the analytical study a computer model that can predict the response of tank wall segments is described and calibrated against the test results. The model is used to carry out a parametric study which investigates additional combinations of reinforcement and loading. The combination of the physical experiments, and the numerical experiments is used to develop a design procedure. The proposed design procedure addresses the leakage limit state directly. It is applicable for fully prestressed, fully reinforced and partially prestressed concrete water tanks.

ACKNOWLEDGEMENTS

This report is reprint of a thesis by the same title, written by the first author under the supervision of the second and the third authors.

The authors would like to acknowledge the following organizations for their financial support: the Natural Sciences and Engineering Research Council of Canada, the Province of Alberta, and the University of Alberta. The donation of materials and components by VSL Corporation, Lafarge Canada Inc., and Inland Cement for the experimental program is gratefully acknowledged.

The assistance and cooperation of Larry Burden and Richard Helfrich of the I.F. Morrison Structural Laboratory, University of Alberta, in the experimental program are gratefully acknowledged. The assistance provided by Dr. Scott D. B. Alexander with the data acquisition system and by the first author's colleagues with the concrete casting is deeply appreciated.

Table of Contents

1- INTRODUCTION	1
1.1 GENERAL	1
1.2 OBJECTIVES OF THIS STUDY.....	2
1.3 SCOPE OF THE REPORT.....	3
1.4 ORGANIZATION OF THE REPORT	3
2- PRELIMINARY REVIEW.....	6
2.1 INTRODUCTION	6
2.2 DESIGN APPROACHES – A LITERATURE REVIEW.....	6
2.2.1 <i>Design Philosophy</i>	6
<i>ACI 350R (1989) “Environmental Engineering Concrete Structures”</i>	7
<i>Portland Cement Association</i>	8
<i>ACI 344 “Design and Construction of Circular Prestressed Concrete Structures” and Prestressed Concrete Institute</i>	9
<i>BS 8007 “Design of Concrete Structures for Retaining Aqueous Liquids”</i>	9
2.2.2 <i>Crack Width Calculation</i>	10
2.3 CASE STUDIES.....	11
2.4 PARTIAL PRESTRESSING – A LITERATURE REVIEW	14
2.4.1 <i>Background</i>	14
2.4.2 <i>Partial Prestressing in Water tanks</i>	16
2.4.3 <i>Crack Width Calculations for Partially Prestressed Concrete</i>	17
2.4.4 <i>Experimental Studies on Partial Prestressing</i>	18
2.5 WATERTIGHTNESS	20
2.5.1 <i>Watertightness Criteria</i>	20
2.5.2 <i>Autogenous Healing</i>	24
2.6 CRACK WIDTH AND STEEL CORROSION.....	26
2.7 SUMMARY.....	26
3- EXPERIMENTAL STUDY	33
3.1 INTRODUCTION	33
3.2 TEST SPECIMENS	33
3.3 FABRICATION OF SPECIMENS	35
3.3.1 <i>Casting and Curing</i>	35
3.3.2 <i>Prestressing the Specimens</i>	36
3.3.3 <i>Grouting the Specimens</i>	37
3.4 MATERIAL PROPERTIES	37
3.4.1 <i>Concrete</i>	37
3.4.2 <i>Non-Prestressed Steel</i>	38
3.4.3 <i>Prestressing Tendons</i>	38
3.5 TESTS SET-UP	39
3.5.1 <i>Eccentric Load Test Set-up</i>	39
3.5.2 <i>Axial-Load Test Set-up</i>	39

3.5.3 <i>Flexural Test Set-up</i>	40
3.6 LEAKAGE TEST	41
3.6.1 <i>Test Set-up</i>	41
3.7 INSTRUMENTATION	42
3.7.1 <i>Non-Prestressed Steel Strain</i>	42
3.7.2 <i>Concrete Strain</i>	42
3.7.3 <i>Loads</i>	43
3.7.4 <i>Specimen Rotation</i>	43
3.7.5 <i>Crack Measurements</i>	43
3.7.6 <i>Leakage Rate</i>	44
3.7.7 <i>Variations in Instrumentation</i>	44
3.8 CONCRETE AND REINFORCEMENT INITIAL STRAINS	44
3.8.1 <i>Initial Strain in Concrete</i>	44
3.8.2 <i>Non-prestressed Steel Strain</i>	45
3.8.3 <i>Prestressed Steel Strain</i>	46
4- TEST RESULTS	62
4.1 INTRODUCTION	62
4.2 CRACK PATTERNS AND SPECIMEN RESPONSE	62
4.2.1 <i>Specimens Tested under Eccentric Load</i>	62
4.2.2 <i>Specimen Tested under Axial Load</i>	68
4.2.3 <i>Specimen Tested under Flexure</i>	70
4.3 MOMENT-CURVATURE CHARACTERISTICS	71
4.4 LEAKAGE TEST RESULTS	72
4.5 EVALUATION OF TEST RESULTS	78
4.5.1 <i>Cracking of Concrete</i>	78
4.5.2 <i>Moment-Curvature Characteristics</i>	80
4.5.3 <i>Leakage Through Cracks</i>	81
5- ANALYTICAL MODEL	111
5.1 INTRODUCTION	111
5.2 DESCRIPTION OF THE ANALYTICAL MODEL	111
5.3 MATERIAL CONSTITUTIVE LAWS	112
5.3.1 <i>Concrete in Compression</i>	112
5.3.2 <i>Concrete in Tension</i>	112
5.3.3 <i>Effect of Creep and Shrinkage</i>	114
5.3.4 <i>Non-Prestressed Steel</i>	115
5.3.5 <i>Prestressing Steel</i>	116
5.4 VERIFICATION OF THE ANALYTICAL MODEL	116
5.5 TENSION STIFFENING MODEL	117
5.6 COMPARISON BETWEEN ANALYTICAL PREDICTIONS AND TEST RESULTS	120
5.7 COMPARISON OF ANALYTICAL PREDICTIONS WITH OTHERS TEST RESULTS	123
6- PARAMETRIC STUDIES	149
6.1 INTRODUCTION	149

6.2 PARAMETRIC STUDY OF STRUCTURAL BEHAVIOUR.....	149
6.3 RESULTS OF THE PARAMETRIC STUDY OF STRUCTURAL BEHAVIOUR.....	150
6.3.1 <i>Moment versus Curvature</i>	150
6.3.2 <i>Depth of Compression Zone</i>	152
6.3.3 <i>Concrete Residual Stresses</i>	153
6.4 SUMMARY OF THE PARAMETRIC STUDY ON STRUCTURAL BEHAVIOUR.....	154
6.4 HYDRAULIC CONDUCTIVITY OF CONCRETE.....	156
7- LIMIT STATES DESIGN FOR LIQUID CONTAINING TANKS	178
7.1 INTRODUCTION	178
7.2 ULTIMATE STRENGTH LIMIT STATE.....	179
7.3 LEAKAGE LIMIT STATE.....	181
7.3.1 <i>General</i>	181
7.3.2 <i>Direct tension</i>	182
7.3.2.1 <i>Prevent Cracking</i>	182
7.3.2.2 <i>Limiting Through Crack Widths Such That Cracks Self-Seal</i>	184
7.3.2.2 <i>Limiting Through Crack Widths Such That Leakage Rates are Acceptable</i>	184
7.3.2.4 <i>Design to Satisfy Permissible Crack Widths</i>	185
7.3.3 <i>Combined Tension and Bending</i>	191
7.3.3.1 <i>Prevent Cracking Completely</i>	191
7.3.3.2 <i>Maintain Minimum Depth of Compression Zone</i>	191
7.4 TRIAL DESIGNS.....	194
8- SUMMARY, CONCLUSION, AND RECOMMENDATIONS	206
8.1 SUMMARY.....	206
8.2 CONCLUSIONS.....	207
8.2.1 <i>Conclusions from Comparison of Existing Specifications</i>	207
8.2.2 <i>Findings from Tests</i>	208
8.2.2.1 <i>Structural Response of Wall Panels</i>	208
8.2.2.2 <i>Leakage Tests</i>	208
8.2.3 <i>Conclusions from the Parametric Studies</i>	209
8.2.4 <i>Conclusions from the Proposed Design Approach</i>	210
8.3 RECOMMENDATIONS FOR FUTURE RESEARCH.....	210
REFERENCES.....	212
APPENDIX A: LISTING OF THE COMPUTER PROGRAM	218
APPENDIX B: TIME-DEPENDENT STRESS AND STRAIN	233
APPENDIX C: SOLVED EXAMPLES	236
EXAMPLE 1 - OPEN TOPPED CIRCULAR TANK	237
EXAMPLE 2 - OPEN TOPPED RECTANGULAR TANK.....	243

List of Tables

<u>Table</u>	<u>Title</u>	<u>Page</u>
2.1	Comparison of crack widths determined using different approaches	28
2.2	Comparison between the various codes, <i>WSD</i>	29
2.3	Comparison between the various codes, <i>USD</i>	29
2.4	k_I values for different crack	30
2.5	Permissible crack widths for water tanks	31
3.1	The variables of the experimental test specimens	47
3.2	Results of ancillary tests of concrete at time of stressing and testing the specimens	48
3.3	Reinforcement properties	49
5.1	Summary of shrinkage and creep effects on the specimens	125
5.2	Material properties for the concrete used in simulating test results	126
5.3	Specimens tested by Alvarez and Marti	126
5.4	The material properties used in Alvarez and Marti specimens	127
6.1	Summary of the variables of the parametric study	160
6.2	Temperature required to equate evaporation and leakage rates	160
7.1	Comparison between failure and design (coded) ultimate load	198
7.2	Width of pre-opening crack for different partial prestressing ratios	198
7.3	Permissible crack widths for water tanks	199

List of Figures

<u>Figure</u>	<u>Title</u>	<u>Page</u>
2.1	The finite element mesh of the large circular tank	32
2.2	Distribution of hoop force	32
3.1	Specimens configurations	50
3.2	Schematic details of specimen 1C40	51
3.3	Details of end anchorage	
	(a) Typical specimen	52
	(b) Specimen 2A	52
3.4	Schematic details of specimen 3C	
	(a) Longitudinal section	53
	(b) Plan	53
3.5	End details of specimen 3C	54
3.6	Distribution of prestressing force along the stand	54
3.7	Eccentric loading test set-up	
	(a) Side view	55
	(b) Plan view	55
3.8	Whiffletree end fitting	56
3.9	Specimen 3C in MTS test machine	56
3.10	Flexure test set-up	
	(a) Side view	57
	(b) End view	58
3.11	Leakage test set-up	
	(a) Section A-A	59
	(b) Section B-B	59
3.12	Leakage test set-up for specimen 3C	60
3.13	Location of the instruments for a typical specimen	61
4.1	Crack pattern of specimen 1C40	83
4.2	Crack pattern of specimen 2A	83
4.3	Crack pattern and mode of failure of specimen 2B	
	(a) Crack pattern	84
	(b) Mode of failure	84
4.4	Crack pattern of specimen 3A	85
4.5	Crack pattern of specimen 3B	85

<u>Figure</u>	<u>Title</u>	<u>Page</u>
4.6	Load versus gross concrete strain for specimen 1C40	
	(a) Tensile strain	86
	(b) Compressive strain	86
4.7	Load versus gross concrete strain for specimen 1C20	
	(a) Tensile strain	87
	(b) Compressive strain	87
4.8	Load versus gross concrete strain for specimen 2A	
	(a) Tensile strain	88
	(b) Compressive strain	88
4.9	Load versus gross concrete strain for specimen 2B	
	(a) Tensile strain	89
	(b) Compressive strain	89
4.10	Load versus gross concrete strain for specimen 3A	
	(a) Tensile strain	90
	(b) Compressive strain	90
4.11	Load versus gross concrete strain for specimen 3B	
	(a) Tensile strain	91
	(b) Compressive strain	91
4.12	Load versus non-prestressed steel stress for specimen 1C40	92
4.13	Load versus non-prestressed steel stress for specimen 1C20	92
4.14	Load versus non-prestressed steel stress for specimen 2A	93
4.15	Load versus non-prestressed steel stress for specimen 2B	93
4.16	Load versus non-prestressed steel stress for specimen 3B	94
4.17	The rotation of the eccentric loading bracket in specimen 1C40 during the test	94
4.18	Mode of failure of specimen 1C20	
	(a) Viewed from the side	95
	(b) Viewed from the compression side	95
4.19	Large deformation of specimen 2A during the test	96
4.20	Wide cracks in specimen 3A	96
4.21	Crack pattern for specimen 3C	97
4.22	Load versus gross concrete strain for specimen 3C	97
4.23	Failure mode of specimen 2C	
	(a) Crack pattern	98
	(b) Concrete spalling on the compression side	98
4.24	Load versus gross concrete strain for specimen 2C	
	(a) Tensile strain	99
	(b) Compressive strain	99

<u>Figure</u>	<u>Title</u>	<u>Page</u>
4.25	Moment versus non-prestressed steel strain for specimen 2C	100
4.26	Examples of strain distribution plotted at each load level using Demec and LVDT readings for specimen 1C40	100
4.27	Moment versus curvature for specimen 1C40	101
4.28	Moment versus curvature for specimen 1C20	101
4.29	Moment versus curvature for specimen 2A	102
4.30	Moment versus curvature for specimen 2B	102
4.31	Moment versus curvature for specimen 3A	103
4.32	Moment versus curvature for specimen 3B	103
4.33	Moment versus curvature for specimen 2C	104
4.34	Leakage rate for the through cracks in specimen 3C	104
4.35	Effect of level of partial prestressing on crack width	105
4.36	Effect of level of concrete cover of non-prestressed steel on crack width	105
4.37	Effect of load eccentricity on crack width (a) Moment	106
	(b) Load	106
4.38	Effect of bond characteristic of tendons on crack width	107
4.39	Effect of level of partial prestressing on the relation between crack width and steel stress	107
4.40	Non-prestressed steel stress versus crack width for flexural and through cracks	108
4.41	Effect of load eccentricity on moment-curvature relationship	109
4.42	Effect of partial prestressing level on moment-curvature relationship	109
4.43	Effect of tendon bond characteristic on moment-curvature relationship	110
4.44	Effect of non-prestressed steel concrete cover on moment-curvature relationship	110
5.1	Concrete stress-strain curves	128
5.2	Tension stiffening models	129
5.3	Stress-strain curve for non-prestressed steel	130
5.4	Stress-strain curve for prestressed steel	130
5.5	Moment versus curvature for specimen 1C40 obtained from the current program and program RESPONSE	131
5.6	Moment versus curvature for specimen 2A obtained from the current program and program RESPONSE	131
5.7	Moment versus curvature for specimen 3B obtained from the current program and program RESPONSE	132

<u>Figure</u>	<u>Title</u>	<u>Page</u>
5.8	Moment versus curvature responses for specimen 3A obtained from different tension stiffening models	132
5.9	Moment versus curvature responses for specimen 1C40 obtained from different tension stiffening models	133
5.10	Moment versus curvature responses for specimen 2A obtained from different tension stiffening models	133
5.11	Load versus strain response for specimen 3C obtained from different tension stiffening models	
	(a) Full response	134
	(b) Response up to yield	134
5.12	Load versus strain response for specimen 3C obtained from the suggested tension stiffening model	
	(a) Full response	135
	(b) Response up to yield	135
5.13	Observed and predicted moment versus curvature responses for specimen 1C40	136
5.14	Moment versus depth of compression zone for specimen 1C40	136
5.15	Moment versus non-prestressed steel stress for specimen 1C40	137
5.16	Load versus concrete tensile strain for specimen 1C40	137
5.17	Load versus concrete compressive strain for specimen 1C40	138
5.18	Observed and predicted moment versus curvature responses for specimen 1C20	138
5.19	Moment versus depth of compression zone for specimen 1C20	139
5.20	Observed and predicted moment versus curvature responses for specimen 2A	139
5.21	Load versus concrete tensile strain for specimen 2A	140
5.22	Observed and predicted moment versus curvature responses for specimen 2B	140
5.23	Observed and predicted moment versus curvature responses for specimen 2C	141
5.24	Observed and predicted moment versus curvature responses for specimen 3A	141
5.25	Moment versus depth of compression zone for specimen 3A	142
5.26	Observed and predicted moment versus curvature responses for specimen 3B	142

<u>Figure</u>	<u>Title</u>	<u>Page</u>
5.27	Observed and predicted load versus elongation for specimen Z1 tested by Alvarez and Marti	
	(a) Full response	143
	(b) Response before yielding	143
5.28	Observed and predicted load versus elongation for specimen Z2 tested by Alvarez and Marti	
	(a) Full response	144
	(b) Response before yielding	144
5.29	Observed and predicted load versus elongation for specimen Z6 tested by Alvarez and Marti	
	(a) Full response	145
	(b) Response before yielding	145
5.30	Observed and predicted load versus elongation for specimen Z7 tested by Alvarez and Marti	
	(a) Full response	146
	(b) Response before yielding	146
5.31	Observed and predicted load versus elongation for specimen Z8 tested by Alvarez and Marti	
	(a) Full response	147
	(b) Response before yielding	147
5.32	Observed and predicted load versus elongation for specimen Z9 tested by Alvarez and Marti	148
6.1	Effect of effective depth on moment versus curvature response	161
6.2	Moment versus curvature for different wall thicknesses	161
6.3	Moment versus curvature for different load eccentricities	162
6.4	Effect of steel ratio on moment versus curvature response for constant ρ_{total}	162
6.5	Effect of steel ratio on moment versus curvature for constant ω	
	(a) $d_p = 150$ mm & $d = 200$ mm	163
	(b) $d = d_p = 200$ mm	163
6.6	Effect of effective depth on compression zone depth	164
6.7	Effect of load eccentricity on compression zone depth	164
6.8	Effect of steel ratio on compression zone depth for constant ρ_{total}	165
6.9	Effect of steel ratio on compression zone depth for constant ω	165
6.10	Effect of load eccentricity on compression zone depth versus non-prestressed steel stress	166
6.11	Effect of steel ratio on compression zone depth versus non-prestressed steel stress ($\omega = \text{constant}$)	166

<u>Figure</u>	<u>Title</u>	<u>Page</u>
6.12	Effect of increasing steel stress on depth of compression zone for different load eccentricities	167
6.13	Effect of increasing steel stress on depth of compression zone for different steel ratios ($\varpi = \text{constant}$)	167
6.14	Compression zone depth versus residual stress at centroid for different load eccentricities	168
6.15	Compression zone depth versus residual stress at centroid for different steel ratios ($\varpi = \text{constant}$)	168
6.16	Compression zone depth versus residual stress at centroid for different wall thicknesses	169
6.17	Compression zone depth versus residual stress at centroid for different effective depths	169
6.18	Effect of changing concrete residual stress for different load eccentricities	
	(a) Concrete extreme fibre stress	170
	(b) Non-prestressed steel stress	170
6.19	Effect of changing concrete residual stress for different steel ratios	
	(a) Concrete extreme fibre stress	171
	(b) Non-prestressed steel stress	171
6.20	Effect of changing concrete residual stress on moment and depth of compression zone for different load eccentricities	
	(a) Moment	172
	(b) Depth of compression zone	172
6.21	Effect of changing concrete residual stress on moment and depth of compression zone for different steel ratios	
	(a) Moment	173
	(b) Depth of compression zone	173
6.22	Load versus strain for axially loaded member with different steel ratios	174
6.23	Axial tension versus steel ratio for different concrete residual stresses	174
6.24	Finite difference mesh	175
6.25	Nodal flow rate below cracks for different depths of compression zone	176
6.26	Horizontal distribution of the flow at different depths	176
6.27	Leakage per square metre versus compression zone depth	177
7.1	Effective tension area as defined by CEB-FIP Model Code 1990	199
7.2	Non-prestressed steel stress versus total reinforcement ratio for a crack width of 0.10 mm	200
7.3	Non-prestressed steel stress versus total reinforcement ratio for a crack width of 0.15 mm	200
7.4	Prestressed reinforcement versus steel ratio for a crack width of 0.10 mm ...	201

<u>Figure</u>	<u>Title</u>	<u>Page</u>
7.5	Prestressed reinforcement versus steel ratio for a crack width of 0.15 mm ...	201
7.6	The minimum depth of compression zone required to control leakage	202
7.7	Non-prestressed steel stress versus eccentricity for different depths of compression zones	203
7.8	Non-prestressed steel stress versus steel ratio for different depths of compression zone	204
7.9	Steel stress obtained using the proposed equation for different prestressing degrees	205
7.10	Steel stress obtained using the proposed equation for different load eccentricities	205
A.1	A spreadsheet contains the input data and part of the output results	231

List of Symbols

A	Crack friction coefficient
$A_{c, eff}$	Effective tension concrete area
A_p	Area of prestressed tendon
A_s	Area of non-prestressed reinforcement (bar)
a	Depth of the rectangular compression block
C	Internal compressive force
c	Depth of compression zone
D	Diameter
d	Effective depth for non-prestressed steel
d_p	Effective depth for prestressed steel
E_c	Elastic modulus of concrete
E_s	Elastic modulus of non-prestressed steel
E_p	Elastic modulus of prestressed steel
e	Load eccentricity
f'_c	Concrete strength
f_{cr}	Concrete cracking stress
f_{cl}	Concrete tensile stress
f_r	Modulus of rupture
f_{sp}	Splitting stress
f_t	Uniaxial cracking stress
f_{pu}	Prestressed reinforcement ultimate strength
f_p	Prestressed reinforcement stress
f_s	Non-prestressed reinforcement stress
f_y	Non-prestressed reinforcement yield stress
H	Water head
h	Thickness
I	Hydraulic gradient
k	Permeability coefficient for concrete
\bar{k}	Permeability coefficient for cracks
k_1	Ratio between effective and surface crack width
$l_{s, max}$	Maximum crack spacing η
L	Crack length
M_D	Service moment due to dead load
M_w	Service moment due to water pressure
N	Tensile force
P_o	Initial prestressing force
P_e	Effective prestressing force
Q	Leakage rate
r	Radius
S	Crack spacing
T	Axial tensile force

T_f	Factored axial tensile force
T_r	Resistance axial tensile force
w	Crack width
w_{eff}	Effective crack width
w_k	Characteristic crack width
χ	Dynamic liquid viscosity
ε	Strain
ε_1	Concrete strain
ε_{cr}	Concrete cracking strain
ε_p	Prestressed steel strain
ε_s	Non-prestressed steel strain
ΔH	The difference in water head at the crack
ϕ	Strength reduction factor
Φ_s / Φ_p	Diameter of bar / strand
η	Modular ratio
φ	Creep coefficient
ρ	Liquid density
ρ_{total}	Total steel ratio
$\rho_{tot, eff}$	Total effective steel ratio
ϖ	$A_s f_y + A_p (0.9 f_{pu})$
ξ	Percentage of water loss
ψ	Bond coefficient as defined by CEB-FIP Model Code 1990

1- Introduction

1.1 General

Concrete is ideally suited for environmental engineering structures such as water reservoirs and sewage treatment tanks. Consequently reinforced and prestressed concrete are the preferred materials for environmental engineering structures. While cylindrical shapes may be structurally best for tank construction, rectangular tanks are frequently preferred for process related reasons.

The structural design of these environmental concrete structures is not covered in Canadian design standards. A variety of foreign sources are frequently used. While all the sources purport to produce safe, leak resistant and durable tanks, the various design standards require significantly different amounts of reinforcement and concrete. The most significant difference appears between the design of reinforced concrete and prestressed concrete tanks. While in the former a significant concrete tensile stress is allowed, a residual net compressive stress is required in the latter. The lack of agreement between the major sources implies that the profession has yet to converge upon a rational solution.

Serviceability limit states are the most important limit states for tanks and they invariably govern the design. Of these, the leakage limit state generally governs over the other serviceability limit states such as deflection. The existing design approaches attempt to control leakage by either completely preventing cracking in prestressed tanks or by limiting cracking to specific widths in reinforced concrete tanks. The various design approaches implement different crack width equations yielding significantly different predictions.

In his historical review, Gogate (1981) stated that one of the earliest documents on the design of concrete liquid retaining structures is due to Gray (1948) who published a textbook about reinforced concrete reservoirs. The book provided convincing arguments for the use of low stresses in the steel reinforcement (80 MPa to 120 MPa) in

the working stress design format. One of the first American documents on the subject appeared in 1942 as a structural design bulletin of the Portland Cement Association ST57 (1942) for the design of circular concrete tanks. This was followed by PCA bulletin ST63 (1963) for the design of rectangular concrete tanks. Many design approaches have evolved since these early references. They are distantly related but with little agreement on design philosophy.

1.2 Objectives of this Study

At a preliminary stage of this research, the existing design approaches for water containment structures were critically reviewed and trial designs were carried out to investigate the practical implications of these design approaches. This preliminary study showed the differences between the existing approaches especially those between the design of reinforced concrete and prestressed concrete tanks. The study also showed the advantages of partial prestressing in water tanks. This is not covered in the current water tank design approaches. It also revealed a growing understanding of phenomena such as watertightness and self-healing of cracks.

As a result of the preliminary study, the objectives of this study were set:

- to develop a rational design procedure for both reinforced and prestressed concrete tanks that assure a safe leak resistant structure.
- to investigate the concept of partial prestressing in liquid storage tanks. This concept is currently used successfully in the design of other types of structures such as bridges and buildings. Understanding the behavior of partially prestressed tanks is the key for providing rational solutions ranging from reinforced concrete at one end of the design spectrum to fully prestressed concrete at the other.

1.3 Scope of the Report

The scope of this report includes a literature review and subsequent trial designs to develop an understanding for the current state of the art. This was followed by an experimental program and subsequent analytical studies.

In the experimental phase a total of eight full-scale specimens, representing segments from typical tank walls, were subjected to load and leakage tests. The test specimens covered a range of prestressed and non-prestressed reinforcement ratios and were subjected to various combinations of axial tension and bending. In the analytical phase a computer model that predicts the response of tank wall segments was written and calibrated against the test results. The model was used to investigate additional factors and to conduct a parametric study. The combination of the experiments and the analytical results were used to propose a tentative design procedure that satisfies the different limit states.

Providing comprehensive design recommendations for water containment structures is beyond the scope of this report. Design considerations such as deflections, seismic design, and design of joints are not covered, but their importance should not be underestimated.

1.4 Organization of the Report

This report consists of eight chapters and three appendices.

Chapter 1 provides a general introduction.

Chapter 2 contains a critical review of the literature and trial designs using the various existing approaches. The results of the trial designs illustrate the practical differences between the various approaches. The concept of partial prestressing in water tanks, watertightness criteria for tanks and durability of tanks are also discussed.

Chapter 3 presents a detailed description of the test specimens, the experimental set-up, and the test procedure.

Chapter 4 provides the detailed test results as well as evaluation of the observed behaviour of all the specimens throughout the course of both loading and leakage tests.

Chapter 5 includes a detailed description of the analytical model employed to simulate the test specimens. Verification of the suggested model against the experimental results and third party test results are also presented in this chapter.

A parametric study is presented in Chapter 6. The analytical model was the basis for this study. The chapter also describes the results of a study conducted to investigate the leakage of concrete tank wall sections.

In Chapter 7, the design limit states for water tanks are discussed in the light of the experimental and the analytical results. A unified approach for the design of water tanks ranging from reinforced concrete at one end of design spectrum to fully prestressed concrete at the other is proposed.

Chapter 8 provides a summary of the research and the conclusions drawn therefrom. Recommendations for future study are also noted.

In Appendix A, a listing of the computer program is given as well as an example of input data and program output.

In Appendix B, the procedure used to calculate time-dependant stresses and strains is illustrated.

Appendix C, contains solved examples to illustrate the application of the suggested design procedure.

This report generally uses the SI system of units. Unless otherwise indicated, the moments are in kNm, forces are in kN and lengths are in millimeters.

The symbols that are used throughout this report are included in the List of Symbols. Some symbols, which are only used in one location and are defined there, are

not included in the List of Symbols. It should be noted that the notations of some equations from other resources, have been modified to make the notations consistent with those used in this report. For example, some authors use “d” for the total thickness. This was replaced by “h” the more commonly used symbol to avoid confusion with the common use of “d” for the effective depth of the reinforcement.

2- Preliminary Review

2.1 Introduction

In this chapter, a critical review of the commonly used design approaches for concrete water tanks is provided. The design philosophy and crack width calculations for each method are compared. This is followed by a description of case studies (trial designs) conducted to illustrate the practical differences between the various approaches. The results of these case studies are then presented. The concept of partial prestressing in concrete members is discussed with emphasis on its application to water tanks. Experimental studies and crack width calculations in partially prestressed concrete members are also presented. Next, the criterion for watertightness in water tanks is described along with the phenomenon of autogenous healing in concrete cracks. Finally the relationship between crack width and reinforcement corrosion is discussed.

The review presented in this chapter focuses on design rather than analysis. Existing Standards and design recommendations used in practice are reviewed. The structural analysis of tanks is also excluded from the scope of this chapter because Wilby's (1977) comprehensive literature survey on that subject showed that elastic (linear) structural analysis is the most common approach.

2.2 Design Approaches – a literature review

2.2.1 Design Philosophy

The limit states for tanks are the ultimate limit state and serviceability limit states which include leakage, durability and deflection limit states. The serviceability requirements invariably govern the design. Within the serviceability requirements, leakage and durability generally govern over deflection limitations. Various design

strategies may be used to create a structure that will satisfy all limit state requirements. This will now be explored.

ACI 350R (1989) "Environmental Engineering Concrete Structures"

Recognizing the need for an organization to provide guidance for the design of environmental engineering structures, ACI formed Committee 350 in 1964. Since its first report in 1971, ACI 350 committee reports have become the most widely used references for the design of reinforced concrete tanks in Canada, the USA, and perhaps the world. The basic philosophy used is to limit the reinforcing steel stresses under normal working loads. This was done exclusively, and explicitly, through working stress design procedures in the early committee reports. In more recent reports, this is done implicitly through a modified ultimate strength procedure. ACI 350 supports both procedures, and has "calibrated" them to produce similar but not necessarily identical designs.

A modified ultimate strength procedure was introduced into ACI 350 in response to changes in the education of American engineers. In the mid 1970's, North American universities stopped teaching working stress design in favour of ultimate strength design. In order to accommodate designers who were unfamiliar with working stress design procedures, Committee 350 introduced an additional load factor called the "sanitary durability coefficient". The demand side of the ultimate limit state equation was artificially increased. A designer using regular ultimate strength design aids would arrive at steel quantities that would produce satisfactory service load stresses in the reinforcement.

ACI 350 contains tables and charts with conservative steel stress limits for specific situations. A modern crack control formulation based on the Gergely-Lutz equation was introduced to permit designers to take advantage of the benefits of using smaller bars at closer spacing. Rather than calculating an explicit crack width, the "Z-factor" approach from ACI 318 was followed. The permissible Z depends upon the severity of the exposure conditions. The more aggressive the exposure, the more

restrictive the Z value. This approach can be used to refine designs based on either the working stress or modified ultimate strength approaches. However, the working stress method is more convenient because it does not require iteration processes to achieve an acceptable value of Z.

ACI 350 recognizes that direct tension is more severe than flexure. In the former, a through crack leading to significant leakage can occur. In the latter, a compression zone on one face of the member reduces the potential for a through crack and significant leakage. These differences are recognized through the use of different allowable working stresses and sanitary durability coefficients.

Shrinkage and temperature related stresses are generally not considered explicitly in ACI 350. Details that reduce these stresses are recommended. More importantly, the minimum shrinkage and temperature reinforcement requirements vary from 0.28% to 0.6% and are thus significantly greater than in ACI 318. The minimum reinforcement is a function of the yield strength of the reinforcement and the distance between shrinkage dissipating joints (e.g. construction joints).

Portland Cement Association

Over the years, Portland Cement Association PCA has published reports on the design of rectangular and circular reinforced concrete tanks (PCA 1942, 1963, 1981, and 1993). They provide tables that assist with the structural analysis of the various tanks (i.e. plate and shell tables). After the appearance of ACI 350, PCA reports tended to support ACI 350 recommendations. The most important difference in the PCA documents is in the establishment of the minimum wall thickness for circular tanks. In addition to a minimum thickness based on constructability, PCA suggests that the wall thickness be such that, in the hoop direction, the wall does not crack under normal service loads. PCA includes an explicit allowance for concrete shrinkage in the calculations.

*ACI 344 "Design and Construction of Circular Prestressed Concrete Structures"
and Prestressed Concrete Institute*

Circular prestressed concrete tanks in North America are generally designed in accordance with the requirements of ACI 344 (1989) or PCI (1987). These documents are rather similar and are based on the philosophy of maintaining the concrete in compression. With this fully prestressed philosophy, concrete tensile stresses are prevented under normal service loads. In general, a residual compression stress of 1.38 MPa (200 psi) is required in the hoop direction under service load. This prevents the formation of through cracks due to direct tension. Tensile stresses due to thermal and moisture gradients are not explicitly calculated. Where these stresses are most important, such as in the upper region of the walls in open-topped above-ground tanks, the nominal residual compression is increased to 2.8 MPa (400 psi).

One of the consequences of the full prestressing philosophy is that there is no benefit of providing non-prestressed reinforcement and additional concrete wall thickness. In fact, one pays a penalty in that additional prestressing is required. Designers are indirectly encouraged to design thin walls with little if any non-prestressed reinforcement.

To resist tensile stresses from vertical bending moments the walls may be prestressed vertically or reinforced with non-prestressed reinforcement. A combination of prestressed and non-prestressed reinforcement may be used. When vertical prestressing is used, ACI 344 requires an average vertical compressive stress of at least 1.38 MPa due to prestressing after all losses.

BS 8007 "Design of Concrete Structures for Retaining Aqueous Liquids"

British Standard BS 8007 (1987) is used occasionally in Canada. From a legal point of view, this is a standard written in mandatory language. The other documents that have been previously discussed are "good practice guides" that offer many helpful suggestions and hints.

BS 8007 is based on limit state design concepts. The basic philosophy is to assess reinforcement requirements on the basis of the crack width limit state under service load. The design is then checked for other limit states. There is no distinction made between crack widths for flexure and direct tension or restrained temperature and moisture effects. For reinforced concrete tanks, the maximum design surface crack widths are limited to 0.2 mm for severe or very severe exposure and 0.1 mm for critical aesthetic appearance situations.

In circular prestressed concrete tanks, zero tension is allowed in the hoop direction while 1.0 MPa flexural tensile stress is allowed due to vertical flexure. In prestressed tanks that are other than circular, the design is based on a 0.1 mm crack width for very aggressive environments and 0.2 mm crack width for other exposures.

2.2.2 Crack Width Calculation

While ACI 344 requires residual compression stress to prevent the formation of cracks, both ACI 350 and BS 8007 standards limit the maximum crack width at the concrete surface to 0.1 or 0.2 mm. However, since each document adopts a different crack width equation, they have different degrees of conservatism. In ACI 350, the Gergely-Lutz equation is the basis of the Z parameter, while in BS 8007 the calculation of the crack width is based on a different empirical approach that is detailed in Appendix B of BS 8007.

A numerical comparison between the two approaches is given in Table 2.1 for typical wall thicknesses subjected to flexure using No. 15 bars at various spacings with 50 mm clear concrete cover. The comparison is extended to include the crack width equations provided by CEB78 (1985) and CEB-FIP Model Code 1990 (1993). Predicted crack widths can vary by more than 200%, with Gergely-Lutz predicting the largest crack widths. For typical practical cases with steel ratios smaller than 1% or with M/M_{cr} smaller than 1.5, the differences in crack width prediction are significant.

2.3 Case Studies

To identify the practical differences between the existing design approaches, two open topped circular tanks were designed. The two tanks have capacities of 650 and 7900 m³ respectively (diameters of 12 and 36 m and heights of 6 and 8 m respectively). The tanks rest on soil and have a membrane floor which is thickened beneath the wall. The structural analysis of each tank was conducted using the finite element program, FEPARCS92 (Elwi 1992), employing a two-dimensional cubic, 4-noded, beam element with axisymmetric formulation. To simulate the soil reaction under the floor, a vertical spring was attached to each node of the floor elements. Figure 2.1 shows the finite element model for the large tank. Each tank was designed as a non-prestressed tank following the requirements of both ACI 350R and BS 8007. The tanks were also designed as prestressed tanks following the requirements of ACI 344, PCI and BS 8007 respectively. The wall was considered hinged at the floor in the non-prestressed tanks. In the prestressed tanks designed by either ACI 344 or PCI, the wall was allowed to slide during prestressing, taking into account the friction of the support pad. A coefficient of friction of 0.2 was assumed. During the application of water pressure on the tank, the wall was considered hinged at the bottom. This is consistent with common construction practices. Figure 2.2 shows the significantly different distributions of the prestressing force in the large tank that result from ACI 344 and BS 8007. The design was conducted with both the ultimate strength design method, *USD*, and working stress design method, *WSD*.

In total, 20 tank designs were generated. Concrete quantities, steel amounts, the calculated crack widths due to applied loads and an approximate estimate of the costs are presented in Tables 2.2 and 2.3 for *WSD* and *USD* respectively. The cost calculations assumed; \$1/kg of non-prestressed steel, \$4/kg of prestressing steel, \$130/m³ of concrete and \$50/ contact m² of form. To ensure consistent comparisons, the BS 8007 crack width prediction equations were used in all cases.

Detailed comparison of the results leads to the following observations.

1. ACI 350's *WSD* and *USD* procedures produce similar results.
2. In small prestressed tanks vertical non-prestressed steel and wall thickness are governed by the minimum value required by each code.
3. In all cases, other than those mentioned in items 1 and 2, *WSD* requires more non-prestressed reinforcement than *USD*. Simple tabulated working stresses give conservative crack widths. While the reduction in the amount of steel required by *USD* causes negligible reduction in the total cost (less than two percent) it results in a significant increase in crack widths. Crack widths are doubled in some cases.
4. Required concrete volumes depend primarily on the minimum wall thickness required for constructability. These minimum thicknesses were sufficient for strength requirements even for the large tank. BS 8007 does not specify a minimum wall thickness. Therefore, a reasonable wall thickness was used to satisfy ease of construction, strength requirements, and the allowed crack width.
5. ACI 350 required 9 percent less nonprestressed reinforcement than "the simple BS 8007" *WSD* but 20 percent more than "the refined BS 8007" design based on crack widths. This difference is because steel stresses smaller than those used by ACI 350 are used in simple BS 8007 *WSD*, while in the refined BS 8007 design the crack width limits are specifically achieved. The ultimate limit state was checked, but never governed.
6. In prestressed tanks, ACI 344 produces the largest vertical non-prestressed steel amount when using *WSD*. This is in part due to the low steel stress of 124 MPa (18 ksi) it recommends. The minimum vertical reinforcement ratio of $0.005 A_c$ required to resist moments from temperature and moisture gradients is a reason for the high steel quantities. Using ACI 344 *USD* requires slightly larger amounts of steel than the other *USD* approaches because it suggests greater minimum vertical steel reinforcement be used.

7. In prestressed tanks BS 8007 requires significantly less prestressing than the other applicable documents, especially in smaller tanks. BS 8007 does not require residual compression in the circumferential direction.
8. In the prestressed tanks, all approaches produce a crack free small tank, but all produce horizontal cracks due to vertical moments in the large tank. ACI 344 always produces the narrowest crack width, especially in *USD*. In the circumferential direction of prestressed tanks there were no cracks. By contrast, a residual compression existed in ACI 344 and PCI solutions as indicated in the last line of Tables 2.2 and 2.3.
9. The crack width in nonprestressed tanks relates to the amount of reinforcement provided. Designs that economized on reinforcement had larger crack widths.
10. In the small tanks, designs that include no prestressing are slightly less expensive than those that use prestressing (2 to 9 percent). For large tanks, prestressing is more economical.
11. When tanks are compared on a crack width basis, prestressed tanks are better. The residual compression stresses, in prestressed tanks, provide additional safety against cracking due to temperature and moisture gradients.
12. For floors, ACI 344 requires the largest amount of reinforcement and BS 8007 requires the smallest. This is because both ACI 350 and PCI require a minimum reinforcement of about $0.003 A_c$ while ACI 344 requires a minimum of $0.005 A_c$ for membrane slabs and $0.006 A_c$ for thickened slabs. In BS 8007 no bottom reinforcement is required for floors of thickness less than 300 mm. Also, $A_{s_{min}} = 0.0035 A_c$ based of one-half the floor thickness.

2.4 Partial Prestressing – a literature review

2.4.1 Background

Around 1940, Abeles (1945) introduced the concept of using a small amount of tensioned high-strength steel to control deflection and crack width while permitting high working stress in the main reinforcement of reinforced concrete. Based on his studies, Abeles advocated that in many designs it is unnecessary to completely eliminate the tensile stress and possible cracking in the concrete. Prestress of a limited magnitude may be applied to counteract only part of the service load so that tensile stress or even hairline cracks could occur in the concrete under full service load. This design approach was termed by Abeles as “partially prestressed concrete”. In general, partial prestressing may mean either or both of the following two conditions:

1. Flexural tensile stresses are permitted in the concrete under service loads, These stresses may be lower than or lead to cracking.
2. A combination of prestressed and non-prestressed reinforcement is employed in the member to resist external loads. The non-prestressed reinforcement may be either ordinary reinforcing steel or non-stressed prestressing steel.

Naaman (1984) proposed that "A necessary and sufficient condition for a member to be called partially prestressed is to contain prestressed and non-prestressed reinforcement intended to resist external loads of the same nature".

Since the 1970's the Canadian concrete design code has permitted partial prestressing based on condition 2. CAN-A23.3-M77 (1977), clause 16.6 allows the use of partially prestressed concrete members "*which derive their strength partly from the use of reinforcement and partly from prestressed tendons...*" This clause has disappeared from the code. The commentary on clause 18.4.3 of the current A23.3-94 (1994) defines partially prestressed members as members in which tensile stress exceeds $0.5\sqrt{f'_c}$. Clause 18.9 of the same code requires minimum bonded non-prestressed reinforcement to control cracking in partially prestressed members.

The American concrete design code provisions have permitted partial prestressing if the concept is defined on the basis of allowing tensile stresses in the concrete under service loads. ACI 318 Building Code implicitly allows partial prestressing, by permitting tensile stresses at service load that started with $0.5\sqrt{f'_c}$ MPa in 1958 and then increased to $1.0\sqrt{f'_c}$ MPa in 1971 if immediate and long-term deflections comply with code limits. The latter value is higher than concrete cracking stresses, which means that cracks are allowed. Partial prestressing is also addressed in the European Specifications (CEB, BS 8110, FIP, SLA).

Partial prestressing has been implemented successfully in buildings and bridges because it utilizes the advantages of both reinforced and fully prestressed concrete. Compared to reinforced concrete it offers better cracking and deflection control and better economy. Compared to full prestressing, partial prestressing also offers better control of camber, a simple layout of prestressing tendons, a higher ductility and energy absorption to failure. Non-prestressed reinforcement used in partial prestressing controls crack width. On the other hand, partially prestressed beams are generally more susceptible to fatigue failure than fully prestressed or reinforced concrete beams. Naaman (1982) indicated that there can be large stress changes in the steel at concrete cracks due to repetitive loads on partially prestressed concrete. In fully prestressed members which by definition are uncracked, the steel stress ranges are small. Brøndum-Nielsen (1984) stated that the stress limits ensuring safety against fatigue may be satisfied even if moderate crack widths are presented. Brøndum-Nielsen argued that the fatigue strength of the anchorage and joints in the tendons is considerably lower than that of the tendons. The fatigue strength of a structure can thus be improved by placing anchorage and joints in zones with small stress variations provided an efficient bond between tendons and concrete is ensured. In addition, durability is a problem for partially prestressed members in comparison to fully prestressed members since they are presumed to be cracked under full service load. The durability concern can usually be addressed with proper design and detailing of the non-prestressed reinforcement.

2.4.2 Partial Prestressing in Water tanks

Unlike buildings and bridges, partial prestressing is not commonly used for liquid retaining structures. ACI 344 (1989) implicitly allows partial prestressing in the vertical direction of circular tanks. In clause 2.3.8 it allows using a combination of prestressed and non-prestressed reinforcement to resist vertical moments. It also states that “*non-prestressed reinforcement should be provided near wall faces in all locations subjected to net tensile stress (after allowing for vertical prestressing, if any) from primary moments*”. ACI 344 does not give any guidance on the crack widths. BS 8007 (1987) appears to allow partial prestressing for non-cylindrical tanks as long as the crack width limits are satisfied (same limits as in reinforced concrete). Partial prestressing does not require additional prestressing when wall thicknesses are increased for constructability, and recognizes the benefits of non-prestressed reinforcement.

To study the influence of using partial prestressing in water tanks, trial designs were carried out. In these studies an 920 m³ open topped rectangular tank (8×20 m and 6 m height) was analyzed using SAP80 (Habib-Allah and Wilson 1984) employing a two dimensional 4-noded shell element. Soil reaction and the wall-floor joints were treated as explained earlier in the circular tanks. The tank was designed as reinforced concrete, fully prestressed and partially prestressed. The structural analysis showed the benefits of providing an edge horizontal beam at the top of the wall. In the case study the presence of that beam reduces the connecting moments in the horizontal direction at wall mid-height from 223 to 153 kNm (40 %) but only increases the maximum vertical moment from 115 to 124 kNm (7.6 %). In the prestressed tanks, prestressing was provided in the vertical direction as well as in the horizontal direction due to the presence of high vertical moments. Since there are no currently available design recommendations for rectangular prestressed tanks, a minimum average prestress of 1.4 MPa was provided in the vertical direction to be consistent with ACI 344. In the horizontal direction, high axial tension accompanies the high bending moments, especially in shallow tanks. This combination makes it impractical to provide full horizontal prestressing sufficient to

produce a residual compression as would be used in the hoop direction of circular tanks. In the case of partial prestressing, the amount of prestressing was adjusted such that the maximum hypothetical tensile stress may exceed the cracking stresses but within the limits specified in BS 8110's (1985) Table 4-2, class 3 prestressing (3.2 to 7.3 MPa).

The estimated cost, using the values stated earlier, for the three (non-prestressed, partially prestressed and fully prestressed) tanks are \$88,350 (\$96/m³water), \$86,350 (\$94/m³ water) and \$103,650 (\$113/m³ water) respectively. In this example, the partially prestressed tank is the least cost solution. The cost study also shows that, for the size studied, the rectangular tanks were generally more expensive than the circular tanks. The crack width calculations showed that, while the crack widths approached 0.15 mm in both the vertical and horizontal directions of reinforced concrete tanks, there were no cracks in the case of partially prestressed tanks. The procedure used in the crack width calculations was based on Tadros (1982) with minor modifications to suit the load cases found in tanks. Even though the partially prestressed tank was designed with tensile stresses that exceed the cracking stresses, the refined crack width calculations based on Tadros (1982) showed that cracks did not form. The above case studies showed the merit of using partial prestressing in water tanks.

2.4.3 Crack Width Calculations for Partially Prestressed Concrete

For partially prestressed members, the presence of prestressed steel complicates crack width calculations by adding more variables affecting the crack width. Prestressed steel type, strands, bars or wires, type of prestressing, pre-tensioned or post-tensioned and level of prestressing are examples of these variables. Krishna Rao and Dilger (1992) presented a critical review of crack-width equations for partially prestressed members. In these members the estimation of non-prestressed steel stress is facilitated by the definition of a fictitious force called the "decompression force". Several researchers use this approach for partially prestressed beams subjected to flexure. The methods need to be extended to combine flexure and tension to suit the loading conditions commonly found in tanks.

2.4.4 Experimental Studies on Partial Prestressing

Because of the importance of serviceability behaviour of partially prestressed elements, many experimental investigations have been undertaken. A selection of experimental programs that dealt with flexure, tension, and static loads (rather than seismic) are presented here.

Stevens (1969) tested three series of fully prestressed, partially prestressed and reinforced concrete simply supported beams designed to have similar ultimate resistance. He proposed the design of partially prestressed beams as fully prestressed up to the point of decompression at the soffit of the beam and as reinforced concrete after that point. He stated that cracking, fatigue and ultimate limit states are likely to be satisfied, when the non-prestressed reinforcement stress under service loads does not exceed 228 MPa or 0.55 times the yield stress.

Bennett and Veerasubramanian (1972) tested thirty-four simply supported 6.0 m beams, with four different cross-sections: rectangular, I-section, T-section and composite T-section. They investigated the effect of the shape of the cross-section and the non-prestressed steel on the flexural behaviour of partially prestressed beams, with particular reference to the deflection, cracks size and the ultimate strength. They concluded that the shape has no effect on flexural cracks and that nonprestressed steel afforded satisfactory control of cracking, even in beams with unbonded prestressed strands, provided that the bonded reinforcement does not yield. They proposed a formula for crack width calculation.

Raju *et al* (1973) tested eight 2.7 m span simply supported pretensioned concrete beams with non-prestressed reinforcement. They proposed a formula to calculate crack width considering the percentage of non-prestressed reinforcement.

Harajli and Naaman (1984, 1989) tested twelve different sets of simply-supported beams. Each set comprised two identical beams. One beam was tested to failure under monotonic loading, while the second beam was tested in fatigue at a constant load range

simulating full live load. Based on test results they developed a model for computing the increase in crack width under cyclic fatigue loading.

Hassoun and Sahebjam (1989) conducted tests on simply supported partially prestressed beams to study the effect of non-prestressed steel on the cracking behaviour. They used test results to develop an expression to calculate the maximum crack width.

Nawy (1989) conducted tests on twenty simply supported pre-tensioned 2.7 m span beams, four two-span continuous beams and twenty-two simply supported post-tensioned beams of 2.3 m span. The major controlling parameters were the amounts of prestressed and non-prestressed reinforcement. Experiments illustrated that the presence of nonprestressed steel in partially prestressed members has a significant effect on crack control such that the cracks become more evenly distributed and the crack spacing and widths become smaller. They also illustrated that an increase in the total steel ratio decreases the crack width and spacing in partially prestressed members.

Based on test results, Nawy proposed a mathematical expression for evaluating crack widths in partially prestressed beams.

Unlike all the above experiments which were conducted on beams, **Alvarez and Marti** (1996) carried out axial tension tests on seven conventionally reinforced and two partially prestressed concrete wall elements. They investigated the influence of some selected parameters on the deformation behaviour and the deformation capacity of structural elements in pure tension. Partial prestressing of the longitudinal reinforcement was one of these selected parameters. They reported the deformation behaviour of each specimen and summarized the effect of the different parameters on the plastic deformation. These tests were used in Section 5.7 to validate the analytical model developed in this report. Further details can be found there.

2.5 Watertightness

2.5.1 Watertightness Criteria

Watertightness is essential for water containment structures. No concrete structure will be perfectly watertight. Some loss of water will occur through uncracked concrete due to permeability, cracks, joints, fittings and incidental defects. The permeability of concrete normally used for water containment structures will result in a very small loss of water (ACI 350/AWWA 400, 1993). On the other hand, joints have a large potential for leakage. Therefore joints require more careful attention during design and construction than other concrete areas. ACI 350/AWWA 400 (1993) states that an expansion joint is more apt to leak than a contraction or control joint, and that all are more apt to leak than a construction joint. Fittings refer to foreign or different materials inserted in, embedded in, or passing through the concrete such as piping. Fittings have the potential for allowing water to follow along the contact surface between the fitting and the concrete. Watertightness criteria usually recognize this potential by not allowing visible leakage at fittings.

Bomhard (1986) differentiates between local and global watertightness. For local tightness, the outer surface of the container may exhibit moist or wet spots at no point. No moist spots implies that the water must evaporate faster than it can permeate through concrete. For global tightness, a specific leakage rate must not be exceeded.

Each of the existing standards specifies certain global leakage rates and requires leak testing to measure the actual leakage rate. The leakage rate is measured by the drop in the water level during the test period. ACI 350/AWWA 400 (1993) allows loss of 0.025 to 0.1 percent of water volume in 24 hours. The specific rate depends upon the water depth and whether the concrete is lined or not. BS 8007 (1987) allows a drop in water level of $1/500^{\text{th}}$ of the average water depth of the full tank (0.2% of water volume) over 7 days.

While both local and global tightness requirements should be met, the global requirements are more important. Satisfying local tightness at all the locations can be done, but at markedly higher costs.

Bomhard states that watertightness requirements could be met by one or a combination of three methods: limiting concrete tensile stress, specifying a minimum depth of concrete compression zone or limiting crack width. Since concrete tensile strength varies considerably, he considers it an unsuitable measure. Bomhard defined three regions in the load-moment interaction diagram. In the first region there are separation (through) cracks, in the second region there is a very small compression zone, and in the third region there is a large compression zone. Prestressing has a considerable effect in preventing leakage in the first two regions. For the region with a sufficiently thick compression zone, Bomhard suggested that tightness will be reached without any tensile stress or crack width limitations and that the watertightness will be more reliable.

Bomhard provided equations to calculate leakage rate Q through uncracked concrete and through cracks given by the following two equations respectively:

$$Q = \frac{k}{\chi} A \frac{\Delta P}{h} \quad (m^3/s) \quad (2.1)$$

$$Q = \frac{\bar{k}}{\chi} w_{eff}^3 L \frac{\Delta P}{h} \quad (m^3/s) \quad (2.2)$$

where,

k is the permeability coefficient for concrete (m^2),

\bar{k} is the permeability coefficient for the crack (non-dimensional),

χ is the dynamic liquid viscosity (1.06×10^{-3} Nsec/ m^2 for water),

ΔP is the pressure drop through the wall,

h is the wall thickness (m),

A is the flow-through surface area in (m^2),

L is the crack length (m), and

w_{eff} is the effective width of the cracks (m) taken as:

$$w_{eff} = \sqrt[3]{2 \frac{(w_1 w_2)^2}{w_1 + w_2}} \quad (2.3)$$

w_1 and w_2 are crack widths from the inner and the outer faces of the wall (m).

Bomhard suggested that k can be taken as 10^{-16} to $10^{-18} m^2$ depending upon the required degree of watertightness, and that \bar{k} will be less than 10^{-2} , which corresponds to laminar flow. He suggested that Eq. 2.2 may be used for open joints. He compared the leakage due to porosity (per unit area) with leakage through a crack (of 0.1 or 0.2 mm width) and found that the ratio varies from 10^{-2} to 10^{-5} . He also compared them to leakage through an open joint (considering joint width 100 times the crack width) and found the ratios will be: $1 : 10^4 : 10^{10}$ for porosity, cracks and joints respectively. Finally, he proposed using 50 mm as a minimum for the compression zone and below this minimum the crack width should be limited to either 0.1 or 0.2 mm.

Imhof-Zeitler (1996) studied the flow of liquids having different viscosity (acetone, water, gas oil, motor oil) in through-cracked structures. He developed the following relationship to predict leakage rate through penetration cracks:

$$Q = \frac{g}{A\chi / \rho} \left[1 + \frac{\Delta H}{h} \right] wL \quad (\text{litre/s}) \quad (2.4)$$

where,

A is a friction coefficient = $12/w^2$ ($1/m^2$),

w is the crack width (mm),

g is the gravity acceleration and,

ρ is the density of the liquid (1000 kg/m^3 for water).

Equation 2.4 is based on flow through slot with plane and parallel walls. Comparing Eqs. 2.4 and 2.2 shows that the coefficient \bar{k} in Eq. 2.2 is approximately replaced by 1/12 (0.083) in Eq. 2.3.

Based on experimental investigation for the flow through cracks, Imhof-Zeitler changed the friction coefficient A to consider the roughness of the crack. He proposed the following two values of A for crack widths greater than or less than 0.1 mm respectively:

$$A = \frac{12}{w^2} \frac{4}{cw^{1.6}} \frac{80}{(14I - 20)} \cdot 10^6 \quad (1/m^2) \quad (2.5)$$

$$A = \frac{12}{w^2} \frac{4}{0.82cw^{0.6} \sqrt{\chi/\rho}} \cdot 10^6 \quad (1/m^2) \quad (2.6)$$

where,

I is the hydraulic gradient ($\Delta H/h$),

$c = 1$ for water soluble liquids and 1.89 for other liquids and,

w is the crack width in mm.

To account for the presence of longitudinal steel, he multiplied A by 1.43 for $w < 0.1$ mm and for steel ratio $> 0.3\%$.

Imhof-Zeitler's experimental results showed that flow behaviour through cracks depends primarily on crack width and roughness. It also depends on liquid properties (viscosity, density, and water solubility) and on the pressure gradient. He concluded that watertightness can not be fulfilled for liquids with low viscosity through separation cracks wider than 0.1 mm. This conclusion is based on testing specimens with thickness of 200 mm under a water head of 1.4 m for 72 hours. He also tested small specimens with a flexural crack and precracked compression zone. He stated that in this case loading conditions and the presence of compression stresses affect watertightness. Tests

showed that the penetration behaviour is influenced also by the percentage of longitudinal reinforcement

2.5.2 Autogenous Healing

The ability of small cracks in concrete to heal themselves in the presence of moisture is called autogenous healing. Autogenous healing reduces and sometimes stops leakage through cracks.

Neville (1981) proposed that autogenous healing is due to the hydration of the unhydrated cement, and may also be aided by carbonation. He stated that the younger the concrete, i.e. the more unhydrated cement it contains, the faster the healing, but healing has been observed at ages up to three years. Neville noted that the application of pressure across the cracks assists in healing.

Murray (1981) conducted experiments to determine a relationship between crack width and the hydraulic conductivity of the crack. The test specimens were 150x150x720 mm blocks of plain concrete cracked in tension and opened to various crack widths ranging from 0.14 to 2.3 mm. Water flow through the crack was recorded but it was allowed to stabilize before recording, so the effect of autogenous healing was not ascertained. The results indicated that parallel-plate theory significantly overestimates the flow rate through a crack. He used the obtained values of hydraulic conductivity for different crack widths as input to a numerical model. He presented a tentative expression that enables one to calculate the maximum allowable crack width that will satisfy certain flow rate limit.

Clear (1985) carried out experiments to investigate the phenomenon of autogenous healing and to determine the relationship between the surface width of a crack in concrete and its effective width. The effective width is defined as the width of a smooth parallel-sided slot that provides equivalent flow through the concrete. Clear defined the factor k_1 as the ratio between the effective crack width. Table 2.4 gives values of k_1 for some simple crack geometries. The experiments showed that parallel-sided cracks,

subjected to a hydraulic gradient of 22.5 with characteristic surface widths up to 0.2 mm heal autogenously such that leakage becomes practically unmeasurable within one week. Tests also showed that the healing mechanism is a combination of mechanical blocking and chemical precipitation of calcium carbonate. Thus filling that the reservoir slowly allows autogenous healing to take place before large pressure gradients develop.

Edvardsen (1996) performed comprehensive and accurate experimental and theoretical studies. He tested small specimens with a single crack as well as 2500x1000x400 mm concrete slabs. He examined many variables include crack width, water pressure, concrete composition, water hardness, skin reinforcement and water additives such as bentonite and silica fume. Experimental results proved that the formation of calcium carbonate crystals in the crack is almost the sole cause of autogenous healing and that the crystal formation is not affected by either concrete composition, or water hardness. Skin reinforcement proved to be highly effective in supporting the autogenous healing process. Edvardsen developed an algorithm that can be used to estimate the reduction in flow rate through a crack as a result of autogenous healing. He finally proposed permissible crack widths for autogenous healing in water-retaining structures vary between 0.05 and 0.2 mm according to the hydraulic gradient as given in Table 2.5. It is noted that there is a distinguish between stationary cracks that do not change width over time and other cracks.

Bick et al. (1997) investigated the penetration of fluids through cracks in concrete. They tested two simply supported 5 m prestressed beams under 4-point loading. The beams were loaded until stabilize cracks were formed. The flow rate through these cracks was examined. They also examined the penetration of eight different liquids through cracks, formed due to axial tension, in 200x200x700 mm concrete prisms. They proposed that the leakage through crack widths up to 0.2 mm can be estimated for a parallel-sided slot with smooth walls multiplied by a reduction factor. Test results suggested that the factor varies from 0.015 to 0.067 with a mean of 0.04. This factor was higher in unreinforced cracks (0.004 to 0.136 with a mean of 0.085). They noted that these values are valid for

liquids that do not react with the hardened cement paste and do not contain suspended particles. In the case of water, the flow rate is considerably smaller due to self healing of the cracks.

2.6 Crack Width and Steel Corrosion

Codes and design specifications have traditionally related durability and reinforcement corrosion to crack width. They specify crack width limits and provide formulas for calculating crack widths. These formulas usually produce different crack widths for the same case as illustrated earlier in the case studies. Beeby (1983), presented a survey of the research carried out on this subject in different countries in Europe and North America. Beeby concluded that crack widths have little influence on corrosion and that the major parameters controlling corrosion are cover and concrete quality. The detailed calculations for crack width as a corrosion control measure in many design recommendations are unnecessary. Brøndum-Nielsen (1984) noted that cracks parallel to the tendons are more dangerous than cracks perpendicular to the tendons, and that the former type is usually not eliminated by prestressing. Naaman (1984) also stated that corrosion may be due to many causes, most of which do not need cracking to be activated and that the best protection against reinforcement corrosion is good quality concrete.

The conclusion is perhaps best stated by Mathieu (1984) as "*Thus, since the very foundation of the cracking serviceability criteria has disappeared, some fresh thinking of this subject is required*".

2.7 Summary

The literature and the case studies presented in this chapter show the differences between the existing approaches for the design of water containment structures. The chapter shows the advantages of implementing the concept of partial prestressing in water tanks. It also presents the trend towards the explicit consideration of watertightness and self-healing of cracks in the design of water tanks.

The experimental and the theoretical work presented in the rest of this report is a step towards the development of a rational design procedure for both reinforced and prestressed concrete leak-resistant tanks. The investigation of partial prestressing in liquid containing structures is included.

Table 2.1 Comparison of crack widths determined using different approaches

Group			h (mm)	Bar spacing (mm)	w_{max} (mm)			
					CEB 78	CEB 90	BS 8007	ACI 350
I	ρ %	0.222	300	300	0.397	0.634	0.385	0.731
		0.333		200	0.363	0.336	0.266	0.431
		0.467		142.9	0.220	0.170	0.181	0.286
		0.667		100	0.135	0.083	0.124	0.187
		0.866		77	0.096	0.049	0.096	0.138
		1.067		62.5	0.075	0.032	0.081	0.109
		1.200		55.55	0.066	0.026	0.073	0.096
II	M/M_{cr}	0.714	300	77	-	0.000	0.041	0.079
		0.833		77	-	0.001	0.053	0.092
		1.000		77	0.057	0.035	0.071	0.111
		1.250		77	0.096	0.049	0.096	0.138
		1.667		77	0.155	0.073	0.140	0.184
		2.500		77	0.261	0.120	0.226	0.277
III	ρ %	0.867	300	77	0.096	0.049	0.096	0.138
		0.650	400	77	0.129	0.083	0.107	0.155
		0.520	500	77	0.161	0.126	0.119	0.174
		0.433	600	77	0.186	0.177	0.131	0.195
		0.325	800	77	0.236	0.213	0.156	0.238

Group (I) : $M/M_{cr} = 1.25$ & A_s is variable

Group (II) : $A_s = 2600 \text{ mm}^2$ & M/M_{cr} is variable

Group (III) : $M/M_{cr} = 1.25$, $A_s = 2600 \text{ mm}^2$ & h is variable.

ρ % = $(A_s / A_c) \times 100$

Table 2.2 Comparison between the various codes, WSD

	ACI 350		ACI 344		PCI		BS 8007				
	A*	B*	A	B	A	B	A	A*	B	B*	
Concrete volume (m ³)											
wall	67.9	271.4	56.6	226.0	46.0	181.0	50.0	50.0	200	244.3	
floor	25.6	225.6	25.6	225.7	25.6	225.7	25.6	25.6	225.7	225.7	
total	93.5	497	82.2	451.7	71.6	406.7	75.6	75.6	425.7	470	
Reinforcement (kg)											
wall	4100	43500	3030	19000	2250	9900	2980	4380	15080	48560	
floor	1300	10170	1970	11500	1000	10100	820	860	6400	6400	
total	5400	53670	5000	30500	3250	20000	3800	5240	25080	54960	
Prestressed steel (kg)	---	---	1290	7215	1290	7215	774	---	6387	---	
The cost (\$)											
Wall cost	35000	169300	38150	167740	35990	152790	35180	33480	157130	170820	
Floor cost	05130	041290	05800	042640	04830	41240	4650	4690	37540	37540	
Total cost	40130	210600	43950	210380	40820	194030	39830	38170	194670	208360	
Cost/m ³ water	61.7	26.6	67.6	26.6	62.8	24.6	61.3	58.7	24.7	26.4	
Crack width(mm)											
Flexure crack	---	0.12	---	0.09	---	0.177	---	---	0.11	0.088	
Direct tension	0.06	0.11	---	---	---	---	---	0.05	---	0.080	
res.comp [‡] .(MPa)	0.8*	2.6*	1.4/2.8	1.4/2.8	1.4/2.8	1.4/2.8	---	1.15*	---	2.94*	

A & A* : The prestressed and the nonprestressed concrete small water tanks respectively
 B & B* : The prestressed and the nonprestressed concrete large water tanks respectively
 ‡ res.comp : The residual compression in circumferential direction after all losses of prestress.
 * : Concrete tensile stress in the circumferential direction rather than residual compression.

Table 2.3 Comparison between the various codes, USD

	ACI 350		ACI 344		PCI		BS 8007				
	A*	B*	A	B	A	B	A	A*	B	B*	
Concrete volume (m ³)											
wall	67.9	271.4	56.6	226.0	46.0	181.0	50.0	50.0	200	244.3	
floor	25.6	225.6	25.6	225.7	25.6	225.7	25.6	25.6	170	225.7	
total	93.5	497	82.2	451.7	71.6	406.7	75.6	75.6	370	470	
Reinforcement (kg)											
wall	4100	43500	3030	15000	2250	8000	2980	3430	13520	36120	
floor	1300	10170	1970	11500	1000	10100	820	860	9700	10000	
total	5400	53670	5000	26500	3250	18100	3800	4390	23200	46120	
Prestressed steel (kg)	---	---	1290	7215	1290	7215	774	---	6387	---	
The cost (\$)											
wall cost	35000	169300	38150	163740	35990	150890	35180	32530	155570	158380	
floor cost	05130	041290	05800	042660	04830	41240	4650	4690	37440	37440	
total cost	40130	210600	43950	206400	40820	192130	39830	37220	193000	195820	
cost/m ³ water	61.7	26.6	67.6	26.1	62.8	24.3	61.3	57.3	24.4	24.8	
Crack width(mm)											
flexure crack	---	0.12	---	0.18	---	0.28	---	---	0.188	0.174	
direct tension	0.06	0.11	---	---	---	---	---	0.14	---	0.199	
res.comp [‡] .(MPa)	0.8*	2.6*	1.4/2.8	1.4/2.8	1.4/2.8	1.4/2.8	---	1.2*	---	3.13*	

The same footnotes as in Table 2.2

Table 2.4 k_1 values for different crack geometries (after Clear)

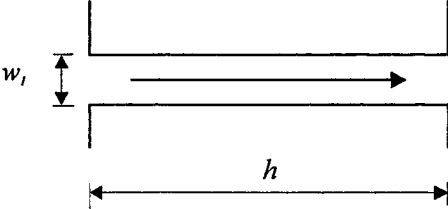
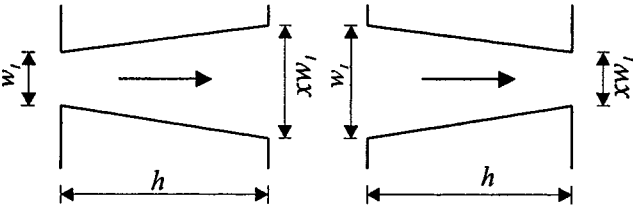
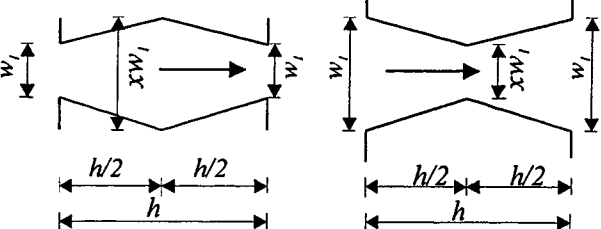
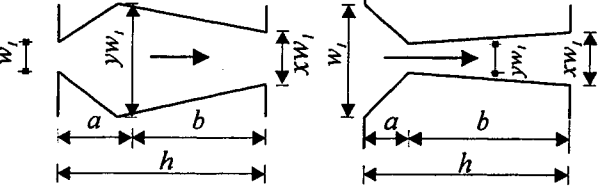
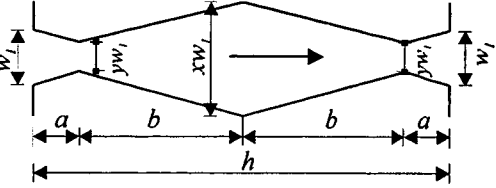
	$k_1 = 1$
	$k_1 = \sqrt[3]{\frac{2x^2}{1+x}}$
	
	$k_1 = \sqrt[3]{\frac{2y^2x^2}{b(y+x)+a(1+y)x^2}}$
	

Table 2.5 Permissible crack widths for water tanks (after Edvardsen)

Hydraulic gradient I	Permissible crack width (mm)			
	Tanks with active cracks			Tanks with stationary cracks
	$\Delta w \leq 10\%$	$\Delta w \leq 30\%$	$\Delta w \leq 50\%$	
≤ 10	0.20	0.15 ~ 0.20	0.10	0.20
10 to 20	0.15	0.10 ~ 0.15	0.05	0.15
20 to 30	0.10	0.05 ~ 0.10	0.05	0.10
30 to 40	-	-	-	0.05

Δw is the variation in crack width with time

3- Experimental Study

3.1 Introduction

This chapter presents a detailed description of the test specimens, the experimental set-up, and the test procedure. The experimental program consisted of two phases. The first phase addressed the structural response of wall panels representing a typical wall segment from a tank with varying reinforcement patterns, prestressing ratios and loading. The second phase addressed leakage rates through cracked wall panels. Eight specimens in all were tested. Six of those were subjected to leakage tests concurrently with structural load application. The goal of the experimental program was to provide data, that does not already exist in the literature, that will be used to develop and calibrate an analytical model.

3.2 Test specimens

The test specimens were selected to represent a typical wall segment from a tank. A typical wall in a tank may be subjected to either flexure, axial tension or both. For that reason three different specimen configurations were chosen, as shown in Fig. 3.1. The test region of the specimen was the central 1.2 m. The central test region was sufficiently far from the end regions to produce a uniform stress state. Table 3.1 shows the details of all specimens and load types.

Six specimens were built with configuration C-I, as shown in Fig. 3.1(a). All had the same dimensions shown except that the height of the eccentric loading brackets was 520 mm in five specimens and 240 mm in specimen 3B. Two 60 mm diameter holes were formed in each eccentric loading bracket spaced at 500 mm centre-to-centre. The “standard” specimen for configuration C-I was 1C40. Figure 3.2 shows schematic details of specimen 1C40 which was reinforced with one layer of non-prestressed reinforcement comprised of four No. 15 bars in the longitudinal direction with 40 mm of concrete cover. Transverse steel of the same diameter spaced at 300 mm was placed above the

main steel. The prestressed steel was six 7-wire size 13 bonded strands. Two strands were placed in each of three metal ducts spaced at 333 mm. The ducts sat on the transverse steel and had a concrete cover of 72 mm. Special reinforcement was added at each end for end anchorage effect as shown in Fig. 3.3. This end anchorage reinforcement consisted of No. 10 closed stirrups surrounding the ducts. Each eccentric loading bracket was provided with vertical reinforcement. This vertical reinforcement was eight 15 mm diameter high-strength threaded rods placed in vertical holes formed in the eccentric loading bracket. Each rod was provided with a 100x100x 20 mm steel plate, washer and nut at each end. The eccentric loading bracket was also provided with four No. 10 vertical stirrups.

All the specimens of configuration C-I had the same reinforcement and concrete cover except as noted in Table 3.1. The concrete cover of specimen 1C20 was 20 mm rather than 40 mm. The reinforcement of specimen 2A was five No. 15 bars. That specimen also had only two strands placed into two ducts. The reinforcement of specimen 3A was only nine strands placed in three ducts with no ordinary reinforcement. The ducts of specimen 2B were not grouted.. Note that the specimens were fabricated and cast upside down and inverted for testing.

Only one specimen, 3C, was cast in configuration C-II, Fig.3.1(b). It was a panel with side dimensions of 1000x3160 mm and a thickness of 250 mm reinforced with top and bottom layers of non-prestressed reinforcement each comprised of two full length No. 15 bars in the longitudinal direction for which the concrete cover was 40 mm. Transverse steel of the same diameter was spaced at 300 mm and tied to the main steel. The prestressed steel was six 7-wire size 13 bonded strands. The strands were fit into three metal ducts spaced at 333 mm, two strands per duct, placed at mid-height with a concrete cover of 105 mm. No. 10 closed stirrups surrounding the ducts were added at each end for end anchorage effect. Before casting the specimen, a 1000x280x25.4 mm steel end plate was placed at each end as shown in Figs. 3.4 and 3.5. The prestressing strands passed through holes drilled in that plate. The four No. 15 non-prestressed

longitudinal reinforcing bars also passed through holes drilled in the end plates and then welded to the plate. To prevent premature failure close to the end-fitting, eight No. 10 bars, four 600 mm long and four 480 mm long, were added symmetrically to the specimen at each end and were welded to the plate in the same manner as the No. 15 bars. Figures 3.4 and 3.5 show these details.

Only specimen 2C was cast in configuration C-III. It was a 1000x3160 mm panel 250 mm thick. The non-prestressed longitudinal reinforcement, the transverse steel and the prestressed steel were similar in amount, size, distribution and end anchorage detail to that of specimen 1C40.

3.3 Fabrication of Specimens

3.3.1 Casting and Curing

All specimens were cast flat on wooden forms. The specimens of configuration C-I were cast inverted such that the top surface during casting was the bottom during the test. The vertical and the horizontal holes in the eccentric loading brackets were formed by installing plastic tubes in the formwork. Prior to casting, 5 mm diameter plugs were silver soldered to two of the reinforcing bars. Two plugs long enough to project about 40 mm from the form holes and spaced at 800 mm were soldered to each bar. They were enclosed in rubber tubes with 10 mm outside diameter. After the concrete had hardened this tube was removed leaving a gap around the plug so that if the reinforcement moved relative to the concrete during testing the plug would not bear on the concrete. During the test a linear voltage differential transducer, LVDT, was connected between the two plugs soldered to one bar.

After casting, the specimens were left to allow for partial set then the exposed surfaces were trowled. The specimens remained exposed for a few hours, and then covered with plastic sheets. After one or two days the sides of the forms were removed. The concrete cylinders and modulus of rupture beams were stripped and placed on top of the specimens. The specimens were then covered for about one week with wet burlap

and plastic sheets. During that week it was ensured that the specimen were kept wet. After that the specimens were lifted from the forms and cured in air.

3.3.2 Prestressing the Specimens

After the curing period the specimens were placed in the test frame where prestressing was to take place. Applying the prestressing force at one end results in a nonuniform strand force distribution because of end anchorage (wedge setting) losses and because of friction along the duct, as shown in Fig. 3.6. To determine that distribution a special procedure is followed. A prestressing chair was supported against the bearing plates embedded in the specimen ends. The prestressing force was applied through a centre-hole hydraulic ram and measured by a centre-hole load cell. A small force was applied and the distance between a mark on the strand and the specimen edge was recorded at both the stressing and fixed ends. The force was increased in steps and at each step the distance at each end was recorded. When the prestressing force reached 80% of the ultimate load of the strand, the end anchorage wedges were seated manually by tapping into place. A 0.12 mm thick trial steel shim was placed between the bearing plate and the wedge anchor. The prestressing force was then reduced by approximately 50% in steps and the strand shortening was measured.

The force was next increased gradually up to the point where the shims could be lifted-off by hand. The difference between that force and the design initial stressing force of 70% of stand ultimate load determined the required thickness of the shims to be added to compensate wedge setting assuming linear response of the strand. The load was then increased to slightly more than the target initial force and the required shims were placed between the bearing plate and the wedge anchor. The 0.12 mm trial shim was introduced again. The force was dropped and then increased again gradually. The force at which the 0.12 mm shim was removed was recorded. This force, P_1 , was considered the initial load at the stressing end of the strand after lock-off. The load was then released completely and the final distance between the reference mark on the strand and the edge of the

specimen was measured. The above procedure was repeated for all the strands from one end.

The stressing set-up was transferred to the other end of the specimen. Each strand was tensioned gradually until the 0.12 mm shim, placed before stressing, could be removed. The load was recorded and considered as the initial force P2 at the dead end. After that the load in the ram was released gradually.

The above stressing procedure was followed to allow: accurate tracing of the strand elongation during stressing; determination of the final elongation; compensation for the wedge-setting losses; and determination of the forces P1 and P2 at each end of the strand after lock-off and before long-term losses.

The stressing sequence of the strands was approximately symmetric with respect to the longitudinal axis of the specimen. Stressing started at the outside strands and moved to the inside strands alternating from side to side.

3.3.3 Grouting the Specimens

All the specimens were grouted except specimen 2B. The grouting mix consisted of water and Portland cement in ratios that varied from 0.40 to 0.42. The grout was injected using a manual pump with reasonable pressure, less than 1 MPA, through a 19 mm hole drilled in the bearing plate. The injection continued from one end until pure grout flowed from the other end. 102x204 mm cylinders were prepared by pouring grout into molds. These cylinders were tested in compression just before testing the specimens to ensure that the grout had adequate strength.

3.4 Material Properties

3.4.1 Concrete

Normal density concrete from a readimix supplier was used. Three loads of concrete were used. Specimens 1C20 and 1C40 were cast in the first placement, 2A, 2B, and 2C were cast next, and 3A, 3B, and 3C were cast last. The mix had a specified 28

day compressive strength of 35 MPa, maximum size of aggregate of 20 mm, Type 50 cement, a 100 mm slump and was non-air entrained. Although the same concrete mix was ordered each time, the concrete compressive strength at the time of testing the specimen varied from 48 to 53 MPa.

Concrete test cylinders and modulus of rupture beams were cast at the same time as the specimens. Eight 152x304 mm cylinders and two 152x152x584 mm beams were cast for each specimen. Three cylinders were tested in compression, one was used for a split cylinder test, and one beam was used for a modulus of rupture test at specimen stressing and testing days.

Details of the concrete strengths for each specimen are given in Table 3.2. The best estimates for the concrete tensile strength were found to be $f_{sp} = 0.53\sqrt{f'_c}$ and $f_r = 0.70\sqrt{f'_c}$. The tensile strengths are consistent with what one would expect for ordinary concrete. The stress versus strain responses for the concrete are reported in Section 5.3.1 where they are compared with a numerical simulation.

3.4.2 Non-Prestressed Steel

Longitudinal and transverse steel used in all the specimens consisted of No. 15 deformed bars. The stirrups were all No. 10 deformed bars. Three tension tests for each size were performed on samples in an MTS 1000 kN universal testing machine in general accordance with CSA G30.18-M92. The tests were stroke controlled. At selected points in the test the stroke was held constant permitting the load to drop to the static value.

3.4.3 Prestressing Tendons

7-wire Size 13 low relaxation strands were used in all the specimens. Three tension tests were performed on samples in the above-mentioned testing machine in general accordance with ASTM.A370-92 The tests were stroke controlled with static readings.

Both reinforcement properties are reported in Table 3.3, while the stress versus strain responses are reported in Sections 5.3.4 and 5.3.5 for non-prestressed and prestressed reinforcement, respectively.

3.5 Tests Set-up

3.5.1 Eccentric Load Test Set-up

The specimens were supported horizontally, as shown in Fig. 3.7 (a) and (b), on roller and knife edge bearings as shown to create a centre-to-centre span of 2500 mm. The specimens were placed between two steel frames 1829 mm apart. Each frame consisted of two W 250x80 beams of span 3962 mm spanning between two W 310x97 steel columns 2134 mm high. Back-to-back C310x32 lateral beam spanned horizontally between the columns to provide reaction points for the loading jacks. Two Dywidag threaded bars of 26 mm nominal diameter were passed through this lateral beam and into the two 60 mm diameter holes formed in each eccentric loading bracket. Each of the two Dywidag bars on the East end was pulled with a 980 kN centre-hole hydraulic jack supported against the lateral beam. The loads were measured using 490 kN centre-hole load cells. On the West end, each of the bars was also connected to 490 kN centre-hole load cell to determine the load. The load was applied simultaneously to both hydraulic jacks with a manually controlled system which used air pressure to activate the hydraulic fluid.

3.5.2 Axial-Load Test Set-up

Specimen 3C was tested vertically in an MTS 6000 kN universal testing machine. The load was transferred between the machine head and the specimen using “clevises and whiffletree” type fittings as shown in Figs. 3.8 and 3.9. These fittings were developed and used by Simmonds *et al.* (1979) with some modifications. These special fittings were connected to a 280x1000x25.4 mm steel end plate at each end of the specimen fitting using eight 19 mm diameter and eight 16 mm diameter bolts. The heads of these bolts were partially embedded in concrete. Before casting concrete a spot of

weld was provided to each head to fix the bolts in their positions perpendicular to the steel plate.

3.5.3 Flexural Test Set-up

Specimen 2C was tested in flexure. It was tested as a simply supported beam under a two-line load system to produce a constant moment region in the middle. The specimen was tested with the tension side up to facilitate taking the readings and conducting the leakage test. The test set-up is shown in Fig. 3.10 (a) and (b). The specimen was held down at both ends using a roller unit consisting of a 25 mm diameter high strength rod between two 30x100x1000 plates. The roller unit was placed under a 38 mm thick steel plate that in turn was placed under a 2-MC 460x86 beam supported on two steel columns. The two upward line loads were located symmetrically and spaced at 1500 mm. Each load was applied through a roller unit similar to that used as a bearing. Each roller unit sat on a 2-C310x45 spreader beam 1200 mm long. At each end two 25 mm diameter high strength threaded bars were passed through the spreader beam to the top of the test set-up and were bolted to 490 kN centre hole load cells bearing on the ends of a 2-50x200x1200 mm plate beam. A 980 kN load cell was centred under that beam. The load cell sat on top of a 980 kN hydraulic jack. The two jacks, one at each line load, were supported on a built-in distributing beam 470mm deep that in turn sat on two 2-MC 460x86 beams mentioned above. The load was monitored with the two 980 kN load cells placed above the jacks and the four small load cells attached to the four 25 mm rods.

As a safety provision, two beams consisting of 2-MC 460x86, 300 mm apart were placed longitudinally at the level of the jacks and supported on 75x50x13 HSS spanning between the two columns. These beams were completely separated and had no effect on the loading system. They are not shown in Fig. 3.10 for clarity.

3.6 Leakage Test

3.6.1 Test Set-up

A 300x1000 mm pressure chamber was placed on the top of the concrete specimen as shown in Fig. 3.11. The four sides of the pressure chamber were C10x8 sections covered with 25 mm thick plexi-glass to permit the observation of any cracking in concrete. A rubber gasket was placed between the chamber and the concrete surface to provide a water tight seal and to eliminate the effect of specimen deformation on the chamber during the test. The chamber was held down by two HSS 76x51x3.8 beams along the long edges of the chamber from the top and two HSS 76x51x3.8 beams in the same direction underneath the specimen. The top and the bottom HSS beams were connected at each end by a 19 mm diameter steel rod and were tightened together to resist the uplift pressure. Spacers were placed between the bottom HSS beam and the specimen to allow the flow of any leaked water. A drip pan larger than the pressure chamber was placed underneath the specimen at the location of the chamber to collect the leaked water into a graduated cylinder for leakage measurements.

The chamber was filled with pressurized water coming from a 520 mm diameter, 540 mm high cylindrical steel container. Air pressure was applied to the water surface inside the cylindrical steel container through a pressure regulator that controlled the water pressure. The applied air pressure was equivalent to an 8 to 10 m head of water. The water container was centred on a load cell calibrated to measure the change in water weight with an accuracy of 10 gm (equivalent to a water volume of 10 ml or 0.00001 m³).

Silicon caulking was applied to the specimen side edges at the location of the chamber to prevent leakage from the slab edges. The caulking layer was covered by steel plates shimmed against the steel rods connecting the top and the bottom HSS beams.

In specimen 3C, which was tested vertically, the pressure chamber was attached to the vertical side of the specimen. The chamber was held in place by running two HSS

76x51x3.8 along each long side of the chamber and running two HSS 76x51x3.8 in the same direction from the opposite side of the specimen then were connected together with 19 mm diameter steel rods. To ensure collecting any water leaking, a sheet steel channel was fabricated and surrounded the specimen directly below the location of the chamber with a slope towards one corner where a graduated cylinder was placed to collect water. Figure 3.12 shows that set-up.

3.7 Instrumentation

For each specimen approximately 50 measurements were recorded at each load level. The measurements included load, elongation, rotation, leakage rate, strain and crack width. Some of these measurements were taken electronically and processed directly using the data acquisition system in the laboratory. Other measurements such as mechanical strain gauges (Demec gauges), crack widths and air pressure were read and recorded manually. Instrumentation for a typical specimen is shown in Fig. 3.13.

3.7.1 Non-Prestressed Steel Strain

Two plugs spaced at 800 mm were silver soldered to each of two reinforcing bars as mentioned in Section 3.3. The change in plug spacing during the test was recorded electronically using a linear variable displacement transducer (LVDT) connecting the two plugs. The average non-prestressed steel strain along the 800 mm gauge length was calculated from LVDT readings. Dividing LVDT readings by the exact gauge length was assumed to produce the strain at the level of the LVDT. The strain at the level of the non-prestressed steel was obtained assuming a linear strain distribution and using the measured strains at the level of the LVDT and the concrete compressive strain at the extreme soffit from Demec gauge readings.

3.7.2 Concrete Strain

Demec discs with a gauge length of 254 mm were glued to the concrete surface as shown in Fig. 3.13. At each load level, all gauges were read twice and reported

manually. If the readings differed significantly, a third reading was taken. The average reading was used in the calculations. The accuracy of the Demec gauge was ± 8.1 microstrain (as reported by the manufacture).

Concrete strain at the specimen mid-height was obtained using the LVDT's 5 and 6 connected between two plugs spaced at 800 mm projected from the concrete. The two plugs were partially embedded in the concrete prior to casting.

3.7.3 Loads

In the eccentric load tests, configuration C-I, the load applied to each of the two East Dywidag bars was measured using the 490 kN centre-hole load cell attached to each rod. The 490 kN centre-hole load cell attached to each of the two West bars measured the force developed in each of these two bars. The four loads were electronically recorded.

In the axial load test, configuration C-II, the load applied to the specimen by the MTS machine was measured by differential pressure transducers contained in the machine.

In the flexure test, the load applied by each of the two 980 kN hydraulic jacks was measured by a 980 kN load cell located above each jack. The force in each of the four rods was measured by a 490 kN centre-hole load cell connected to each rod.

3.7.4 Specimen Rotation

Two electronic rotation meters were mounted on the two eccentric loading brackets of the specimen at the same level of the Dywidag bars.

3.7.5 Crack Measurements

Crack widths were measured at each load level after cracking using a microscope with an optical scale graduated to 0.0254 mm (0.001 in.). The cracks were marked during

the test. A 100x 100 mm grid was marked on the specimen and the crack profile was mapped after the test.

3.7.6 Leakage Rate

Two estimates for the leakage rate were obtained. One estimate came from the volume of water that was collected in the graduated cylinder. The other estimate came from the change in weight of the cylindrical water supply container. The accuracy of the leakage rate estimates is discussed in Section 4.4.

3.7.7 Variations in Instrumentation

The instrumentation of all specimens was similar with the following exceptions. The spacing between the two top LVDTs in specimen 2A was 400 mm because the specimen had five No. 15 bars rather than 4 bars. The two rotation meters in specimen 2C, which was a panel tested in flexure, were mounted at the mid-depth above the supports. There were no top LVDTs in specimen 3A because there was no non-prestressed longitudinal steel. Specimen 3C, which was a panel tested vertically under axial load, was reinforced with non-prestressed steel in both faces. Hence, two LVDTs were used to measure the strain of the bars in each face.

3.8 Concrete and Reinforcement Initial Strains

3.8.1 Initial Strain in Concrete

The specimens were covered with wet burlap and plastic sheets for about one week after casting. It was ensured during that week that the specimens were kept wet. After that, the specimens were lifted from the wooden form and the Demec strain gauges were installed. Curing in air was continued until the specimens were prestressed. The tests were conducted a few weeks after stressing. Concrete age varied from 60 to 170 days at testing. A series of Demec readings was taken as follows:

- reading # 1: immediately after Demec installation while the specimen still wet;

- reading #2: immediately before tendons stressing;
- reading #3: immediately after tendons stressing;
- reading #4: 24 hours after stressing;
- reading #5: 72 hours after stressing;
- reading #6: at the day of testing, before start of loading,
- reading # 7: at each load level.

The above Demec readings were used to trace the strain history of the specimen as follows:

- reading # 1 was considered as the initial reading;
- shrinkage strain of concrete before stressing = reading #2 - reading # 1
- concrete strain due to stressing = reading # 3 - reading # 2
- 24 hour creep and shrinkage strain in concrete = reading # 4 - reading # 3
- readings taken 72 hours after stressing were identical with those taken 24 hours after the stressing,
- shrinkage and creep strain of concrete after stressing = reading # 6 - reading # 3
- initial strain in concrete at testing = reading # 6 – reading # 1
- actual concrete strain at any load level = reading # 7 – reading # 1

3.8.2 Non-prestressed Steel Strain

Non-prestressed steel strain at the beginning of the test was determined from Demec reading # 6 - # 1 and an assumed linear strain distribution. This initial steel strain, which was compressive, was algebraically added to the steel strain obtained from LVDT readings at any load step.

3.8.3 Prestressed Steel Strain

The prestressing force, P1 and P2, at each end was obtained immediately after the prestressing process as explained in Section 3.3.2. The average of these two forces, P1 and P2, was considered as the prestressing force in the strand. The forces in all the strands were averaged to get the average strand force in the specimen. The corresponding stress was calculated. The strand stress-strain curve was then used to obtain the initial strain in the strand before long-term losses.

The prestressing losses due to shrinkage and creep of concrete were considered from the concrete strains at the level of the tendons resulting from Demecs reading # 6 - # 3. This strain was subtracted from the initial strain in the tendon to produce the average strain in the strand at the beginning of the test.

Table 3.1 The variables of the experimental test specimens

Configuration	Specimen	Load		Concrete cover (mm)	Reinforcement		Bond of tendons
		Type	Eccentricity (mm)		Non-prestressed	7-wire size 13 strands	
C-I	1C40	M & T	530	40	4 No. 15	6 in 2 ducts	bonded
	1C20	M & T	530	20	4 No. 15	6 in 2 ducts	bonded
	2A	M & T	530	40	5 No. 15	2 in 2 ducts	bonded
	2B	M & T	530	40	4 No. 15	6 in 2 ducts	unbonded
	3A	M & T	530	40	—	9 in 3 ducts	bonded
	3B	M & T	260	40	4 No. 15	6 in 2 ducts	bonded
C-II	3C	T	0.0	40	4 No. 15	6 in 2 ducts	bonded
C-III	2C	M	—	40	4 No. 15	6 in 2 ducts	bonded

Notes:

M : Bending moment

T : Tensile axial load

The distinguishing variable of each specimen (related to specimen 1C40) is shaded

Table 3.2 Results of ancillary tests at time of stressing and testing the specimens

Specimen	at stressing							at testing						
	Age days	f'_c MPa	$f'_{c-average}$ MPa	f_{sp} MPa	$\frac{f_{sp}}{\sqrt{f'_c}}$	f_r MPa	$\frac{f_r}{\sqrt{f'_c}}$	Age days	f'_c MPa	$f'_{c-average}$ MPa	f_{sp} MPa	$\frac{f_{sp}}{\sqrt{f'_c}}$	f_r MPa	$\frac{f_r}{\sqrt{f'_c}}$
1C20	16	38.6	38.32	2.92	0.47	2.47*	0.399	44.1	44.82	3.66	0.55	4.33	0.65	
		38.4						45.2						
		38.0						45.2						
1C40	13	37.5	37.54	1.79**	0.29	4.16	0.6789	47.7	46.92	3.03	0.44	4.52	0.66	
		37.6						47.9						
								45.2						
2A	44	44.3	44.40	2.68**	0.40	3.83	0.5748	55.1	52.92	4.08	0.56	5.96	0.82	
		47.7						53.2						
		41.1						50.5						
2B	49	41.6	44.58	4.12	0.62	4.67	0.6994	49.1	47.21	4.52	0.66	5.19	0.76	
		45.6						48.1						
		46.5						44.4						
2C	55	45.9	44.44	3.87	0.58	4.8	0.7201	47.4	47.84	4.06	0.59	5.19	0.75	
		43.9						48.3						
		43.5												
3A	26	39.8	38.12	3.84	0.62	3.9	0.6317	47.9	46.90	3.49	0.51	5.19	0.76	
		37.8						46.9						
		36.8						45.9						
3B	43	42.1	43.65	4.12	0.62	4.86	0.7356	49.5	48.78	3.26	0.47	5.45	0.78	
		43.8						48.1						
		45.0												
3C	40	41.3	40.82	4.01	0.63	4.99	0.781	45.6	46.19	3.32	0.49	5.64	0.83	
		40.3						46.8						

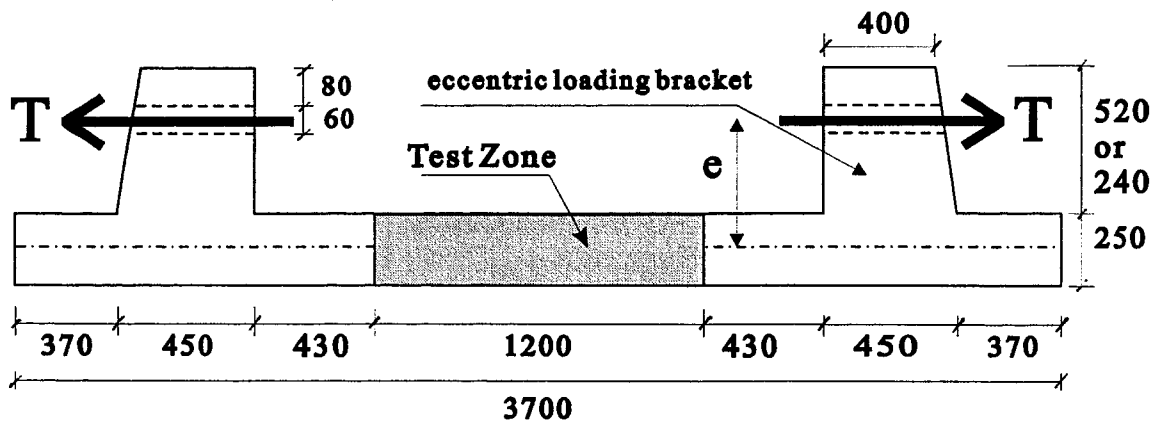
* the beam was cracked before testing

** the cylinder cracked from one side

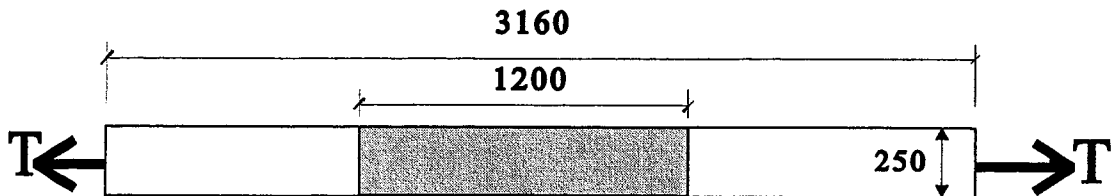
Table 3.3 Reinforcement properties

		No. 10 bar	No. 15 bar	Size 13 strand
Modulus of elasticity	(MPa)	200000	190000	200000
Yield stress	(MPa)	440	430	1650*
Static yield stress	(MPa)	422	417	1605*
Ultimate strength	(MPa)	715	700	1903
Strain hardening strain	(microstrain)	5170	5120	-
Ultimate strain	(microstrain)	125500	125000	63200

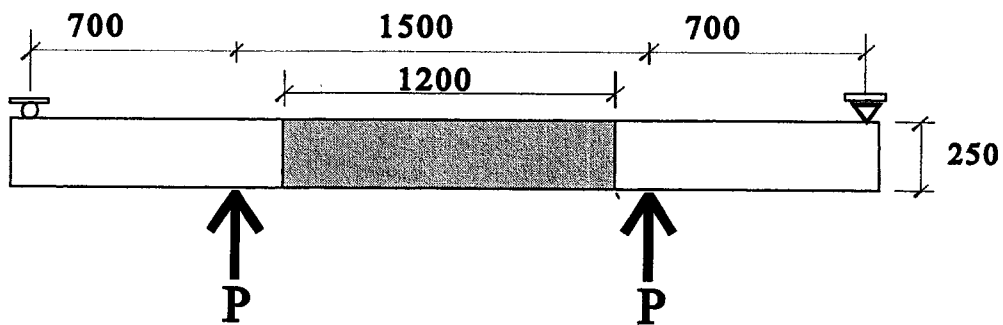
* taken as the stress at an elongation of 1.0% as defined by CSA G279



(a) Configuration C-I (eccentric load)



(b) Configuration C-II (axial load)



(c) Configuration C-III (flexure)

All specimens 1.0 m wide

Figure 3.1 Specimens configurations

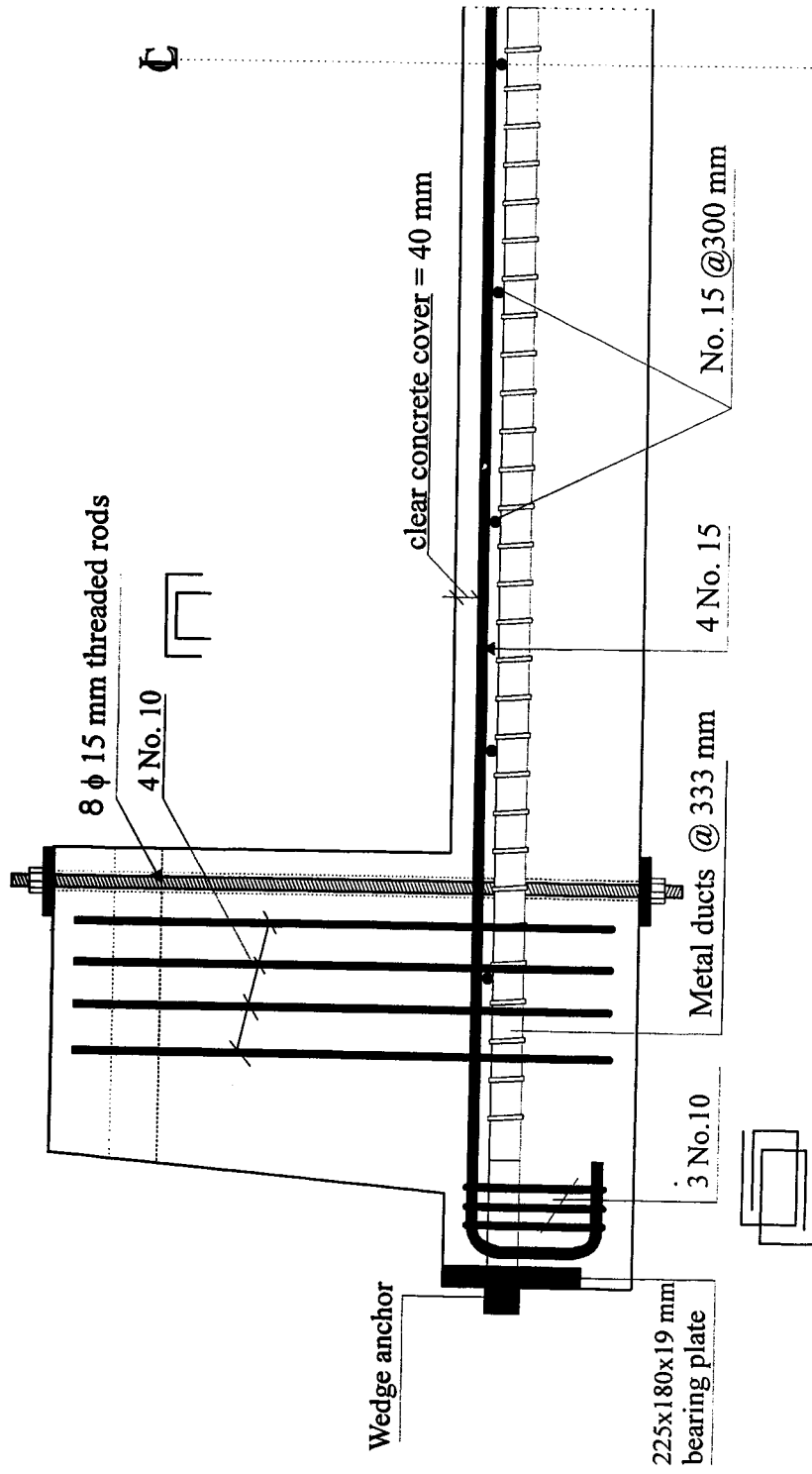
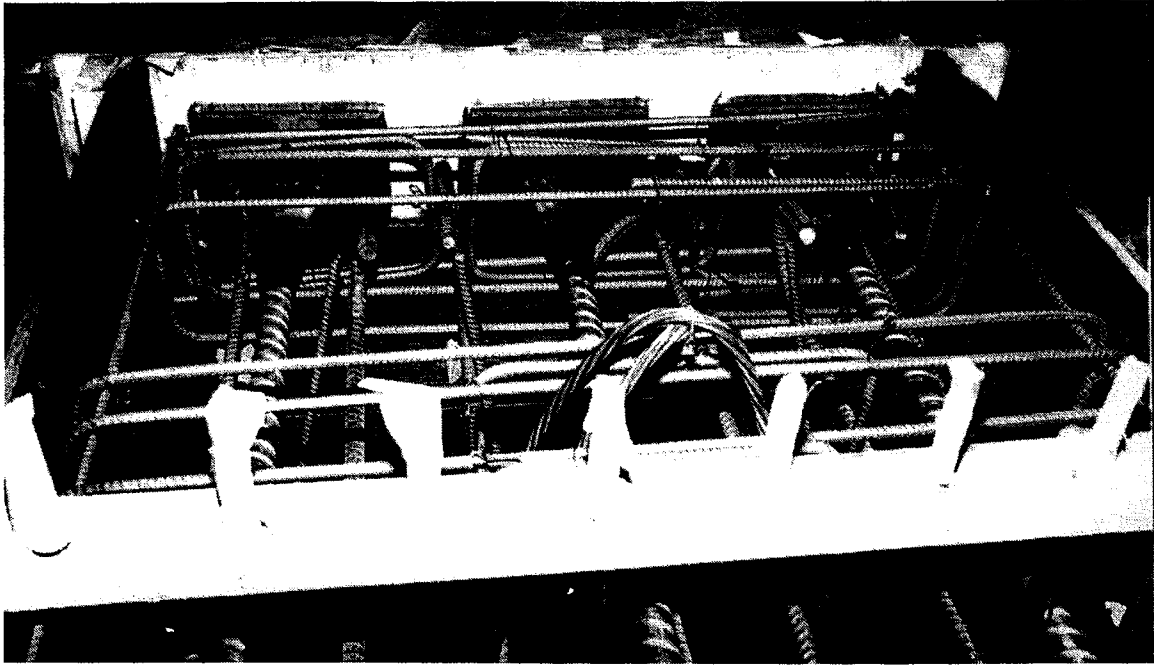
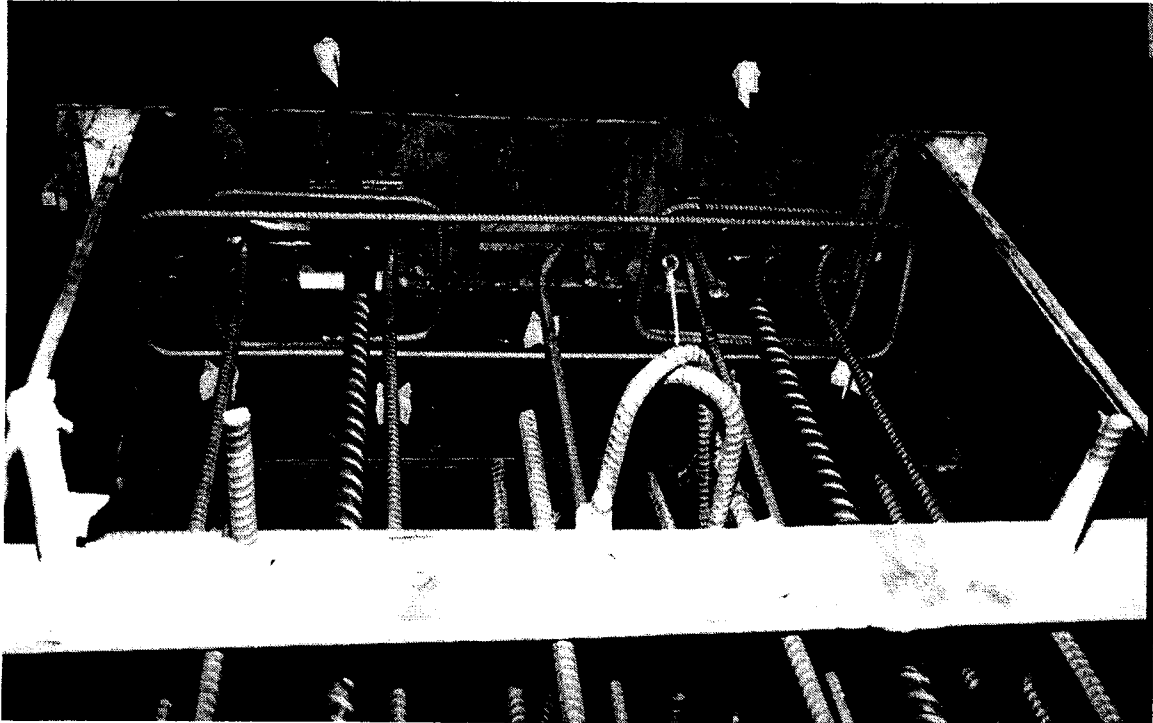


Figure 3.2 Schematic details of specimen 1C40



(a) Typical specimen



(b) Specimen 2A

Figure 3.3 Details of end anchorage

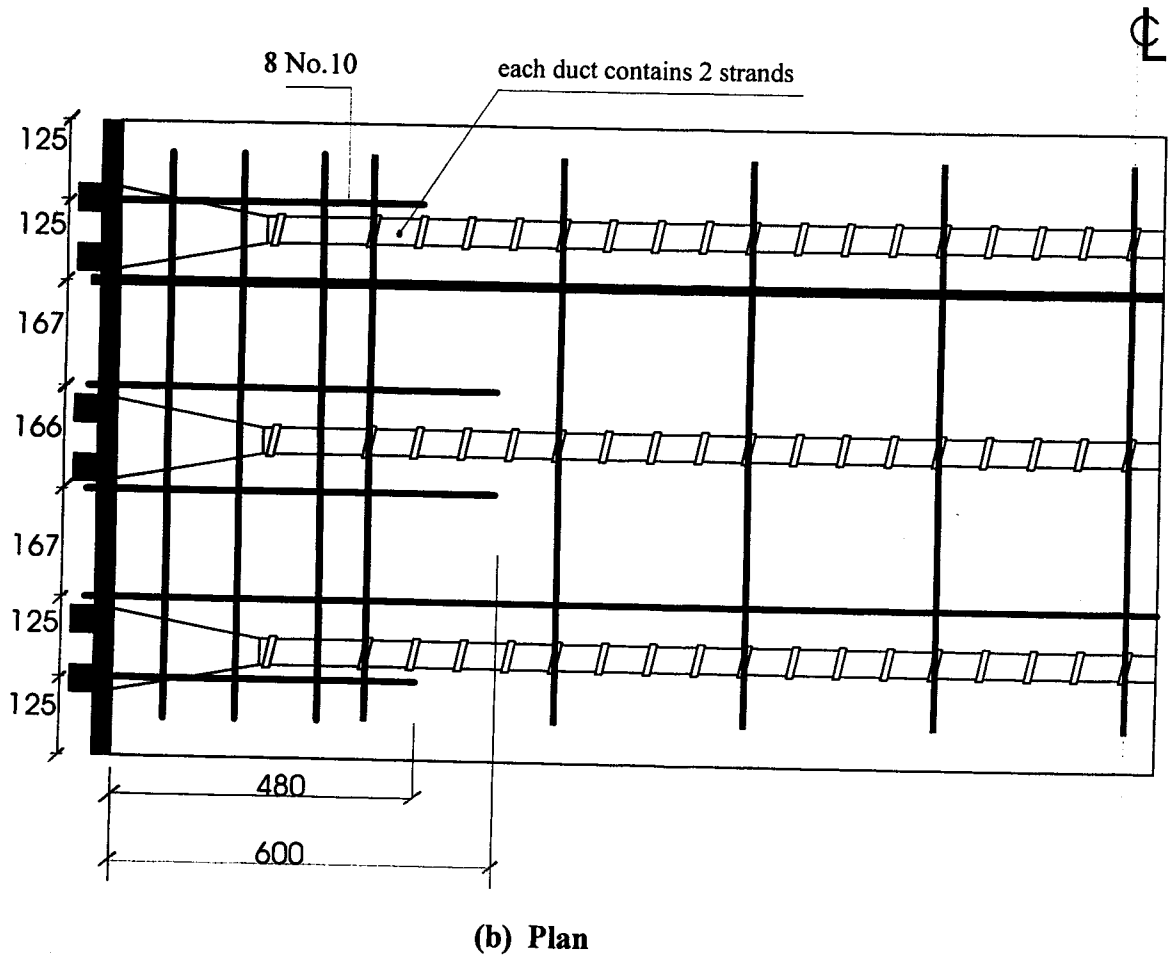
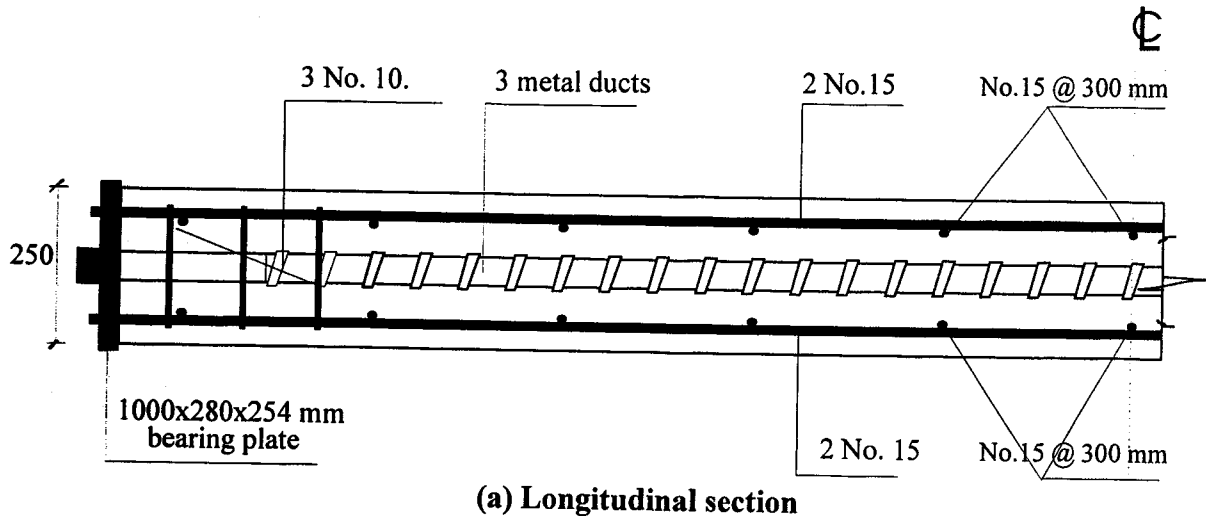


Figure 3.4 Schematic details of specimen 3C

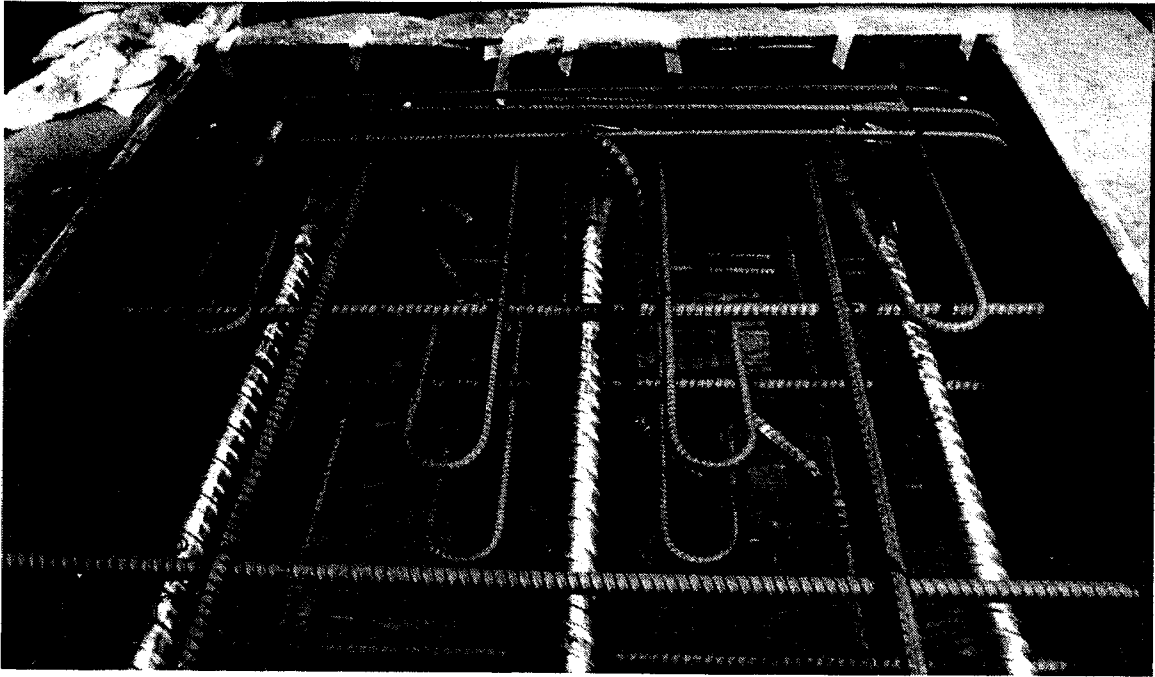


Figure 3.5 End details of specimen 3C

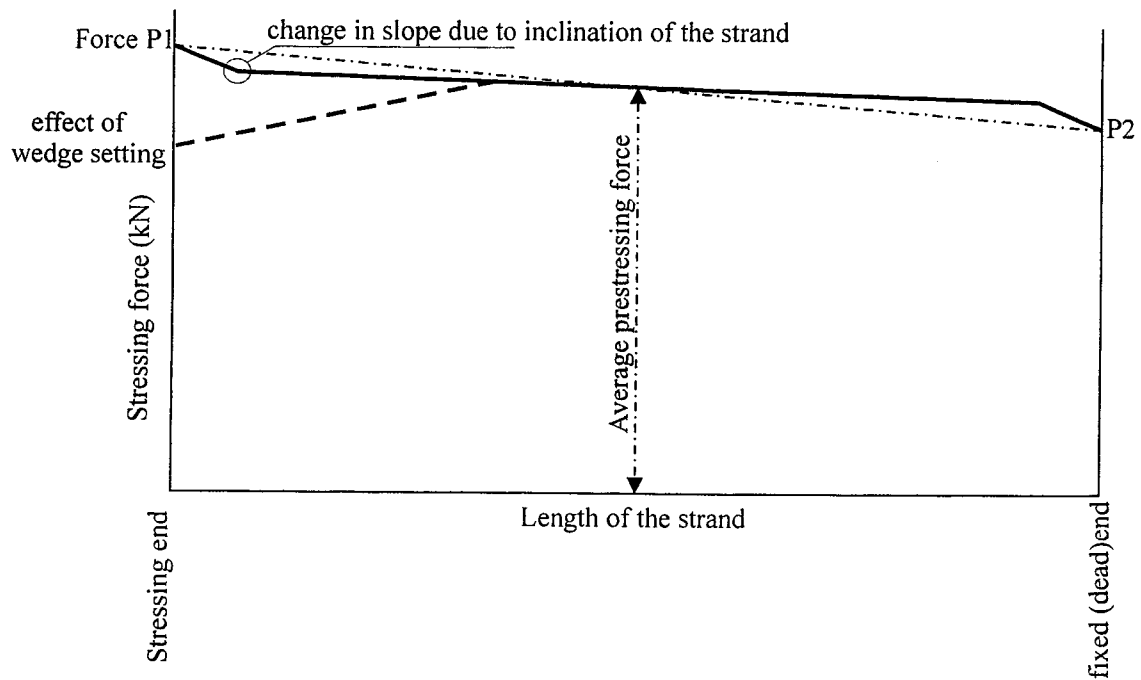
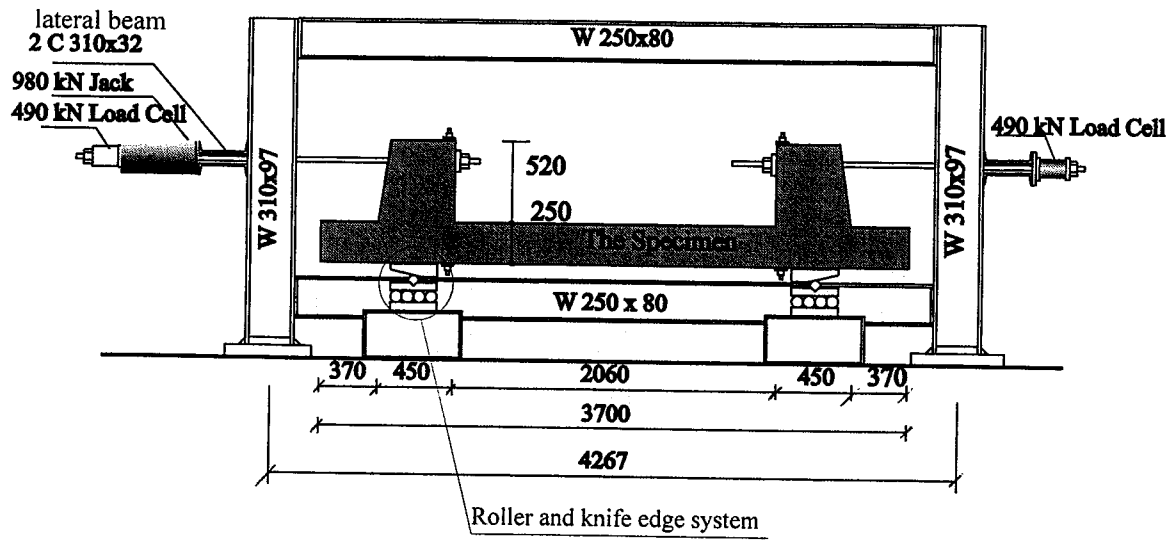
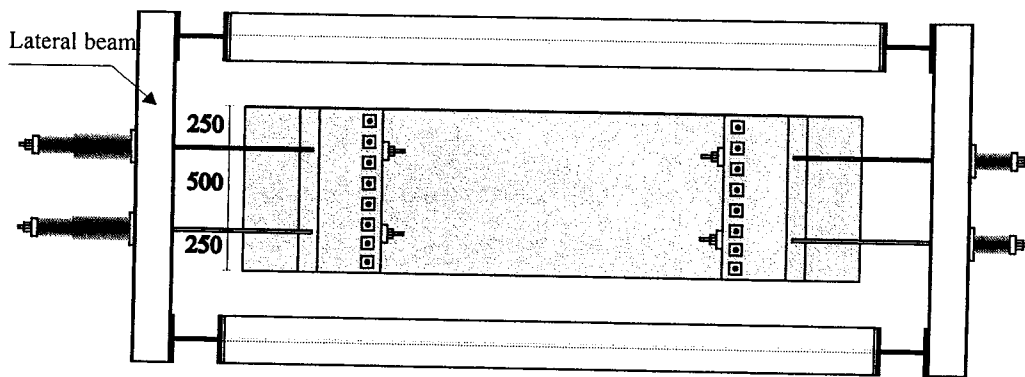


Figure 3.6 Distribution of prestressing force along the strand



(a) Side view



(b) Plan view



Figure 3.7 Eccentric loading test set-up

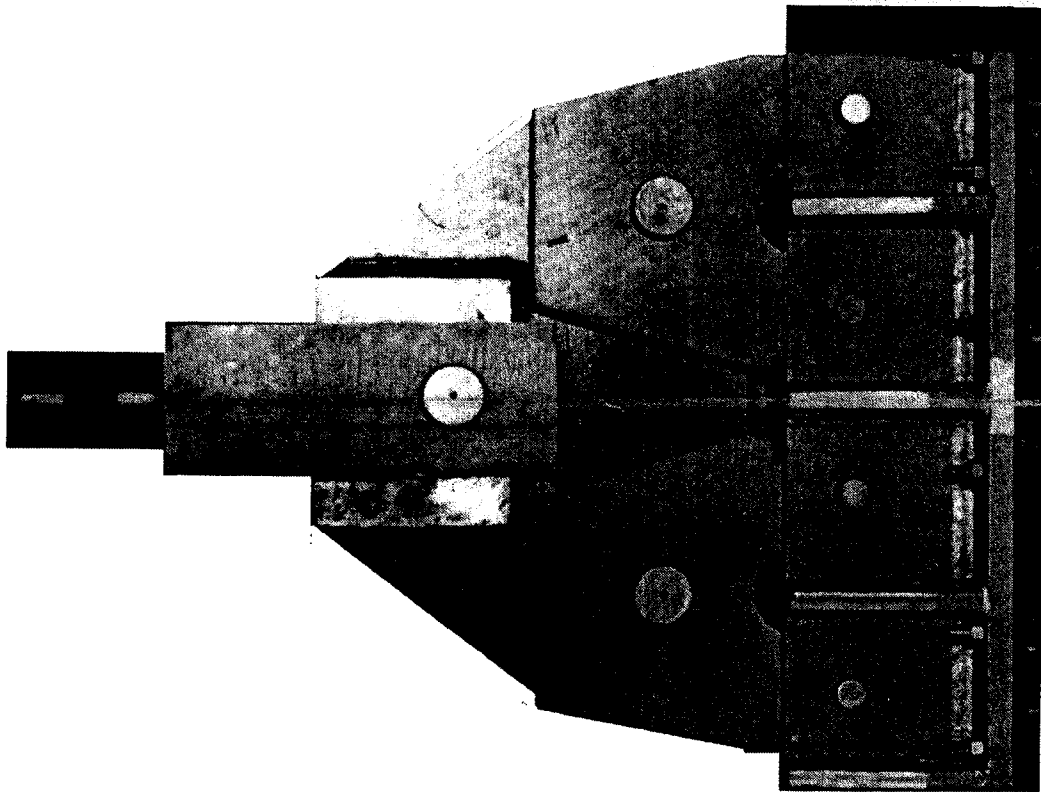


Figure 3.8 Whiffletree end fitting

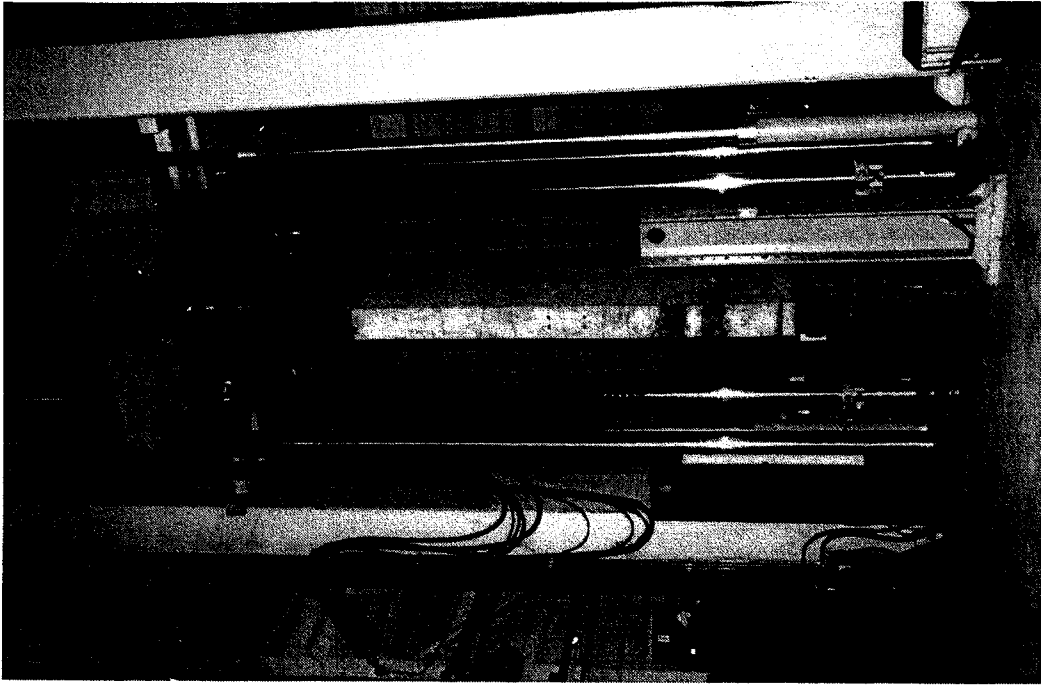


Figure 3.9 Specimen 3C in MTS test machine

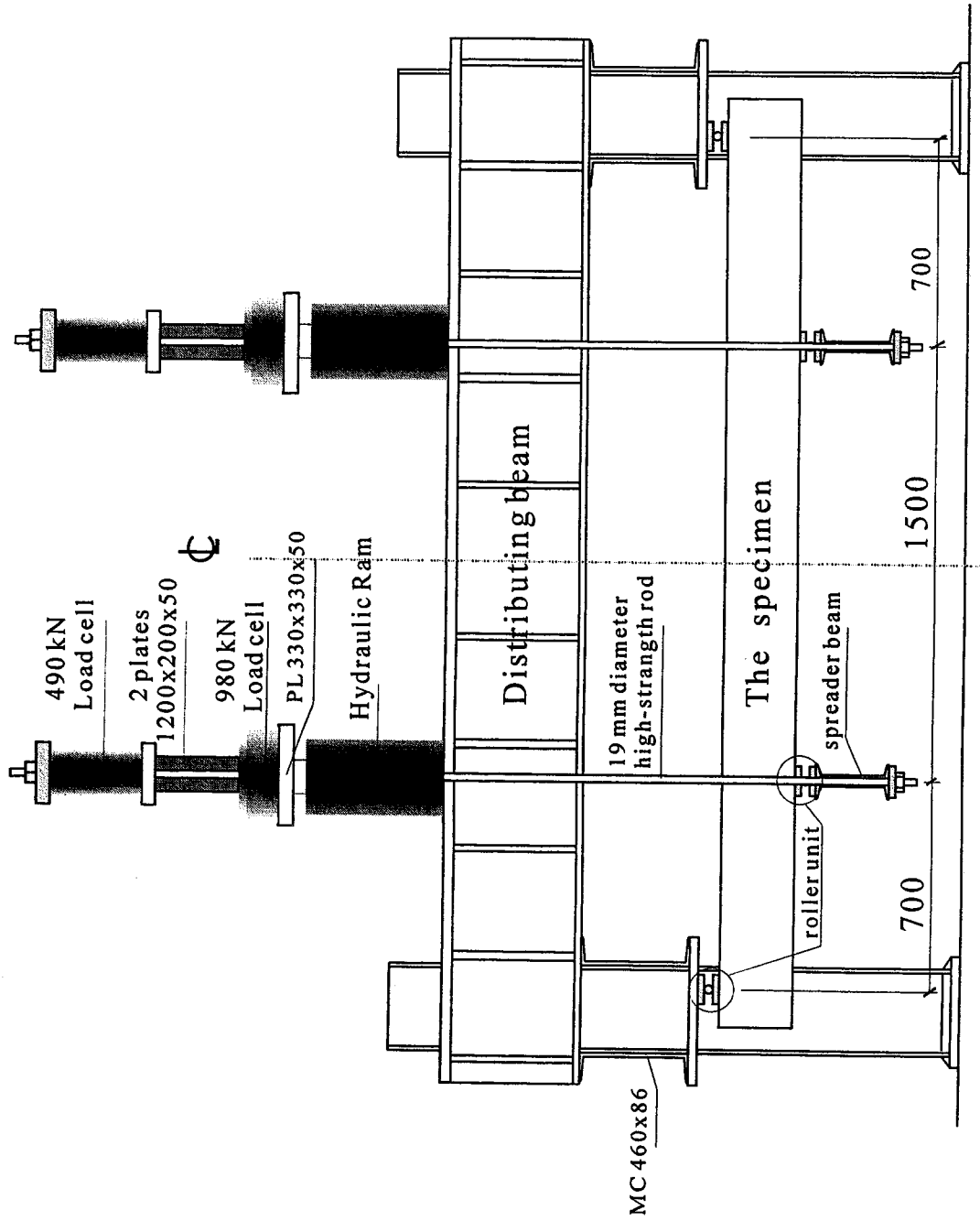


Figure 3.10 (a) Side view of flexure test set-up

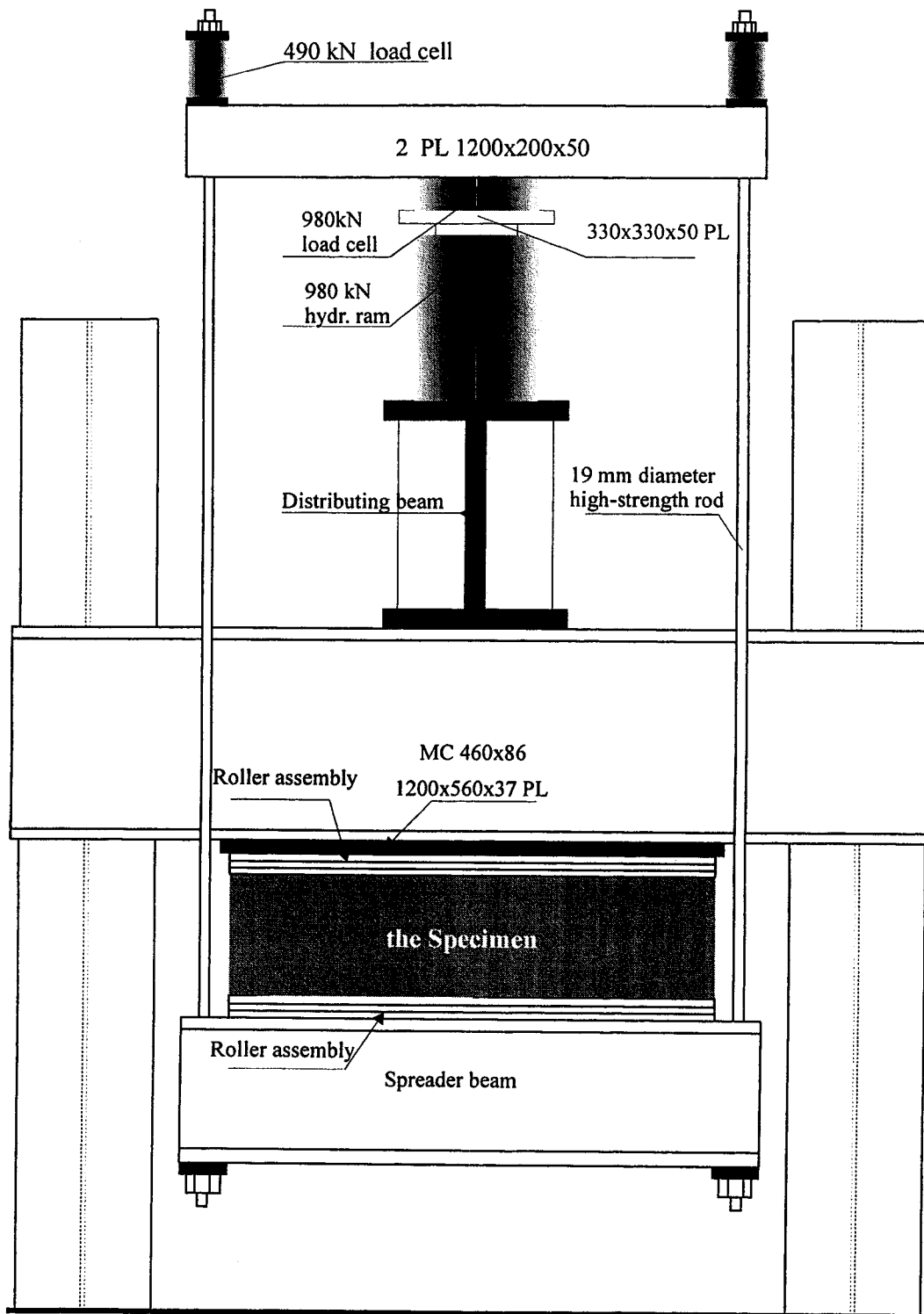


Figure 3.10 (b) End view of flexure test set-up

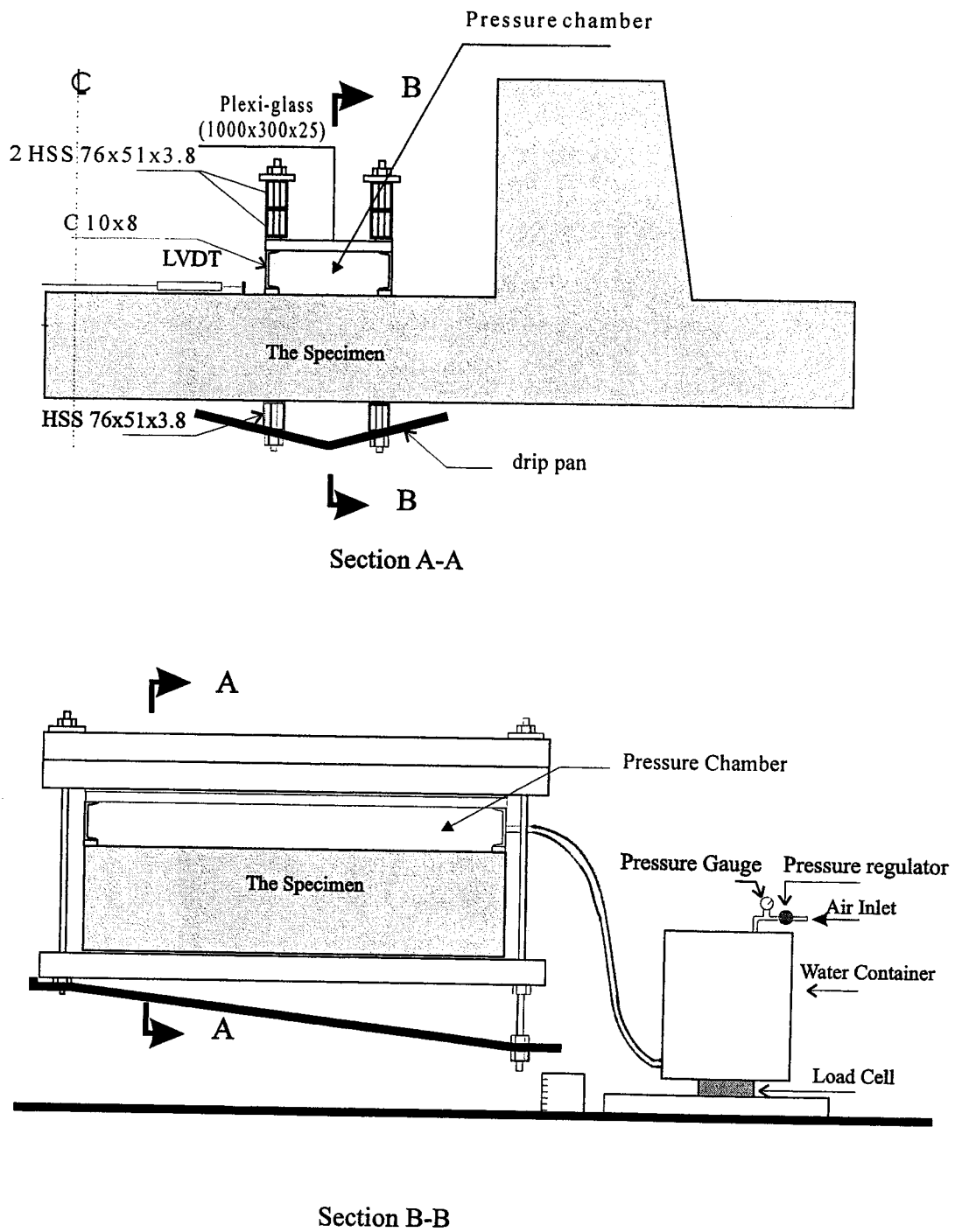


Figure 3.11 Leakage test set-up

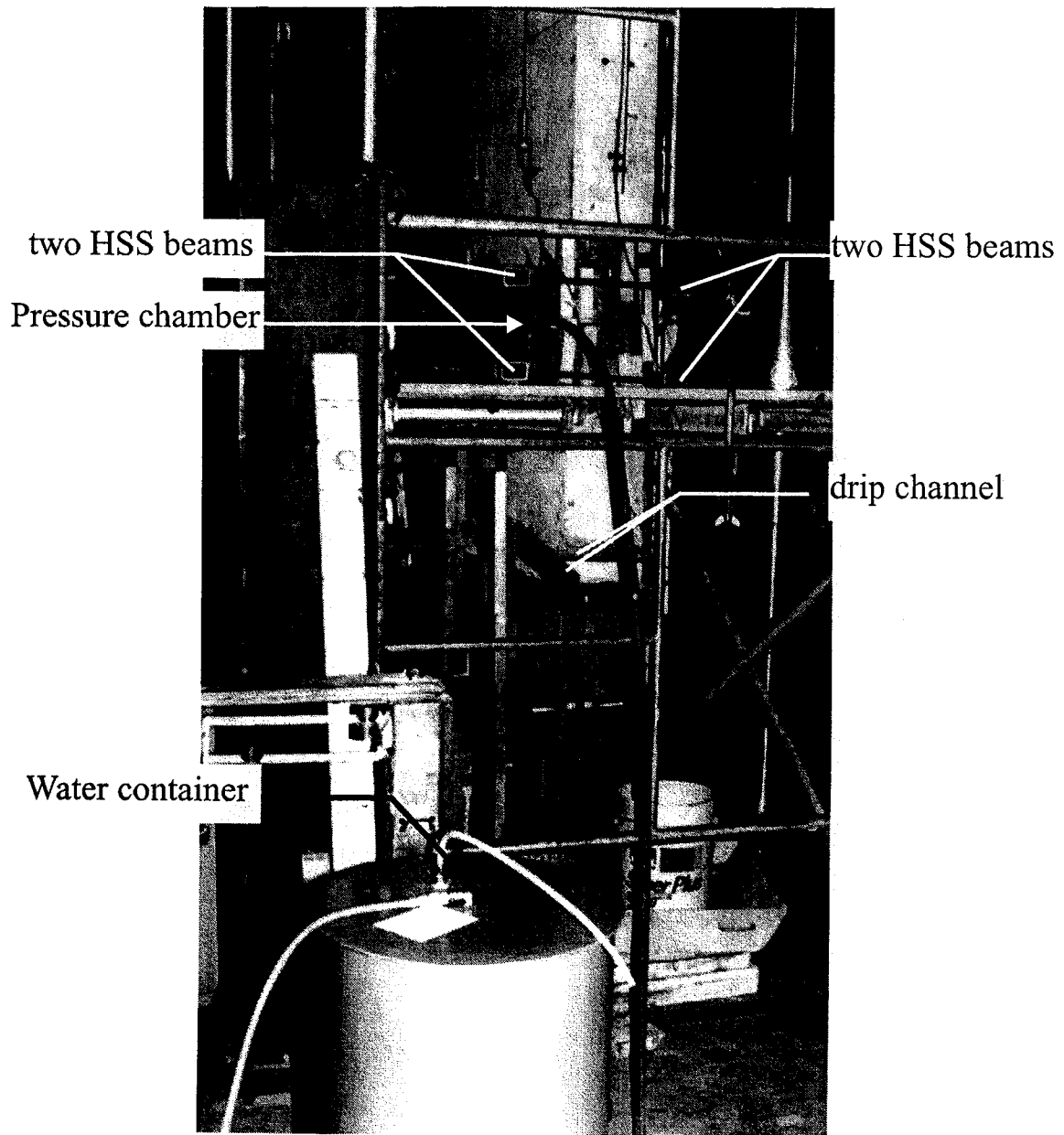
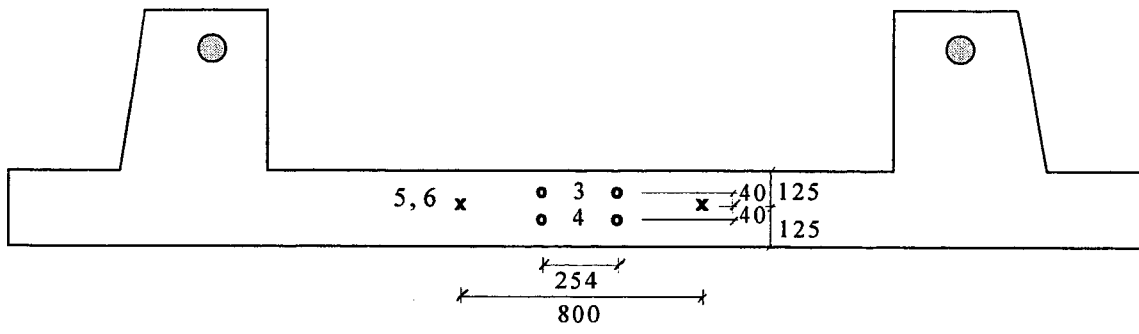
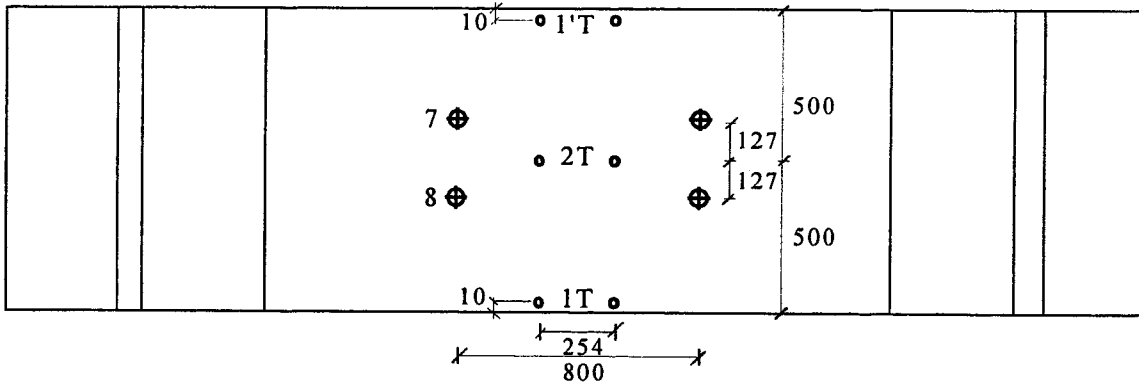


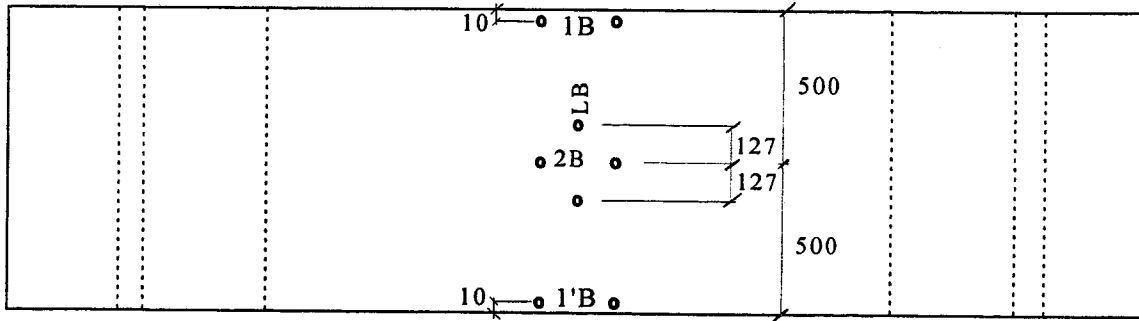
Figure 3.12 Leakage test set-up for specimen 3C



Elevation



Top Plan



Bottom Plan

x LVDT point for concrete
 o Demec point

⊕ LVDT point for non-prestressed steel
 ⊙ Rotation transducer

Figure 3.13 Location of instruments for a typical specimen

4- Test Results

4.1 Introduction

This chapter presents the test results and the observed behaviour of all the specimens. Test variables included concrete cover, load eccentricity, prestressed to non-prestressed steel ratios and bond of tendons. Crack patterns and structural response of the individual specimens are presented in Section 4.2. The specimens are classified into three categories according to the nature of the test. The first category includes specimens tested under eccentric load starting with the standard specimen 1C40. The second category includes specimen 3C tested under axial tension and the third includes specimen 2C tested under flexure only. Moment-curvature characteristics are discussed in Section 4.3 followed by leakage test results given in Section 4.4. Finally, Section 4.5 presents an evaluation of test results.

4.2 Crack Patterns and Specimen Response

4.2.1 Specimens Tested under Eccentric Load

In this group of specimens a tensile load was applied to the Dywidag bars attached to the eccentric load brackets. The test zone in the middle of the specimen was thus subjected to that tensile force accompanied by a bending moment equal to the force times the eccentricity. The eccentricity was approximately 520 mm in all the specimens of this category except specimen 3B which had an eccentricity of 260 mm. The self-weight of each specimen in this group produced a bending moment at the mid-span of 3.6 kNm that counteracts the moments due to the applied load. Demec and LVDT readings at zero applied load were considered the initial strains. Hence, the strains due to this latter moment were not considered and consequently the self weight moment is not included in the figures of Chapter 4 or this discussion. The effect of the dead load is considered in Section 5.6 in which the results of the analytical model are compared with test results.

Figures 4.1 through 4.5 show some significant crack features at the termination of the tests. Figures 4.6 through 4.11 show the gross concrete tensile and compressive strain histories versus the applied test load obtained from the Demec points shown in Fig. 3.13. Figures 4.12 through 4.16 show the non-prestressed steel strain history obtained from LVDT readings. The strains are thus the average steel strain within the gauge length of the LVDT. A detailed description of the response of each specimen is given below.

4.2.1.1 Specimen 1C40

Specimen 1C40 is considered the standard specimen. The load was applied in increments of 10 kN. The first observed transverse crack occurred on the tension side at a load level of 157 kN in the middle zone of the specimen. When the load was kept constant at 160 kN to take a set of readings, other transverse cracks spaced at 300 mm started to appear. These cracks formed at the location of the transverse steel. Some of these cracks extended to the full width of the specimen when the load was increased. Observation of the edges (sides) of the specimen showed that these cracks penetrated partially through the thickness of the specimen. The depth of penetration increased with increasing load. At a load level of 220 kN a new crack formed between each of the existing cracks. With increasing load, no new cracks were observed but existing cracks continued to widen. A crack that formed at the intersection with the eccentric loading brackets became very wide by the end of the test, as shown in Fig. 4.17, and consequently the rotation of these two brackets increased. Because of that rotation, a local bend of the Dywidag rods was noticed at a load of 365 kN where the rods touched the edges of the 60 mm holes formed in the brackets. It was decided to terminate the load and reposition Dywidag rods in the holes to eliminate the contact. The specimen was reloaded and at 405 kN, the loading was terminated due to spalling of the concrete at the bottom of the specimen under the crack at the eccentric load bracket. The crack pattern at the termination of the test is shown in Fig. 4.1. The regularity of the cracks is clear from the figure. The depth of the compression zone at the cracks at the termination of the test

was an average of 65 mm. Due to the uncertainty in identifying the precise crack tip location. The compression zone depths are considered to be accurate within ± 10 mm.

The load versus gross concrete tensile strain plots are given in Fig. 4.6(a). The influence of crack propagation on gross concrete strain is clearly seen. The plot obtained from Demec 1T is stiffer than the other two curves. The cracks at 1T formed at a higher load and were narrower than the cracks formed at the location of the other two Demecs. However, each of the three curves generally has three stages. The first stage is linear up to first cracking. The second stage is from first cracking up to yielding of the prestressed steel. The third stage is from steel yield to concrete failure. It can also be observed from Fig. 4.6(a) that the three curves at the cracking load are still on the negative side of the strain axis which means that the concrete strain is still compressive. This is because the plotted strain includes also concrete strain due to stressing and time effects, shrinkage and creep. If concrete strain due to time effects was excluded from the plot, the strain at cracking would be tensile and in the range of concrete tensile strain. To do that the vertical axis was shifted to the left by an amount equal to that due to shrinkage and creep. This shown by the vertical dashed line in Fig. 4.6(a).

Load versus concrete compressive strain curves are given in Fig. 4.6(b). The three curves are very close since no crack effect is involved.

Figure 4.12 shows a clear sudden change in the non-prestressed steel strain curves at cracking but no such change can be seen at yield of the non-prestressed steel. It is thought that at that loading level the prestressed steel is carrying most of the applied load. Hence, the effect of non-prestressed steel is insignificant. For that reason the second cusp of the curve occurred at a strain equivalent to yield of the prestressed steel. The vertical dashed line to the left of the origin accounts for creep and shrinkage strains as was in Fig. 4.6(a).

4.2.1.2 Specimen 1C20

Unlike the other specimens in which the concrete cover to the non-prestressed steel was 40 mm, specimen 1C20 had a concrete cover of 20 mm. During the test, the behaviour of specimen 1C20 was similar to that of specimen 1C40 except that the cracking load and the failure load were slightly higher. This slight difference is expected since the effective depth of the non-prestressed steel in specimen 1C20 is 20 mm larger. The first crack occurred at a load of 170 kN and was located exactly at the mid-span. Similar to specimen 1C40, a small increment of the load caused a set of additional cracks with a uniform spacing. At a load of 240 kN a new crack formed between each of the existing cracks. The test was terminated at a load of 420 kN when spalling of the concrete occurred close to the eccentric loading bracket as shown in Fig. 4.18. At the end of the test the average depth of the compression zone, as observed from the crack penetration on the edges of the specimen, was 80 mm. The camber was 16 mm at the end of the test.

The concrete strains in Fig. 4.7(a) show that the plot obtained from Demec 1T is much softer than the other two plots. Three cracks occurred in 1T, while only one crack occurred in each of the other two locations (2T and 1' T).

Figure 4.7(b) shows that the concrete compression strain curves are very close due to the absence of cracking on the compression face of the specimen.

Figure 4.13 shows that the non-prestressed steel behaviour is similar to that in specimen 1C40, but it seems that a sudden movement occurred in LVDT # 8 after cracking. This movement affected that LVDT readings.

4.2.1.3 Specimen 2A

The variable in specimen 2A was the reinforcement. It had five No. 15 bars and two strands instead of four No. 15 bars and 6 strands as used in the other specimens. This significant reduction in prestressed steel led to a significant reduction in both cracking

and ultimate loads. First cracking occurred at a load of 80 kN. The test was terminated at a load of 290 kN due to large deformation of the specimen. At a load of 80 kN a set of cracks formed at the location of the transverse steel. With increased load, the cracks extended until a load of 140 kN at which a new crack appeared between each existing crack. With subsequent load, no more cracking was observed but rather only the widening of the existing cracks. Figure 4.19 shows the large deformation and crack widths of the specimen during the test. The depth of the compression zone was as small as 30 mm. Figure 4.2 shows the regular crack pattern that developed. The crack widths reached 5 mm before termination of the test.

In Fig. 4.8 (a), the Demec 2T was lost when a crack occurred at the location of one of the Demec points, and the point fell off. It should also be noted that Demec 1T is softer between 120 kN to 200 kN. In this range Demec 1T include one more crack than the other demec gauges and the common crack was approximately 0.12 mm wider at 1T location.

Figure 4.14 shows that the non-prestressed average steel strain for the two LVDT's are in good agreement except for the last few readings where one LVDT deviated.

4.2.1.4 Specimen 2B

This specimen is similar to specimen 1C40 except that the tendons were not grouted. Unbonding affected the behaviour of this specimen during the test. The first cracking was observed at a load of 150 kN. At a load of 160 kN, more cracks appeared. For purposes of the leakage test, the specimen was unloaded then reloaded in the next day. More cracks occurred when the load was increased beyond 160 kN. Unlike the other specimens, the cracks were random and wider. There was no apparent relationship between the cracks and the location of transverse reinforcement. At a load of 400 kN, the test was terminated after spalling of the concrete on the compression side at the location of the leakage test set-up as shown in Fig. 4.3. Figure 4.3 also shows the crack pattern at

the end of the test. The average depth of the compression zone at the end of the test was about 50 mm. It can be concluded that unbonding the strands, in the specimen studied, had no effect on the cracking load or on ultimate load but it affected the specimen's behavior after cracking.

The effect of cracking on load versus gross concrete tensile strain curves is shown in Fig. 4.9(a). The response obtained from Demec 1'T is softer than Demec 1T response than that of 2T. One crack was formed at Demec 2T while two cracks were formed at the location of both 1T and 1'T. Those at 1'T were wider. Load versus average non-prestressed steel strain plots are given in Fig. 4.15. There is very good agreement between the gauges.

4.2.1.5 Specimen 3A

This specimen was reinforced with 9 prestressed strands and no non-prestressed longitudinal steel. It represents fully prestressed concrete. One crack occurred at a load of 180 kN. At 190 kN, a set of additional cracks were observed. They were regular and formed at the location of the transverse steel. Unlike all the previous specimens no additional cracks occurred with increasing load. The cracks merely widened with additional load. Figure 4.20 shows the wideness of the cracks during the test. Figure 4.4 shows the crack pattern after the termination of the test.

The crack penetration into the specimen showed a cracking phenomena unique to specimen 3A. As evident in Fig. 4.4, every crack branched into two cracks at a load of 220 kN. This happened at approximately the same level as the bottom of the metal duct. The two branches of the original crack continued penetrating with increased load. Some of them branched again into two cracks. Two crack branches from different original cracks extended until intersecting. The concrete spalled at this location along the entire width of the specimen at a load of 410 kN. The test was terminated. At failure, the average depth of compression zone was 45 mm except at the location of the crushing where it was 30 mm. The cracks were as wide as 8 mm.

The load versus gross concrete tensile strain curves given in Fig. 4.10(a) coincide because one crack formed at a load of 130 kN along the full width of the specimen and passed through the three Demecs locations. No more cracks formed at Demecs locations other than this primary crack. Figure 4.10(b) shows that the three compressive strain responses are very close but two of the three Demecs detached at a load of 380 kN. The remaining Demec recorded concrete compressive strain that reached 4500 microstrain.

4.2.1.6 Specimen 3B

The load eccentricity of 260 mm in this specimen was one-half of the eccentricity in the other specimens. The first cracking was observed at a load of 300 kN. This load produces the same moment resulting from a load of 150 kN in specimen 1C40 which means that cracking started approximately at the same moment in both specimens. A set of transverse cracks occurred along the specimen span at load of 300 kN. This set of cracks was spaced at 300 mm and was aligned with the transverse reinforcement. By increasing the load new cracks formed but unlike the other specimens, the new cracks were random and occurred at different loads and at different spacing. The last crack formed at a load of 580 kN. After that, the cracks extended and widened. The test was terminated at a load of 860 kN when it was noticed that two of the Dywidag bars had elongated significantly. The cracks were 7 mm wide, the rotation of the eccentric load brackets was 6.5° , and the average depth of the compression zone was 50 mm. The cracks pattern after the termination of the test is shown in Fig. 4.5.

As with the other specimens, the concrete strains and non-prestressed steel strain are shown in Figs. 4.11 and 4.16.

4.2.2 Specimen Tested under Axial Load

Specimen 3C was tested in axial tension using the MTS 6000 kN universal test machine as described in Section 3.7.2. This test lasted for eight days due to leakage tests that were performed on this specimen while under load. On the first day, the load was applied gradually. The eight LVDTs readings were recorded electronically every 40 kN,

or less, while Demec readings were taken every 200 kN. The first cracking appeared at a load of 1040 kN. It consisted of two through transverse cracks, labeled A and B in Fig. 4.21, located at transverse steel bar positions 900 mm apart. The load was increased to 1090 kN at which point a new through crack, labeled C, occurred following the transverse steel. The load was released gradually. After unloading, the cracks did not close completely. Permanent crack widths varied from 0.025 mm to 0.10 mm. The leakage test followed at this point with the full details in Section 4.4. For four days part of the leakage test was conducted and on the fifth day the specimen was reloaded. The load was increased and kept constant on the specimen at a level of 730 kN for another two days for leakage test purposes. During these two days the load was decreased to 580 kN. After that the load was increased again. Widening of the existing cracks was observed. At a load of 1100 kN a new transverse through crack, Labeled F, occurred, as shown in Fig. 4.21. Another transverse through crack, labeled G, occurred at a load of 1160 kN. With increasing the load the existing cracks became wider and new irregular cracks occurred near the ends of the specimen. At a load of 1600 kN a loud bang was heard from the specimen indicating a fracture of the reinforcement after which the load dropped. The load was released gradually.

The strain of some non-prestressed steel bars at failure measured with the LVDTs reached 30,000 microstrain. The strain of the prestressed strands was 36,200 microstrain, the difference arising from the initial prestressing strain. The stress-strain curves of the No. 15 bars and the 7-wire size 13 strands used in this test indicate that while this measured strain is less than 25% of the ultimate strain of No. 15 bars, it exceeds 58% of the ultimate strain of the strands. Similar failures occurred in tension tests of strand coupons. Some coupons failed at a strain lower than 30,000 microstrain due to fracture at the ends of the sample (at the grip with the machine head). This comparison suggests that the fracture occurred to one or more wires in the strands and most probably at the ends. Figures 4.21 presents the crack pattern of the specimen after the test.

LVDT readings were close at all six locations. Similar behaviour was observed from the Demec readings. Figure 4.22 represents average readings of all six LVDTs as well as a plot representing average readings of the six Demec gauges. The last readings of Demec strain gauges were taken at a load of 1500 kN. Very significant elongation occurred for the specimen beyond that load until steel fracture took place at a load of 1600 kN. The curves are linear up to cracking. After cracking and due to unloading and reloading processes and the creep of concrete, a horizontal shift is observed followed by strain hardening up to a strain equivalent to yielding of the prestressed steel where a rapid reduction in the slope of curves is observed. The curves continue with that slope until fracture occurs.

4.2.3 Specimen Tested under Flexure

Specimen 2C was tested under pure flexure as a simply supported slab 1000 mm wide with a 2900 mm span. It was loaded with two line loads 1500 mm apart giving 700 mm shear span on each end. According to the chosen structural system the bending moment due to the applied load along the middle half-span of the specimen is assumed to be constant with a value of $(0.70 \times \text{jack load})$ kN. The pressure on the two hydraulic jacks was controlled manually, hence the two loads were not exactly equal. Therefore, the moment in the test region was calculated using the average load. The Demec and LVDT readings give the values of gross strain at the mid-span. The specimen self-weight and the loading apparatus produced a bending moment of 6.3 kNm that counteracts the moments due to the applied load. Demec and LVDT readings at zero applied load were considered the initial strains. Hence, the strains due to this latter moment were not considered and consequently the self weight moment is not included in the figures of Chapter 4 or this discussion. The effect of the dead load is considered in Section 5.6 in which the results of the analytical model are compared with test results. The first observed cracking occurred on the tension side at a bending moment of 104 kNm in the middle zone of the specimen. The cracks formed in the transverse direction at spacing of 300 mm, coinciding with the locations of the transverse steel. The load was terminated

for leakage test purpose. After two days the specimen was reloaded. With increasing the load, some of the existing cracks extended to the full width. The crack depth increased with increasing load. At a moment of 118 kNm new crack formed on each side of the central crack. The two new cracks extended to the full width of the specimen at a moment of 141 kNm. With increasing load, additional cracks occurred outside the central 600 mm portion of the span. The new group of cracks occurred between the first set of cracks in an irregular inclined pattern. As the moment increased beyond 187 kNm, no new cracking was observed but rather only the widening of existing cracks. At a moment of 262 kNm the load was terminated because of spalling of the concrete on the compression side within the middle zone of the specimen next to the location of the East line load. The crack pattern at the termination of the test is shown in Fig. 4.23. The crack depths indicated that the average depth of the compression zone after the termination of the test was 68 mm along one side of the specimen and 92 mm along the other.

Moment at mid-span versus gross concrete tensile and compressive strains are plotted in Fig. 4.24. The concrete strains in these plots were obtained from Demecs readings. The three plots in Fig. 4.24(a) are very close except three readings of Demec 1'T. Crack widths readings showed that even though one crack passed by the three Demecs, it was wider at the location of 1'T during that load range. Compressive strain plots are very close due to the absence of cracking.

Figure 4.25 shows moment versus non-prestressed steel strain responses. There is a difference between the responses of the two LVDTs which starts from the beginning and reduces gradually through the test. This suggests that cracking had nothing to do with that difference. Rather, it seems that there was a problem with one of the LVDTs.

4.3 Moment-Curvature Characteristics

The concrete strain distribution was measured at three locations across the mid-span of the specimen, on the centre and at each edge, using Demec strain gauges. The Demecs mounted on the top and the bottom surfaces on the centre gave the strain

distribution at this location. The strain distribution at each edge was obtained from four Demecs mounted at the top, at the bottom and 40 mm above and below the mid-depth. For each specimen the three strain distributions were plotted at each load level. The non-prestressed steel strains obtained from the LVDT readings at the same load levels were plotted in the same plots at the position of the non-prestressed steel. Samples of these plots are given in Fig. 4.26.

The strain distributions obtained from the three sets of Demec gauges were used to calculate three different values of curvatures at each moment level. Two other curvature values were calculated using the strain values obtained from LVDT readings (LVDT 7 and 8). LVDT readings were considered as an extension of the concrete strain at the level of the LVDT and were used in conjunction with concrete compressive strain obtained from Demecs strain gauges. Figures 4.27 through 4.33 give moment-curvature diagrams for all the specimens except specimen 3C, which was tested under axial tensile load. The moment versus curvature response for the different specimens exhibit similar features. Each diagram is essentially linear up to cracking. Beyond cracking a change of the slope is observed. The second reduction of slope occurs due to yielding of the prestressed steel. In most specimens yielding of the non-prestressed steel has no significant effect on the response since the force carried by the non-prestressed steel is small comparable to that carried by prestressed steel. Only the moment-curvature response of specimen 2A, given in Fig. 4.29, shows the influence of yielding of the non-prestressed steel. The area of the non-prestressed steel in this specimen was more than five times that of the prestressed steel.

4.4 Leakage Test Results

After testing the first two specimens 1C40 and 1C20, it was noted from the measured crack widths that the cracks pattern and widths were in general symmetric with respect to the specimen mid-span. It was also noted that the cracks occurred at the location of the transverse steel as described in the preceding Sections. Hence, it was decided to conduct leakage tests on the subsequent specimens such that a steel "water"

chamber was placed at the location of the first transverse bar outside the gauge length of the LVDTs in order not to interfere with strain readings taken at mid-span. It was also decided to rely on the symmetry of the crack pattern and assume that the width of the concrete cracks occurring inside the chamber were equal to the corresponding crack on the other side of mid-span. The leakage tests were conducted on the remaining six specimens during the course of the loading tests described in Section 4.2. This section presents a detailed description of the leakage test results for the individual specimens presented in the same order in which they were tested.

The first leakage test was conducted on specimen 2A. Before the loading portion of the test was started the water chamber was filled with water under a pressure of 35 kPa and left for 24 hours to ensure that the concrete inside the chamber was saturated. At the start of the load test the pressure was increased to 80 kPa which is equivalent to about an 8 m head of water. A crack formed inside the chamber at a load of 80 kN as a part of the first set of cracks. The second set of cracks in the specimen occurred, as mentioned in Section 4.2.1.3, at a load of 140 kN. No leakage was observed until a load of 180 kN. At that load the width of the crack inside the chamber at the surface was estimated to vary from 0.30 to 0.48 mm with an average of 0.39 mm. At that load water started leaking from the north vertical edge of the specimen at the location of the chamber. The leaking water was collected and the corresponding time was recorded. Leakage continued from this side with a flow rate increased from 7 ml/min at a load of 200 kN to 150 ml/min at a load of 232 kN. At the same time the average width of the crack inside the chamber increased from 0.5 to 1.7 mm respectively. At that load the pressure on the water was released. It was discovered after the test that when the crack penetrated through the depth of the specimen it caused a cut in the silicon "caulking" which started to leak through that cut. Leakage occurred despite the presence of the sheet of steel clamped against this membrane. However, throughout the test there was no sign of water leakage or even wetness at the bottom of the specimen, the compression side. This means that although the water was able to overcome the resistance of the caulking membrane and the sheet of steel, it was not able to flow through the concrete compression zone.

It was noted that the crack inside the chamber did not close completely after the termination of the load in almost all the specimens and that it was wider than any other crack. Hence, the width of the crack inside the chamber was estimated using the width of the similar crack from the other half of the specimen. The effect of lateral water pressure on the crack surface is believed to be small.

In specimen 2B, the same procedure of filling the chamber with pressurized water was followed. The concrete crack inside the chamber was observed at the cracking load of 150 kN. Once the crack occurred a limited leakage was observed from one vertical edge. It was decided to shut off the water pressure and terminate the load to fix this side by adding more caulking material. A steel plate was also added to increase the support of the steel sheet. On the next day, water pressure was applied and the specimen was reloaded. At a load of 160 kN the existing crack inside the chamber extended to the full width of the specimen and changed direction running diagonally to the corner of the chamber. When this crack approached the edge of the specimen and passed under one corner of the water chamber water started leaking from the gasket and continued with an almost constant flow rate of 35 ml/min. At a load of 200 kN, a second main crack occurred inside the chamber followed by a group of random short cracks. At a load of 280 kN one of these small cracks extended outside the chamber. Water started to flow profusely from this crack causing the leakage test to be terminated. At the maximum load, the average width of the crack inside the chamber was estimated to be 0.38 mm. No sign of leaking or wetness was observed at the bottom of the specimen. That is, there was no leakage through the specimen. All of the leakage was through breaches in the sealing system.

The third leakage test was conducted on specimen 3A. In that specimen more precautions were taken to avoid leaking from the vertical sides of the specimen. Two layers of the caulking material were applied on the concrete sides and left for six hours to set. A third layer was applied on the steel sheet, then the sheet was compressed against the specimen side to ensure good contact. A steel plate was used to apply compression to

the steel sheet. As in the previous tests the pressurized water was applied to the specimen 24 hours before the test and increased to 80 kPa at the time of the test.

At a load of 190 kN a crack occurred inside the chamber. The width of this crack was estimated at that load to be only 0.05 mm. At a load of 240 kN, with the crack width estimated to be 0.34 mm, slight leakage was observed through the north side of the specimen. The precautions taken to prevent such leakage were not entirely successful, but they did reduce the rate of leakage significantly. Leakage from that side continued at an almost constant rate of 27 ml/min. Continuous observation for the bottom of the specimen showed no leakage and the surface was completely dry. At a very high load of 340 kN, a diagonal crack formed inside the chamber extended to the corner of the chamber and a considerable leakage was observed. The crack inside the chamber was wider than 1.25 mm at that load. The water pressure was released and the leakage test was terminated.

The next specimen tested was specimen 3B. In this specimen the load eccentricity was small. Cracking inside the chamber occurred at a load of 300 kN. With increasing load, a crack, K, running in the longitudinal direction of the specimen was observed inside the chamber at a load of 500 kN. This crack extended outside the chamber and started leaking at a load of 540 kN. The pressure was temporarily released. The part of that crack outside the chamber was dried then sealed using epoxy. After drying the epoxy was covered with a steel plate held in place with weights. The water pressure was applied again and the loading increased. This treatment was successful in preventing leakage from that spot. Also there was no leakage from the vertical sides in that specimen. At a load of 700 kN crack K extended and water started to flow through it with high rate. The leakage test was terminated at that load with an estimated surface width of the crack inside the chamber of 2.0 mm. Again no sign of leakage or wetness was observed on the compression side.

The last leakage test on a specimen with flexural cracks was conducted on specimen 2C, which was tested under flexure only. A new procedure was followed in

this test to ensure that the chamber would be centered on a crack. The specimen was loaded first without the water chamber. The load was increased until first cracking was observed at a bending moment of 104 kNm. It was decided to place the water chamber on a crack occurred within the zone of constant moment but outside the zone in which strain measurements are taken. While the specimen was under load and the crack was open, the vertical part of the crack from each side were filled with caulking material. After removing the loads the vertical crack closed with that material inside it. After removing the loads from the specimen the water chamber was centered on the chosen crack. The two vertical sides of the specimen at the location of the chamber were sealed as described for specimen 3A. After one day with the sides dry, the chamber was filled with water under a pressure of 35 kPa and left for one day. The next day the specimen was reloaded and the load increased gradually. At the same moment at which cracking started during the first loading cycle, 104 kNm, a diagonal crack formed inside the chamber and extended to the outside. Leakage started through this crack. The water pressure was temporary shut off to permit sealing of this crack. The part of the crack outside the chamber was dried then sealed with epoxy and covered with a steel plate held in place with weights. The water pressure was applied again but once the load was increased, the diagonal crack extended to intersect with the closest main crack and leaking started along this main crack. It was decided then to terminate the leakage test. There was no leaking from compression side of the specimen at any time during the test.

All the previously described leakage tests were conducted on flexural cracks with compression zones. In specimen 3C leakage through a “through crack” was investigated. To ensure that the water chamber would be centered on a crack, the specimen was loaded first without the water chamber. At a load of 1040 kN two through cracks occurred, crack A and B shown in Fig. 4.21. By increasing the load to 1090 kN a third through crack, crack C, occurred. Crack C was chosen to be in the centre of the water chamber because it does not interfere with LVDTs and Demec strain gauges. The average width of crack C at a load of 1100 kN was 0.43 mm on the north of the specimen and 0.21 mm on the south face. It was decided to place the water chamber on the north side where the

crack was wider. The specimen was unloaded and the average width of crack C was measured. It was 0.10 mm from the north side and 0.03 mm from the south side. The two sides of the specimen at the location of the water chamber were sealed as described for specimen 3A. The sides were left to dry and after two days the chamber was filled with water under a pressure of 70 kPa while the specimen is unloaded. A few minutes after filling the chamber, water started to leak from the crack inside the chamber. Due to a problem occurred in the pressure regulator, water pressure increased to 120 kPa for about 20 minutes. The leaking water was collected and leaking rate was recorded. Leakage rate was low and significantly reduced until leaking completely stopped at 330 minutes from the start of the leakage test.

It was intended to investigate the phenomena of autogenous healing (sealing) of the crack. Hence, after the crack self sealed for the first time, it was left for 48 hours under the same water pressure without load on the specimen. After 48 hours the specimen was loaded gradually. The crack started to leak once the load reached 730kN. At that load, the width of the crack inside the chamber was estimated to be 0.25 mm at the waterside and 0.01 mm at the other side. The testing machine pressure valve was locked to keep the same load of 730 kN acting on the specimen. Leaking water was collected and leakage rate was recorded. Leakage rate gradually reduced, and after 48 hours with the specimen still loaded the crack sealed itself again and leakage completely stopped. During that period it was observed that the load reduced to 580 kN.

The load was increased gradually. At a load of 840 kN the leakage started again and there was a spot along the crack where something like a hole in concrete occurred. Water jetted through this hole. Leakage test was terminated because of the very high flow. At that load, 840 kN, the width of the crack inside the chamber was estimated to be 0.36 mm at water side and 0.14 mm at the other side. The estimation of the width of the crack inside the chamber was based on measuring the width of crack A. Crack width readings taken after removing the chamber showed that cracks A and C generally had the same width at the same loads.

Figure 4.34 shows autogenous healing of the crack inside the chamber in the two cases described above. The readings of the load cell, on which the water container was supported, were very accurate (± 10 gm). It was also sensitive to any change in the pressure on the water surface. Water was moving back and forth between the container and the chamber, due to any minor change in air pressure, causing fluctuations in load cell readings. Any sudden change in air pressure, caused a jump in load cell readings. Hence, the plotted leakage rate recorded manually was more useful. It was based on the volume of water collected in the graduated cylinder.

4.5 Evaluation of Test Results

In this section an evaluation and comparison of test results will be presented. The evaluation will address the cracking behaviour of the specimens emphasizing the effect of the different variables investigated in the experimental study. Leakage through cracks and moment-curvature relationships of the specimens will be also evaluated. Other aspects of test results will be presented later through a comparison with the analytical model.

4.5.1 Cracking of Concrete

4.5.1.1 Effect of Partial Prestressing Level on Cracking

Figure 4.35 shows the relationship between crack width and bending moment for three levels of partial prestressing ($A_s/A_p = 0, 1.3, 5.1$). It is noted that although the crack initiation in the fully prestressed specimen, 3A ($A_s/A_p = 0$), was delayed due to prestressing, once it cracked the cracks were always wider than those of partially prestressed specimen. This would be expected since the transformed cracked stiffness is smaller. The rate of crack width increase, described by the slope of the curve, was also higher in the fully prestressed. On the other hand, specimen 2A ($A_s/A_p = 5.1$), that had low prestressing started cracking at the lowest moment but the rate of crack width increase was low prior to yielding of the steel and significantly increased after that. Generally at the same load, the crack widths in the case of partial prestressing ($A_s/A_p =$

1.3) were narrower than those of the fully prestressed case or the very lightly prestressed case ($A_s/A_p = 5.1$). The above observations show the merit of partial prestressing in controlling the cracking behaviour of concrete.

4.5.1.2 Effect of Concrete Cover on Cracking

Figure 4.36 shows that the crack width versus moment plots for the case of 20 and 40 mm concrete covers are very close. This suggests that, at the same moment, the effect of the concrete cover on crack width for partially prestressed concrete is not significant. However, that conclusion can not be generalized because it is based on only one test with specific partial prestressing level and load eccentricity.

4.5.1.3 Effect of Eccentricity on Cracking

Figure 4.37 (a) and (b) show the effect of eccentricity on crack behaviour. In Fig. 4.37(a) for the same moment the smaller the eccentricity, the higher the axial tension, and the wider the cracks. In addition, the rate of crack width increase is highest for the specimen of smallest eccentricity. In Fig. 4.37(b), which gives the relationship between crack width and load, the comparison between through and flexural cracks is not necessarily realistic because, as described earlier, specimen 3C that had through cracks was loaded, unloaded, and reloaded. The load was kept constant for two days then increased. The other two specimens with flexural cracking were subjected to only one cycle of loading. If specimen 3C were loaded like the others for only one cycle, the crack widths would be less. This also indicates that one should not be relied on crack widths taken from first cycle of loading since the reopened cracks are generally wider. In either case of loading, it is clear that through cracks occurred at higher axial load but once they occurred they become wide. Testing the specimen with through cracks showed that pre-cracking effects significantly affects the cracking behaviour of the specimen. In the test the first crack occurred at a load of 1040 kN with a width of 0.10 mm but after reloading the width of the pre-opened crack was 0.20 mm at a load level of 600 kN.

4.5.1.4 Effect of Bond Characteristic of Tendons on Cracking

Figure 4.38 shows the relationship between crack width and moment for two specimens. In one specimen the tendons were ungrouted. Even though the cracking moment and the ultimate moment were almost the same for the two specimens, the behaviour of the two specimens between these two limits was different. The cracks in the case of unbonded tendons were significantly wider and the crack pattern was completely different as described in Section 4.2.1.4.

4.5.1.5 Effect of Non-prestressed Steel Stress on Cracking

Figure 4.39 shows the crack width versus non-prestressed steel stress relationship for two different partial prestressing levels, namely $A_s/A_p = 5.1$ and 1.3 , respectively. The figure shows that partial prestressing level has an insignificant effect. This conclusion is expected because it has been shown (Gergely and Lutz, 1968, and Nawy and Huang, 1977) that a crack width can be expressed as a direct function of the average strain in the steel and crack spacing. Hence for the same crack spacing and the same steel strain, the crack width should be the same.

Figure 4.40, in contrast to Fig. 4.39, presents the significant difference in crack width at the same steel stress between flexural cracks and through cracks. Again, this difference may be due to the loading procedure followed in testing the specimen with the through crack. The plot shows that for similar steel stresses, the through cracks are much wider than the flexural cracks.

4.5.2 Moment-Curvature Characteristics

The moment curvature plots show the same trends as load-strain plots. Figures 4.41 through 4.44 show the effect of the different variables on the moment-curvature responses.

In Fig. 4.41 the effect of the axial tension in increasing the specimen ductility is shown. This is expected since the axial tension reduces the depth of the neutral axis and hence the compression zone.

Figure 4.42 shows the effect of partial prestressing. Comparing the two plots of the fully prestressed case and the case of A_s/A_p of 1.3 shows that while the maximum moment of the fully prestressed specimen is slightly higher, the curvature, which reflects ductility, in the case of partial prestressing is generally higher. The moment capacity of the fully prestressed case was slightly higher because its reinforcing index was higher. The reinforcing index is a direct function of the summation of the yield force of the non-prestressed steel and the yield stress of the prestressed steel. The ductility of concrete elements depends globally on the ductility of the reinforcement; prestressing steel is less ductile than non-prestressed steel. Therefore, the fully prestressed specimen was less ductile. This decrease in ductility favors partial prestressing which combines the advantages of both fully prestressing and fully reinforcing. The specimen with very light prestressing, $A_s/A_p = 5.1$, (close to reinforced concrete) was the most ductile but its flexural capacity was significantly lower. It also cracked earlier.

The effect of bond characteristics of the tendons on the moment-curvature diagram is shown in Fig. 4.43. It is observed that the specimen with unbonded tendons is slightly more ductile due to the wide cracks that occurred in it. It can be also observed from Fig. 4.44 that increasing the concrete cover increases ductility.

4.5.3 Leakage Through Cracks

Leakage tests were conducted on six specimens. In five specimens the cracks were flexural with a compression zone. In the pure tension specimen, a through crack penetrated the whole depth. In the case of flexural cracks, there was no leakage from the compression side in all five specimens tested. Even when water leaked from either the top or the sides of the specimens, the crack widths that leaked were very wide. The load that caused leakage was beyond the service load. It is also well known that water always

follows the path of least resistance. Since water was able to overcome the resistance provided by the caulking, sheet steel and steel plate, this may indicate that flow through these constraints was easier than leaking through the compression zone. From these observations it can be concluded that the presence of the compression zone, in the tested specimens, prevented leakage. Thus, a design strategy for flexural members may be based on providing a minimum thickness of compression zone rather than limiting steel stresses or crack widths.

In the case of through cracks, autogenous healing occurred for the pre-opened crack within five hours during which rate of leaking was very low. For a crack width of 0.25 mm from the water side and 0.1 mm from the other side, autogenous healing occurred in less than two days and the leakage rate decreased dramatically in the first few hours of that period. Thus, design strategy for tension members that develop through cracks may be based on restricting the crack widths so that autogenous healing can occur. Also, one may design so that while leakage may occur, the rate is within acceptable values.

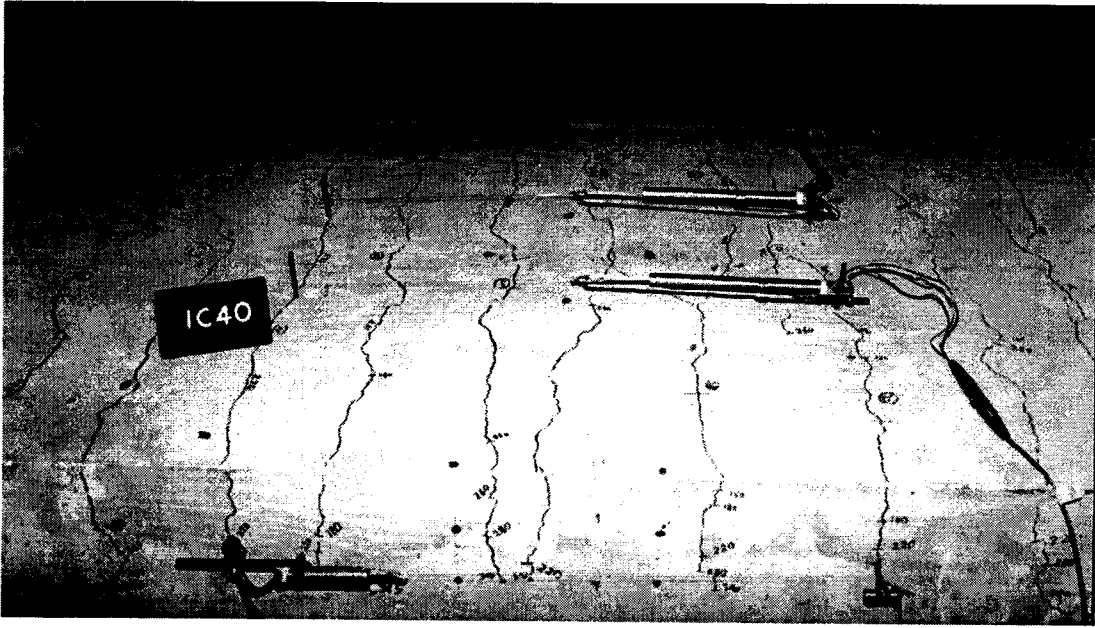


Figure 4.1 Crack pattern of specimen 1C40

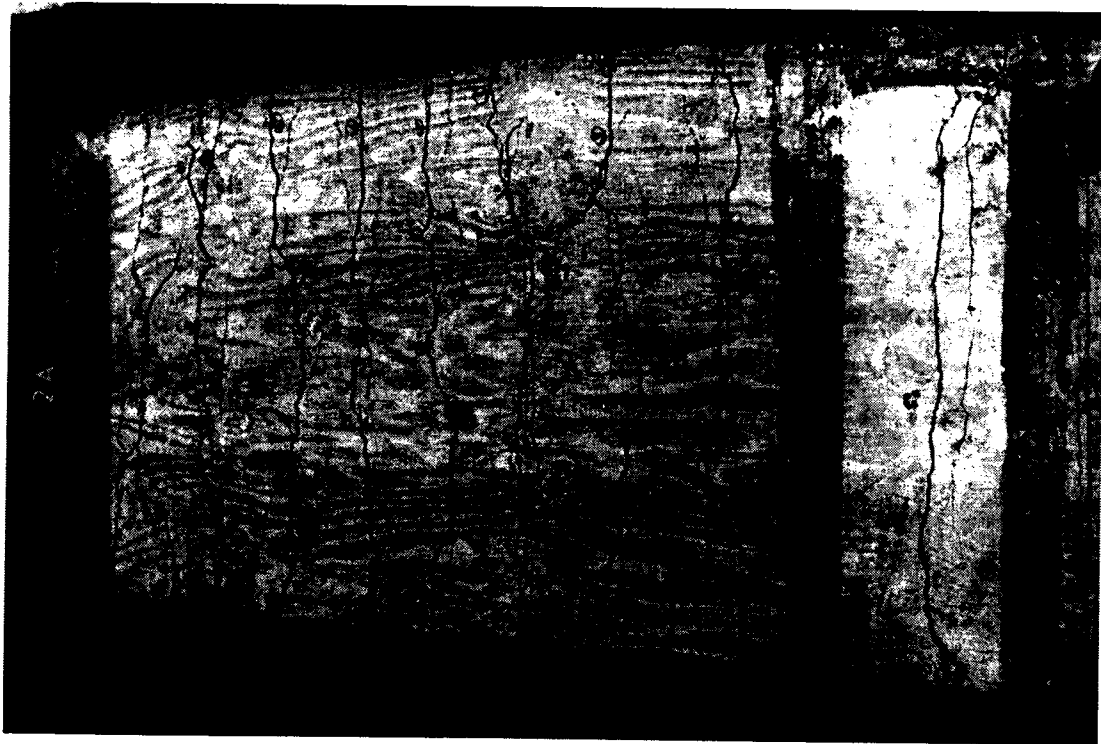
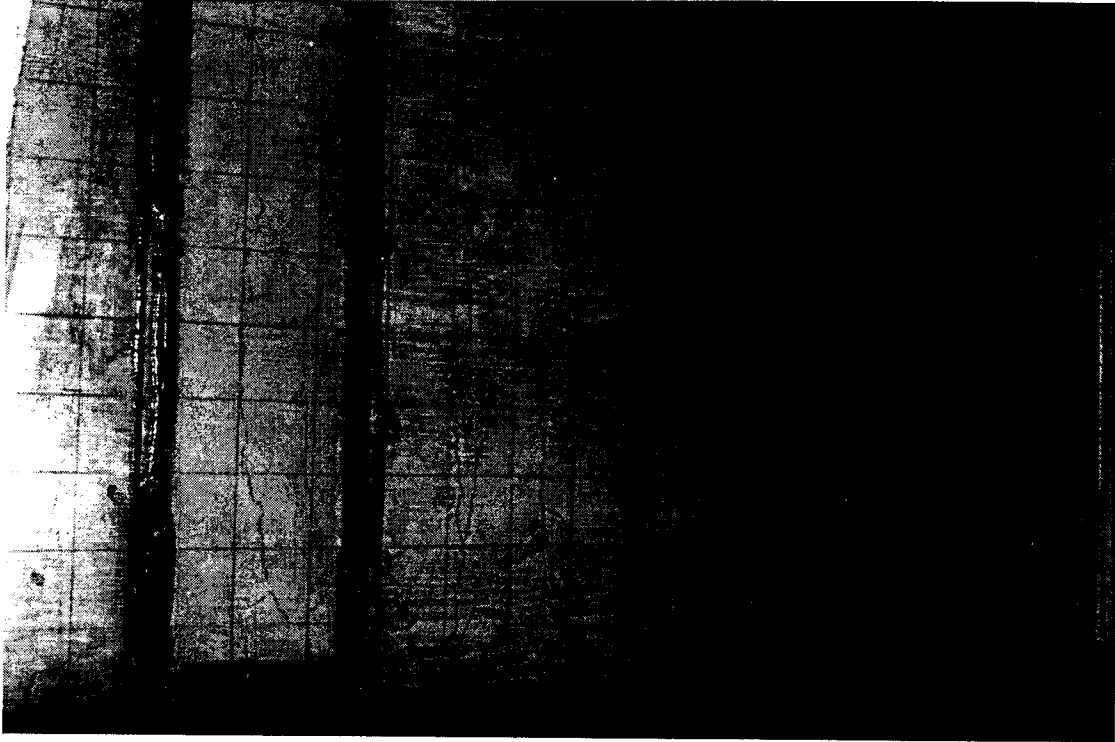
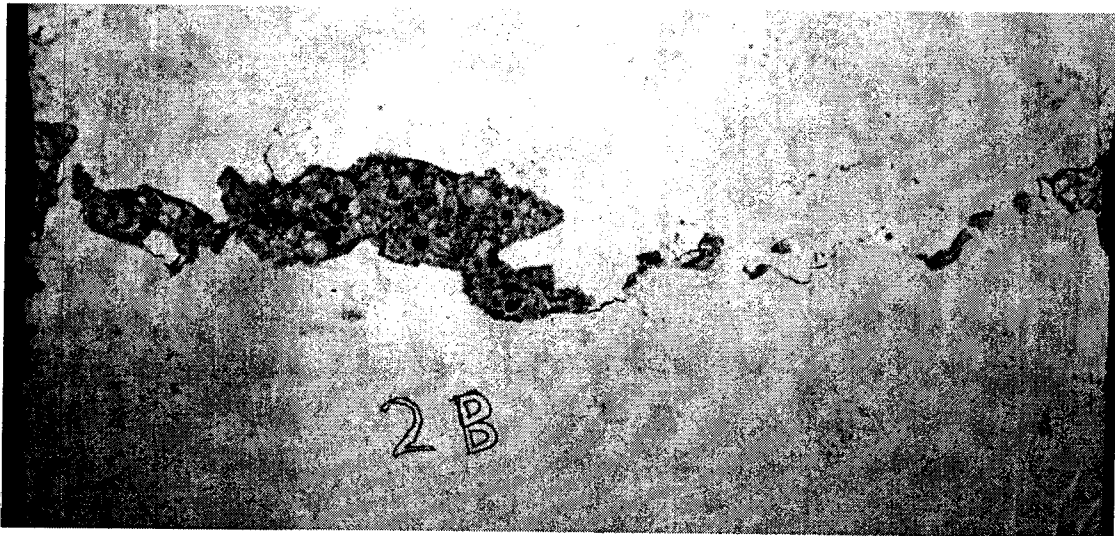


Figure 4.2 Crack pattern of specimen 2A



(a) Crack pattern



(b) Mode of failure

Figure 4.3 Crack pattern and mode of failure of specimen 2B

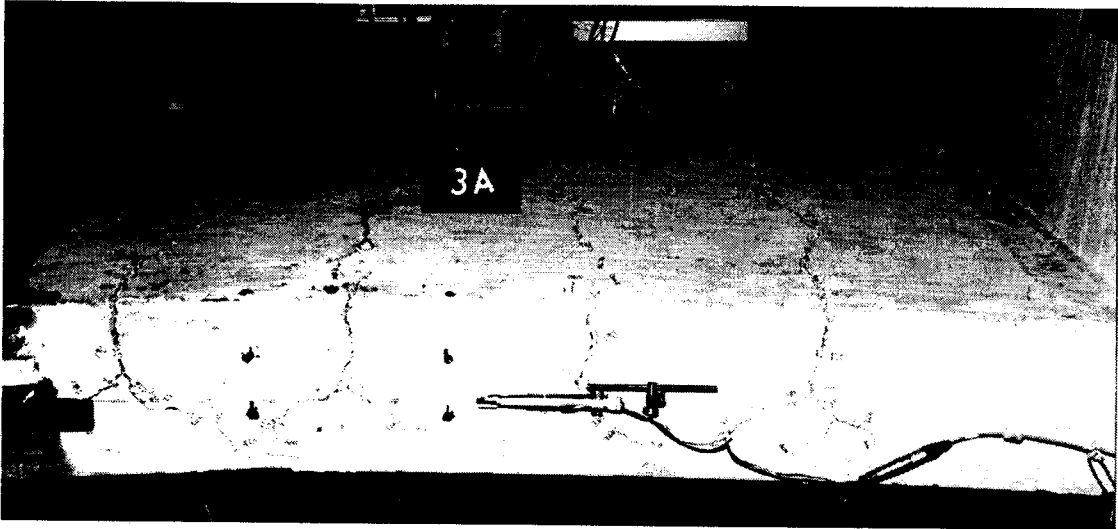


Figure 4.4 Crack pattern of specimen 3A

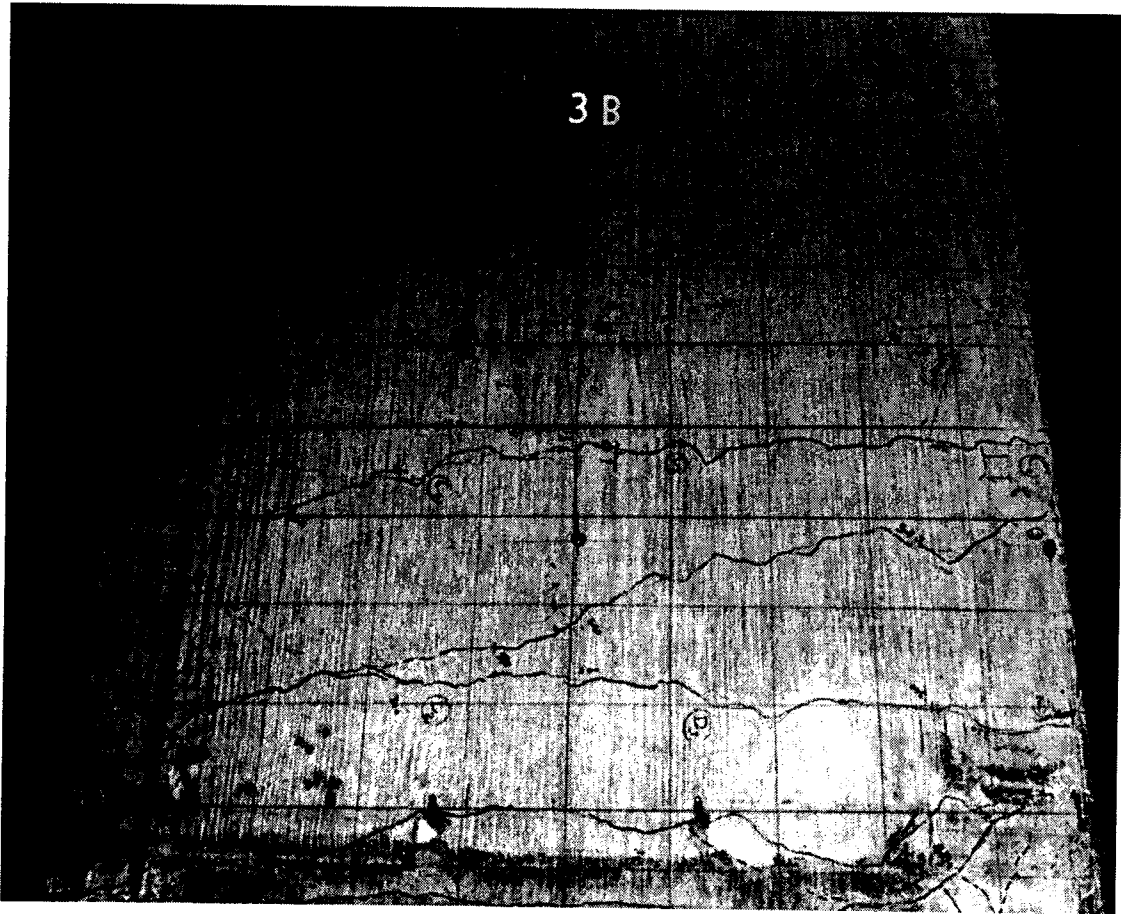
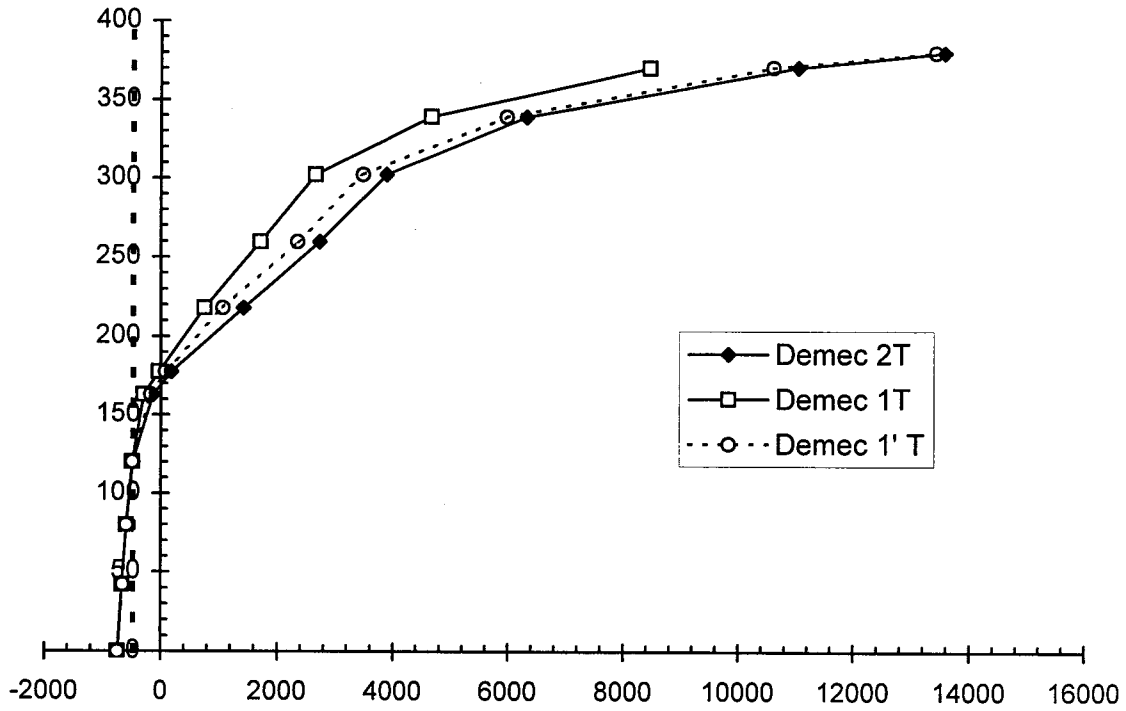
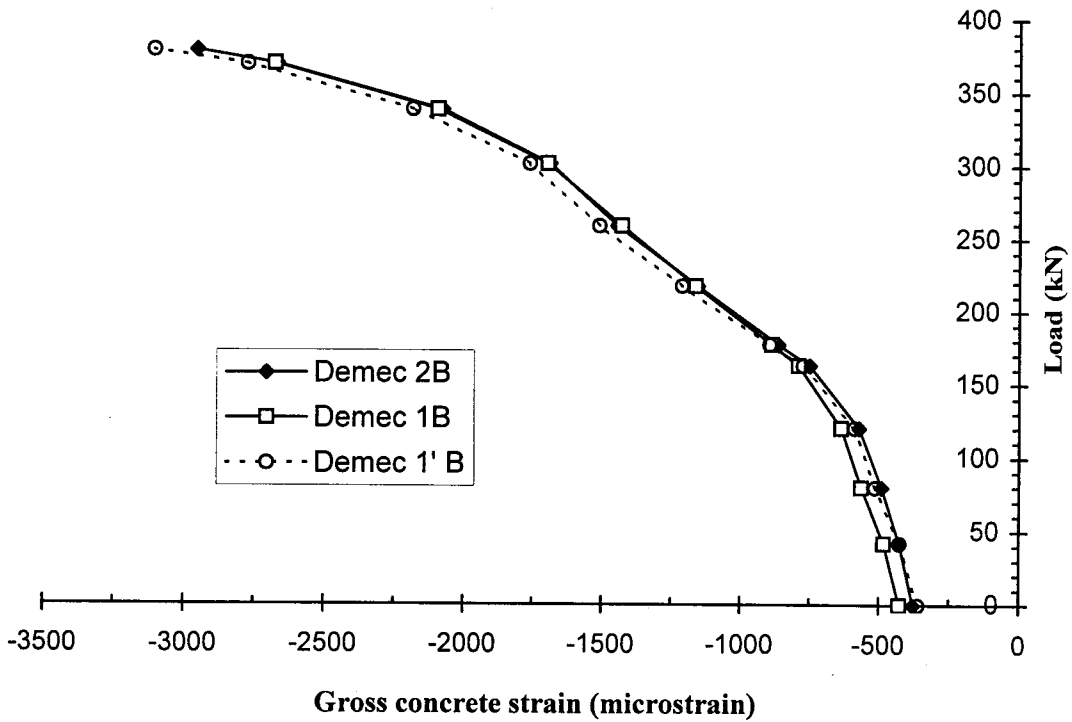


Figure 4.5 Crack pattern of specimen 3B

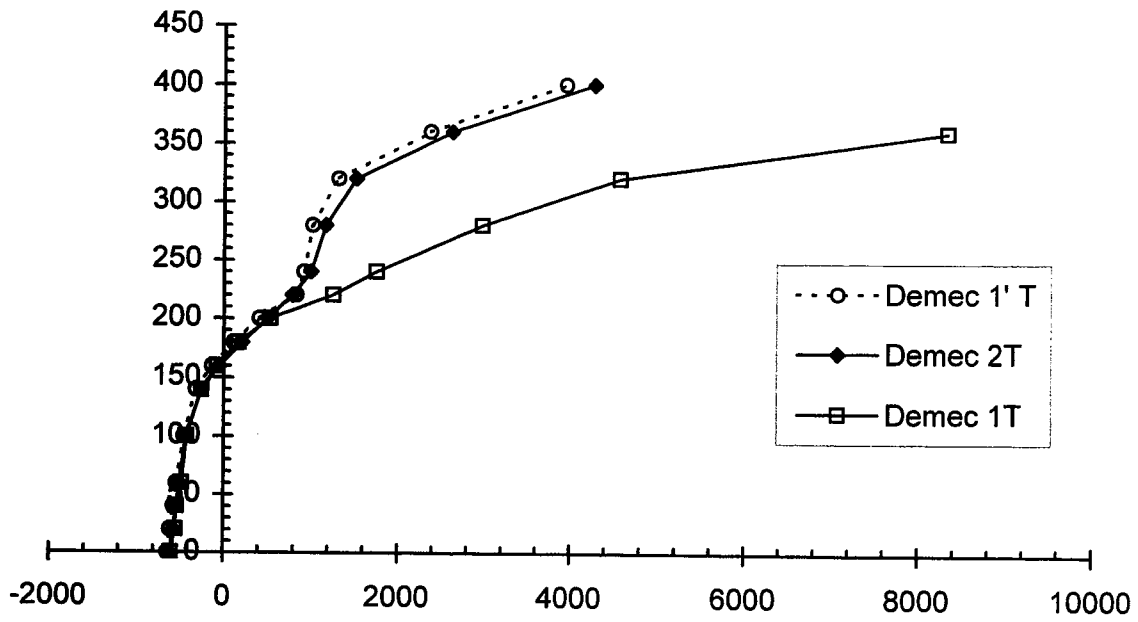


(a) Tensile strain

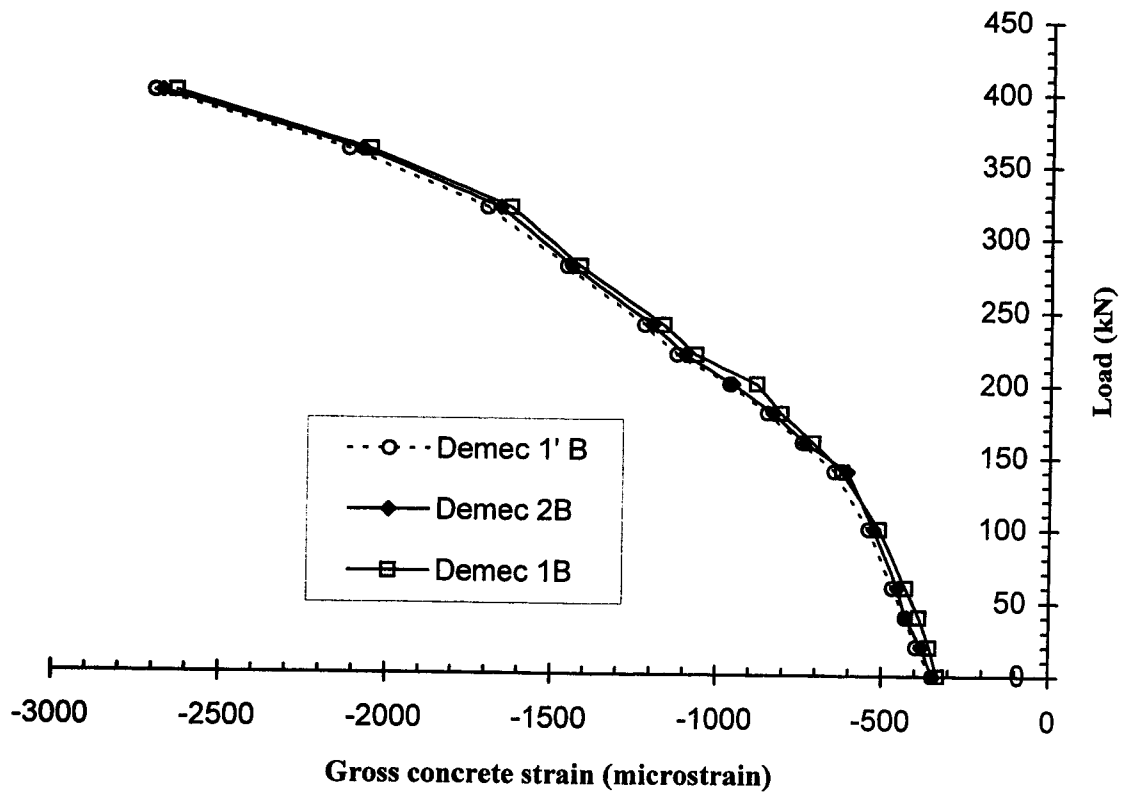


(b) Compressive strain

Figure 4.6 Load versus gross concrete strain for specimen 1C40

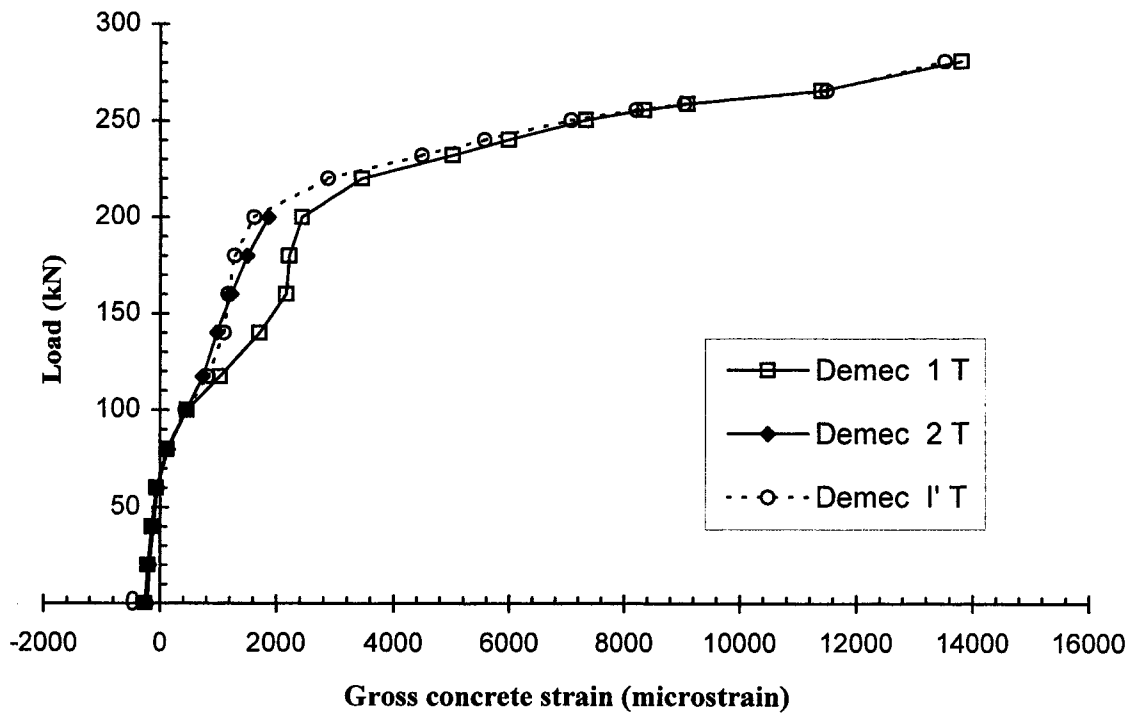


(a) Tensile strain

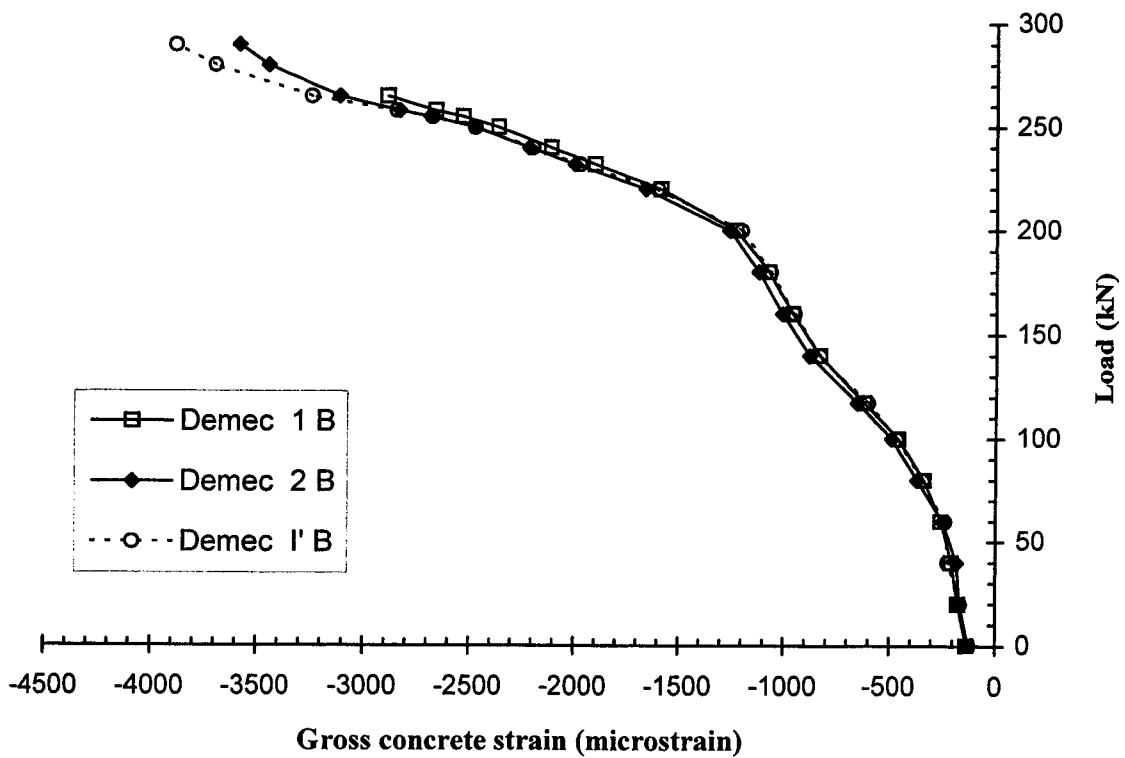


(b) Compressive strain

Figure 4.7 load versus gross concrete strain for specimen 1C20

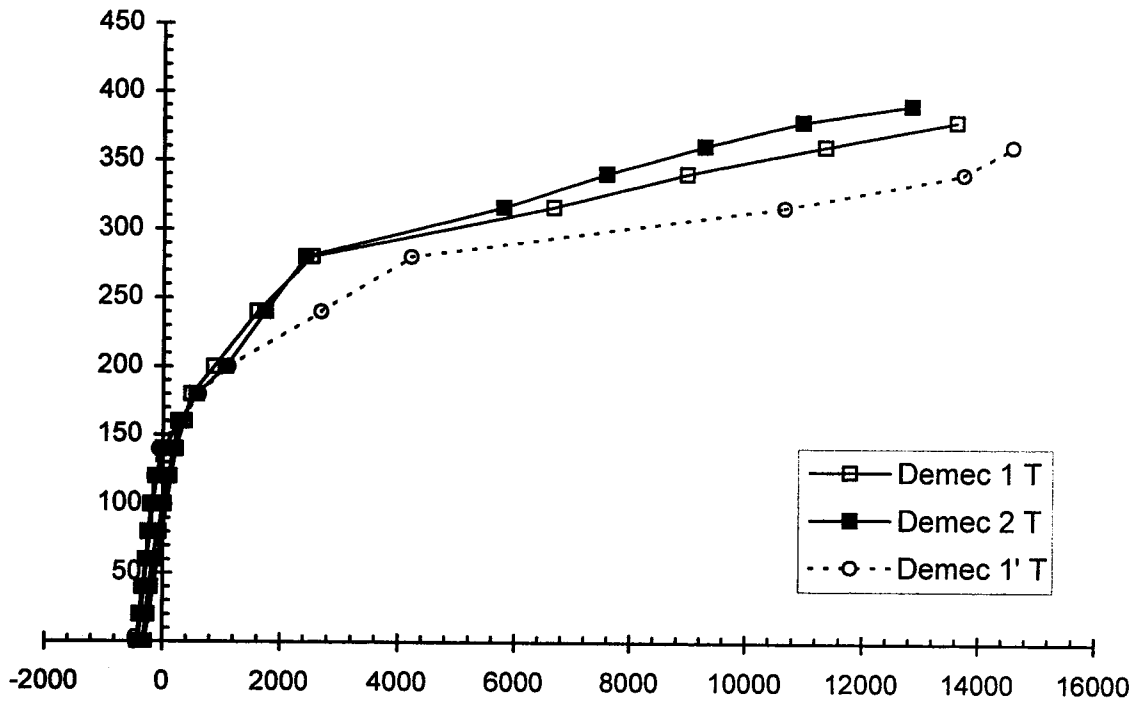


(a) Tensile strain

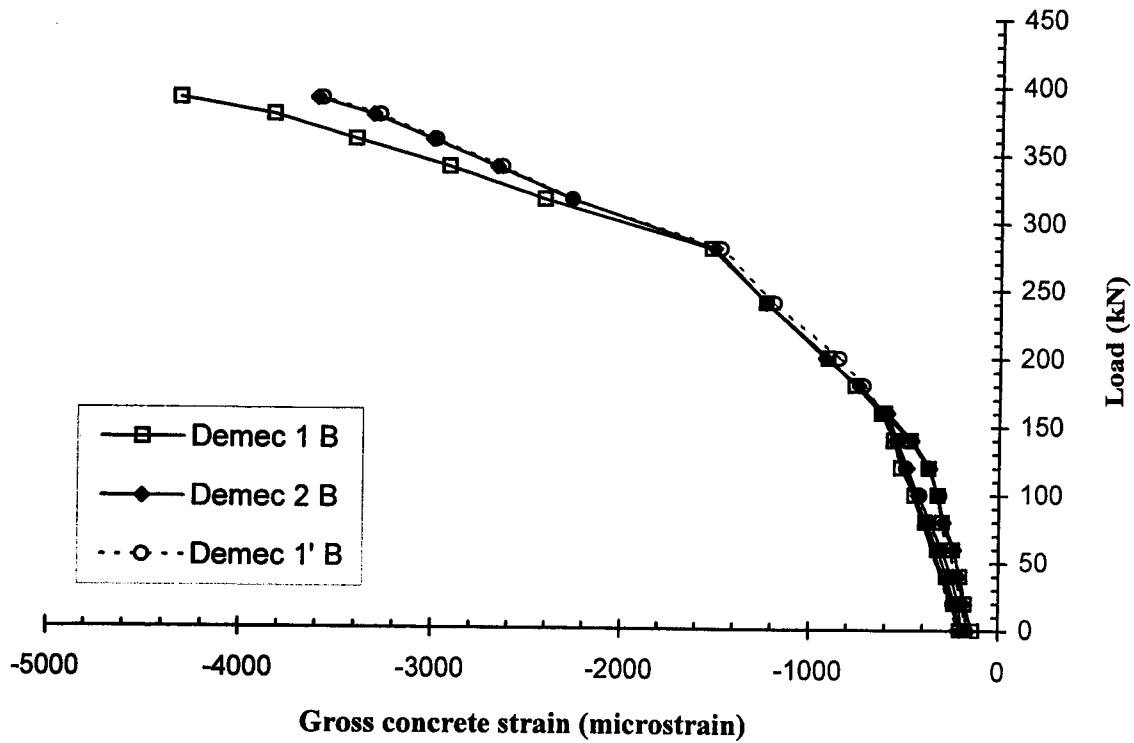


(b) Compressive strain

Figure 4.8 Load versus gross concrete strain for specimen 2A

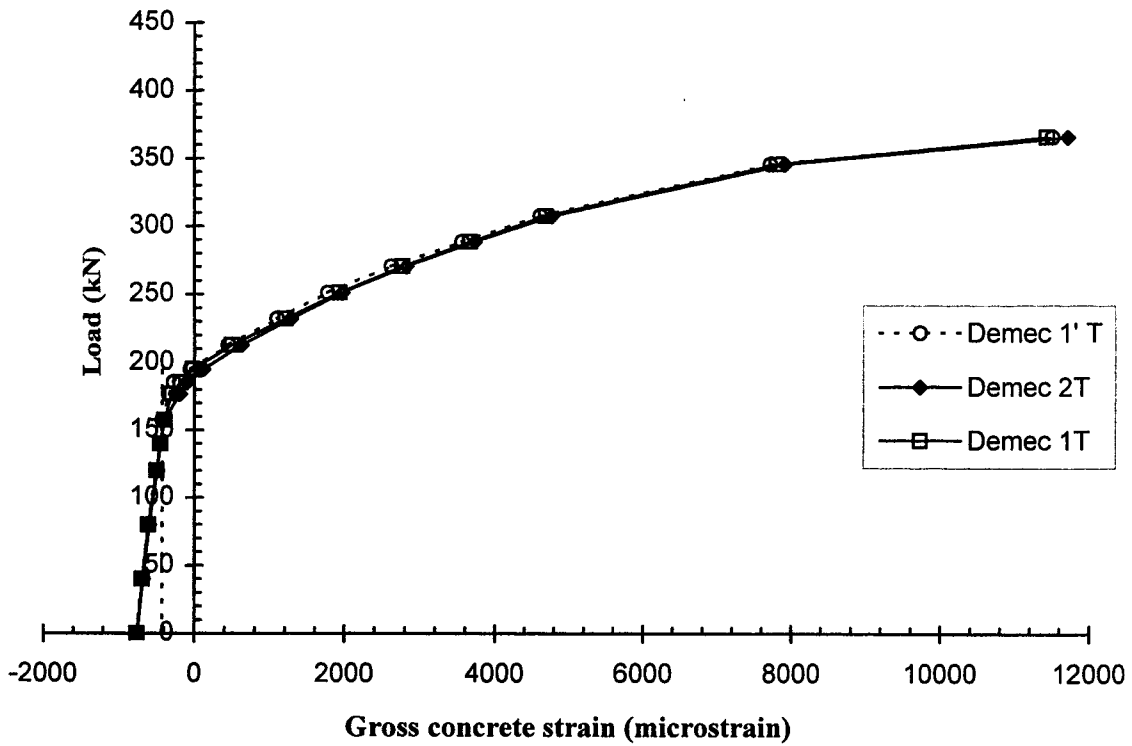


(a) Tensile strain

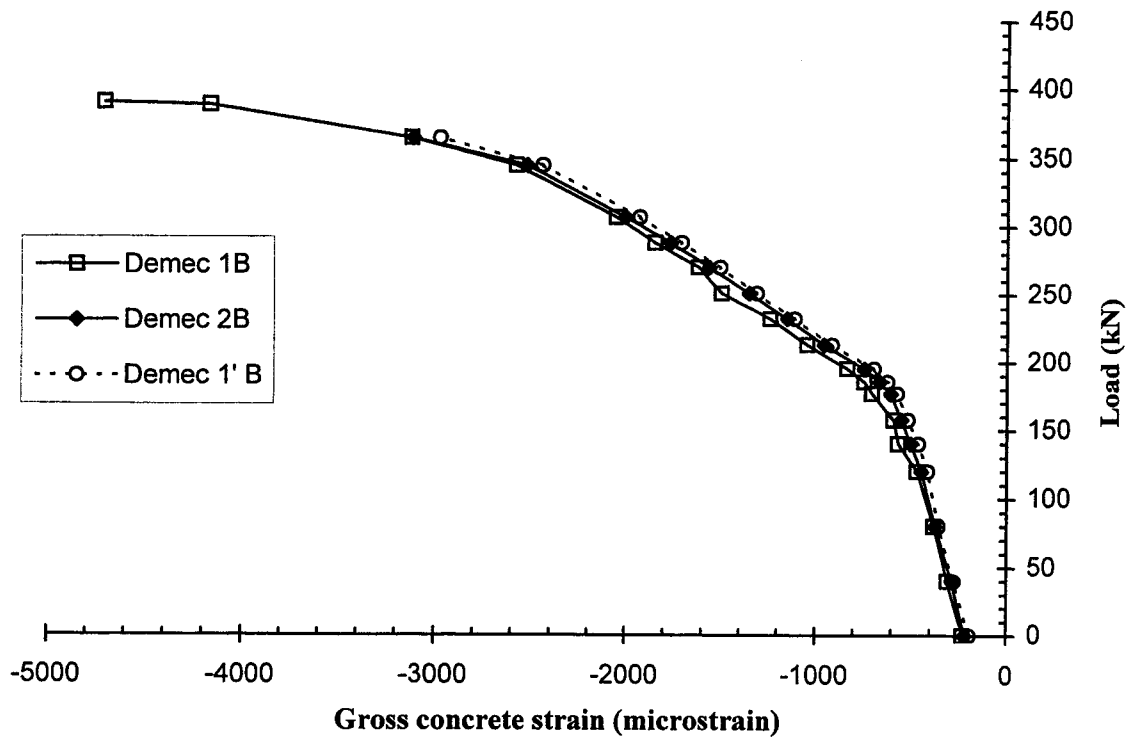


(b) Compressive strain

Figure 4.9 Load versus gross concrete strain for specimen 2B

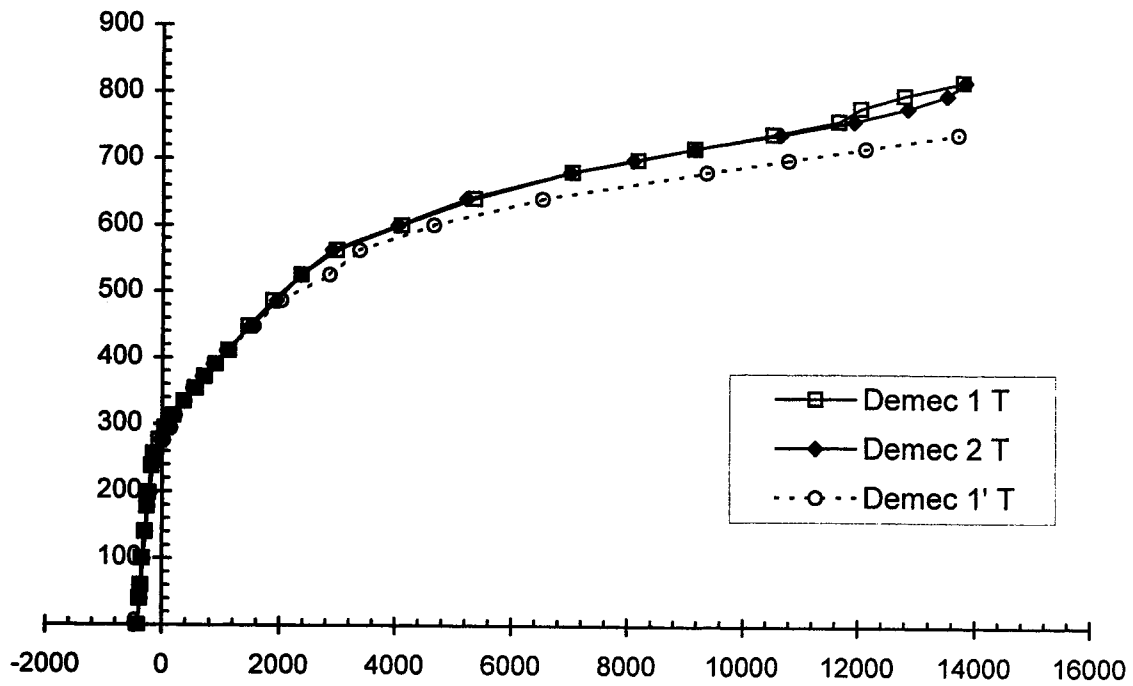


(a) Tensile Strain

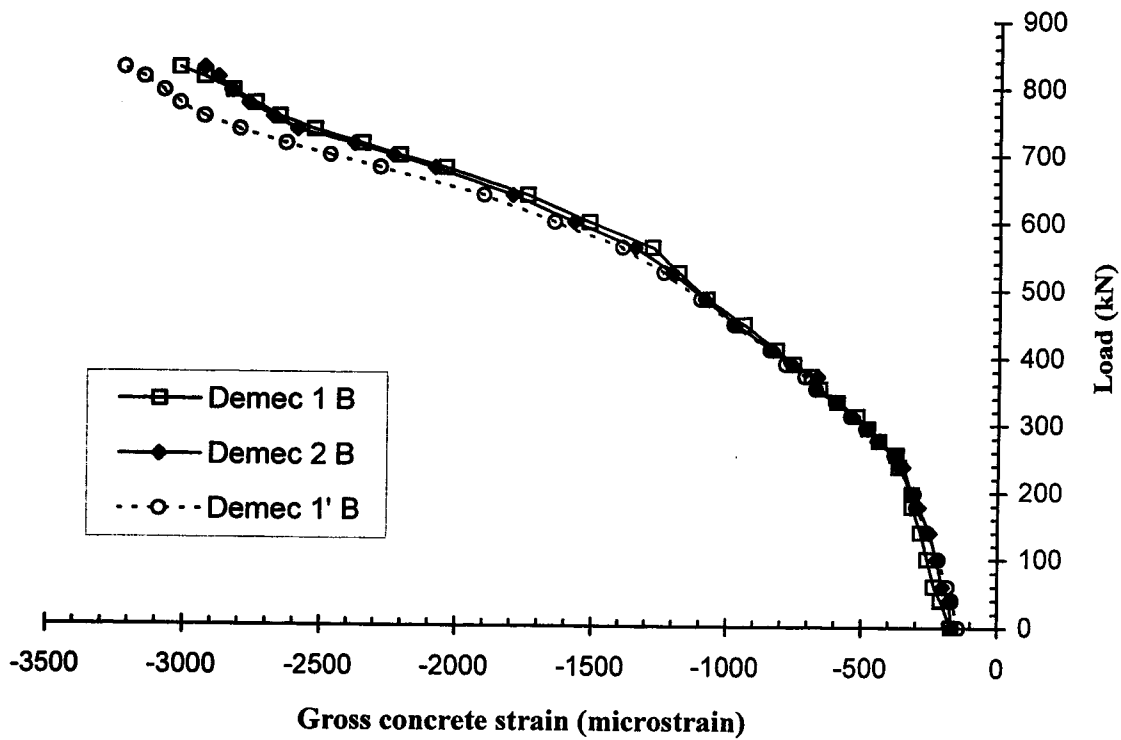


(b) Compressive Strain

Figure 4.10 Load versus concrete strain for specimen 3A



(a) Tensile strain



(b) Compressive strain

Figure 4.11 Load versus Gross concrete strain for specimen 3B

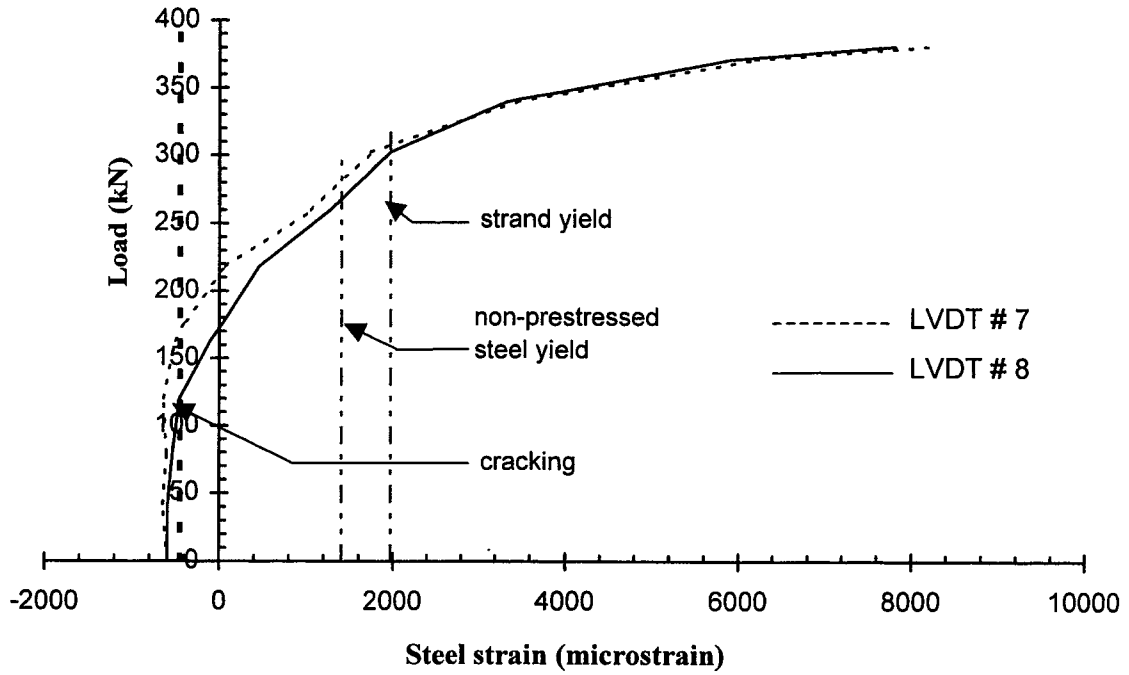


Figure 4.12 Load versus non-prestressed steel stress for specimen 1C40

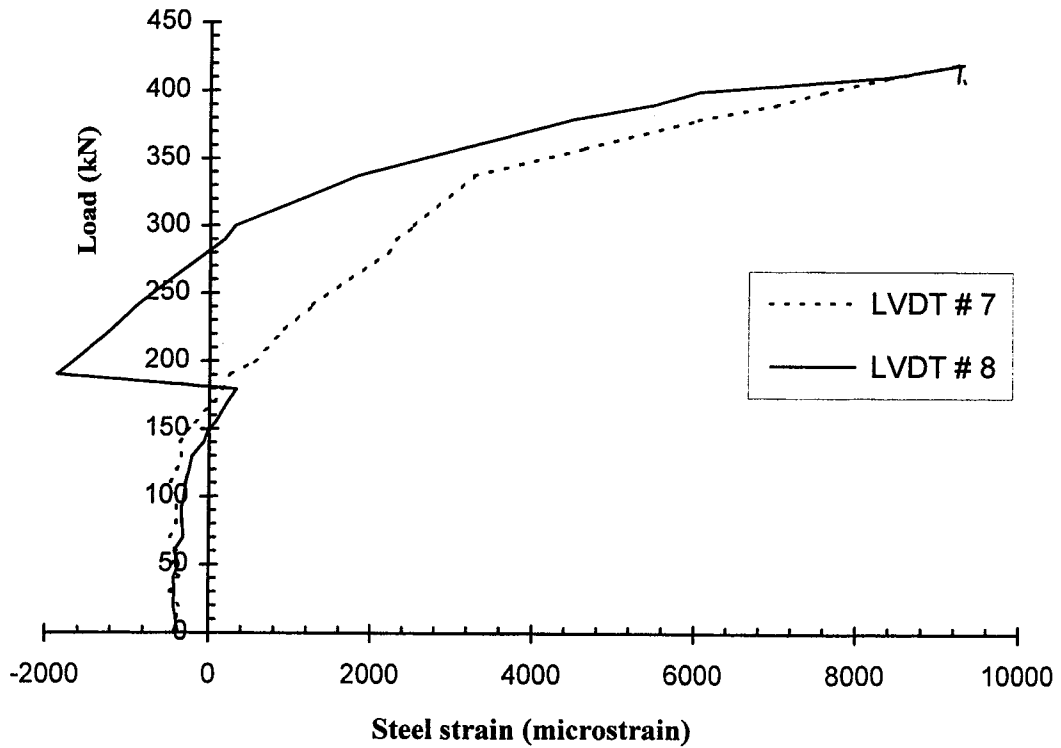


Figure 4.13 Load versus non-prestressed steel stress for specimen 1C20

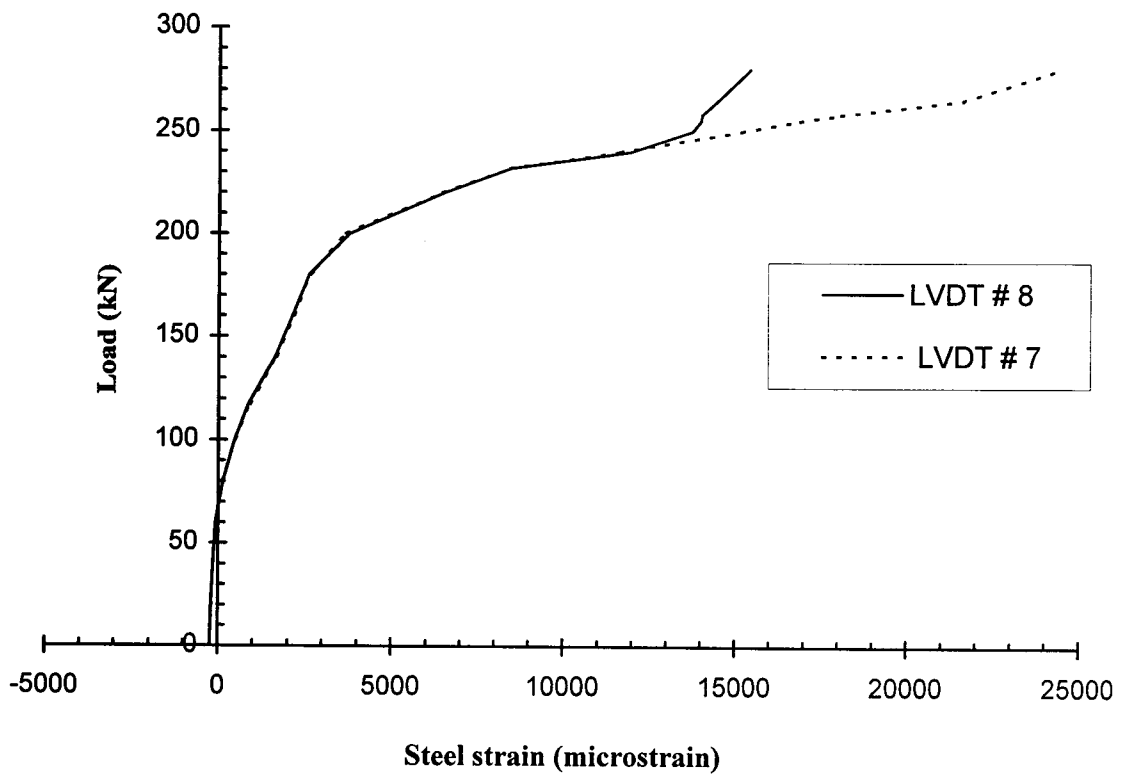


Figure 4.14 Load versus non-prestressed steel stress for specimen 2A

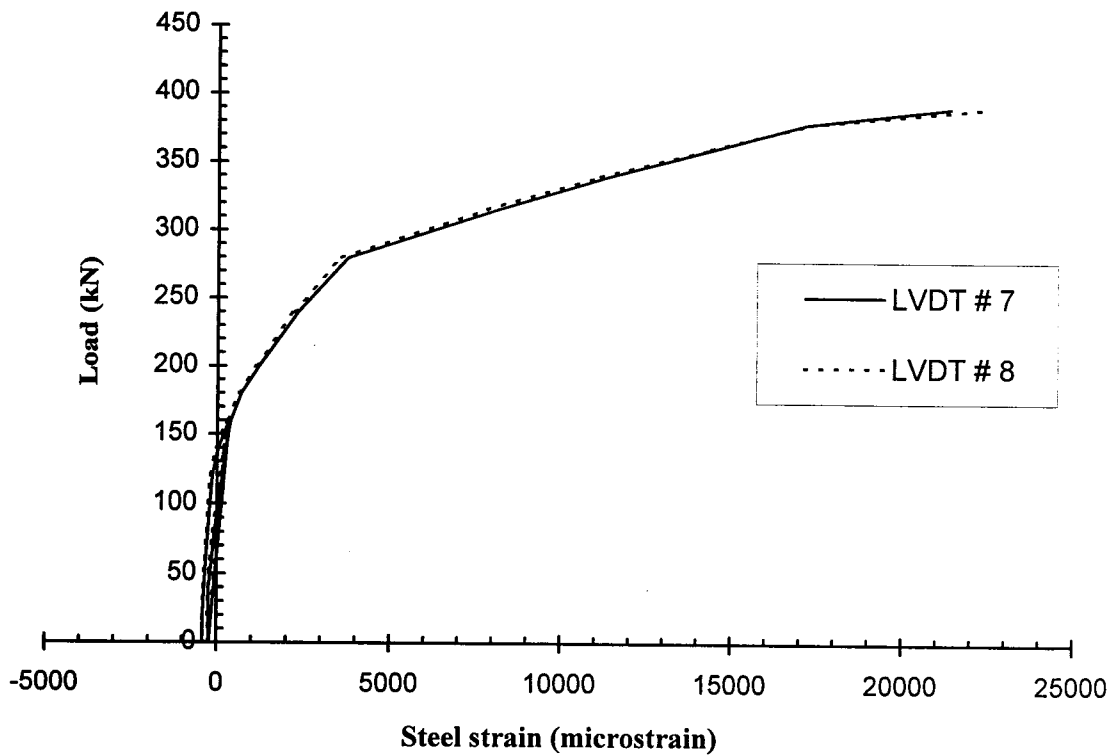


Figure 4.15 Load versus non-prestressed steel stress for specimen 2B

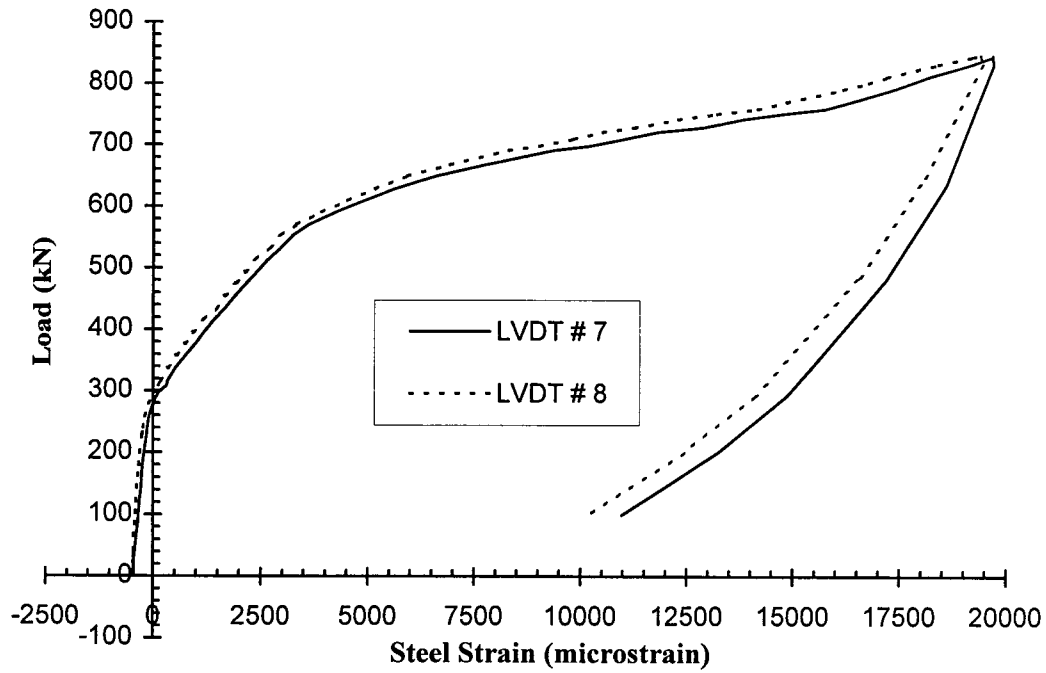


Figure 4.16 Load versus non-prestressed steel strain for specimen 2B

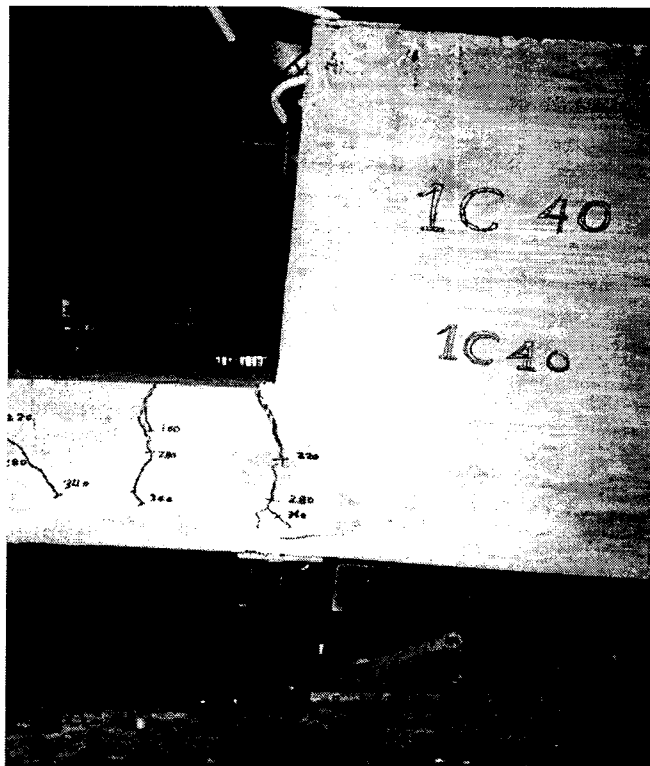
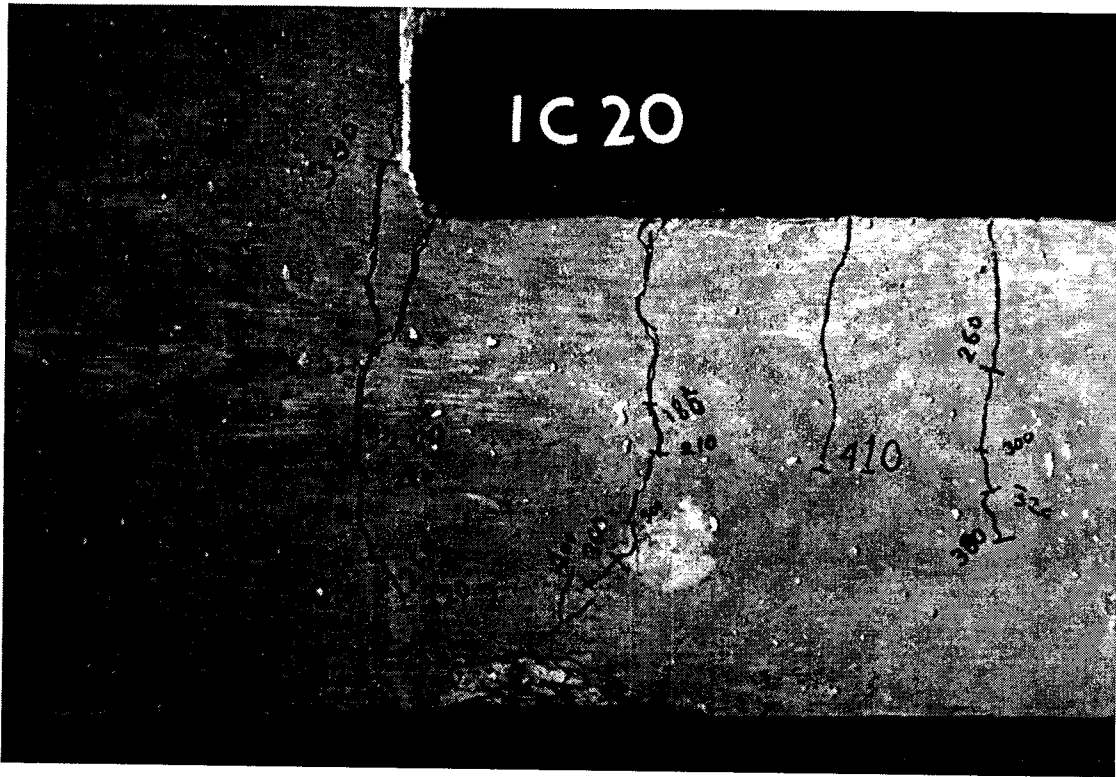


Figure 4.17 The rotation of the eccentric loading bracket in specimen 1C40 during the test



(a) Viewed from the side



(b) Viewed from the compression side

Figure 4.18 Mode of failure for specimen 1C20

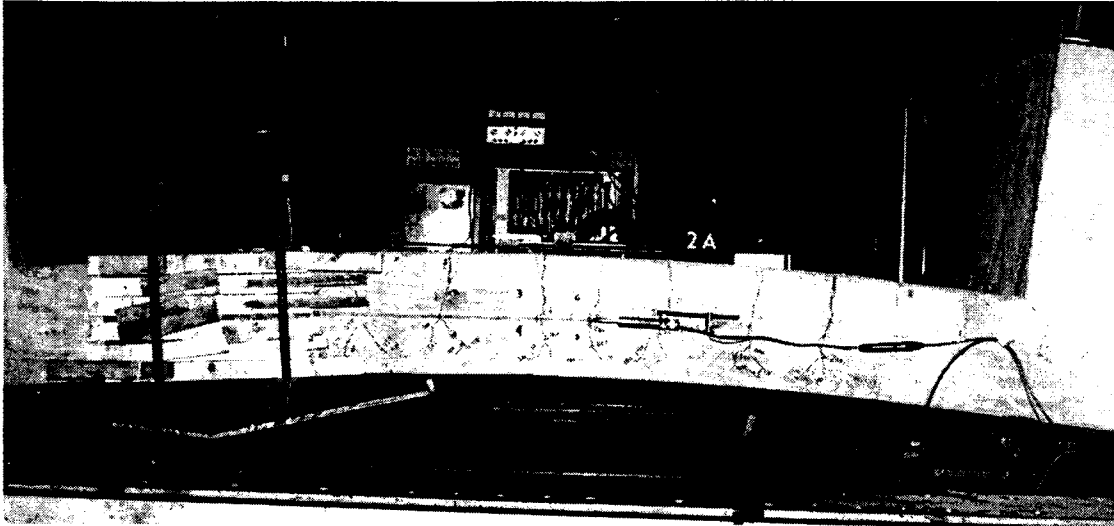


Figure 4.19 Large deformation of specimen 2A during the test

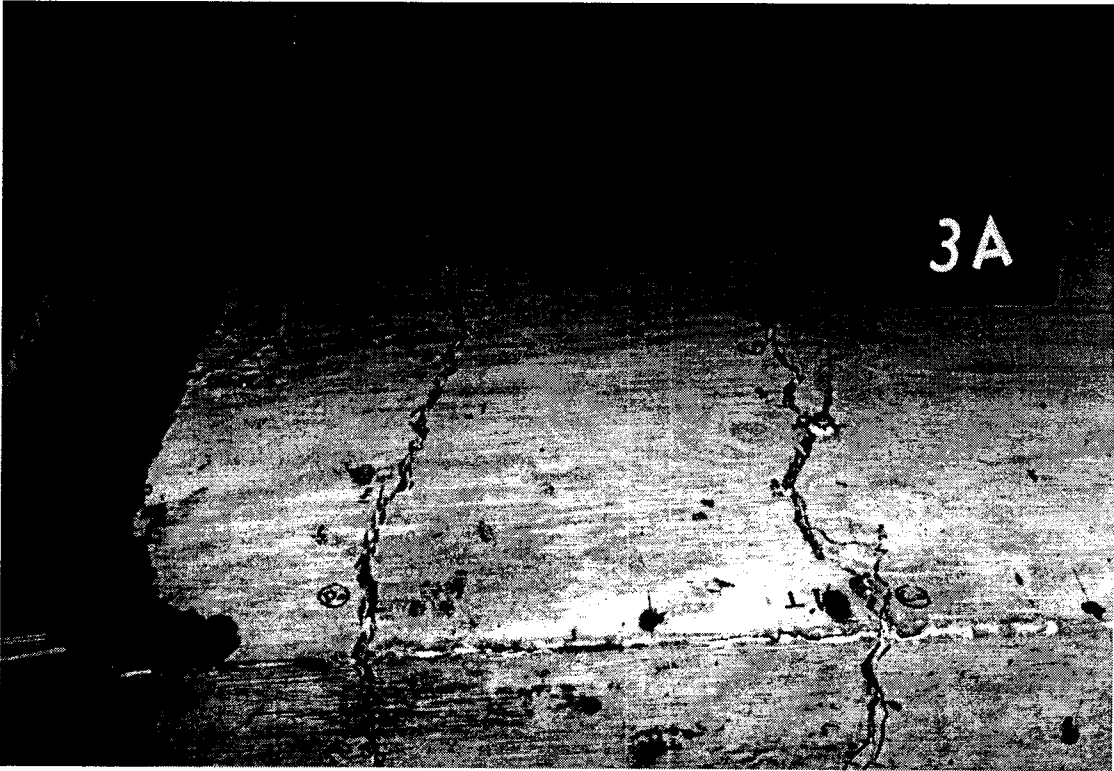


Figure 4.20 Wide cracks in specimen 3A

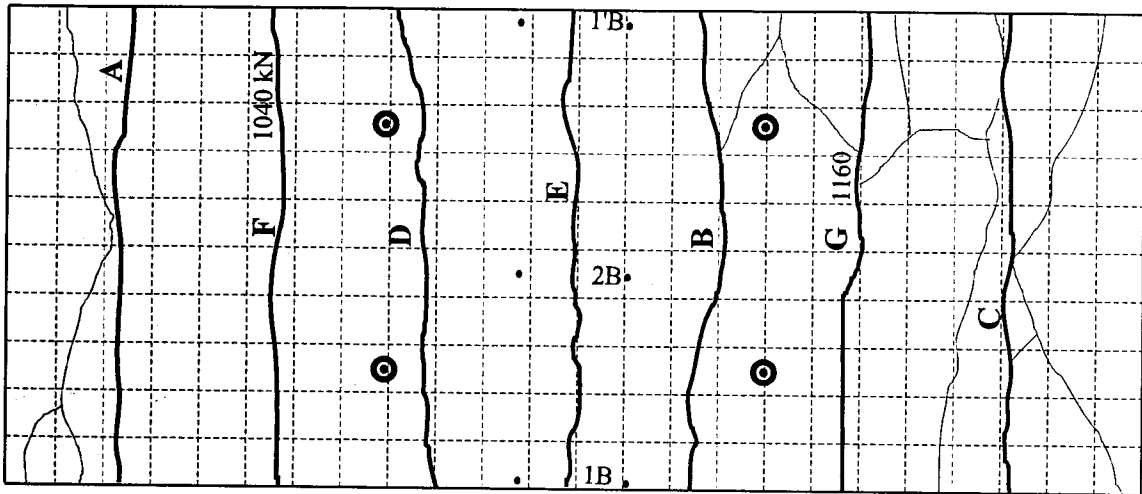


Figure 4.21 Cracks pattern for specimen 3C

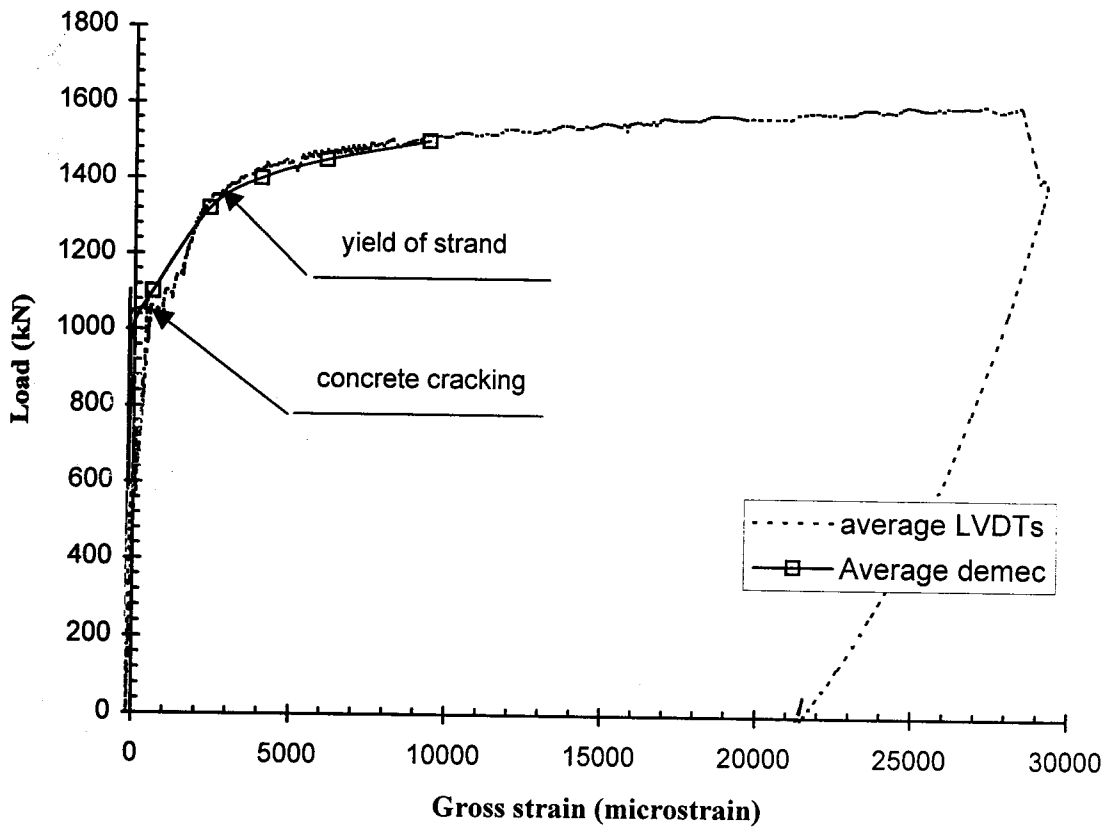
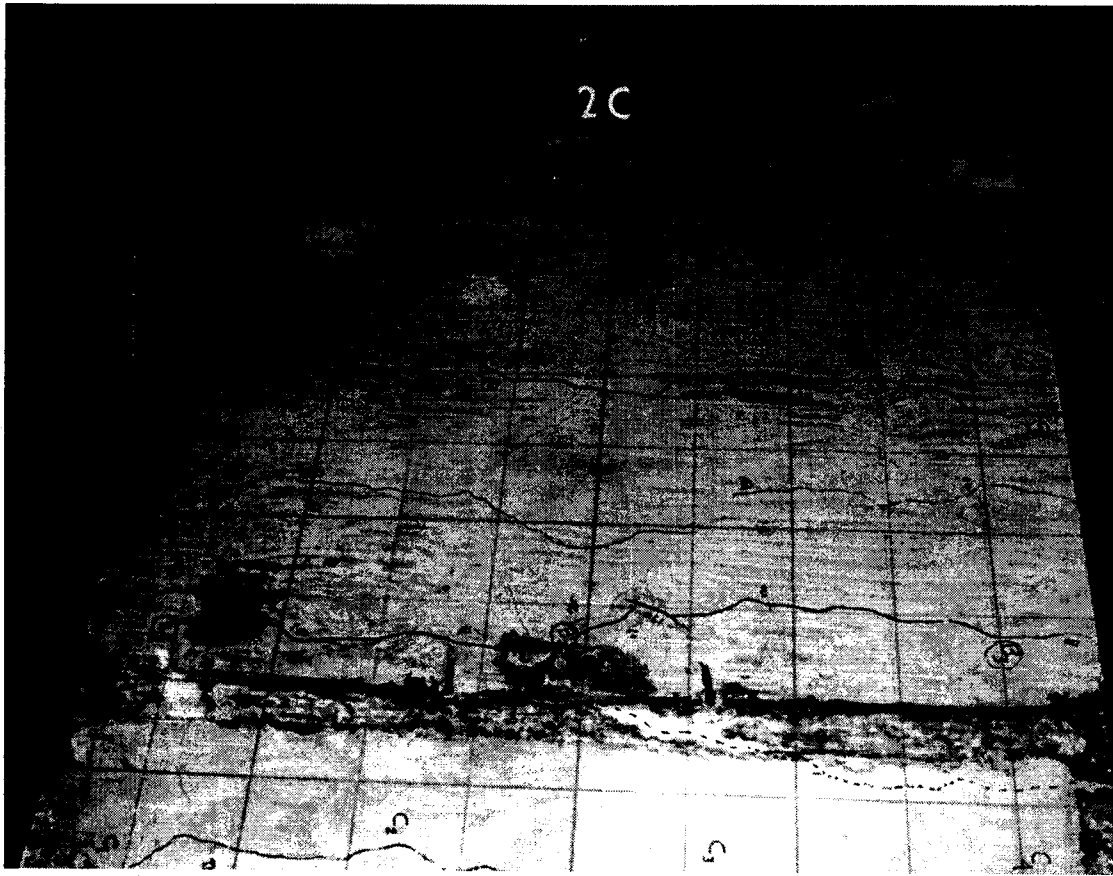
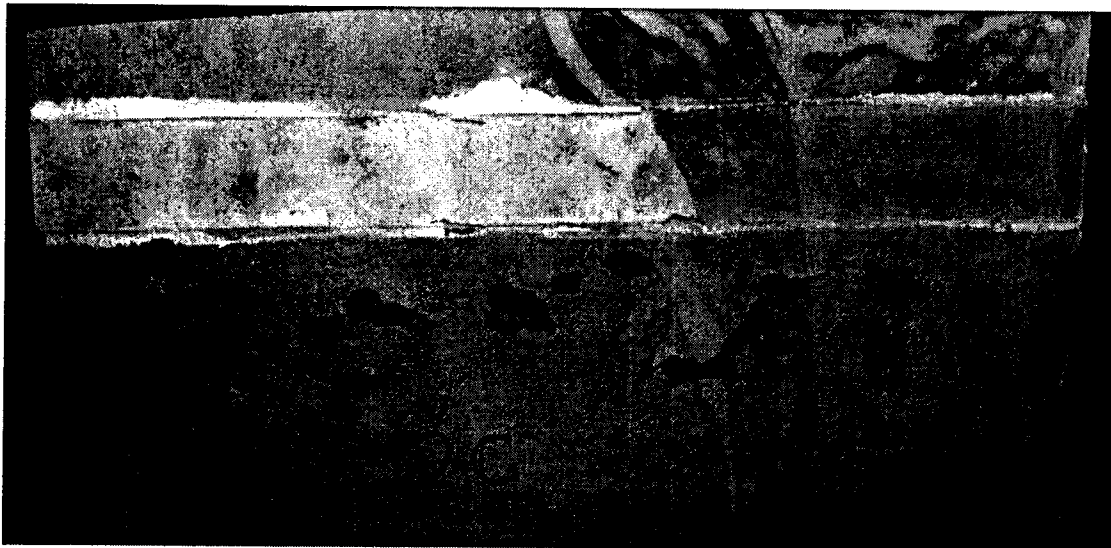


Figure 4.22 Load versus gross concrete strain for specimen 3C



(a) Crack pattern



(b) Concrete spalling on the compression side

Figure 4.23 Failure mode of specimen 2C

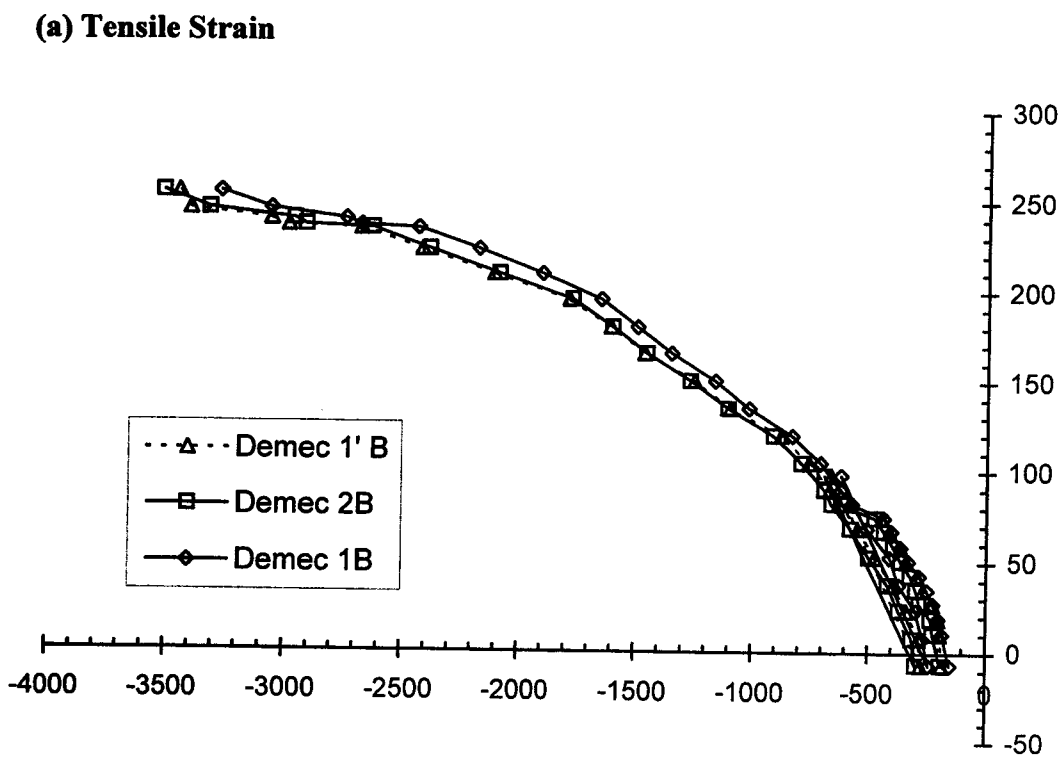
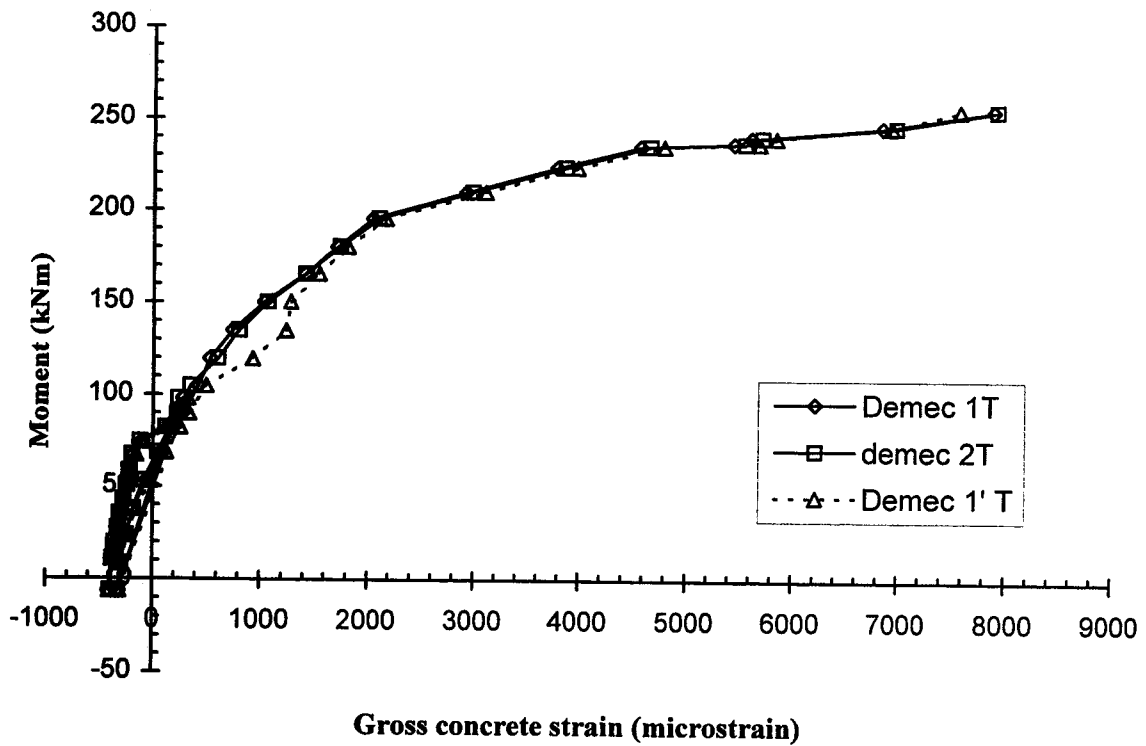


Figure 4.24 Moment versus gross concrete strain for specimen 2C

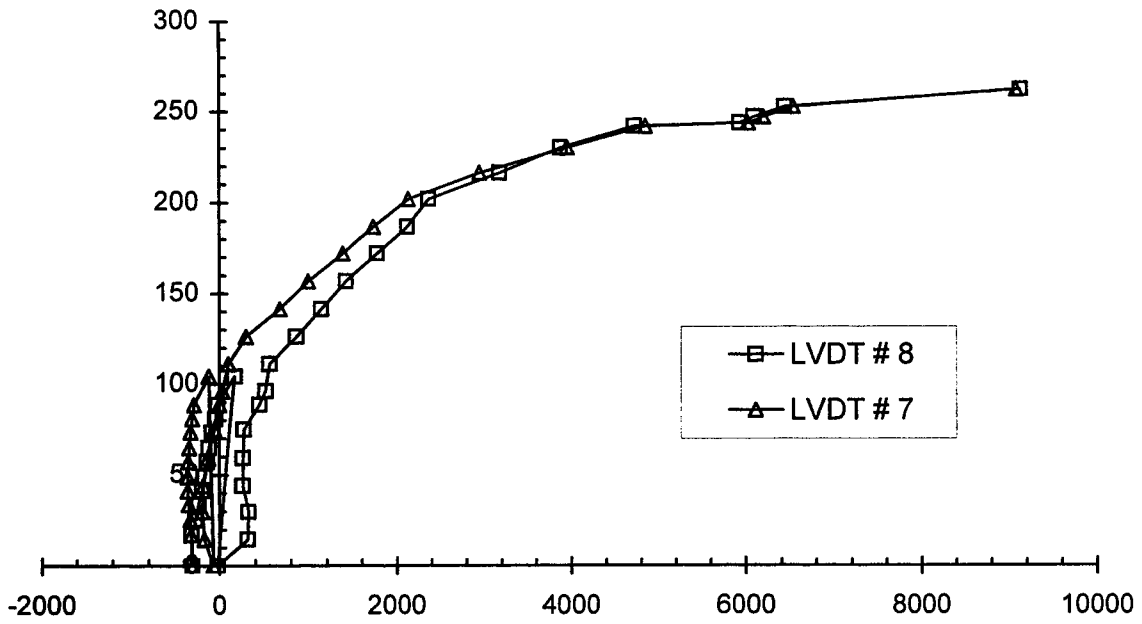


Figure 4.25 Moment versus non-prestressed steel strain for specimen 2C

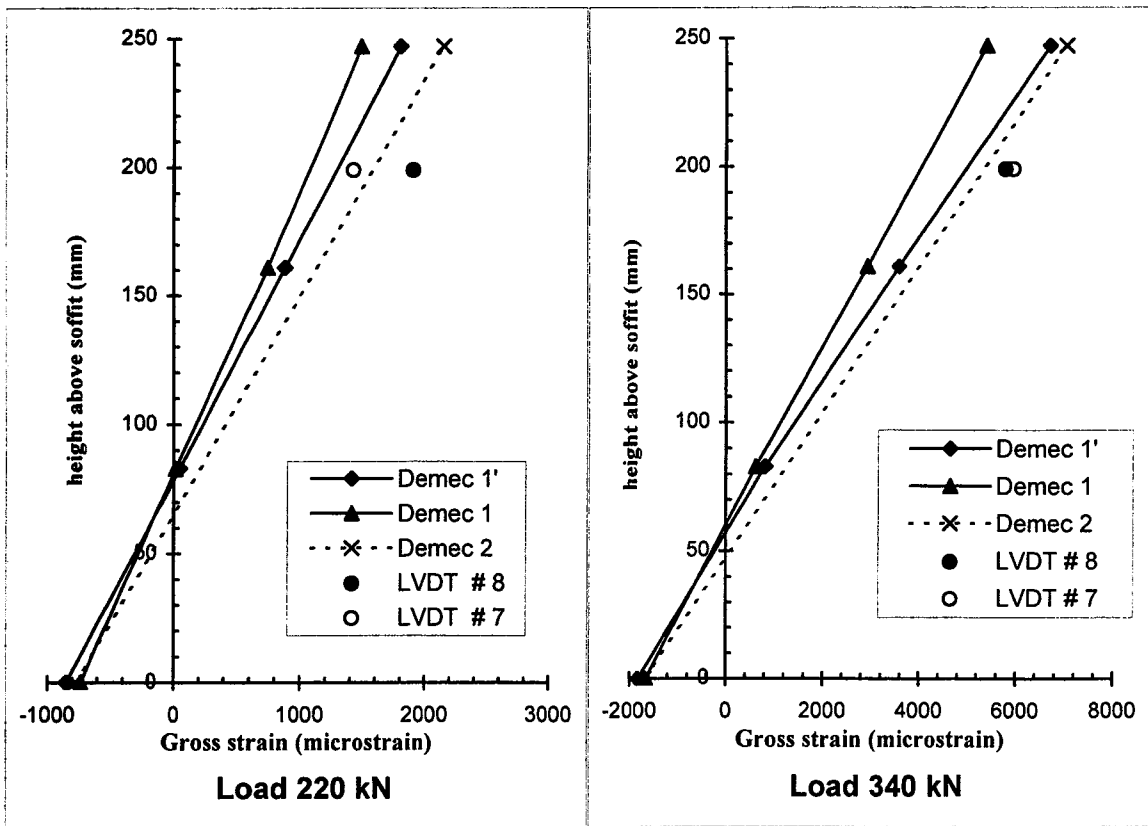


Figure 4.26 Examples of strain distribution plotted at each load level using Demec and LVDT readings for specimen 1C40

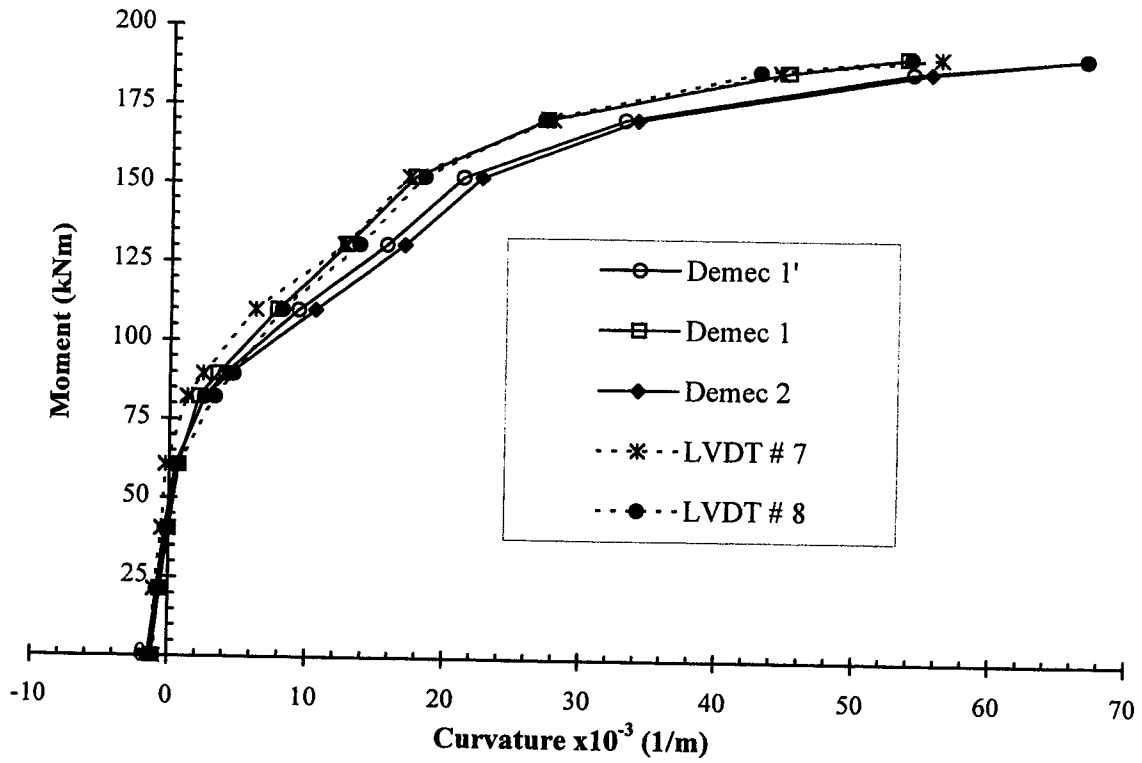


Figure 4.27 Moment versus curvature for specimen 1C40

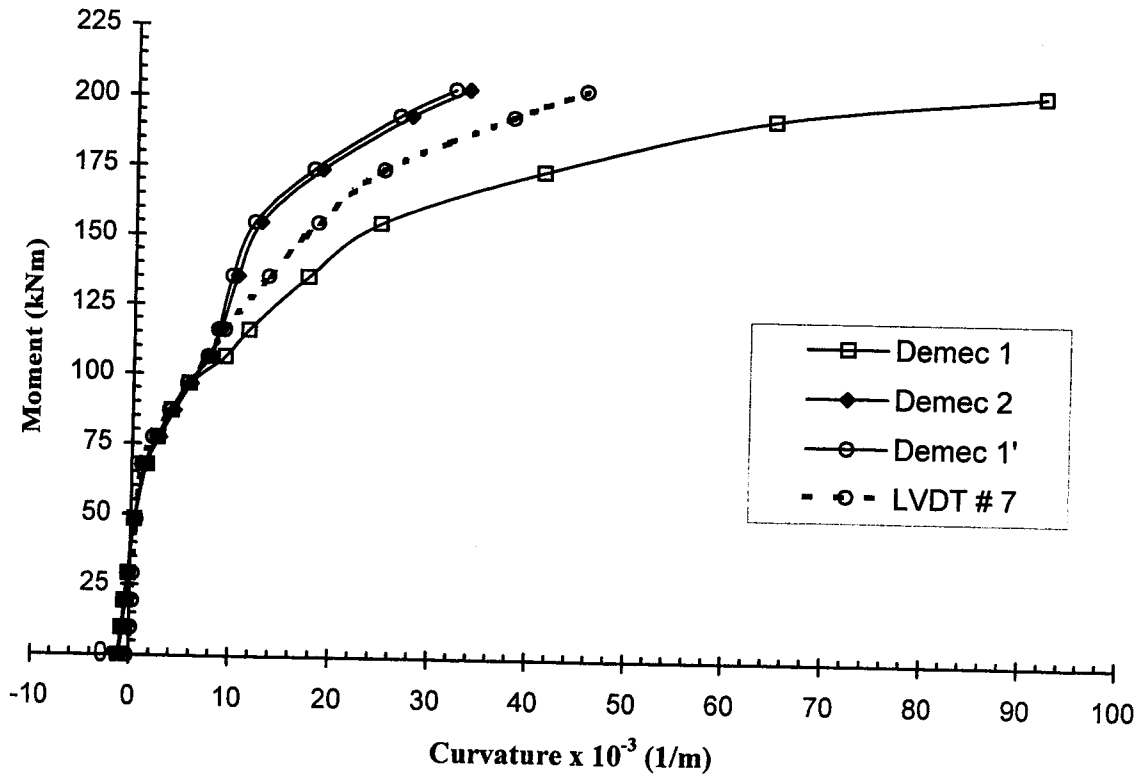


Figure 4.28 Moment versus curvature for specimen 1C20

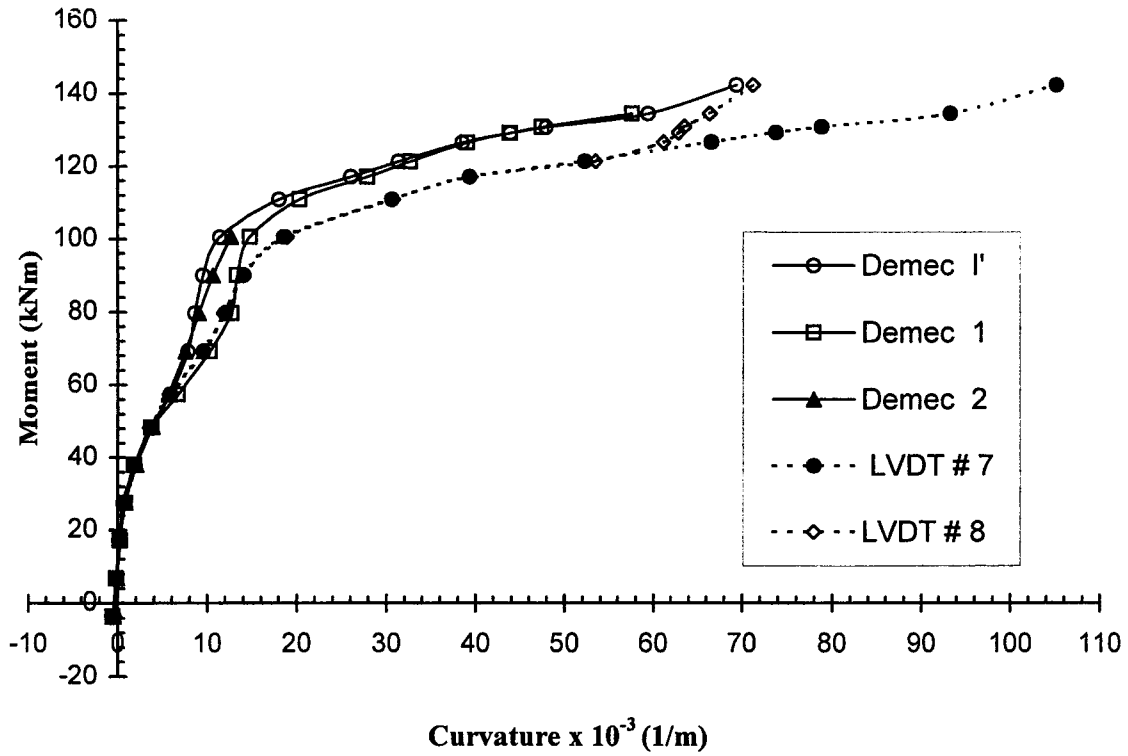


Figure 4.29 Moment versus curvature for specimen 2A

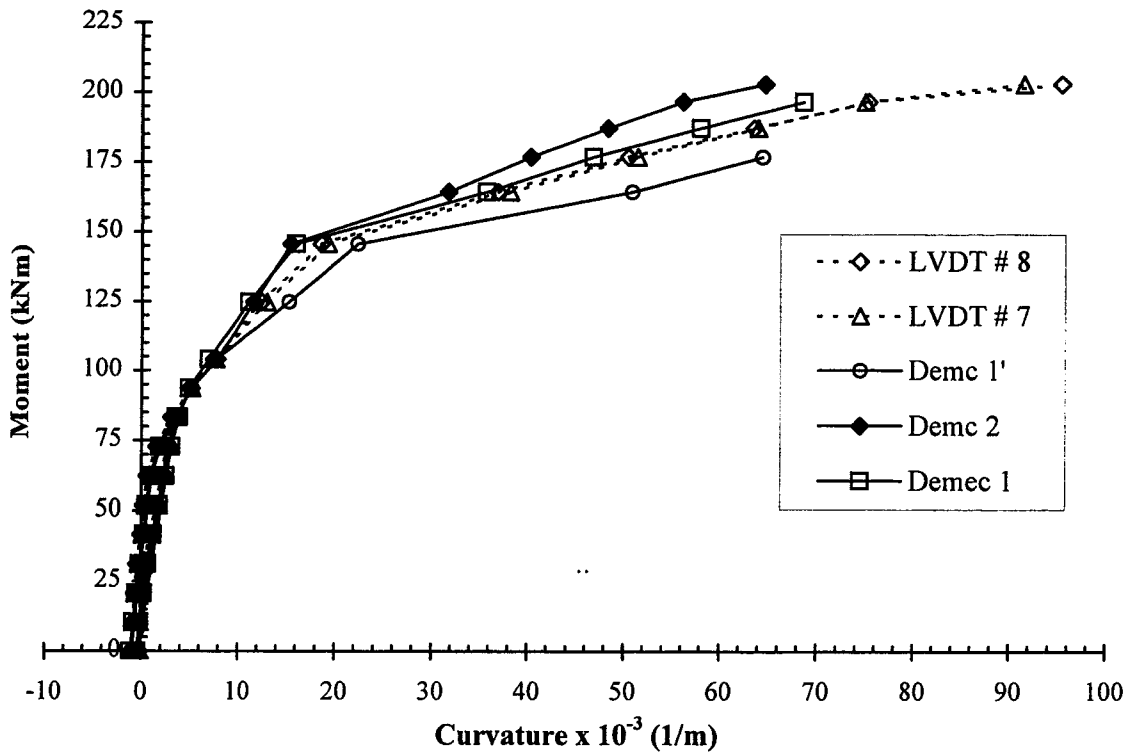


Figure 4.30 Moment versus curvature for specimen 2B

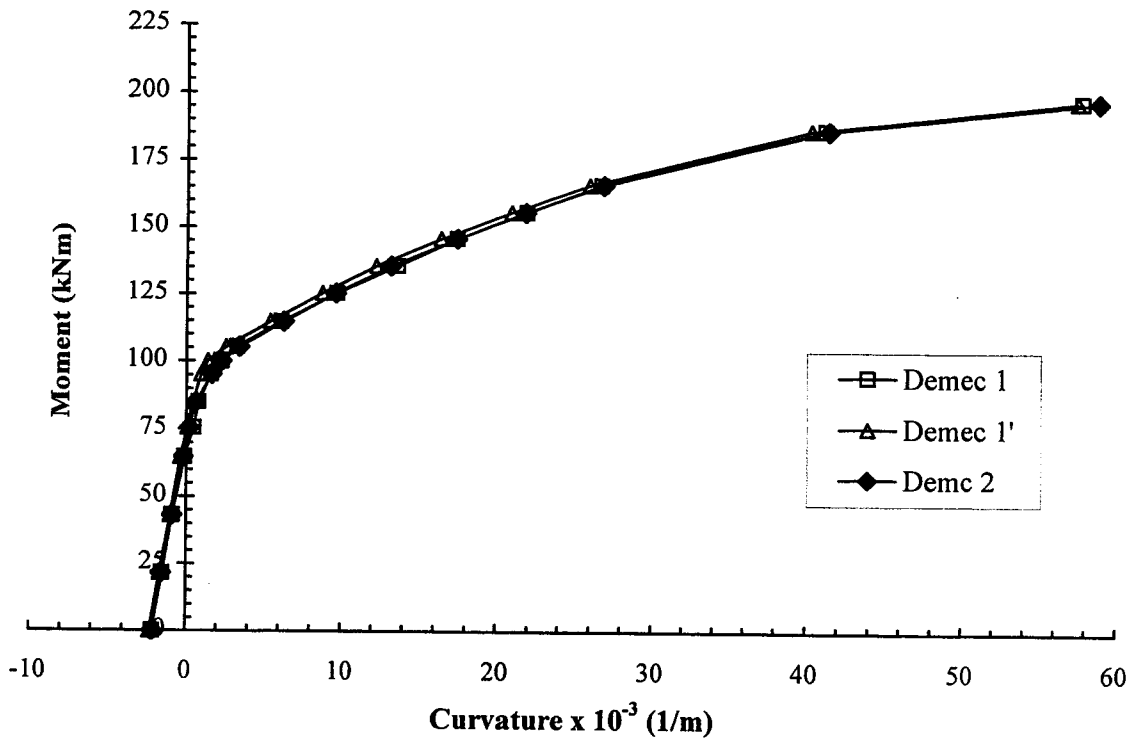


Figure 4.31 Moment versus curvature for specimen 3A

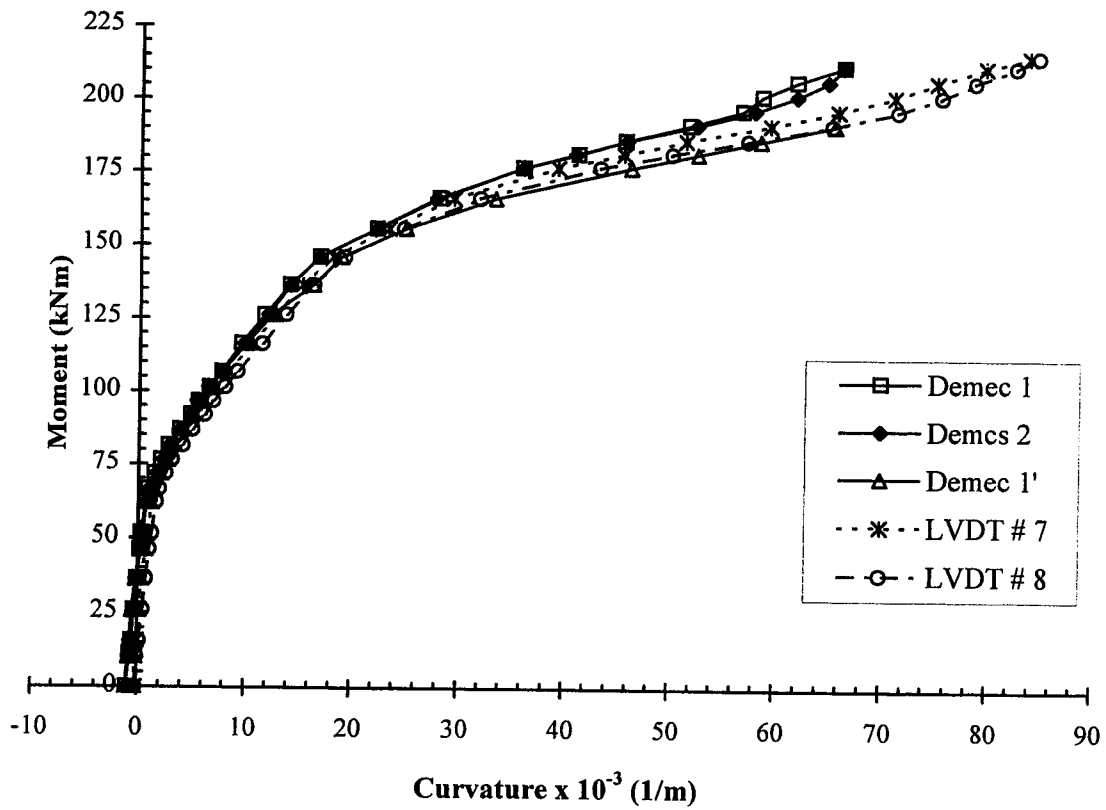


Figure 4.32 Moment versus curvature for specimen 3B

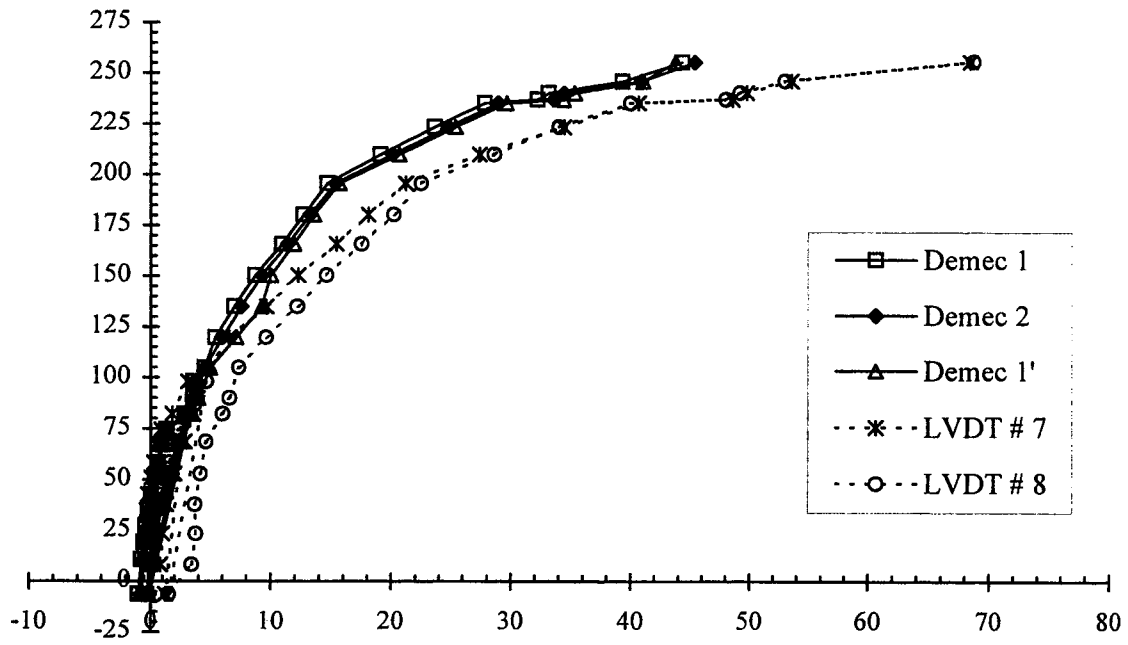


Figure 4.33 Moment versus curvature for specimen 2C

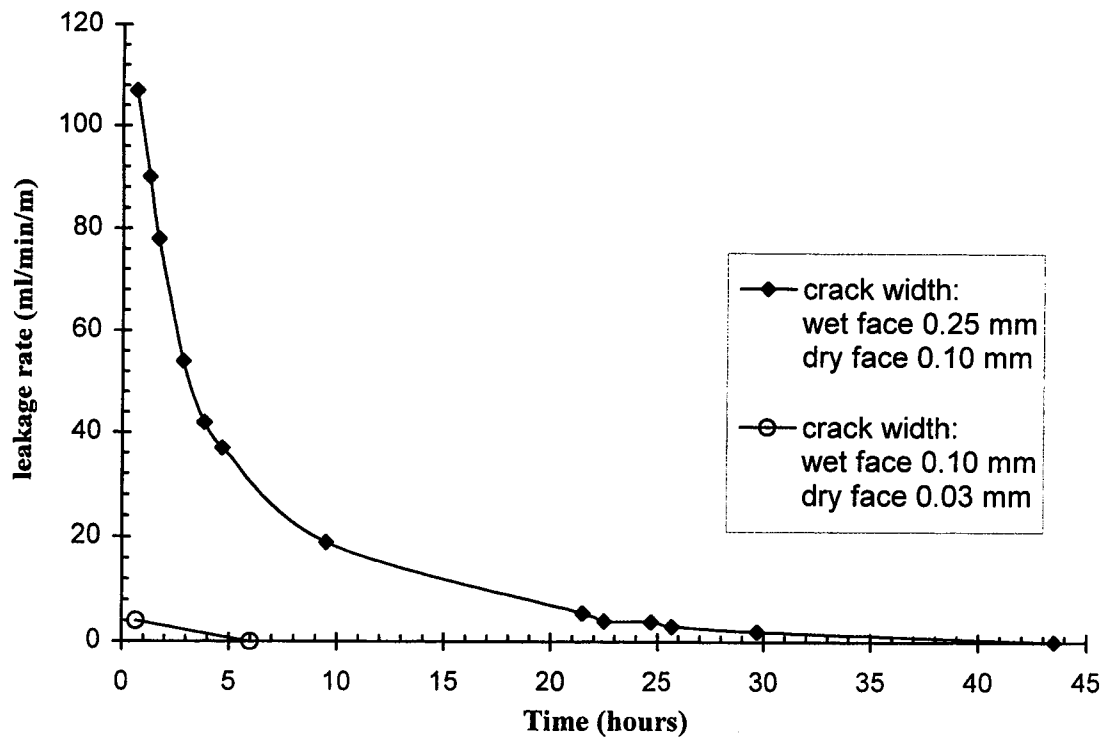


Figure 4.34 Leakage rate for the through cracks in specimen 3C

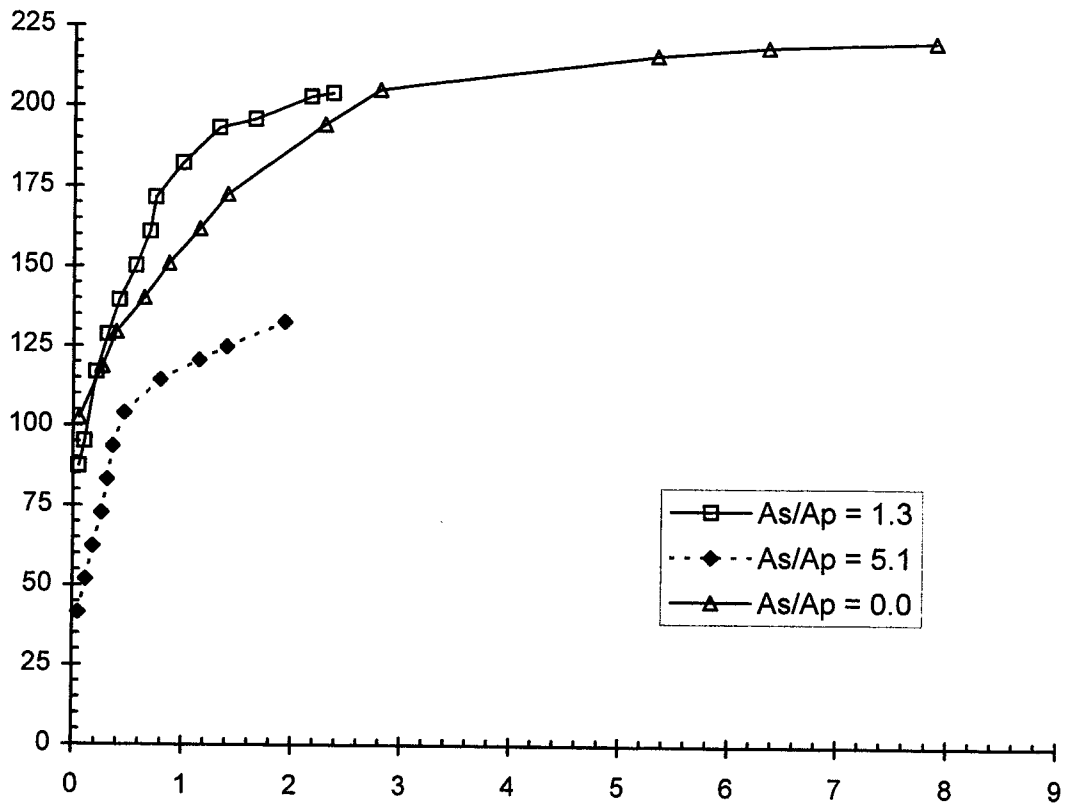


Figure 4.35 Effect of level of partial prestressing on crack width

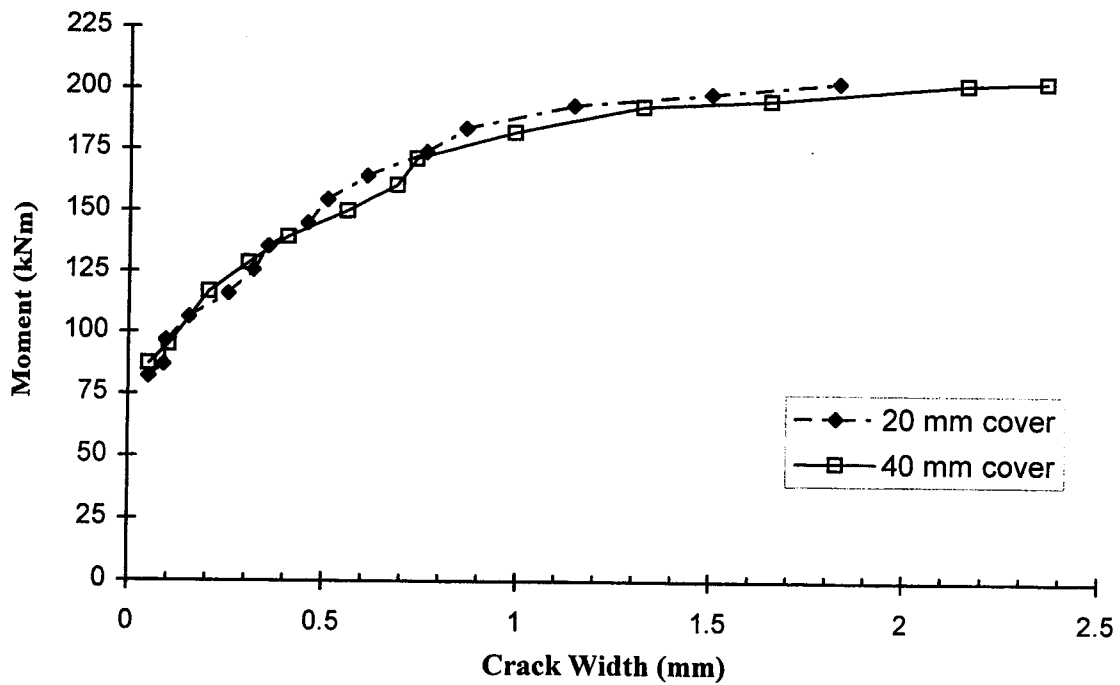
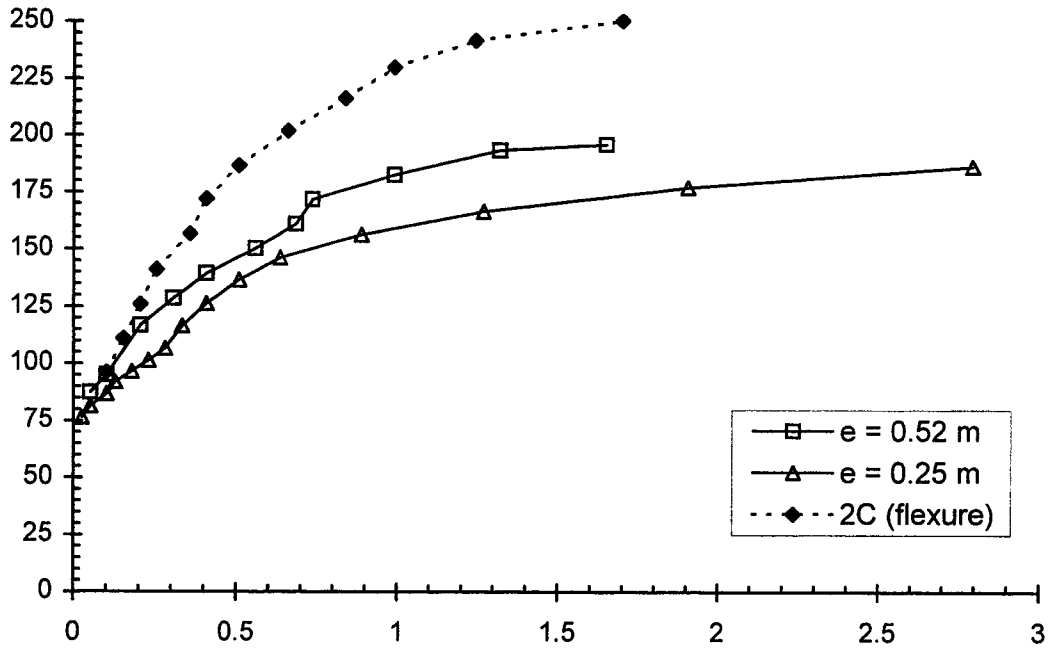
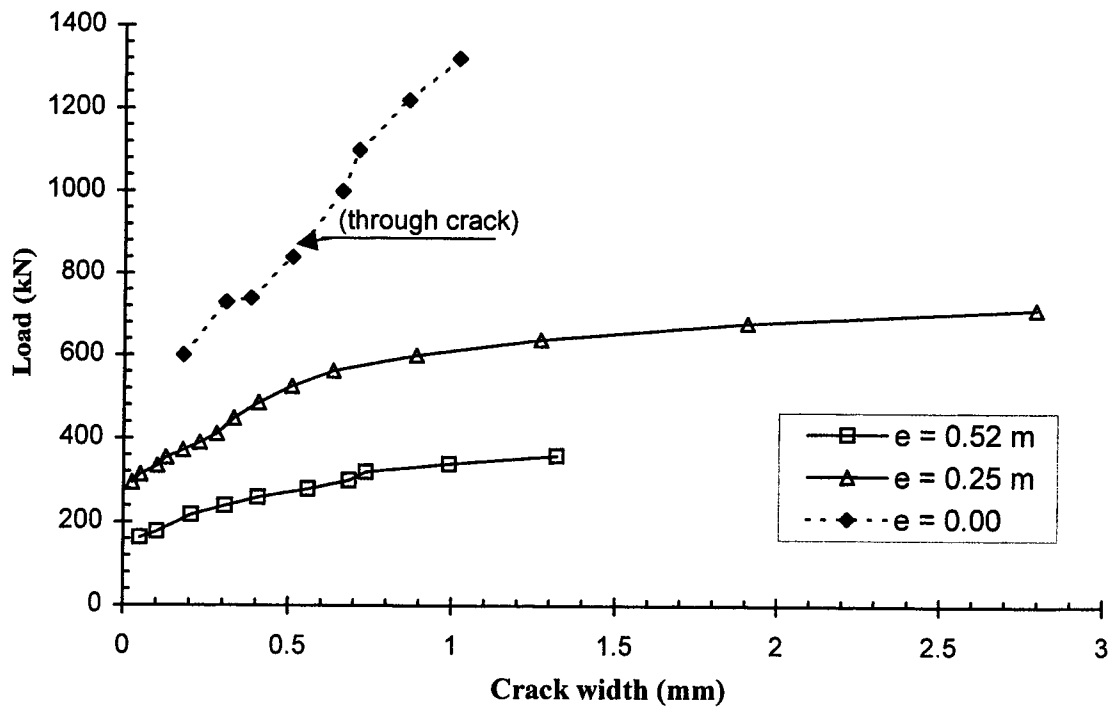


Figure 4.36 Effect of concrete cover of non-prestressed steel on crack width



(a) Moment



(b) Load

Figure 4.37 Effect of load eccentricity on crack width

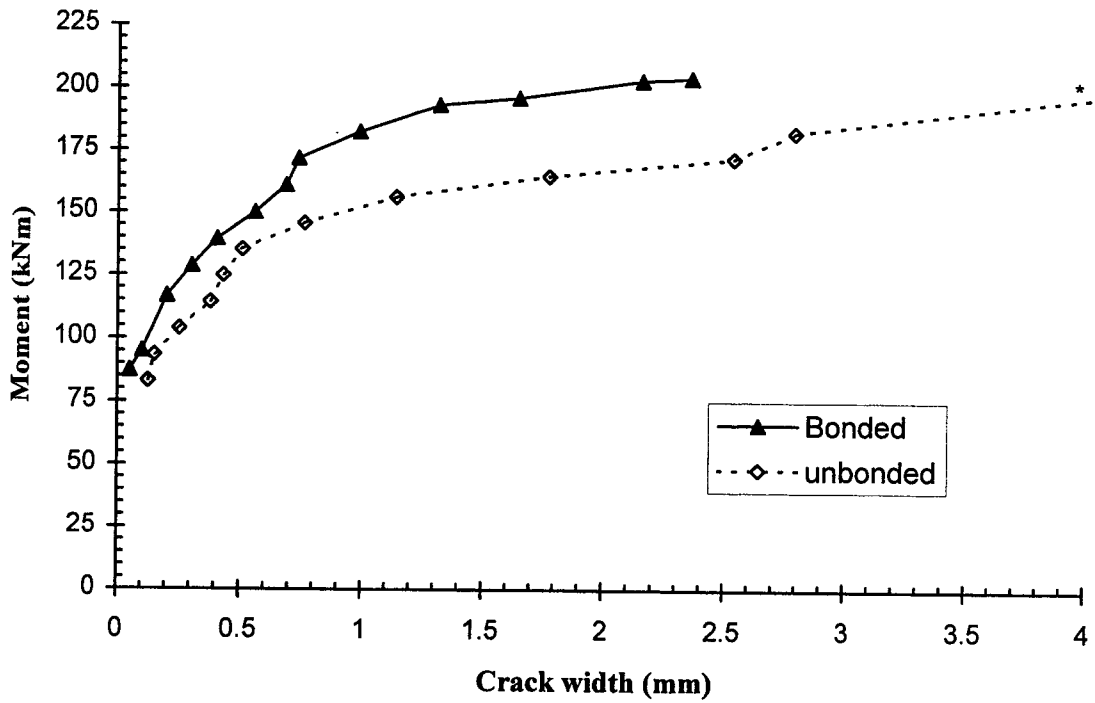


Figure 4.38 Effect of bond characteristic of tendons on crack width

(* the last data point at crack width 8 mm is not shown)

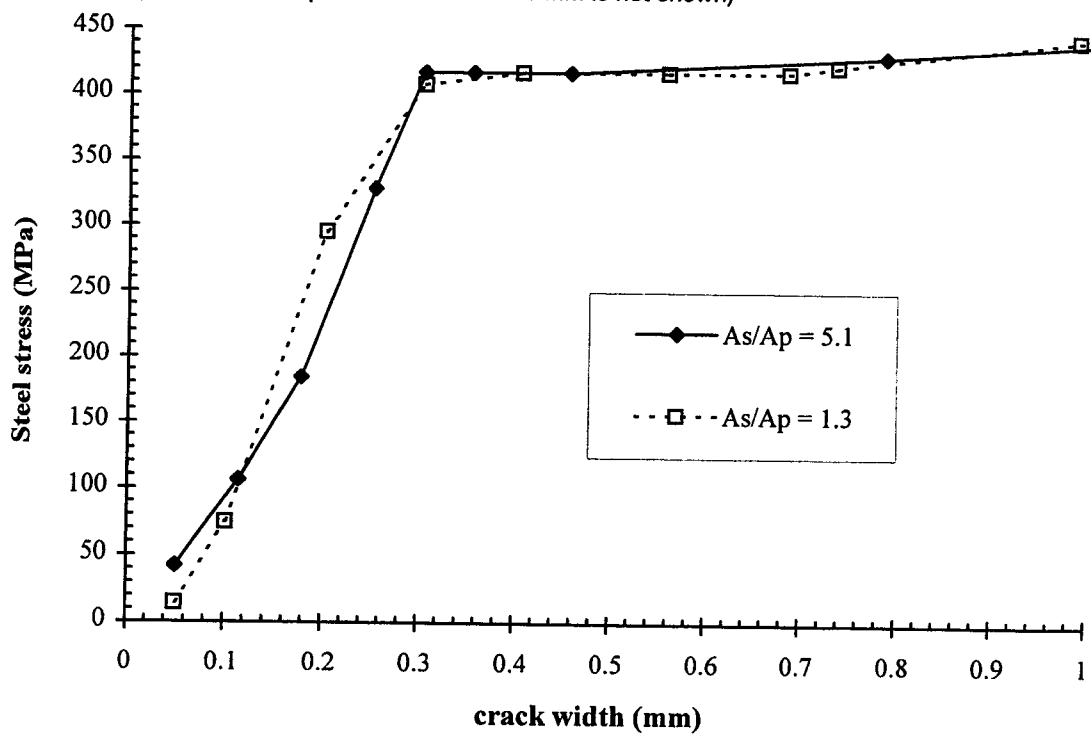


Figure 4.39 Effect of level of prestressing on the relation between crack width and steel stress

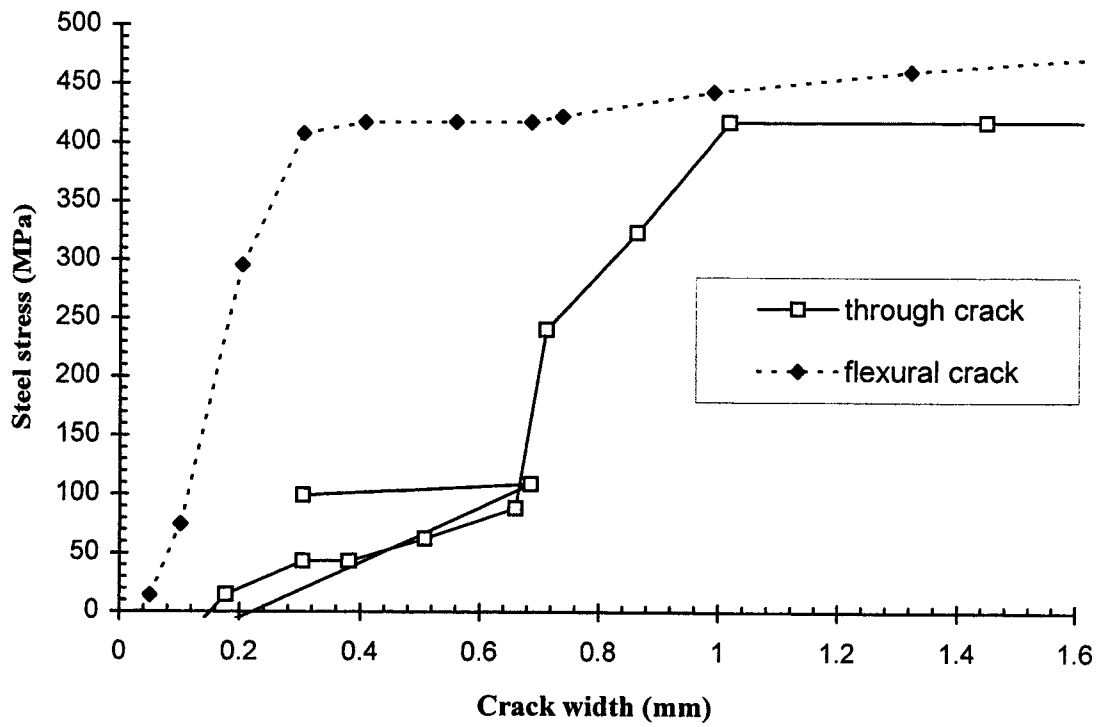


Figure 4.40 Non-prestressed steel stress versus crack width for flexural and through cracks

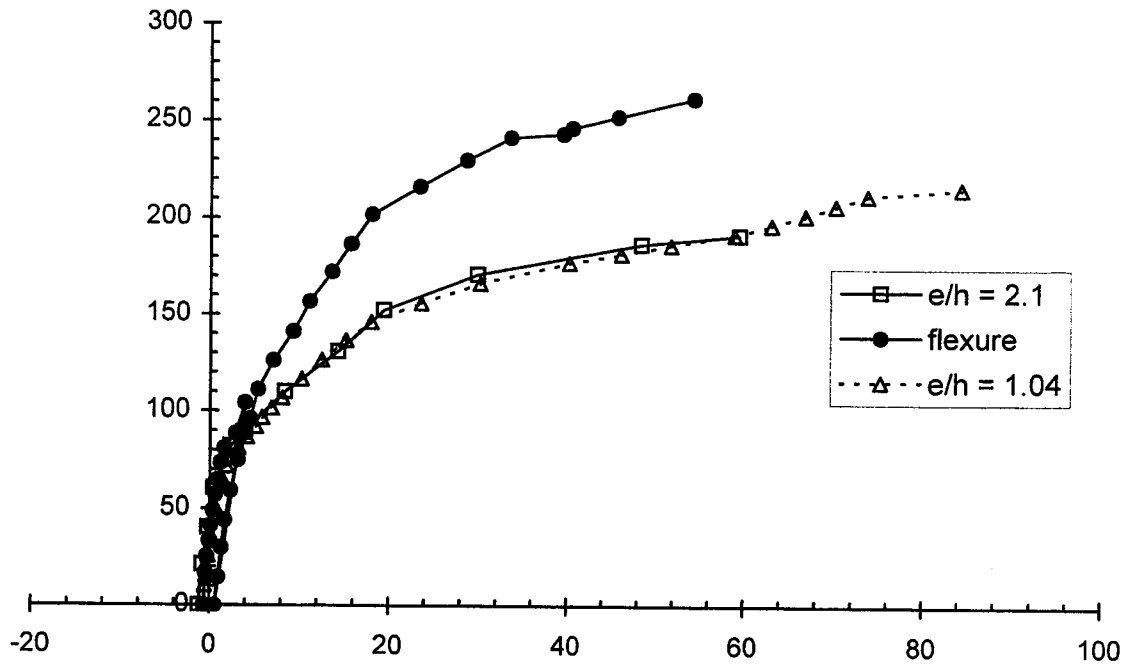


Figure 4.41 Effect of load eccentricity on moment-curvature relationship

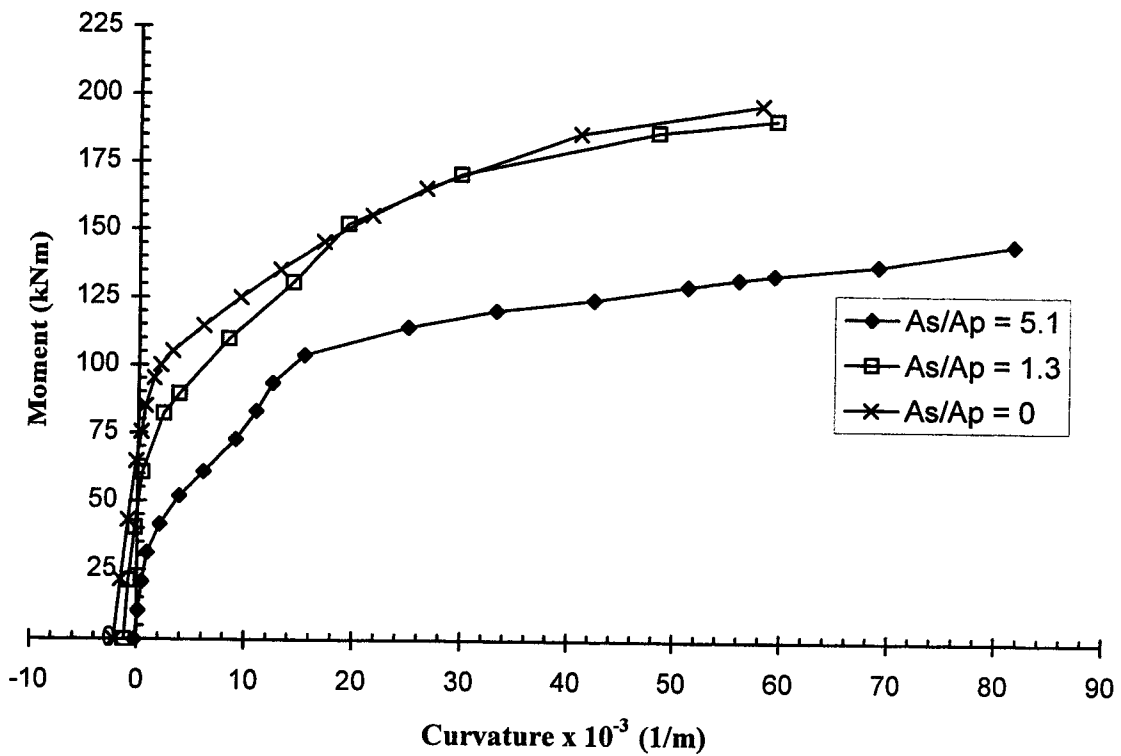


Figure 4.42 Effect of partial prestressing level on moment-curvature relationship

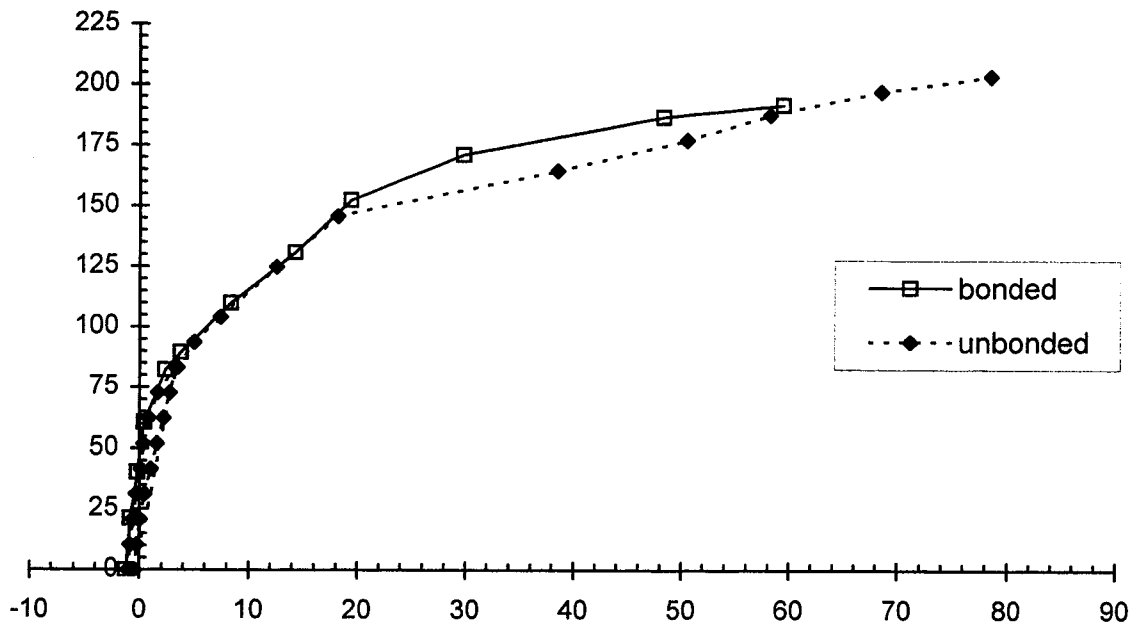


Figure 4.43 Effect of tendon bond characteristics on moment-curvature relationship

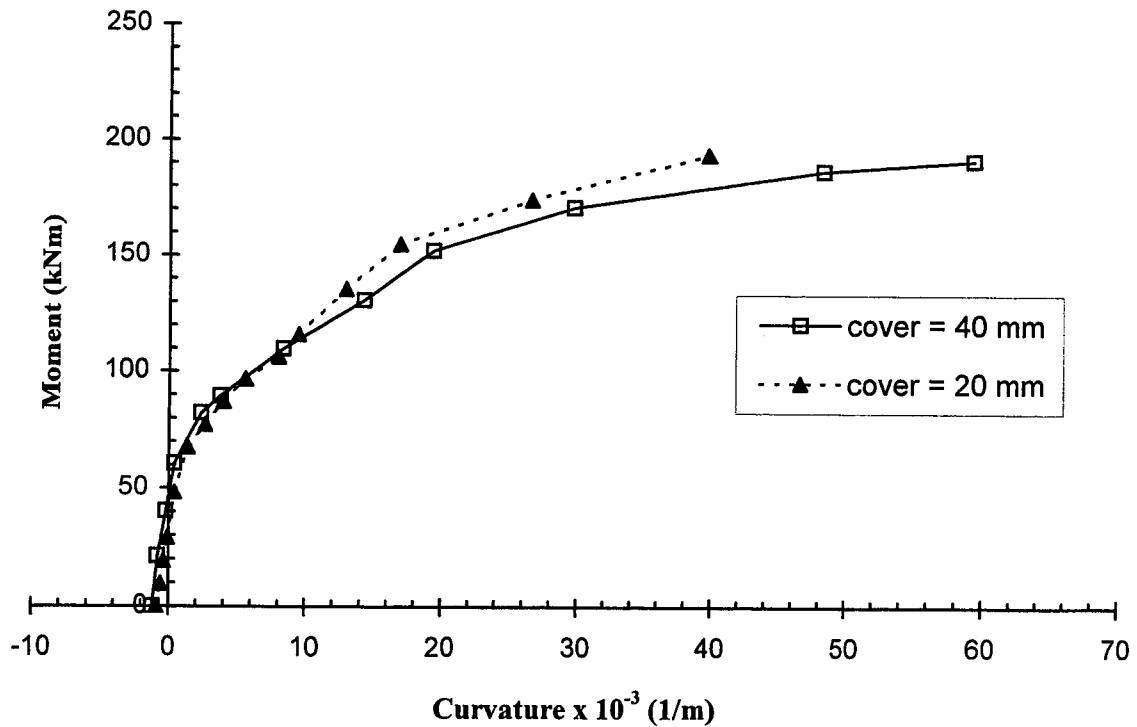


Figure 4.44 Effect of non-prestressed steel concrete cover on moment-curvature relationship

5- Analytical Model

5.1 Introduction

This chapter presents a description of an analytical model written using Visual Basic to analyze partially prestressed concrete sections. Description of the model, the material constitutive laws used in it and a verification of it are given in Sections 5.2 through 5.5. The model was employed to simulate the experimental test specimens. The results of the simulations are presented in Section 5.6. It was also used to model third-party test specimens, which are presented in Section 5.7.

5.2 Description of the Analytical Model

A Visual Basic computer program was developed to perform a plane section analysis of reinforced, prestressed and partially prestressed concrete sections. In performing this analysis, a linear strain distribution is assumed over the cross section at all load levels. The corresponding stresses are obtained from stress-strain relationships. The cross section is divided into 100 layers and a numerical integration is used to obtain the corresponding forces and moments.

The program starts by calculating concrete strains corresponding to zero external loading then increases the concrete strain at the extreme fibre on the compression side, by increments of 25 microstrain (compression) until failure. For each increment, the model calculates, by trial and error, the other extreme fibre strain that satisfies a given eccentricity. Consequently, for this strain distribution, the program calculates moment, axial load, curvature, concrete compressive stress at extreme fibre, non-prestressed and prestressed steel stresses and the depth of the compression zone. The program recognizes failure when the strain at any of the concrete extreme fibres, non-prestressed steel or prestressing steel, exceeds its ultimate strain. The program considers the effect of creep and shrinkage of concrete and calculates deformations and forces before and after

considering this effect. The program displays the results directly on a spreadsheet and automatically creates plots for moment versus curvature and other responses.

The input of the program includes: section and material properties, reinforcement area, load eccentricity, initial strain in concrete due to shrinkage and creep, creep coefficient, free shrinkage strain and prestressing steel initial strain. The material models for concrete, non-prestressed steel and prestressed steel are grouped in a separate module as separate functions to facilitate modifying any one of them without affecting the rest of the program. A listing of the program is provided in Appendix A.

5.3 Material Constitutive Laws

5.3.1 Concrete in Compression

Compressive tests were conducted on three concrete cylinders for each specimen on the same day as the test, as described in Chapter 3. In addition to concrete strength, the full response of the cylinder was obtained for each compression test. Two and sometimes three stress-strain curves were obtained for each specimen from the cylinder compression tests. Curve fitting was used to produce relationships simulating an average stress-strain response for each specimen. This average curve was unique for each specimen and used in the analytical study. Each curve consists of different cubic relationships for ascending and descending branches. Figure 5.1 shows examples of these curves.

5.3.2 Concrete in Tension

While tensile behavior in concrete usually does not significantly affect the ultimate strength of a member, the effect of tensile stresses in concrete must be taken into account when the serviceability characteristics of a member are needed. It is known that reinforced concrete can display significant additional stiffness after cracking due to tension stiffening. This effect is simulated using stress-strain relationships for concrete in

tension so that the strain and curvatures obtained would represent average values in the cracked zone rather than the peak values at crack locations.

Several tension stiffening models are proposed in the literature. Three models were examined in the present study. These three models are those of Vecchio and Collins (1986), Massicotti *et al.* (1990) and Foster (1992). The three models are plotted in Fig. 5.2 for three different partial prestressing ratios. A description of these models is given below.

Vecchio and Collins (1986) proposed the following equation to simulate the post-cracking behaviour of reinforced concrete based on correlation with test data:

$$f_{cl} = \frac{f_{cr}}{1 + \sqrt{200\varepsilon_1}} \quad (5.1)$$

This equation was modified later as given by Collins and Mitchell (1987) to

$$f_{cl} = \alpha_1 \alpha_2 \frac{f_{cr}}{1 + \sqrt{500\varepsilon_1}} \quad (5.2)$$

The factors α_1 and α_2 represent bond characteristics of tendons and load history respectively. Collins and Mitchell (1987) suggested that the cracking stress of concrete be taken as:

$$f_{cr} = 0.33\sqrt{f'_c} \quad (5.3)$$

Massicotte *et al.* (1990) derived stress-strain relationships modeling the post-cracking behavior. Equilibrium of forces between the cracked and the uncracked regions is considered at control points that represent the states of stabilized cracking and yielding of reinforcement at the crack. The curve is assumed to be quadratic between these two points. Concrete tensile stress is considered zero when the average strain in the member reaches the reinforcement yield strain. The curve is considered linear between this point

and the point of yielding of reinforcement at the crack. Detailed equations can be found in Massicotte *et al.* (1990).

Foster (1992) modified the linear relationships suggested by Al-Manaseer and Phillips (1987) to recognize the fact that concrete cracking may occur at values considerably lower than the uniaxial cracking stress, f'_c . The stress-strain curve after cracking is defined by:

$$f_{c1} = f_{cr} \left(\alpha_2 + \frac{(1 - \alpha_2)(\alpha_1 - \frac{\epsilon_1}{\epsilon_{cr}})}{(\alpha_1 - 1)} \right) \leq f_{cr} \quad \text{for } \epsilon_1 < \alpha_1 \epsilon_{cr} \quad (5.4 \text{ a})$$

$$f_{c1} = \alpha_2 f'_c \leq f_{cr} \quad \text{for } \epsilon_1 \geq \alpha_1 \epsilon_{cr} \quad (5.4 \text{ b})$$

In this equation the factors α_1 and α_2 are material constants, different than those used by Vecchio and Collins. In using this model to simulate his own test results, Foster used $\alpha_1 = 10.0$ and $\alpha_2 = 0.3$ and he estimated the concrete cracking stress to be in the range of $0.3\sqrt{f'_c}$ to $0.4\sqrt{f'_c}$ to best match the observed test results. Furthermore, when Foster used the model to simulate others test results he always used α_1 as 10.0 but changed α_2 in the range of 0.2 to 0.8 to match test results. This wide range of α_2 implies that Foster considered that the average tensile stress could remain higher than 0.8 of the cracking stress at fairly high average strains.

The three tension stiffening models were incorporated in the developed analytical model to simulate the response of some tested specimens. The results are presented in Section 5.5.

5.3.3 Effect of Creep and Shrinkage

Creep and shrinkage of concrete directly affect the strain and consequently the curvature of a member. Creep and shrinkage also induce stresses in a restrained concrete member producing additional axial forces and moments. This effect is calculated in the

analytical model by employing the method described by Ghali and Favre (1986). However, there was no need to calculate theoretical values for the creep coefficient, ϕ , or shrinkage strain, ϵ_{cs} , of the tested specimens. The change of concrete strain due to shrinkage and creep was already measured during the test as explained in Chapter 3. Therefore, the measured strains were used to calculate realistic values of ϕ and ϵ_{cs} that were used in the analytical model in conjunction with the measured strains to calculate the change in stresses and consequently moments and loads. A summary of the effect of shrinkage and creep on the tested specimens is given in Table 5.1 and the procedure used in these calculations is explained in Appendix B.

It should be noted that in the test results the initial load was considered zero while the effect of shrinkage and creep of concrete was included in initial strain readings. This means that shrinkage and creep effects were considered only on deformations not loads. Therefore, in comparing analytical and experimental results, the predicted values of loads and moment were those without shrinkage and creep effects while the predicted values for deformations and stresses were those including that effect.

5.3.4 Non-Prestressed Steel

The two stress-strain curves obtained from tension tests on coupon samples of the reinforcement were simulated in the analytical study by a model consisting of three stages described by the following relationship:

$$f_s = E_s \epsilon_s \quad \epsilon_s \leq \epsilon_y \quad (5.5 \text{ a})$$

$$f_s = f_y \quad \epsilon_y < \epsilon_s \leq \epsilon_{st} \quad (5.5 \text{ b})$$

$$f_s = 369604\epsilon_s^3 - 105391\epsilon_s^2 + 10015\epsilon_s + 368 \quad \epsilon_{st} < \epsilon_s \leq \epsilon_u \quad (5.5 \text{ c})$$

Equation 5.5 is plotted in Fig. 5.3 against tension test results. Equation 5.5 is shifted from the test results by the difference between the observed yield stress and the static yield stresses.

5.3.5 Prestressing Steel

The stress-strain response for prestressing steel obtained from the tension tests described in Chapter 3 was modeled using the modified Ramberg-Osgood function recommended by Mattock (1979) up to a strain of 38000. After that strain the slope of the curve, obtained from the test, reduces. The part of stress-strain response between a strain of 38000 until ultimate strain was modeled using a quadratic function.

$$f_p = E_p \varepsilon_p \left(A + \frac{1-A}{[1+(B\varepsilon_p)^C]^{1/C}} \right) \quad \varepsilon_p < 38000 \quad 5.6(a)$$

$$f_p = -92822 \times 10^{-12} x^2 + 0.010587x + 1527 \quad 38000 \leq \varepsilon_p < 63200 \quad 5.6(b)$$

The modulus of elasticity E_p is 200000 MPa. The three constants A, B and C which define the Ramberg-Osgood function are taken as 0.03, 116.5, and 10 respectively. Figure 5.4 shows a plot of this equation against the curves obtained from the tension tests.

5.4 Verification of the Analytical Model

Specific problems were analyzed manually in a spreadsheet and the results of each step were verified carefully against that obtained using the developed model. The model was also verified against the program RESPONSE (Collins and Mitchell, 1991). Some tested specimens were simulated using both RESPONSE and the developed model. During this comparison, the material constitutive laws used in the developed model were chosen to be the same as used in RESPONSE. The simulation was performed for three specimens subjected to eccentric tension. With two different partial prestressing ratios, A_s/A_p , of 1.3 and 5.0, and two different eccentricities of 520 and 260 mm for specimens 1C40 and 2A, and specimens 1C40 and 3B, respectively. Moment versus curvature diagrams resulting from the two programs for the three specimens are plotted against the corresponding experimental results and shown in Figs. 5.5 through 5.7. It is clear that responses obtained from the two programs completely

coincide. However, responses obtained from both programs are stiffer than the response of the tested specimens in the range between cracking and yielding and softer after that. This discrepancy was the reason that led to the development of the analytical model rather than relying on an existing program like RESPONSE. It is believed that using appropriate material models, particularly the tension stiffening model, can produce better results.

5.5 Tension Stiffening Model

The three tension stiffening models described in Section 5.3 were incorporated in the developed analytical model to simulate the response of four tested specimens. Three of these specimens, specimens 3A, 1C40 and 2A, were tested under eccentric tension with the same load eccentricity but with three different partial prestressing ratios, A_s/A_p , of 0.0, 1.3 and 5.0, respectively. Specimen 3C tested under axial tension was also simulated. Figures 5.8 to 5.10 give moment versus curvature diagrams for the three specimens 3A, 1C40 and 2A respectively. The curves obtained using the three tension stiffening models are plotted in each figure together with two additional plots. One plot represents the experimental results (the average of Demecs and LVDT readings) and the second gives the analytical model results neglecting the contribution of concrete after cracking. The figures show that the predicted responses by all the three tension stiffening models are stiffer than the experimental results in the region of service loading, between cracking and yielding. At higher loads the three models predict a softer response than the tests, with the Massicotte model producing the lowest moments and the Foster model producing the highest moments. Figure 5.2 explains this difference since the descending part of Massicotte's model has the steepest slope and vanishes completely when the average concrete strain equals the non-prestressed yield strain, while the Vecchio and Collins and the Foster models continued beyond this strain with a considerable concrete tensile stress. Vecchio and Collins (1986) stated that significant tensile stresses were found in the concrete between the cracks even at very high average tensile strain. Experiments conducted by Gilbert and Warner (1978) showed also that concrete

maintains an average tensile stress varying between 0.3 to 0.7 f_{cr} even at high average tensile strain.

Figure 5.11(a) shows load versus gross concrete strain diagram for specimen 3C obtained by using the three tension stiffening models and from experimental test data. In this case Foster also significantly overestimates the section capacity while Massicotte underestimates it. Vecchio and Collins model on the other hand accurately predict the ultimate capacity of the section. The first part of the load-strain curves are enlarged in Fig. 5.11 (b) to study the impact of using these models on the prediction of the serviceability response of the member subjected to axial load. The figure yields many observations. The predicted cracking load, which is the same for the three models depending on the value specified for concrete cracking stress, was higher than that obtained from the test. The discontinuity of Vecchio and Collins model at cracking stress led to a drop in the load-strain curve which is inconsistent with test results. On the other hand, the constant concrete stress after cracking in the Foster model led to an increase and then a gradual decrease in the load, which also is inconsistent with test results. The steep decrease in concrete stress in the Massicotte model and neglecting the concrete contribution after yielding of the reinforcement affected the global behaviour.

The above observations led to the developing of a tension stiffening model that better simulates the present test results. This model has the following features: a lower cracking stress than $0.33\sqrt{f'_c}$ suggested by Mitchell and Collins, and concrete tensile stresses that gradually decrease after cracking without a sudden drop. Concrete still has some tension stress after the yielding of steel but not as high as in the Foster model.

With all the differences among the existing tension stiffening models and the scatter in test data collected by Vecchio and Collins (1986), there was no need to complicate the model. Therefore, the suggested tension stiffening model consists of two parts describing the post-cracking behaviour. The first part is non-linear and represents the gradual reduction in concrete tensile stress during the progress of cracks until a state

of stabilized cracking is achieved. The second part represents the stress history after that and can be constant or linear with a very flat slope. The model is plotted in Fig. 5.2 against the other three models and is given by the following equation:

$$f_{c1} = f_{cr} \left(\beta_2 + \frac{(1 - \beta_2) \left(\beta_1 - \frac{\epsilon_1}{\epsilon_{cr}} \right)^2}{(\beta_1 - 1)^2} \right) \leq f_{cr} \quad \text{for } \epsilon_1 < \beta_1 \epsilon_{cr} \quad (5.7 a)$$

$$f_{c1} = \beta_2 f_{cr} \leq f_{cr} \quad \text{for } \epsilon_1 \geq \beta_1 \epsilon_{cr} \quad (5.7 b)$$

In this equation the constant β_1 represents the extension of the non-linear part of the curve beyond the concrete cracking strain while β_2 represents the portion of cracking stress that remains after stable cracking. It was found from simulating the present experiments with this tension stiffening model that β_2 can be taken in the range of 0.3 to 0.5, while β_1 can be approximately taken as 15, and can be increased if the eccentricity or the ratio A_s/A_p increases. Increasing the ratio between the load at which stable cracking occurs and the cracking load is the reason for increasing β_1 . On the other hand, a significant reduction in β_1 should be considered in either partial prestressing with unbonded tendons or full prestressing.

As detailed in Chapter 4, in most specimens, a second and final set of cracking occurred after the first set. The ratio between the two loads at which these two sets occurred was about 1.4. In specimen 2A where A_s/A_p was high and in specimen 2C tested under flexure the ratio was about 1.75. In the case of full prestressing, specimen 3A, no second set of cracking occurred and in specimen 2B, unbonded tendons, random and very wide cracks occurred at different load levels due to lack of bond.

This model was used to predict the response of specimen 3C tested under axial tension, and the results are plotted in Fig. 5.12. Figure 5.12 (a) shows the full load verses concrete strain diagram, while Fig. 5.12 (b) shows the response to approximately the

level of the service load. In general, the two figures exhibit good agreement between the suggested model and test results.

The proposed tension stiffening model was incorporated in the proposed analytical model which was used to predict the response of all the tested specimens. The response predictions are presented in the next section.

5.6 Comparison between Analytical Predictions and Test Results

The eight tested specimens were modeled using the analytical model described earlier. The material properties for concrete used in this study and the parameters of the tension stiffening model are given in Table 5.2. The results for individual tests are presented below. The comparison between predicted and observed values included failure loads, moment versus curvature response, moment versus depth of compression zone, moment versus non-prestressed steel stresses and concrete tensile and compressive strains versus load. Detailed comparisons are provided for the standard specimen 1C40. For all the other specimens, only moment versus curvature response is shown unless certain response exhibits certain features. To account for the effect of dead load, the stresses due to the dead load moments were theoretically calculated for the uncracked transformed section. The corresponding strains were obtained by dividing these stresses by the concrete modulus of elasticity used in the analytical model. The obtained strains at the extreme fibres were approximately 11 microstrain for configuration C-I specimens and 20 microstrain for specimen 2C. These strain values are a result of a bending moment at the mid-span due to dead load of 3.6 and 6.3 kNm respectively. These dead load moment and the corresponding strains (and the curvatures) are added algebraically to the test results presented in the figures of this chapter to insure a consistent comparison with the analytical model. The latter predicts the total resistance of the wall section. The failure moments described below are those include the dead load moment.

For specimen 1C40, the analytical model predicted failure at a load of 404 kN when the concrete compressive strain exceeded the ultimate strain. This compares

favourably with the observed failure load of 405 kN that occurred due to crushing of the concrete on the compression side. The moment versus curvature, moment versus depth of compression zone and moment versus non-prestressed steel stresses are plotted in Figs. 5.13 through 5.15 respectively. From the results presented in these figures it can be seen that a good correlation exists between the test and the analytical model. Plots of the measured and the modeled concrete tensile and compressive strains versus load are given in Fig. 5.16 and 5.17 respectively.

The model predicted failure for specimen 1C20 by crushing of the concrete at a load of 393 kN. This load is 6.5% less than the observed failure load of 420 kN which occurred due to concrete crushing. The moment versus curvature and moment versus the depth of the compression zone graphs are given in Fig. 5.18 and 5.19, where it can be seen that the model was slightly stiffer than the test for a limited range of loading but in general a good correlation exists between the analytical and test results. Plots of concrete extreme fibre strain versus load produce the same conclusion.

For specimen 2A, where $A_g/A_p = 5.0$, the predicted failure of 294 kN due to crushing of concrete compares favourably with the observed failure load of 290 kN which occurred due to crushing of concrete. In both cases failure occurred well after yield of the non-prestressed steel. Comparing the predicted moment versus curvature graph with the experimental curve given in Fig. 5.20 shows that excellent correlation exists up to yielding of the non-prestressed steel where the modeled curve became softer. The load versus concrete tensile stress plots in Fig. 5.21 give similar results. Test results showed that tensile strains measured using Demec strain gauges were lower than tensile strains obtained from LVDT readings. Hence, concrete tensile strains at the extreme fibres obtained by interpolated LVDT readings were plotted on the same graph. The interpolated LVDT readings show better correlation than Demec points readings.

For specimen 2B, where the tendons were unbonded, the analytical model predicted failure at a load of 398 kN when the concrete compressive strain exceeded the ultimate strain. This compares favorably with the observed failure load of 400 kN that

occurred due to crushing of concrete on the compression side. However, the model was initially stiffer but became softer at high loads as shown in Fig. 5.22.

For specimen 2C tested under flexure, the predicted failure moment, 242 kNm, was slightly less than the observed value of 260 kNm. However both of them were due to crushing of concrete on the compression side. Figure 5.23 that shows plots of moment versus curvature indicates good agreement between test and analytical model although the model is slightly softer at high moments.

In specimen 3A, which was fully prestressed, the model predicted failure due to crushing of concrete at a load level of 385 kN which is only 6% less than the observed failure load of 410 kN. The moment versus curvature and moment versus depth of compression zone are given in Figs. 5.24 and 5.25 respectively. An excellent agreement can be seen in the latter figure while in the former the model predicted stiffer response for a range of load after cracking. It should be noted that during the test, the Demec points became loose during the last three load increments.

When modeling specimen 3B that had a load eccentricity half that of the other specimens, it was found that using the concrete cracking stress, f_{cr} , as $0.23\sqrt{f'_c}$ predicted a significantly low failure load. Therefore, unlike the other specimens, f_{cr} was taken as $0.33\sqrt{f'_c}$ and the tension stiffening parameter β_2 was taken as 0.6. This slightly increased the predicted failure load to 760 kN due to concrete crushing while the observed failure load was 860 kN with a difference of 13%. Increasing the value of f_{cr} used in the analysis, however, made the response of the specimen stiffer than the observed behaviour as shown in Fig. 5.26. The comparison presented in this figure indicates that, in general, a good correlation exists between the experimental test and the analytical model within the service load only. This implies that the model predicts the serviceability behaviour well. It should be noted that the rotation of the eccentric loading brackets reached 6.5° by the end of the test, which reduced the eccentricity and consequently increased the ultimate load.

5.7 Comparison of Analytical Predictions with Others Test Results

Some of the experimental studies carried out to investigate the serviceability of reinforced, prestressed and partially prestressed concrete members are presented in Chapter 2. Most of these studies were concerned about crack widths and the parameters affecting cracking. Most of the tests were conducted on beams subjected to bending moment and reported only crack widths and the beam deflection. Among the few tests conducted on specimens subjected to axial tension, those conducted by Alvarez and Marti (1996) were modeled and the results are presented in this section.

Alvarez and Marti (1996) carried out tension tests on seven conventionally reinforced and two prestressed concrete wall elements to investigate the influence of some selected parameters on the deformation behaviour and the deformation capacity of structural elements in pure tension. Partial prestressing of the longitudinal reinforcement was one of these selected parameters. All nine test specimens were 1000x3000 mm, 220 mm thick rectangular panels. The characteristics of the specimens are given in Table 5.3. Table 5.3 indicates that the non-prestressed reinforcement had high ductility in seven specimens and low ductility in two specimens, **Z4** and **Z5**. The properties of the materials used in these specimens are given in Table 5.4. The four reinforced concrete specimens **Z1**, **Z2**, **Z8** and **Z9** that were reinforced with high ductility non-prestressed steel and the two partially prestressed concrete specimens **Z6** and **Z7** were chosen for analytical modeling.

It was reported that failure of specimens **Z1**, **Z2** and **Z8** was caused by rupture of the longitudinal reinforcing bars while in test **Z9** some bar couplers at the edges of the specimen broke before reaching the expected mode. Failure of the partially prestressed test specimens **Z6** and **Z7** was initiated by rupture of wires in the post-tensioning tendon. The reinforcing bars failed only after a further increase of the imposed elongation. It was also reported that specimens **Z1**, **Z2** and **Z8** failed at an average concrete strain less than one half of the ultimate strain of steel. In the two partially prestressed test specimens **Z6**

and **Z7** the strain at failure was only 20% of the non-prestressed steel ultimate strain and approximately 53% of the prestressed steel ultimate strain.

The concrete cracking stress used in the model varied between $0.23\sqrt{f'_c}$ and $0.20\sqrt{f'_c}$ to match test results. The tension stiffening parameter β_1 was taken 15 and β_2 varied between 0.2 and 0.35. Figures 5.27 through 5.32 show load versus elongation plots for specimens **Z1**, **Z2**, **Z6**, **Z7**, **Z8** and **Z9** respectively. The elongation was measured for a gauge length of 1800 mm. In general, a good correlation exists between test and modeled values keeping in mind that the modeled non-prestressed steel stresses were the static values. For the prestressed steel, only the dynamic stresses were reported and were used in the model. Hence, the model curves are closer to the static readings in the load-elongation plots for reinforced concrete specimens **Z1**, **Z2**, and **Z8** as shown in Fig. 5.27, 5.28 and 5.31 respectively. In the partially prestressed specimens **Z6** and **Z7**, that had A_s/A_p of 1.173 and 0.587 respectively, the model curves, shown in Figs. 5.29 and 5.30, are closer to the dynamic readings especially in specimen **Z7**. The model curve continued until the axial load became equal to the steel area times the ultimate steel stress, which means that steel strain at a crack reached the ultimate strain. The reinforced concrete specimens **Z1**, **Z2**, and **Z8** failed at a gross strain less than one half the steel ultimate strain due to strain localization. The partially prestressed specimens **Z6** and **Z7** also failed at a low gross strain due to rupture of wires in the tendons. The comparison between model and test responses for specimen **Z9**, shown in Fig. 5.32, is only for the response before yield since specimen **Z9** failed in this load range when some bar couplers at the edges of the specimen broke.

Table 5.1 Summary of shrinkage and creep effects on the specimens

Specimen	ϕ	ϵ_{cs} microstrain	Δf_s MPa	ΔN_s kN	ΔM_s kN	ΔN_c kN	ΔM_c kNm	ΔN_{total} kN	ΔM_{total} kNm
1C40	0.4018	-385	-84.8188	-67.855	-5.15698	119.1633	0.400082	51.3083	-4.7569
1C20	0.446	-189	-49.6533	-39.7227	-3.89282	64.08245	0.520471	24.35978	-3.37235
2A	0.664	-147	-32.6665	-32.6665	-2.48266	34.38736	0.138948	1.720845	-2.34371
2B	0.521	-133	-38.6561	-30.9248	-2.45853	46.73518	0.351942	15.81034	-2.10658
2C	0.253	-169	-37.0093	-29.6074	-2.30938	60.76407	0.216594	31.15664	-2.09279
3A	0.446	-230	-43.092	0	0	500.321	0.10153	500.321	0.10153
3B	0.521	-132	-39.9424	-31.9539	-2.58827	44.81677	0.374654	12.86283	-2.21361
3C	0.466	-127	-33.25	-26.6	0	23.99534	-1.3E-15	-2.60466	-1.3E-15

Δf_s change in non-prestressed steel stress
 ΔN_s change in steel internal force
 ΔM_s change in steel internal moment
 ΔN_c change in concrete internal force
 ΔM_c change in concrete internal moment
 ΔN_{total} change in total internal force
 ΔM_{total} change in total internal moment
 ϵ_{cs} shrinkage strain
 ϕ creep coefficient

Table 5.2 Material properties for the concrete used in simulating test results

Specimen n	f'_c MPa	ϵ_{co}	E_c MPa	$f_{cr} / \sqrt{f'_c}$	β_1	β_2
1C20	45.7	-0.0023	32000	0.21	15	0.30
1C40	45.7	-0.0023	32000	0.21	15	0.30
2A	51.9	-0.0026	32500	0.23	15	0.45
2B	48.2	-0.0027	32000	0.23	4	0.35
2C	48.6	-0.0027	34200	0.23	20	0.50
3A	47.0	-0.0031	27200	0.23	4	0.45
3B	44.2	-0.0028	30000	0.33	15	0.45
3C	46.6	-0.0029	27100	0.18	21	0.30

Table 5.3 Specimens tested by Alvarez and Marti

Test Specimen	Z1	Z2	Z3	Z4	Z5	Z6	Z7	Z8	Z9
Non-prestressed Steel A_s [mm ²]	2156	2156	2156	2156	2156	1232	616	1540	431 2
Prestressed Steel A_p [mm ²]	0	0	0	0	0	1050	1050	0	0
Type of steel	H	H	H	N	L	H	H	H	H
Transverse reinforcement A_{st} [mm ²]	250	250	0	250	250	250	250	250	250
Target strength of concrete f'_c [MPa]	50	90	50	50	50	50	50	50	50

The variable in each specimen is shaded

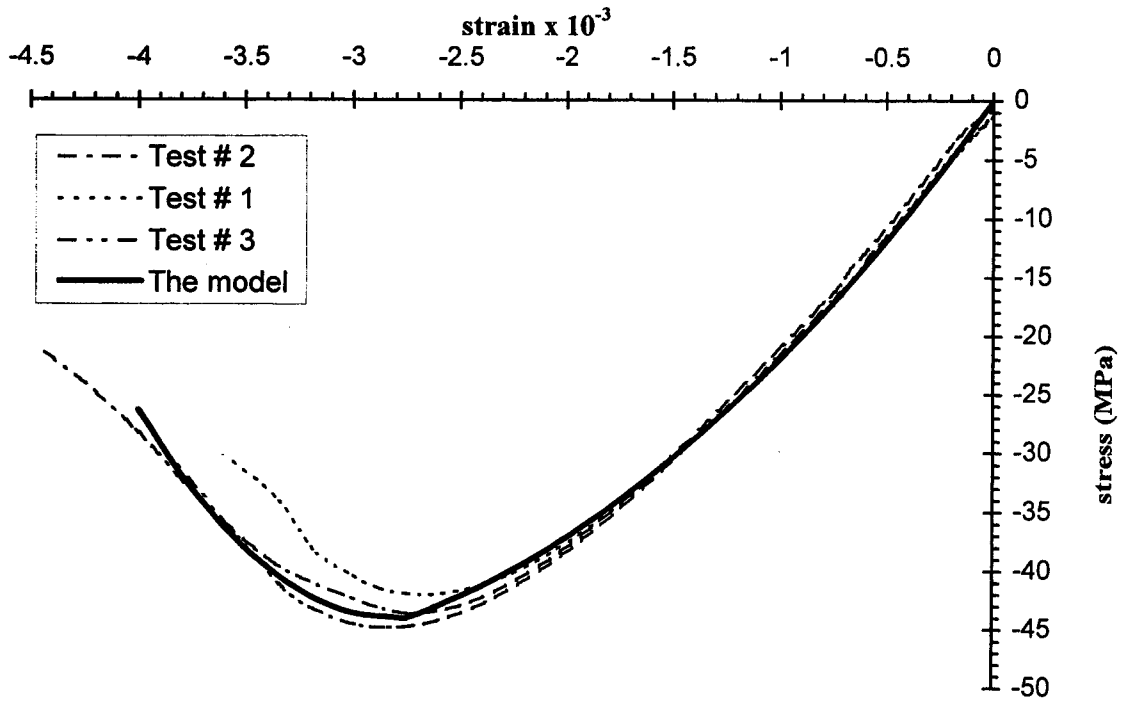
H : Highly ductile non-prestressed steel

N & L : two types of low ductile non-prestressed steel

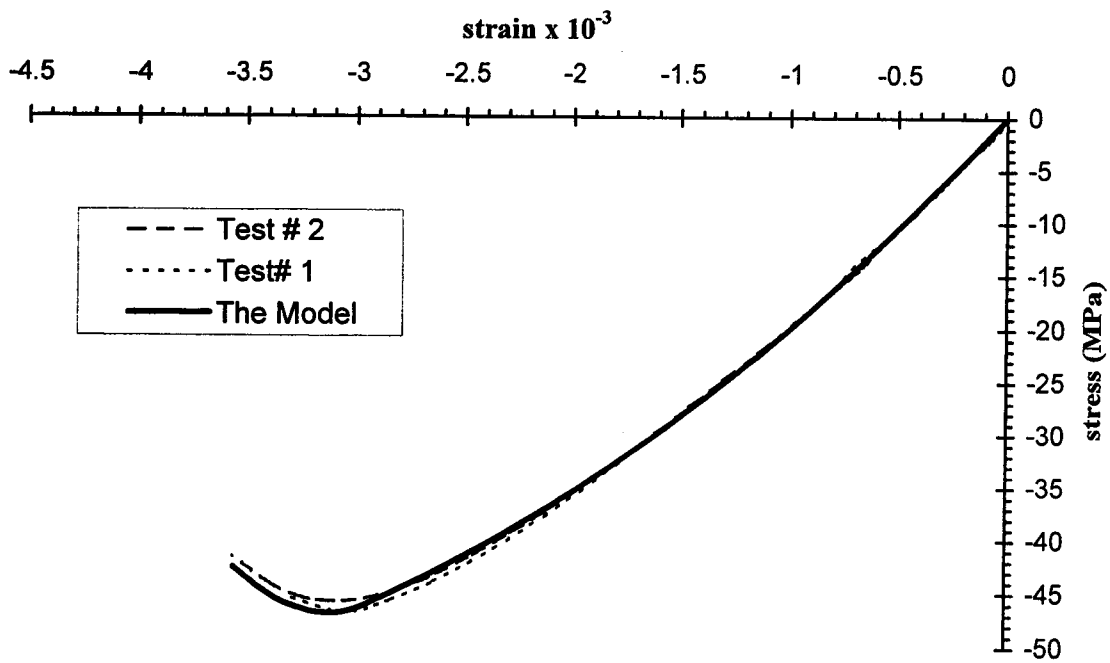
Table 5.4 The Material properties used in Alvarez and Marti specimens

Specimen	Z1	Z2	Z3	Z4	Z5	Z6	Z7	Z8	Z9
Concrete:									
Age of specimen	79	70	27	45	25	107	89	42	93
Density	2387	2477	2386	2371	2410	2403	2406	2404	2393
f_c	50.5	79.6	48.3	50.0	49.1	51.9	50.7	50.7	47.0
Tensile strength	3.68	5.65	3.42	3.60	3.30	3.52	3.51	3.51	3.22
Splitting stress	3.96	6.23	4.21	4.02	3.85	3.53	4.50	4.50	3.09
ϵ_{co} †	2.53	2.42	2.33	2.64	-	2.11	2.24	2.24	2.25
Modulus of elasticity	38.7	41.5	32.8	31.2	-	34.2	35.0	35.0	32.5
Non-prestressed steel:									
Diameter	13.96	13.96	13.96	13.94	13.90	13.96	13.96	13.96	13.96
Yield stress	488.1	488.1	488.1	576.6	586.9	488.1	488.1	488.1	488.1
Static yield stress	471.7	471.7	471.7	557.0	566.3	471.7	471.7	471.7	471.7
Ultimate strength	614.7	614.7	614.7	604.8	620.6	614.7	614.7	614.7	614.7
Static ultimate strength	583.4	583.4	583.4	572.1	584.0	583.4	583.4	583.4	583.4
Yield strain	2.06	2.06	2.06	-	-	2.06	2.06	2.06	2.06
Ultimate strain	124.7	124.7	124.7	32.3	26.4	124.7	124.7	124.7	124.7
Modulus of elasticity	217.9	217.9	217.9	213.2	214.6	217.9	217.9	217.9	217.9
Prestressed steel									
Yield stress (0.2% offset)						1625	1625		
Ultimate strength						1836	1836		
Ultimate strain						45	45		
Modulus of elasticity						196.2	196.2		

† concrete compressive strain corresponding to f_c



(a) Specimen 3B



(b) Specimen 3A

Figure 5.1 Concrete stress-strain curves

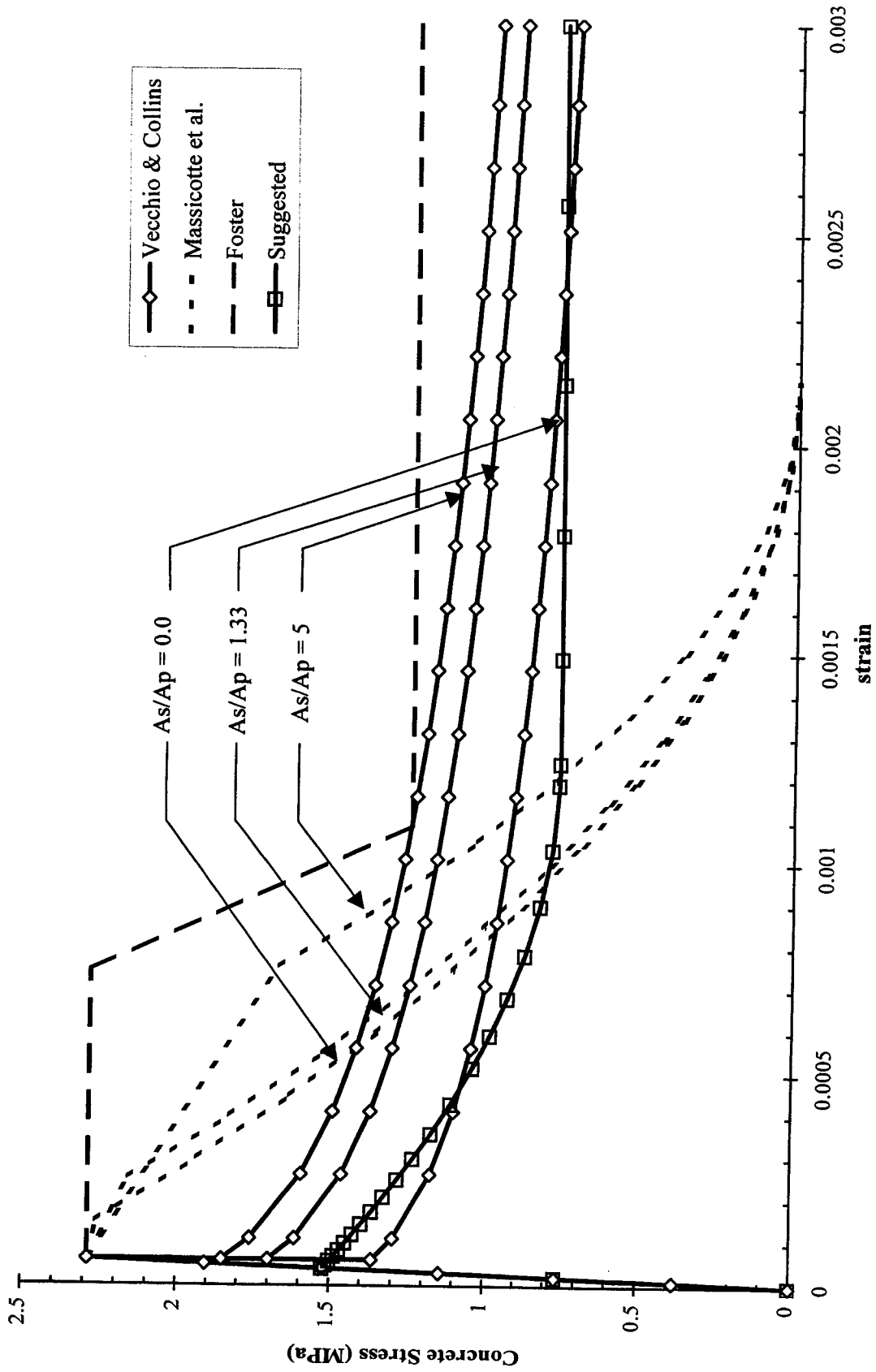


Figure 5.2 Tension stiffening models

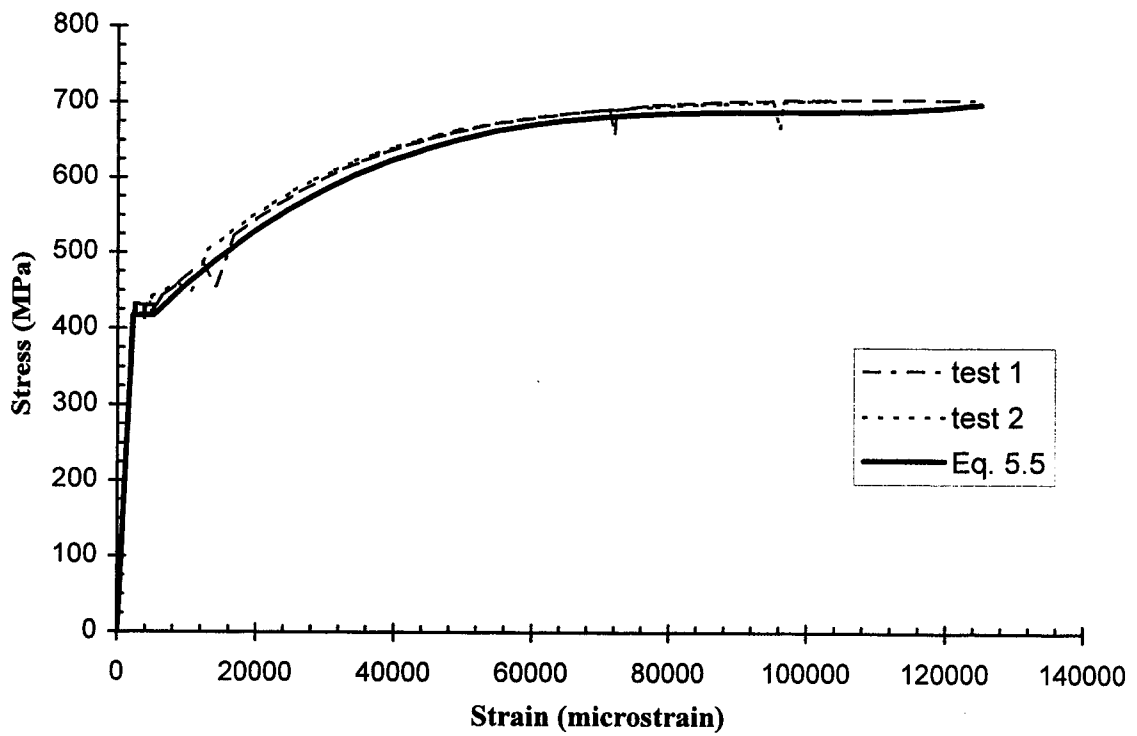


Figure 5.3 Stress-strain curve for non-prestressed steel

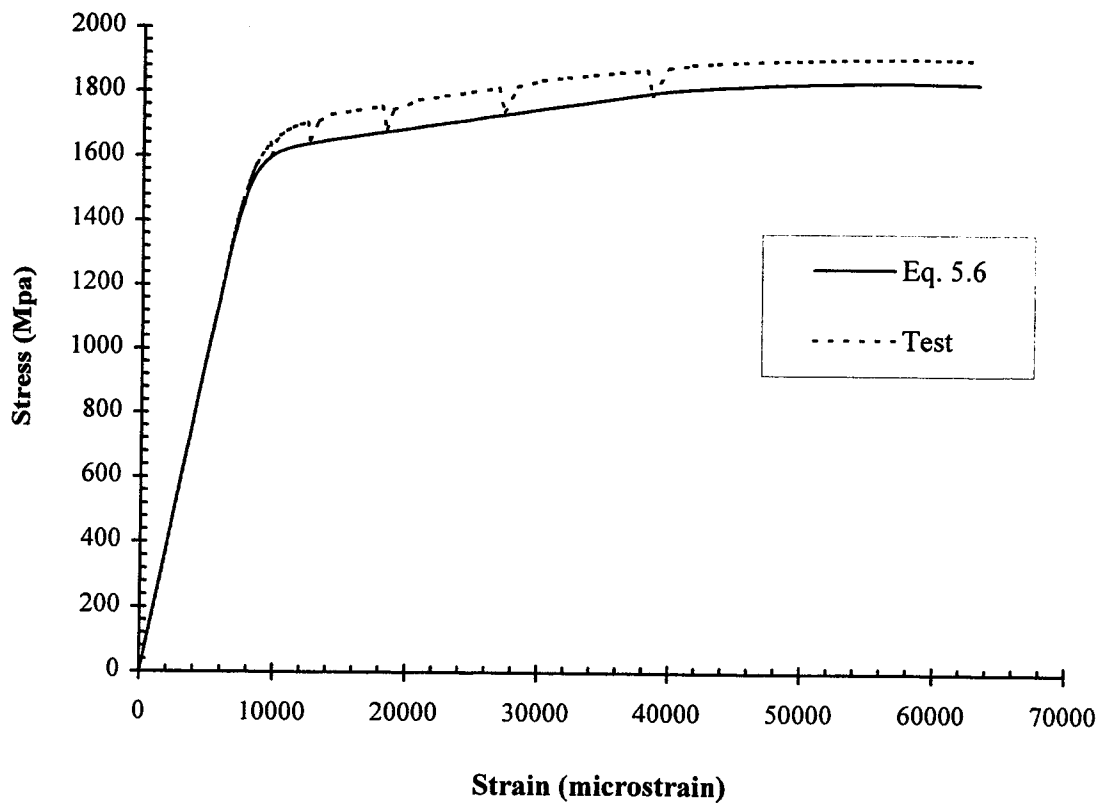


Figure 5.4 Stress-strain curve for prestressing steel

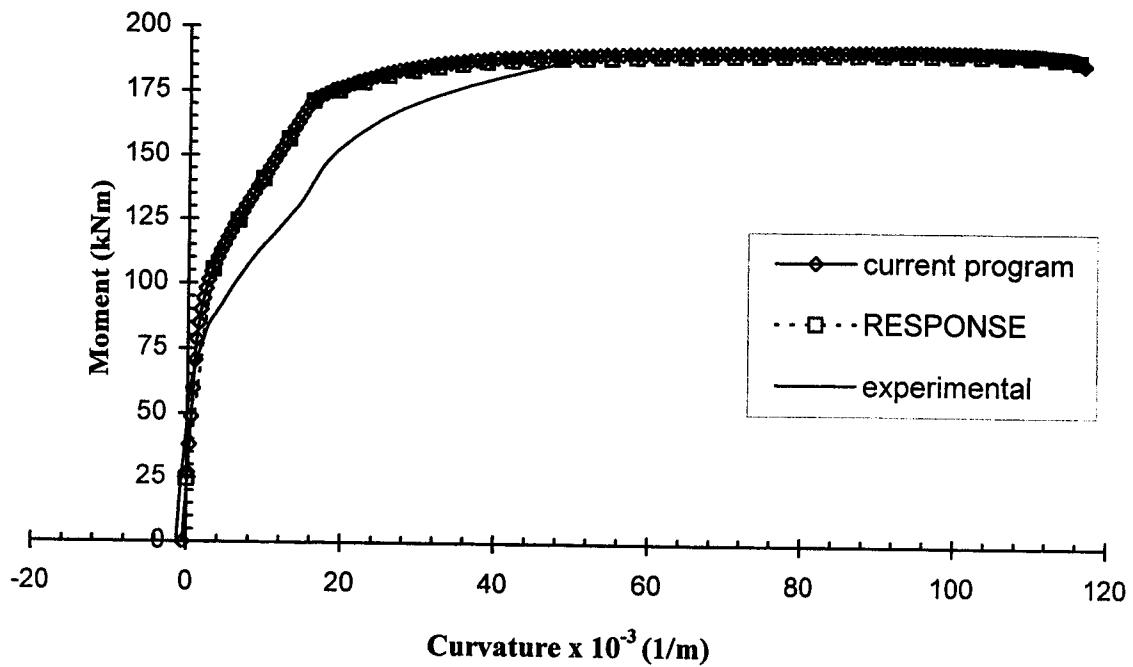


Figure 5.5 Moment versus curvature for specimen 1C40 obtained from the current program and program RESPONSE

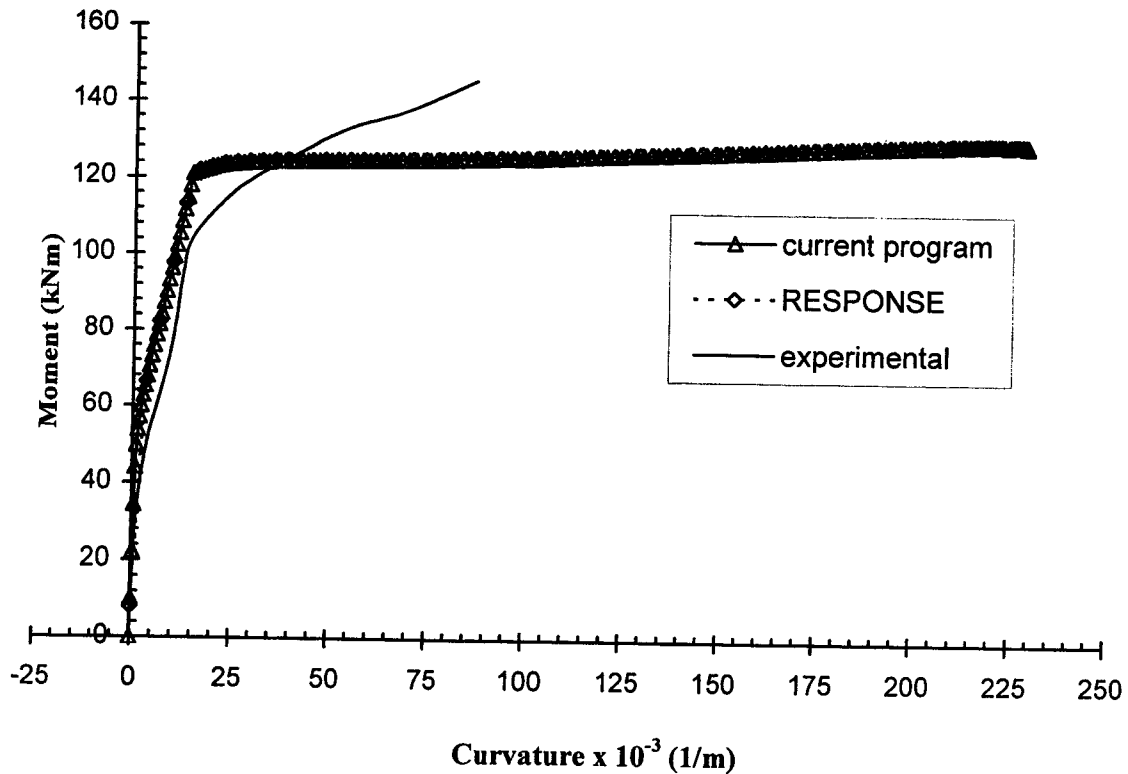


Figure 5.6 Moment versus curvature for specimen 2A obtained from the current program and program RESPONSE

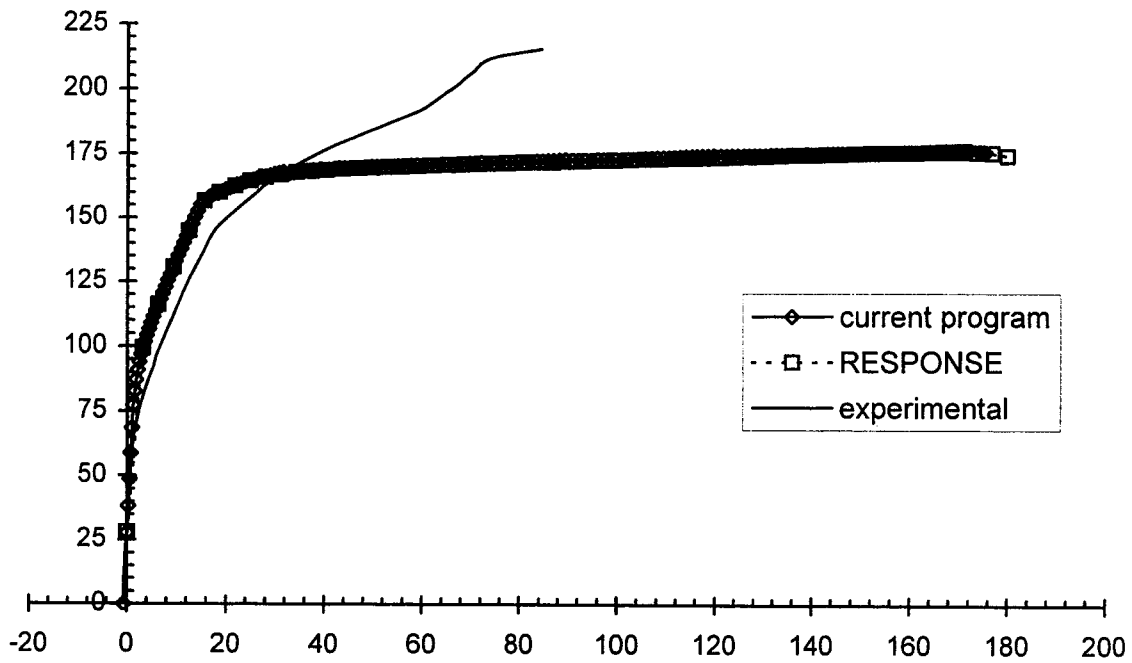


Figure 5.7 Moment versus curvature response for specimen 3B obtained from the current program and RESPONSE

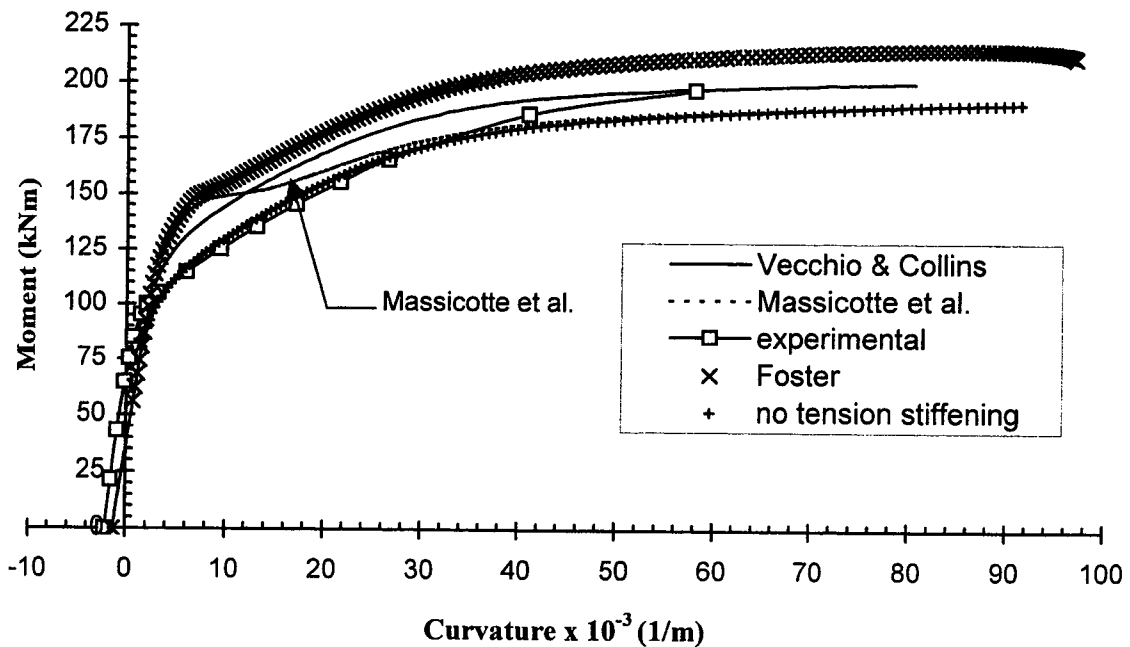


Figure 5.8 Moment versus Curvature response for Specimen 3A obtained using different tension stiffening models

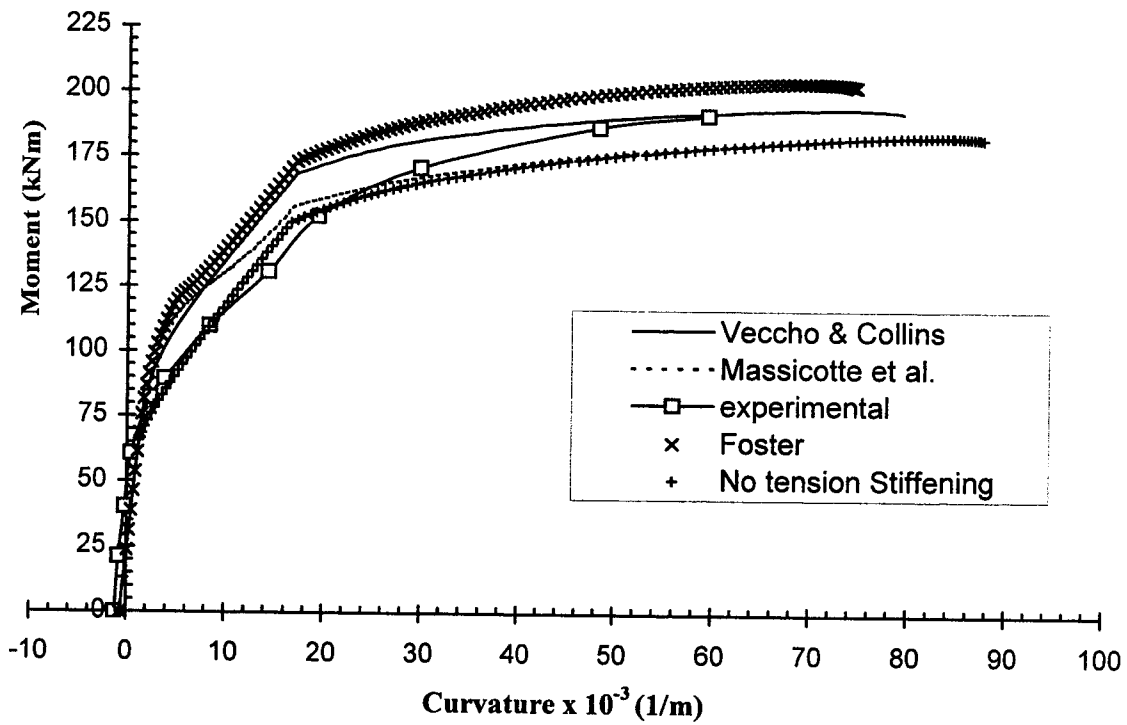


Figure 5.9 Moment versus curvature response for specimen 1C40 obtained using different tension stiffening models

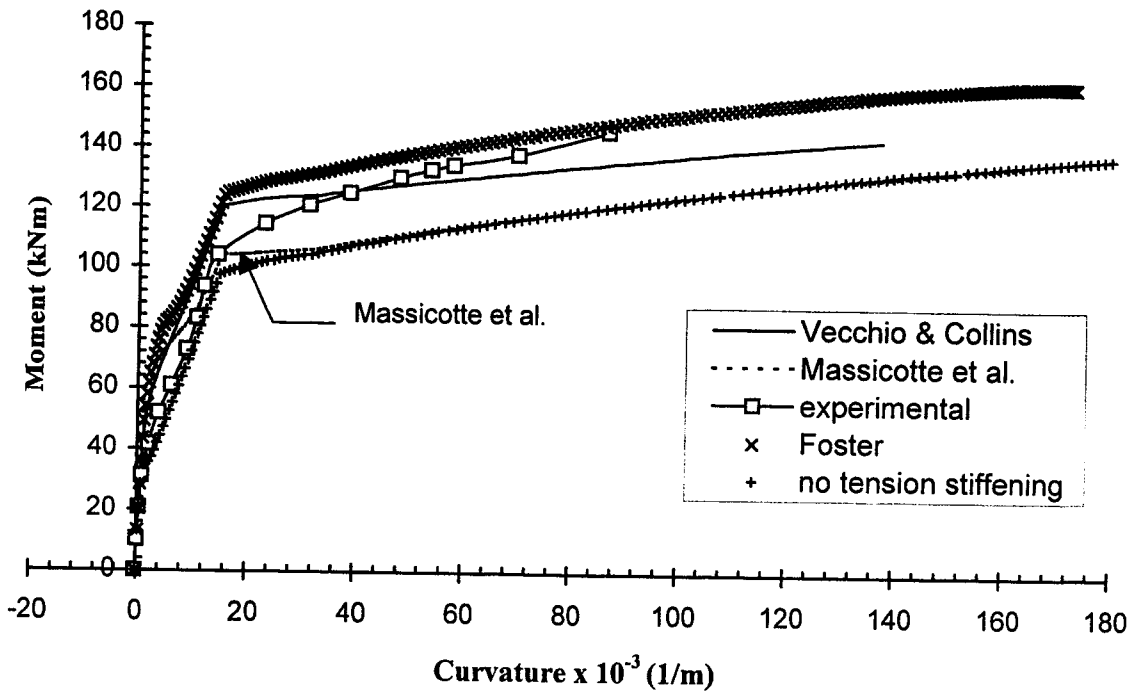
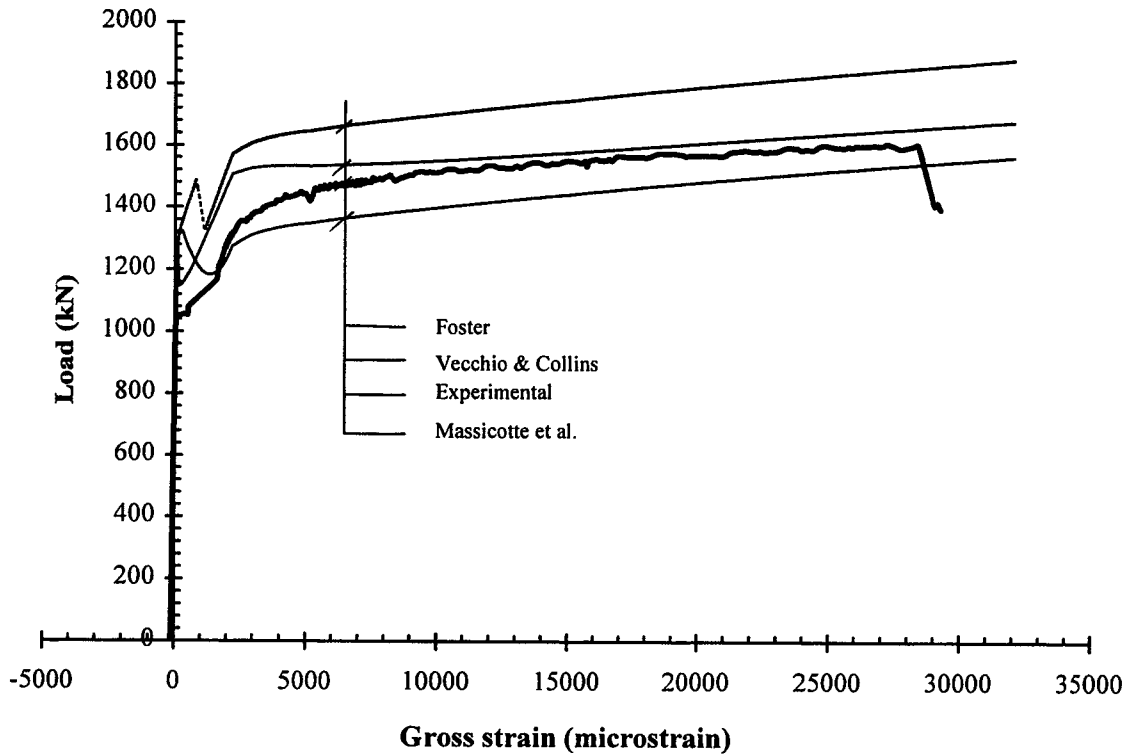
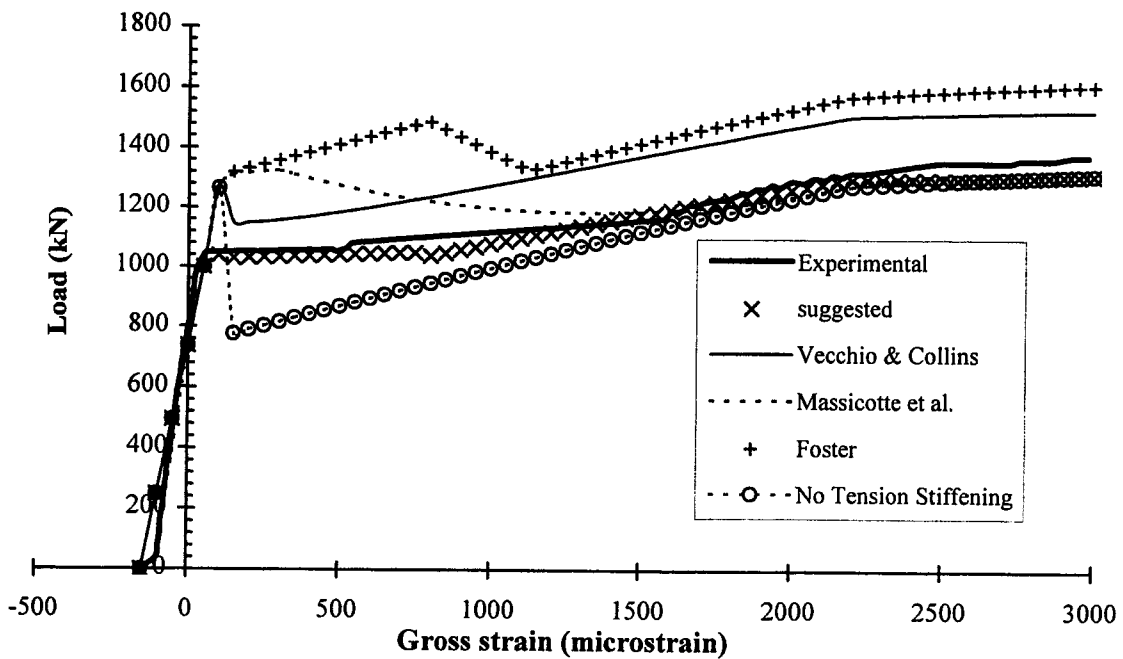


Figure 5.10 Moment versus curvature response for specimen 2A obtained using different tension stiffening models

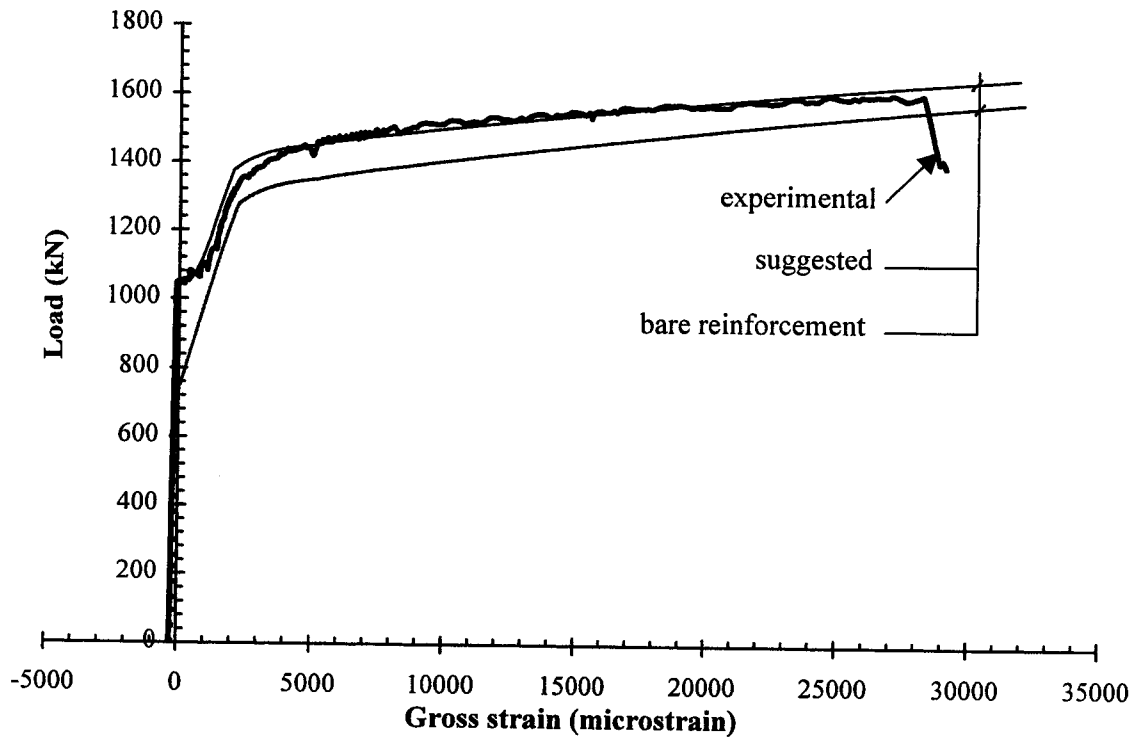


(a) Full response

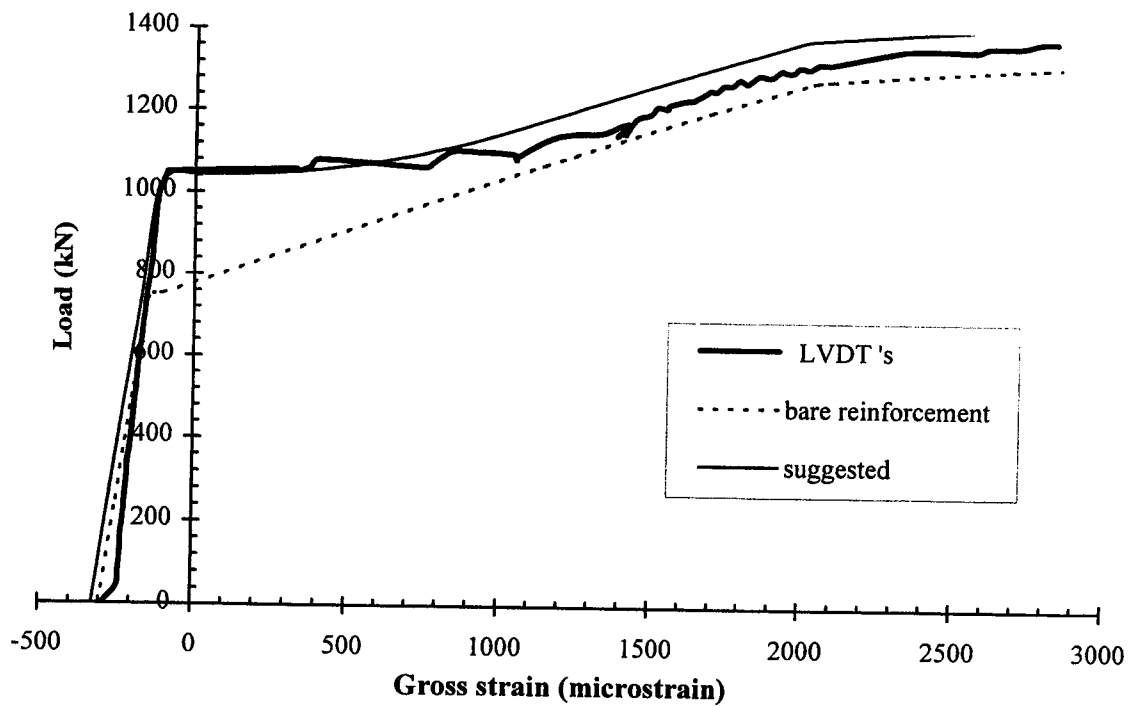


(b) Response up to yield

Figure 5.11 Load versus strain response for specimen 3C from different tension stiffening models



(a) Full response



(b) Response before yield

Figure 5.12 Load versus strain response for specimen 3C obtained from the suggested tension stiffening model

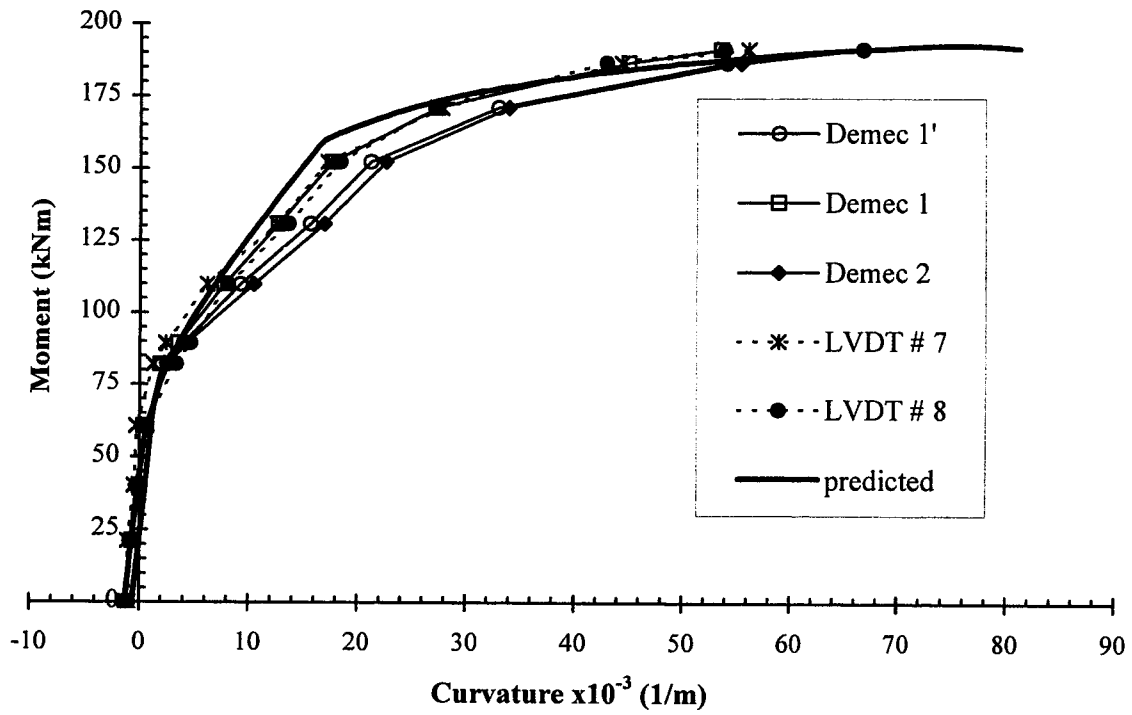


Figure 5.13 Observed and predicted moment versus curvature responses for specimen 1C40

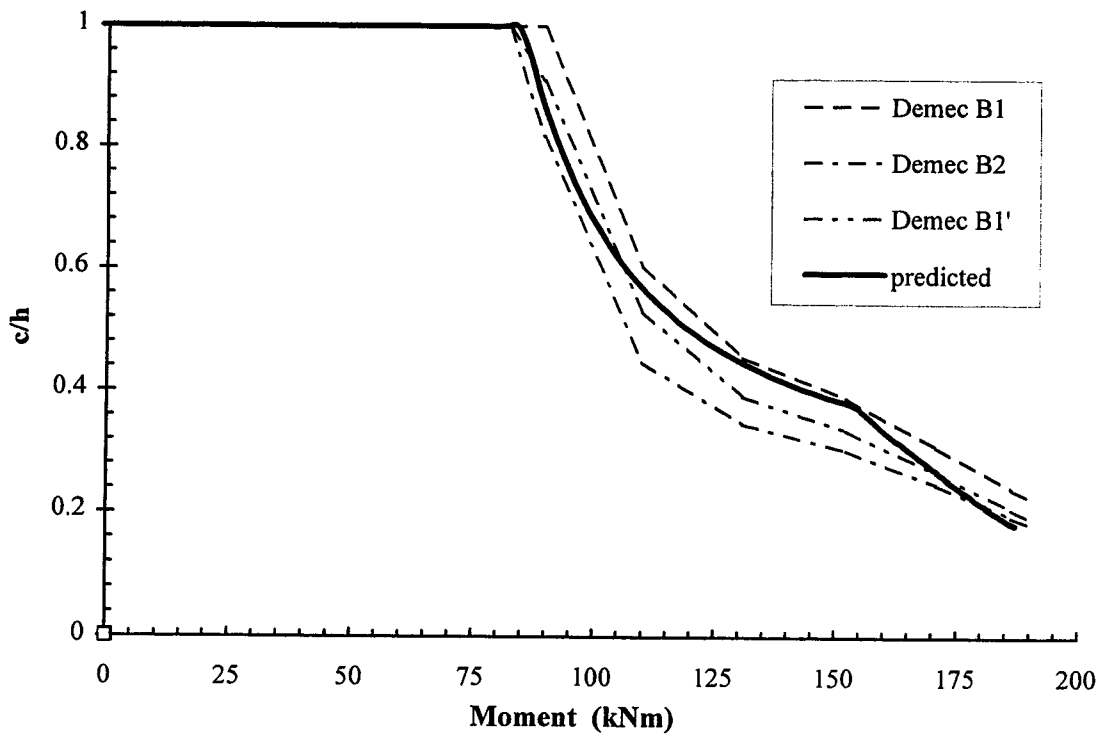


Figure 5.14 Moment versus depth of compression zone for specimen 1C40

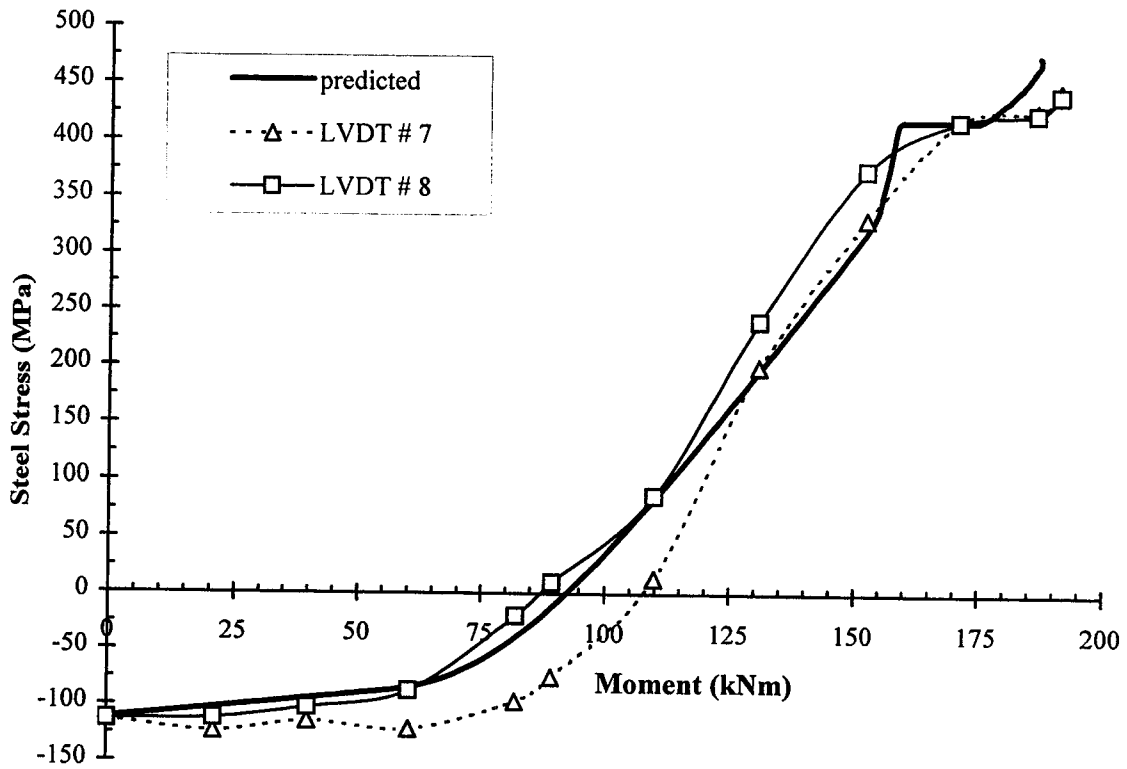


Figure 5.15 Moment versus non-prestressed steel stress for specimen 1C40

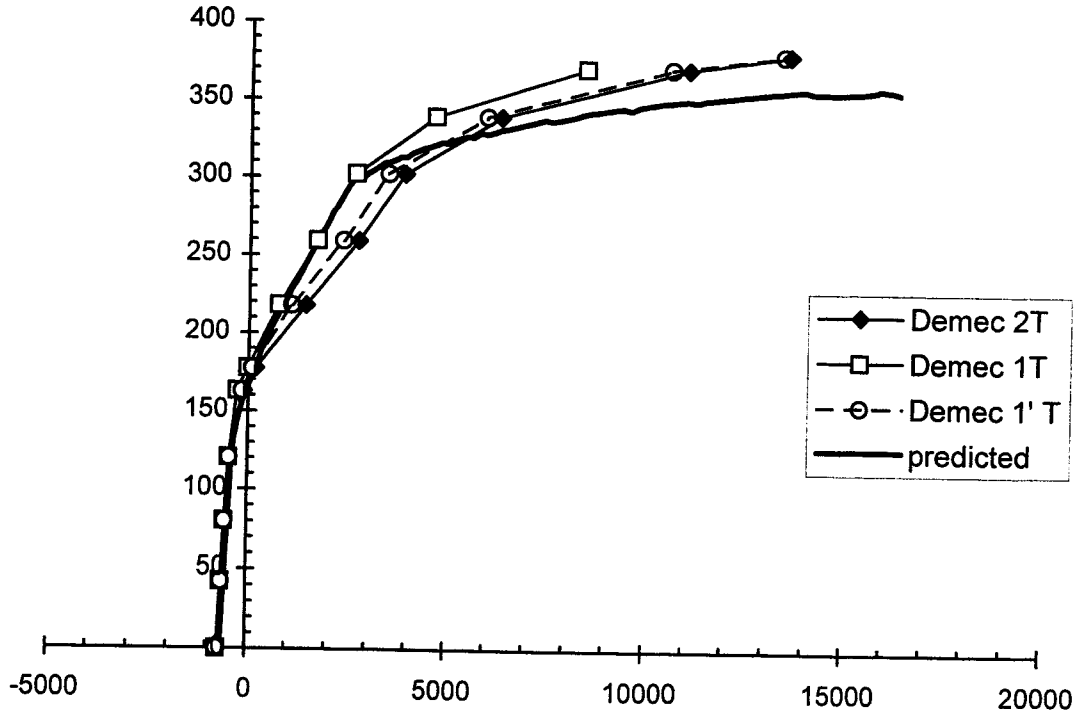


Figure 5.16 Load versus concrete tensile strain for specimen 1C40

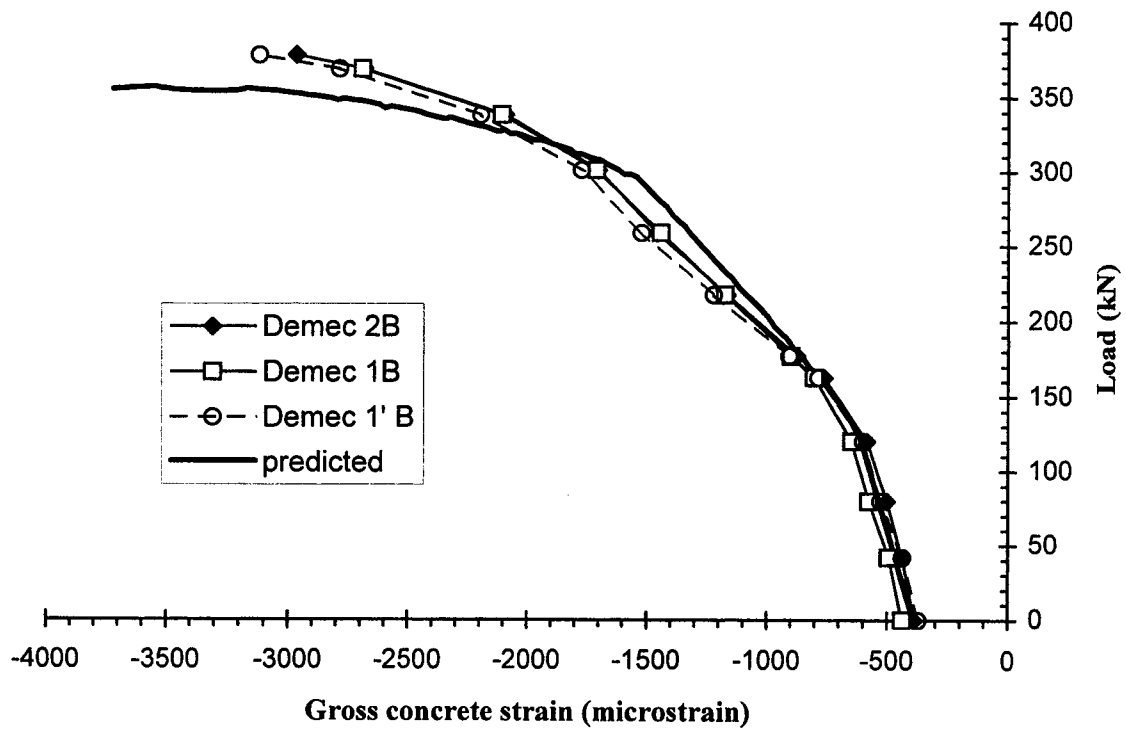


Figure 5.17 Load versus concrete compressive strain for specimen 1C40

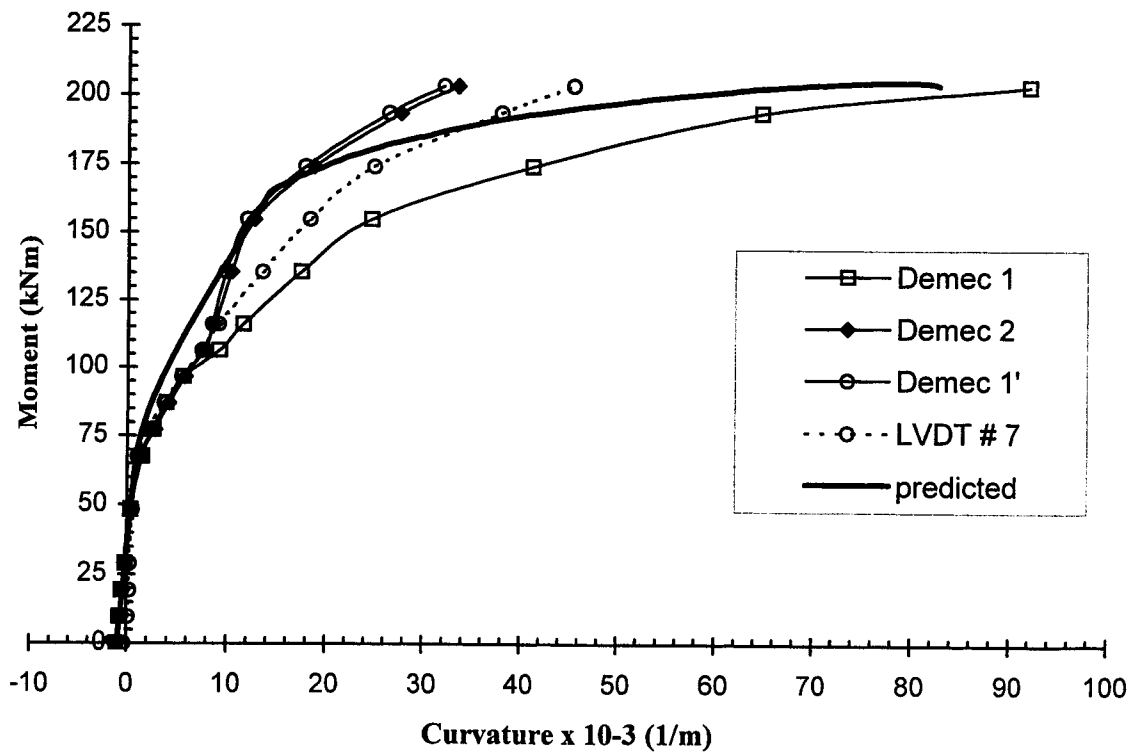


Figure 5.18 Observed and predicted moment versus curvature responses for specimen 1C20

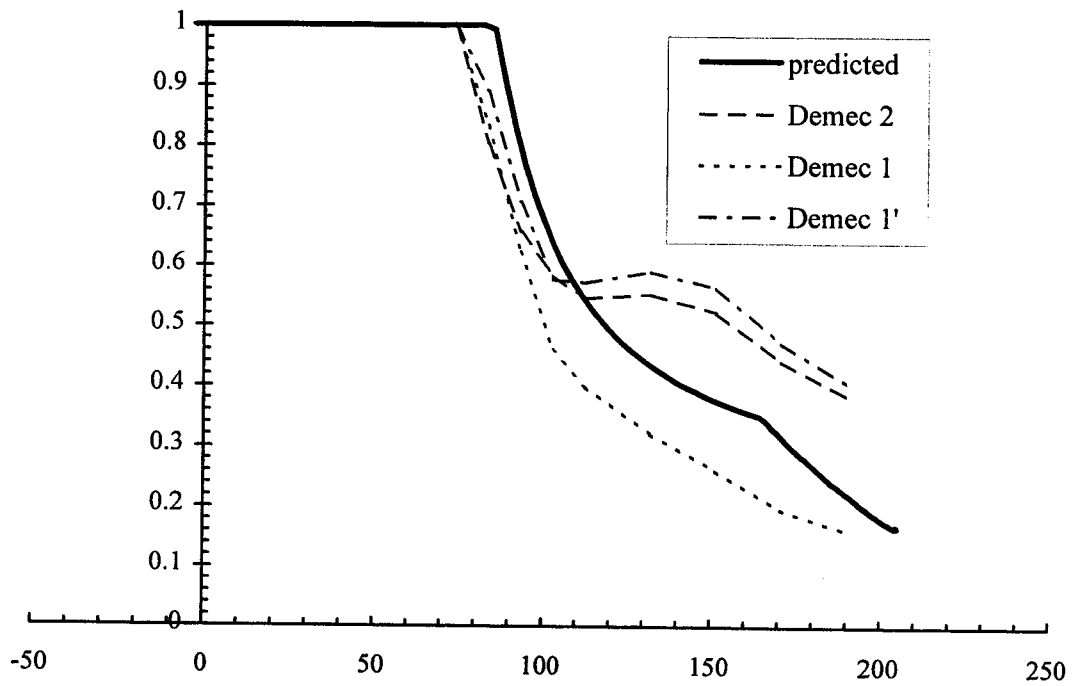


Figure 5.19 Moment versus depth of compression zone for specimen 1C20

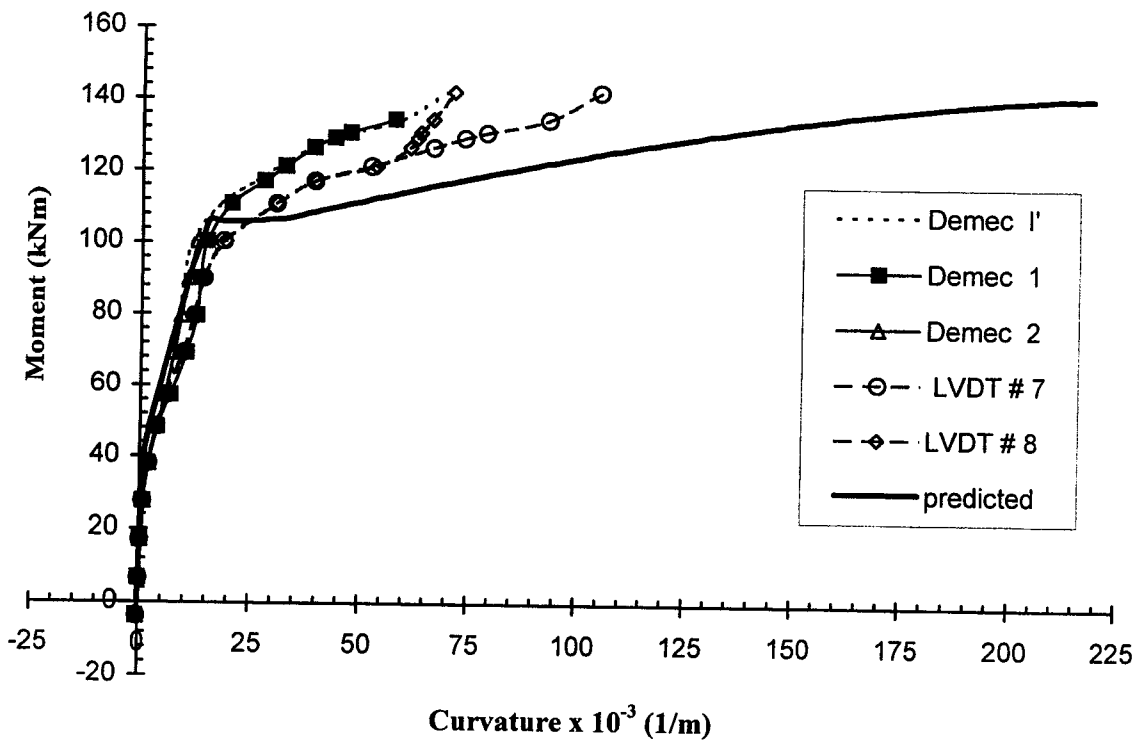


Figure 5.20 Observed and predicted moment versus curvature responses for specimen 2A

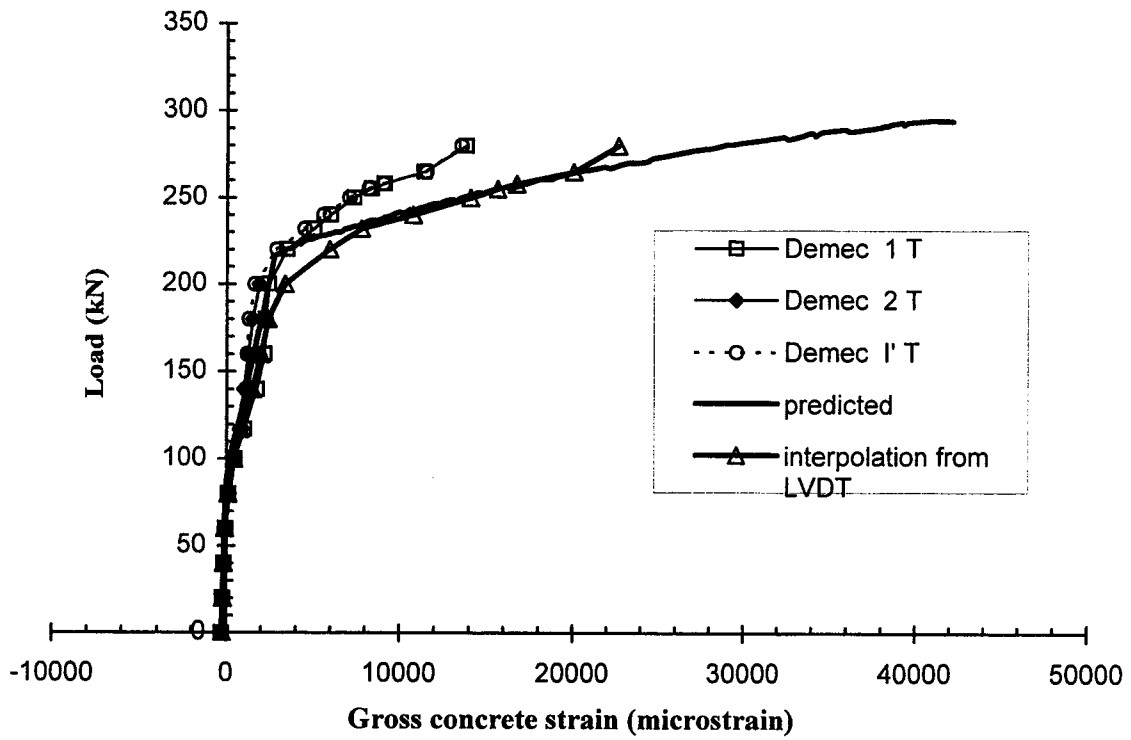


Figure 5.21 Load versus concrete tensile strain for specimen 2A

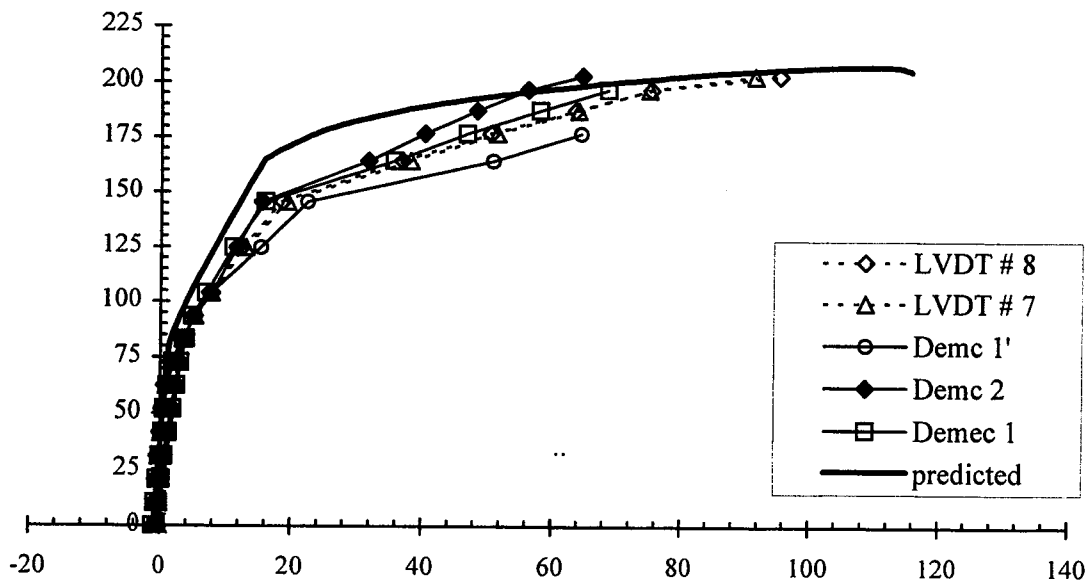


Figure 5.22 Observed and predicted moment versus curvature responses for specimen 2B

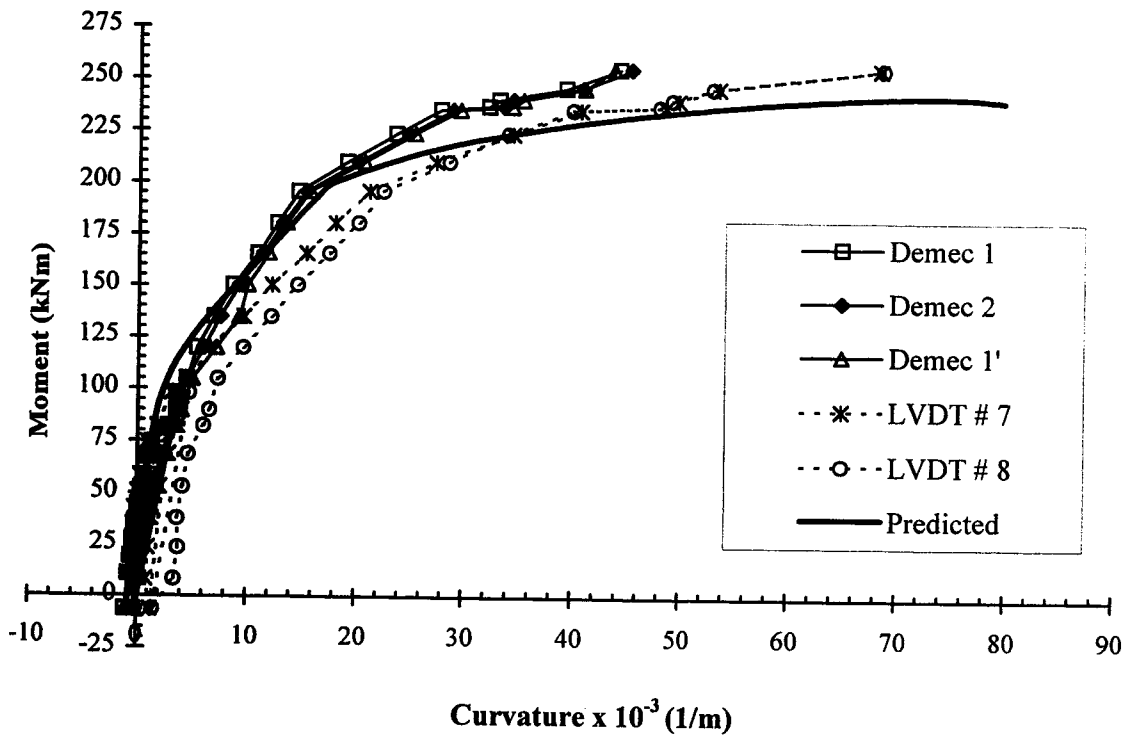


Figure 5.23 Observed and predicted moment versus curvature responses for specimen 2C

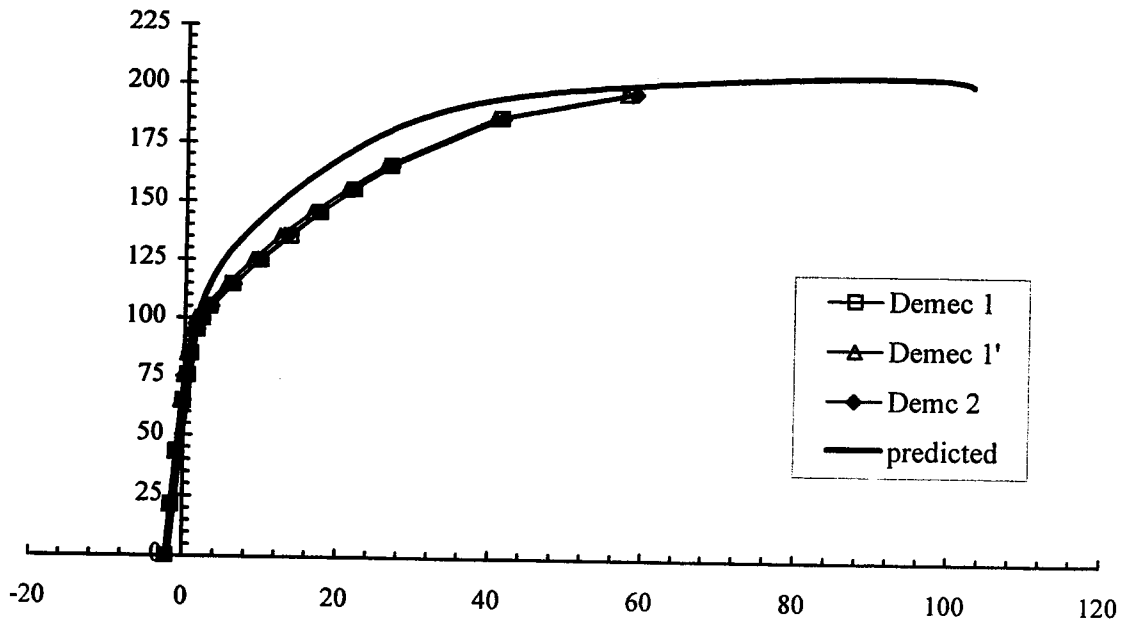


Figure 5.24 Observed and predicted moment versus curvature responses for specimen 3A

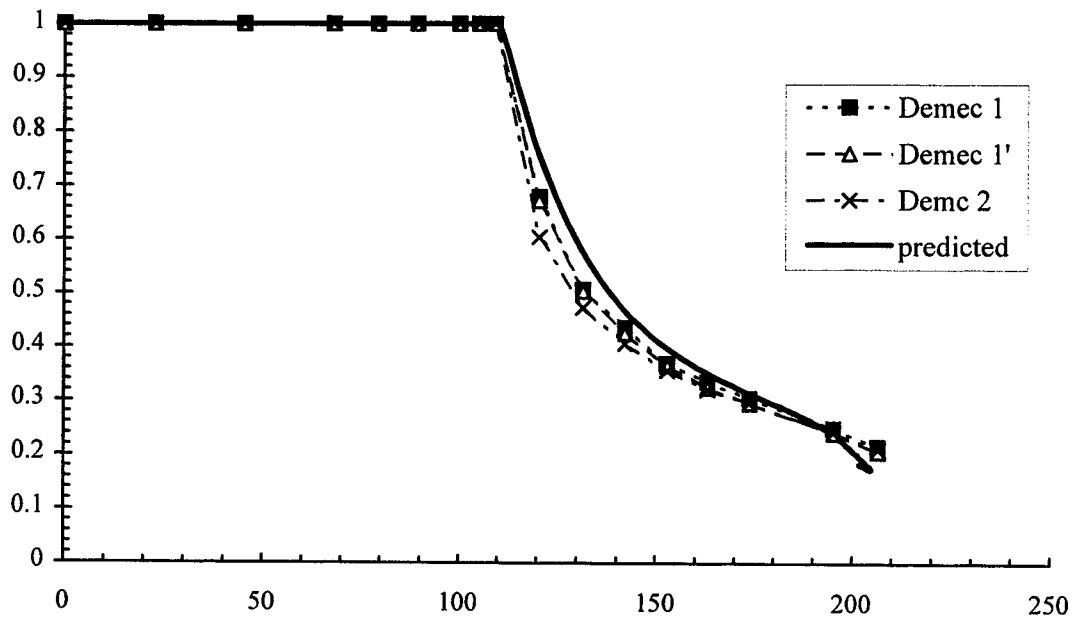


Figure 5.25 Moment versus compression zone depth for specimen 3A

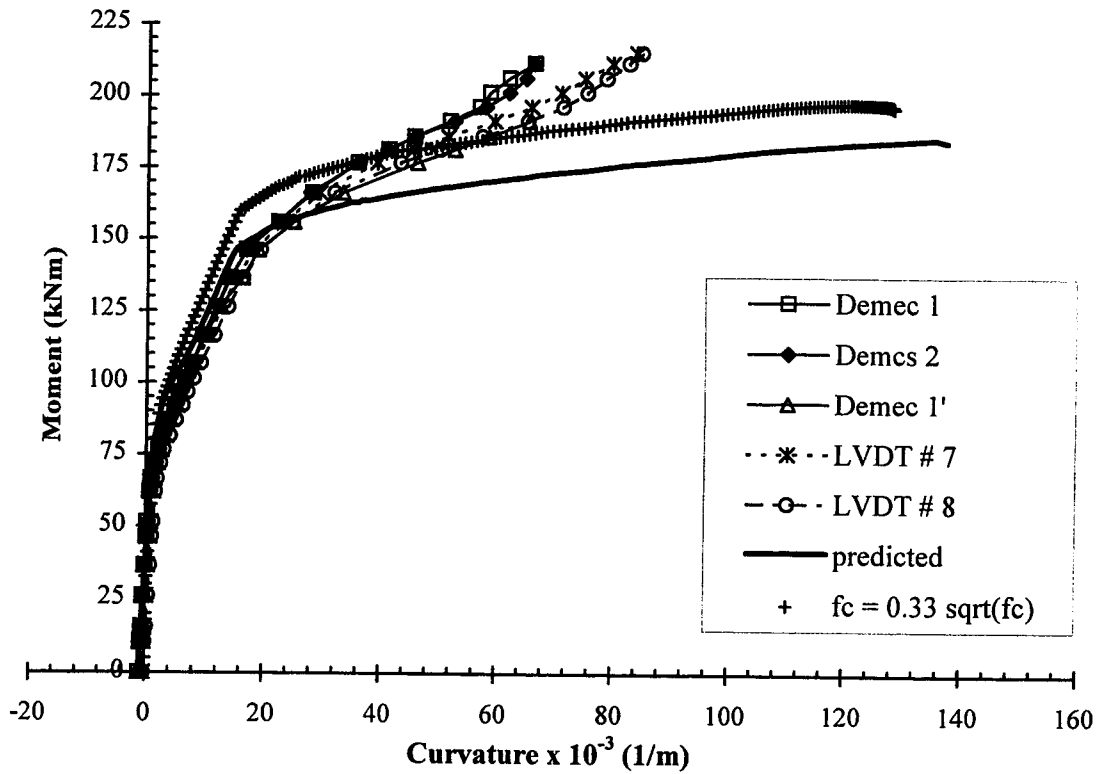
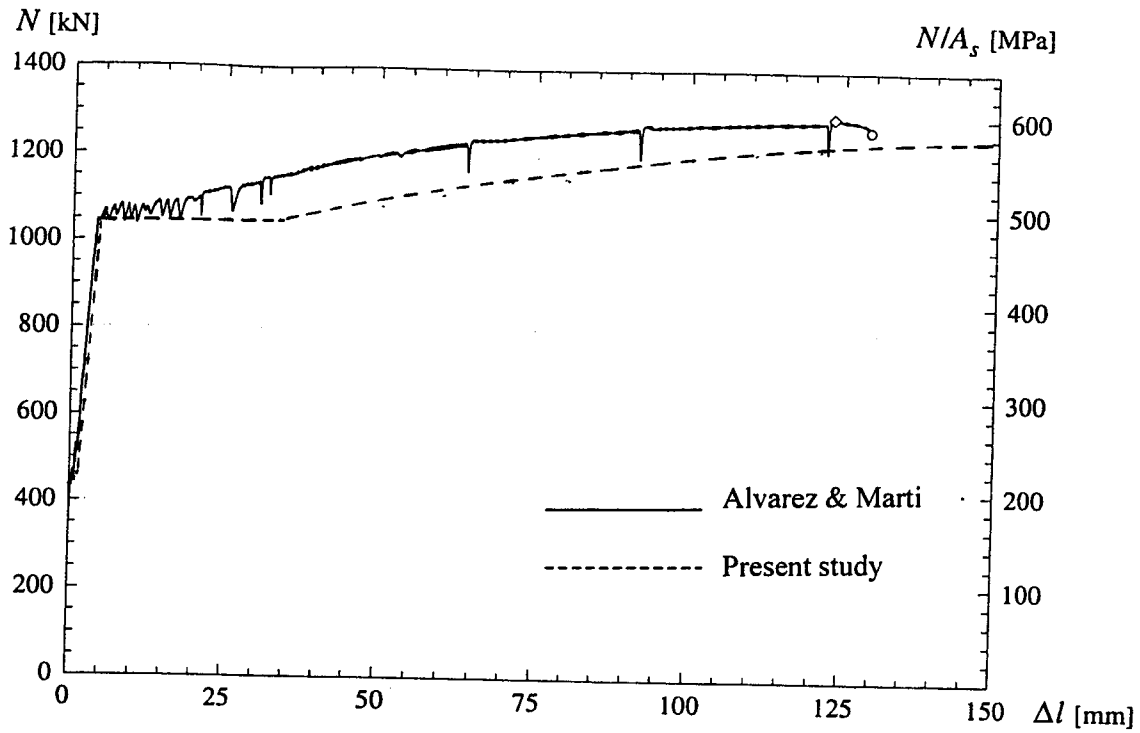
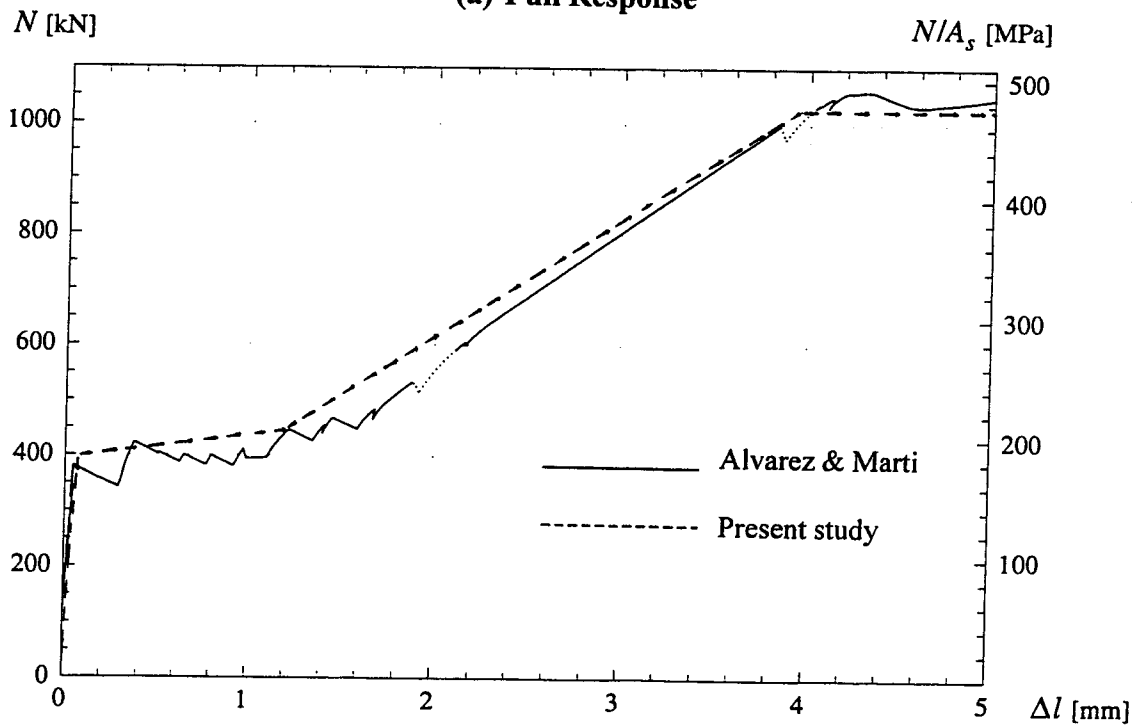


Figure 5.26 Observed and predicted moment versus curvature responses for specimen 3B

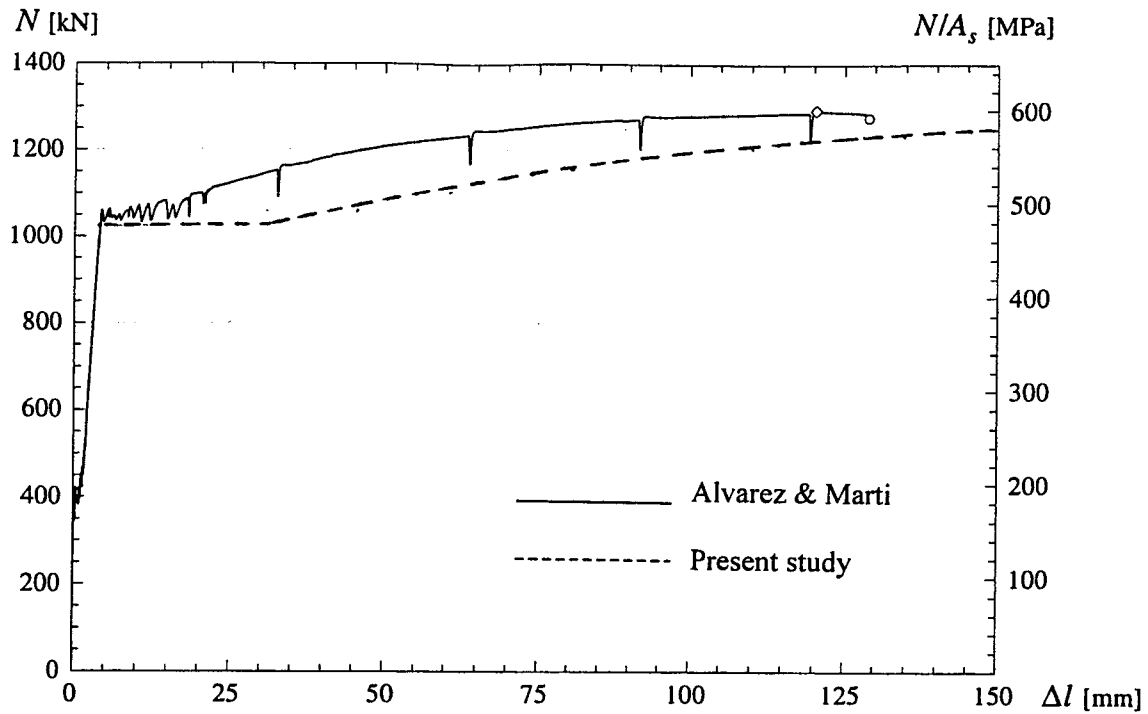


(a) Full Response

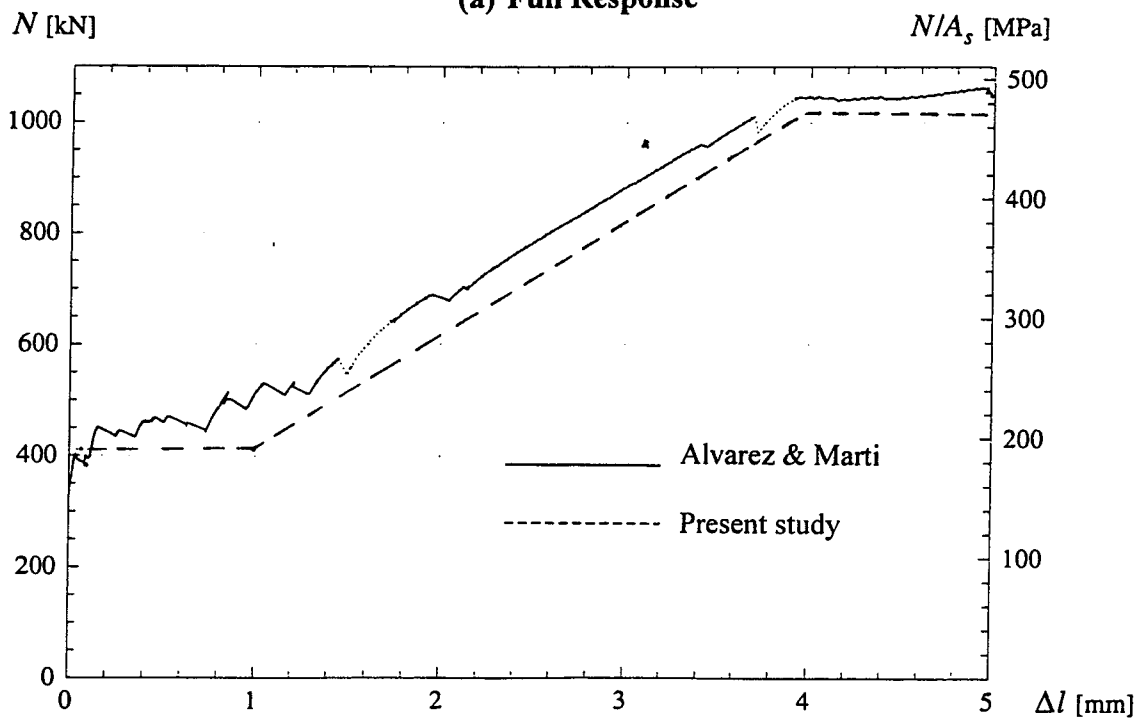


(b) Response before yielding

Figure 5.27 Observed and predicted load versus elongation for specimen Z1 tested by Alvarez & Marti

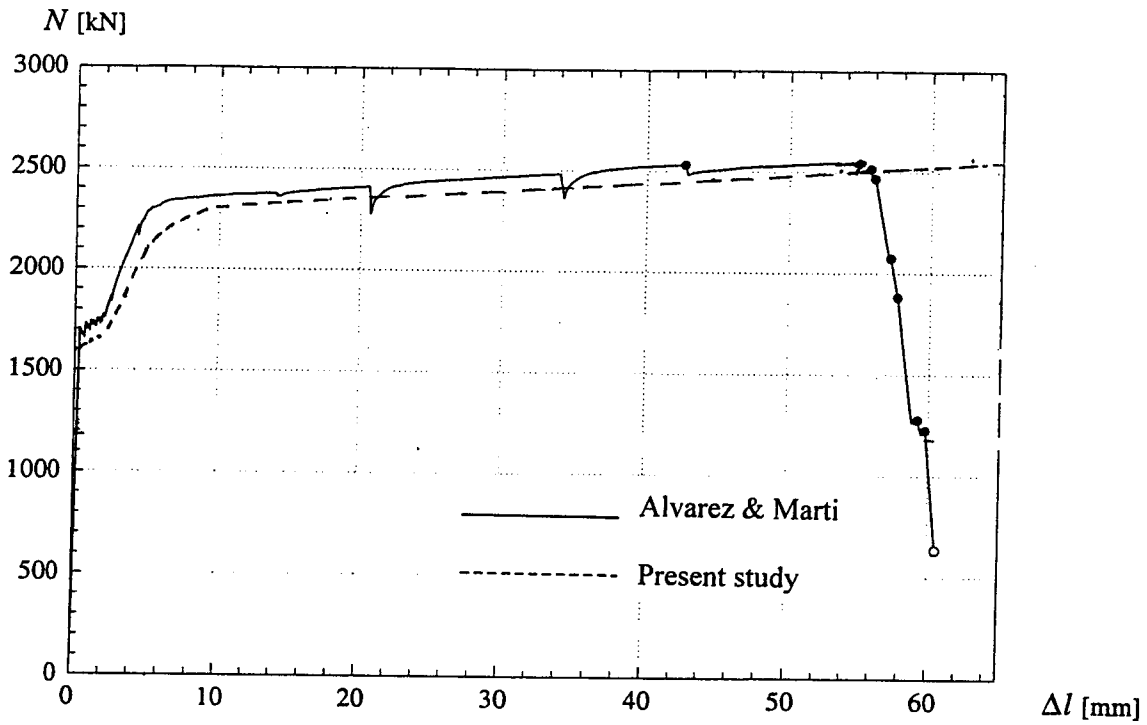


(a) Full Response

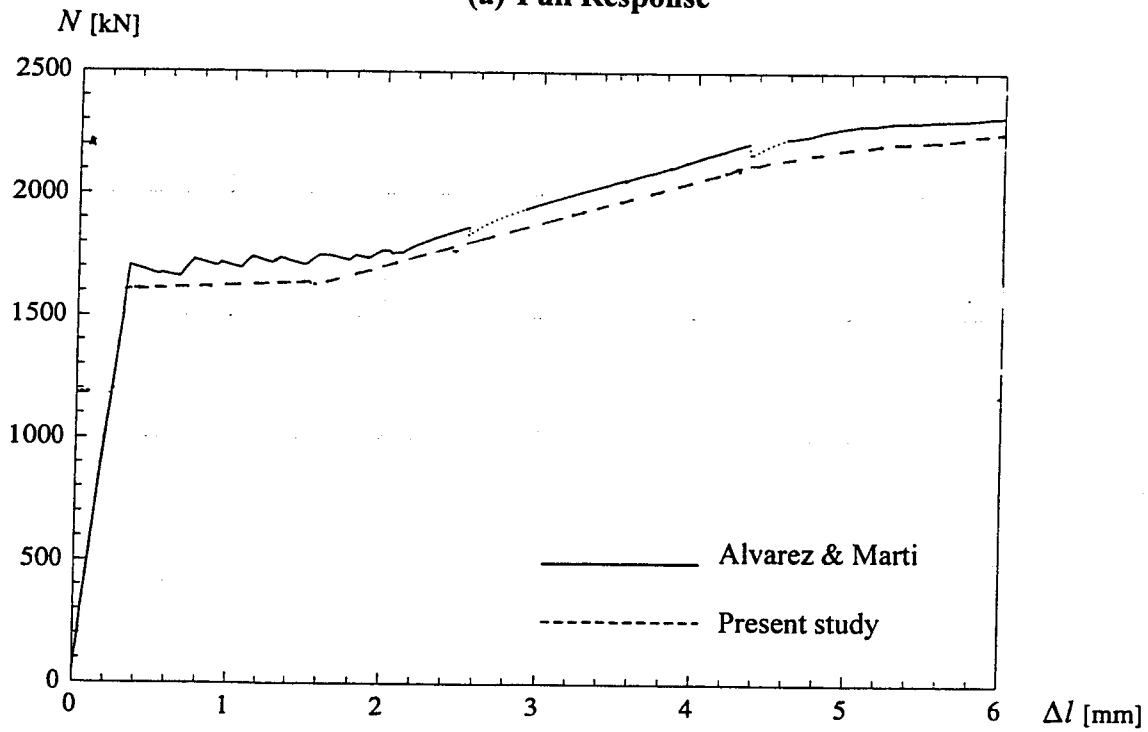


(b) Response before yielding

Figure 5.28 Observed and predicted load versus elongation for specimen Z2 tested by Alvarez & Marti

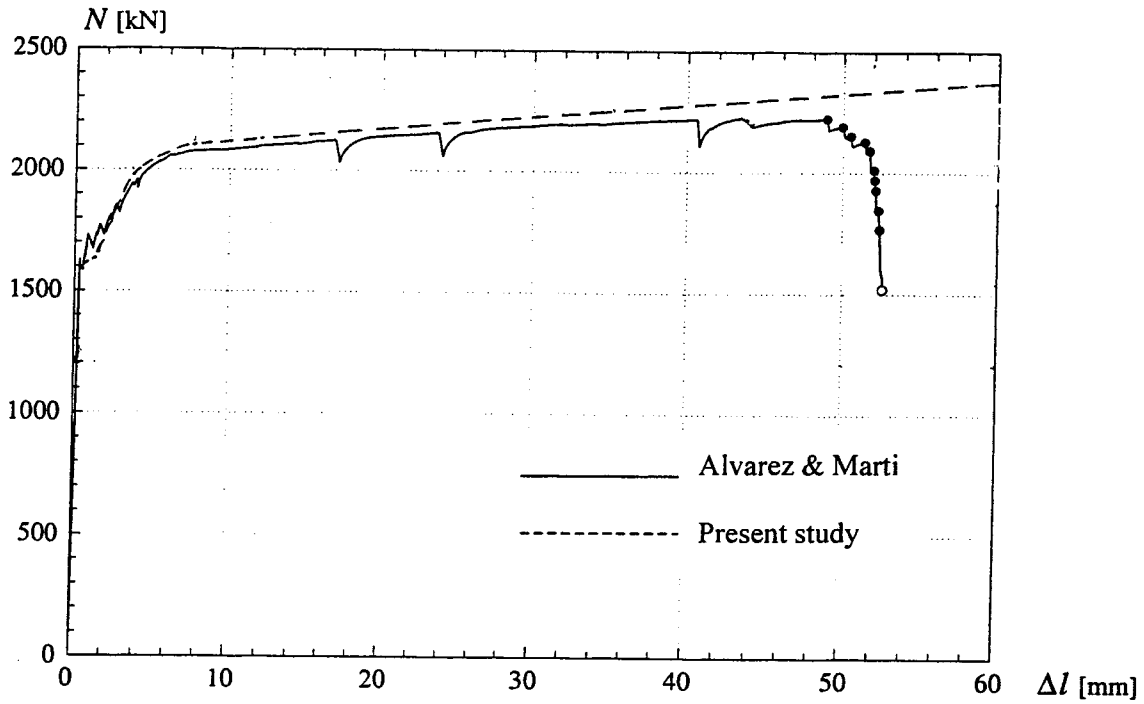


(a) Full Response

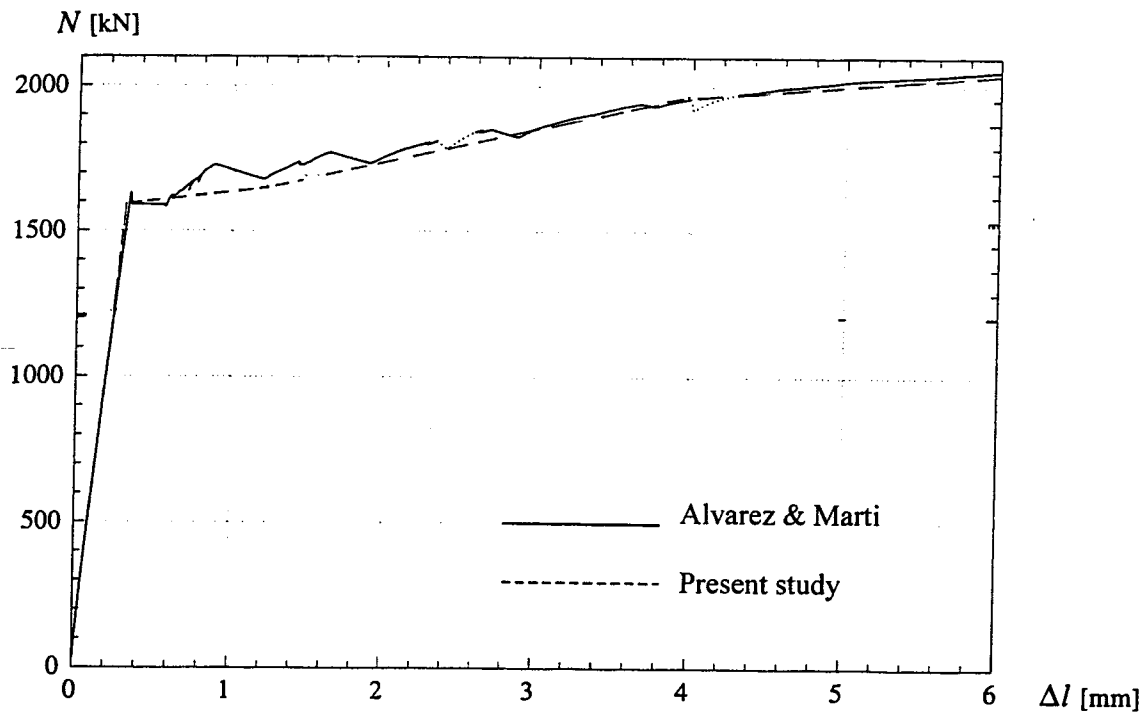


(b) Response before yielding

Figure 5.29 Observed and predicted load versus elongation for specimen Z6 tested by Alvarez & Marti

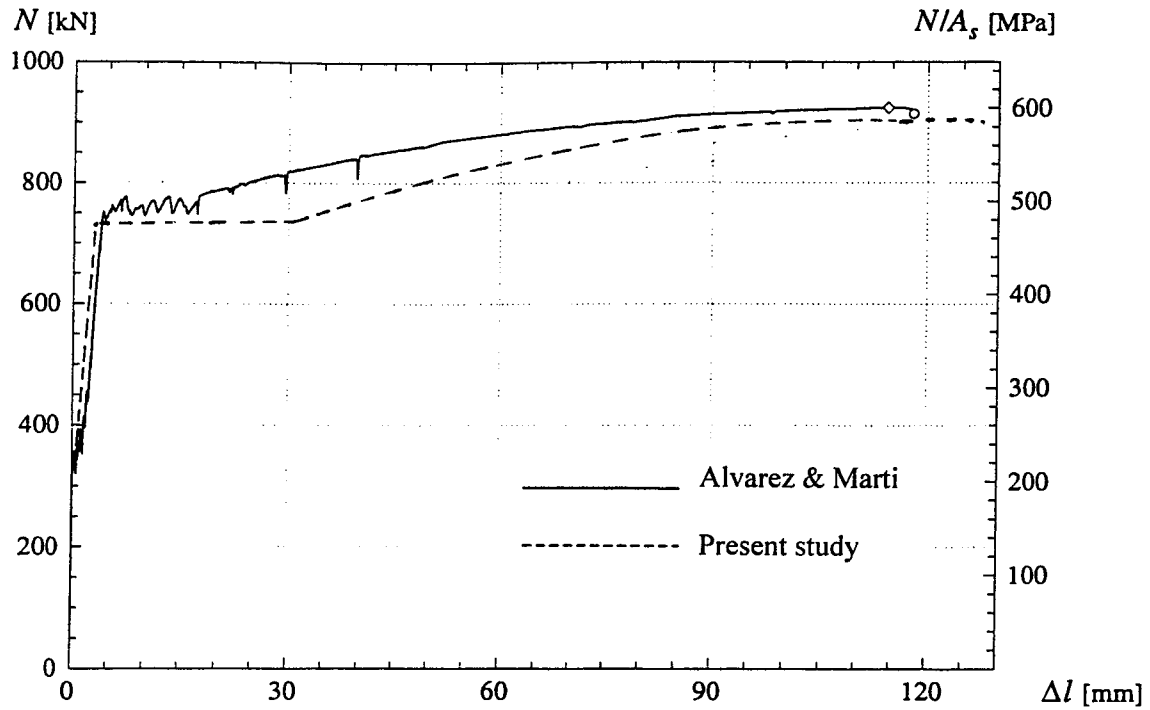


(a) Full Response

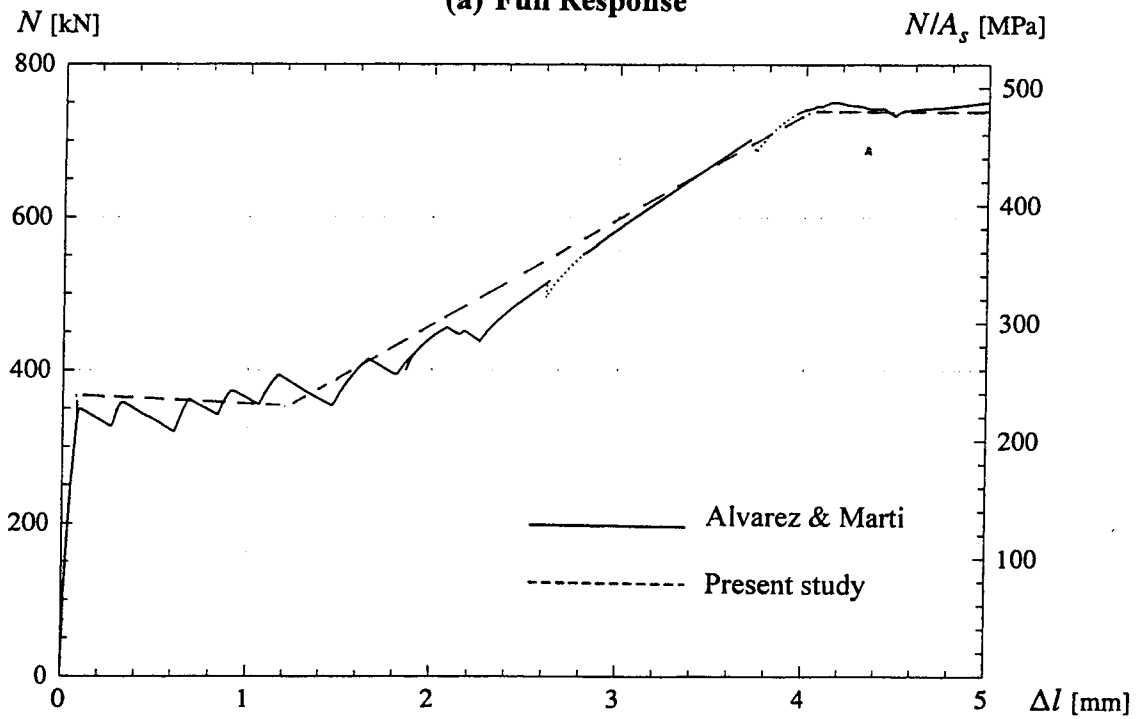


(b) Response before yielding

Figure 5.30 Observed and predicted load versus elongation for specimen Z7 tested by Alvarez & Marti



(a) Full Response



(b) Response before yielding

Figure 5.31 Observed and predicted load versus elongation for specimen Z8 tested by Alvarez & Marti

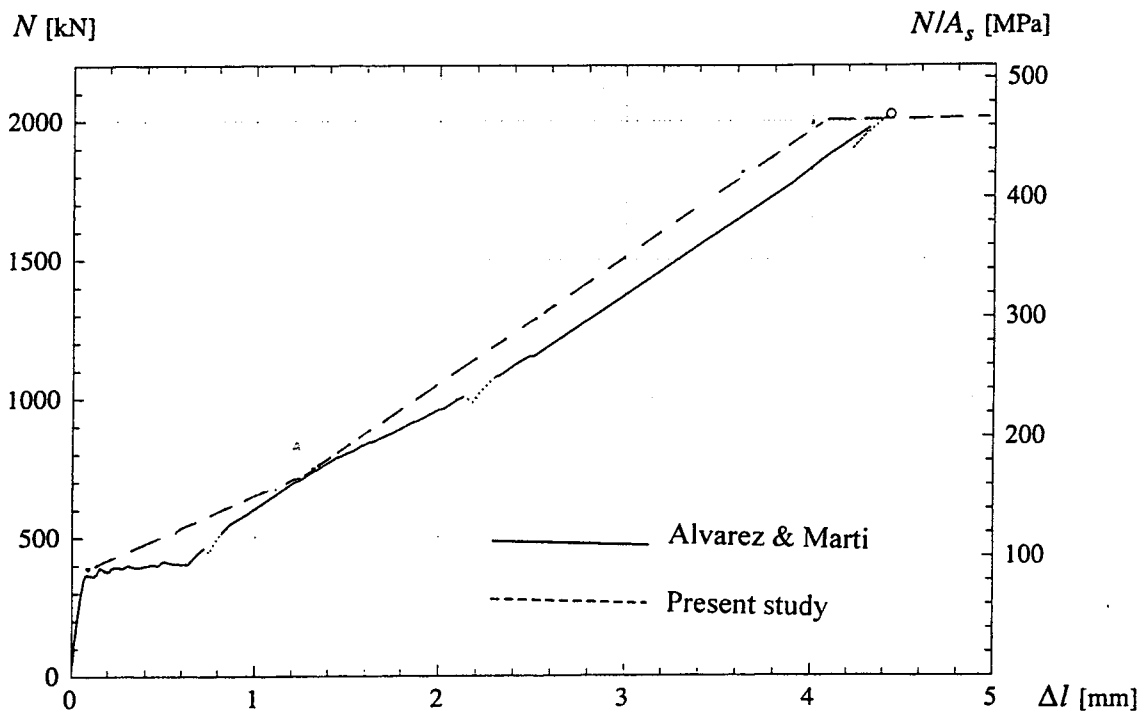


Figure 5.32 Observed and predicted load versus elongation for specimen Z9 tested by Alvarez & Marti

6- Parametric Studies

6.1 Introduction

Two parametric studies are presented in this chapter. First, the developed analytical model was used to carry out a parametric study of the structural response of wall panels to extend the range of the available test results. Section 6.2 gives the basic variables studied followed by the results given in Section 6.3. This study is summarized in Section 6.4. Finally, Section 6.5 describes a study conducted to investigate the hydraulic conductivity through cracks and the compression zone of the concrete section.

6.2 Parametric Study of Structural Behaviour

The experimental study investigated the effect of four parameters on the behaviour of partially prestressed wall segments in concrete water tanks. These four parameters are:

1. The effective depth of non-prestressed steel. Two values for concrete cover were tested, namely 20 mm and 40 mm (i.e. $d = 222$ and 202 mm respectively).
2. The partial prestressing ratio expressed as the ratio between non-prestressed and prestressed steel area A_s/A_p for which three ratios were tested namely 0.0, 1.3 and 5.0.
3. Load eccentricity, e ; for which four eccentricities were tested, namely pure moment, $e = 520$ mm, $e = 260$ mm and axial tension ($e/h = \infty, 2.08, 1.04$ and 0.0 respectively).
4. Bond characteristics of tendons; bonded and unbonded.

The restrictions on the number of physical tests limited the number of values studied for each of the four parameters not to mention other parameters. The present analytical model, which yielded satisfactory agreement with test results, was used to generate a parametric study. With the exception of bond characteristics of tendons, the parametric study addressed the same parameters investigated in the experimental tests with more values and wider range. In addition to these parameters, the effects of the

effective depth of prestressed steel and the concrete wall thickness were studied. The parametric study did not address some parameters such as the method of prestressing, post-tensioning versus pre-tensioning, and type of tendons; strands versus wires or bars.

The basic concrete section used in this parametric study had a width of 1000 mm and a thickness of 250 mm which is the minimum thickness required by the North American standards and recommendations for constructability. The section was reinforced with non-prestressed steel of area $A_s = 800 \text{ mm}^2$ at an effective depth, d , of 200 mm and prestressed steel of area $A_p = 800 \text{ mm}^2$ at an effective depth, d_p , of 150 mm. The stress-strain relationships for both steel types were those used in modeling the experimental tests. The concrete uniaxial compressive strength f'_c was selected equal to 45 MPa, a cracking stress of concrete of $0.23\sqrt{f'_c}$ was used, and the concrete compressive strain corresponding to f'_c , ϵ_{co} , was set to 0.0023. A summary of the variables studied in the parametric study is given in Table 6.1. The table indicates that a total of 51 wall sections were analyzed. For each case the analytical model generated several relationships including moment versus curvature, moment versus depth of compression zone (c), load versus c , extreme fiber concrete compressive stress f_c versus c , non-prestressed steel stress f_s versus c and concrete stress at mid-depth versus c . The results of the parametric study are presented in several forms to delineate the behaviour of each parameter.

6.3 Results of the Parametric Study of Structural Behaviour

6.3.1 Moment versus Curvature

Figures 6.1 through 6.5 show the effect of the different studied parameters on moment-curvature relationships. Figure 6.1 indicates that the non-prestressed steel effective depth, d , has no effect before cracking. Reducing d slightly softens the response after cracking. This slight effect is due to the fact that the contribution of non-prestressed steel on the total moment is insignificant in the partially prestressed concrete sections

studied. On the other hand, the same figure shows the significant effect of increasing prestressed steel effective depth, d_p , on increasing the cracking moment and post-cracking moments. In the case studied the ultimate moment is increased by about 70%. Because, in this example, the prestressing steel contributes about 80% of the tensile force, increasing its effective depth improves the moment resistance more than increasing the effective depth of the non-prestressed reinforcement. The significant effect of wall thickness on the moment is clear in Fig. 6.2; increasing the thickness by 20%, from 250 to 300 mm, increased the moments by about 40% for the case studied.

It can be observed from Fig. 6.3 that load eccentricity, e , has a great effect on the ultimate curvature; reducing the eccentricity dramatically increased the section deformation but decreased the moment resistance. The effect of partial prestressing on moment-curvature relationships is demonstrated in Figs. 6.4 and 6.5 for two partial prestressing ratios. The first is the A_s/A_p ratio that satisfies the condition that the total steel in the section, $A_s + A_p$, is constant, i.e. $\rho_{total} = \text{constant}$. The second is the A_s/A_p ratio that satisfies the relationship: $\varpi = A_s f_y + A_p (0.9 f_{pu}) = \text{constant}$. Here the ultimate capacity of the section is the same for any A_s/A_p ratio. The case of steel ratios that satisfy $\rho_{total} = \text{constant}$, Fig. 6.4, exhibits the well-known difference between reinforcement and prestressing steel. The former produces larger deformation with lower moment capacity. In the case of the steel ratios that satisfy $\varpi = \text{constant}$, Fig. 6.5 (a), all A_s/A_p ratios achieved the same ultimate ductility but do not have the same ultimate moment. All of the curves intersect at a moment of 156 kNm. At that moment $f_p j d_p / f_s j d = 0.9 f_{pu} / f_y$, and since all the steel ratios satisfy the relationship: $A_s + A_p (0.9 f_{pu} / f_y) = \text{constant}$, the resulting moment is constant for all steel ratios. The ultimate moments vary because the effective depth for non-prestressed steel and prestressed steel were not the same. To overcome this difference the section was reanalyzed with $d = d_p = 200$ mm. The resulting moment versus curvature diagrams are given in Fig. 6.5 (b). The small differences which still exist in ultimate moments are because the ratio between f_p and f_s at ultimate is not exactly $0.9 f_{pu} / f_y$ due primarily to the strain hardening of non-prestressed steel.

6.3.2 Depth of Compression Zone

Test results indicate that no leakage occurs through flexural cracks as long as a compression zone exists. The depth of the compression zone seems to be an effective parameter in preventing leakage.

Figures 6.6 through 6.9 give the depth of the compression zone, c , versus moment for the studied parameters. It can be observed from the figures that while changing d has almost no effect on c , increasing d_p significantly increases c . Figure 6.7 indicates that even after cracking members with $e/h > 0.5$ still have a considerable compression zone. Figures 6.8 and 6.9 illustrate the efficiency of prestressed tendons in increasing c for steel ratios with $\rho_{\text{total}} = \text{constant}$ and $\varpi = \text{constant}$ respectively.

Some design procedures such as ACI 350 (1989) are based on limiting the non-prestressed steel stress under service loads. The limiting stress typically varies from 100 MPa to 200 MPa depending upon the exposure conditions, bar size and whether the section is subjected to direct tension or flexure. The limiting stress does not depend on load eccentricity or partial prestressing ratio. For this range of steel stress Fig. 6.10 shows that for a constant e/h , there is virtually no difference in the depth of the compression zone. It also shows that e/h has a considerable influence on the depth of the compression zone. Figure 6.11 shows that for the typical steel stress limit, the impact of A_s/A_p is less significant than that of e/h .

Figure 6.12 shows the effect of increasing the allowable steel stress on the depth of the compression zone. Doubling the steel stress reduces c by only 25%. Figure 6.12 also shows that the value of c becomes constant for each steel stress when e exceeds about four times the thickness. The same effect is illustrated in Fig. 6.13 for different A_s/A_p with constant ϖ . The reduction in c in this case is less than 20% with a considerable compression zone for all steel ratios.

6.3.3 Concrete Residual Stresses

In the design of circular prestressed concrete tanks, ACI 344 requires that full prestressing be used in the circumferential direction, subjected to axial tension, with a residual compressive stress in concrete of 1.38 MPa (200 psi). ACI 344 allows partial prestressing in the vertical direction but specifies that the average compressive stress due to prestressing after all losses is 1.38 MPa. Since the section is only subjected to moment, the concrete compressive stress at mid-thickness must be less than 1.38 MPa. This indicates that a residual compressive stress is also required in the vertical direction at the section mid-thickness.

The concrete stress at mid-thickness is plotted versus depth of compression zone c and shown in Figs. 6.14 through 6.17 for different load eccentricities, steel ratios with constant ω , wall thickness, d and d_p respectively. Figure 6.14 shows that for a specific residual concrete stress (RCS), for instance -1.38 MPa, the depth of the compression zone is greater for smaller eccentricities. This is rational since the stress gradient is small when load eccentricity is small. Figure 6.15 shows that a RCS of -1.38 MPa can not be achieved beyond a certain partial prestressing ratio, $A_s/A_p = 8$ in the figure. Below this limiting ratio, the change in steel ratio slightly affects the depth of the compression zone corresponding to RCS of -1.38 MPa. Figures 6.16 and 6.17 show that the effect of wall thickness on c is significant and that both of d and d_p have little effect on c . At a RCS of -1.38 MPa, increasing the wall thickness from 190 to 300 mm caused a 70 mm increase in the depth of the compression zone.

While it ensures that most or all of the section is in compression, a RCS of -1.38 MPa yielded, in the studied cases, a steel stress, f_s , ranging from 0.03 to 0.12 of the yield stress. The smaller the eccentricity, or the larger the A_s/A_p ratio, the lower is f_s . On the other hand, a RCS of -1.38 MPa yielded in the cases studied cases a reasonable concrete compressive stress f_c that ranged between 0.2 and 0.4 f'_c .

In order to overcome the drawbacks resulting from specifying a RCS of -1.38 MPa, two alternative values for residual concrete stresses (RCS) at mid-depth were investigated. Figures 6.18 and 6.19 present the impact of changing RCS from -1.38 to 0.0 and 1.0 MPa on f_s and f_c for different load eccentricities and mechanical steel ratios respectively. It can be observed from the figures that this change in RCS increased f_s , 70% in the first figure. The percentage of increasing f_s in Fig. 6.19 varies from 50 to 500%. This change in RCS also increased f_c by smaller percentages. However, both f_c and f_s are still within reasonable limits. The effect on bending moment and depth of compression zone c is illustrated in Figs. 6.20 and 6.21 for different load eccentricities and steel ratios with constant ω respectively. Reducing RCS increased the carried moment which, with the exception of the cases with very small eccentricities, is still in the acceptable stage between cracking and yielding moments particularly for high partial prestressing ratios. Furthermore, this change in RCS does not significantly reduce c which is still more than 110 mm in the studied cases.

For the case of axial tension, Fig. 6.22 shows plots for load versus concrete strain for different steel ratios with constant ω . The plots indicate that while the ultimate capacity is the same for all steel ratios, the cracking load increases and the deformation reduces with increasing prestressed steel in the section. It should also be realized that specifying a residual compressive or even zero stress in the concrete means that the stress in the non-prestressed steel will be either compressive or zero. The only way to utilize the presence of non-prestressed steel in the section is by allowing some tensile stress in the concrete. For instance allowing only 1.0 MPa tensile stress, although it produces f_s of only 8.0 MPa, significantly increases the capacity as shown in the Fig. 6.23. It should be noticed that concrete, non-prestressed and prestressed steel all contributed in this increment in load.

6.4 Summary of the Parametric Study on Structural Behaviour

The aim of this parametric study was to provide further insight into the behaviour of partially prestressed sections subjected to combinations of axial load and

moment. A second objective was to examine existing codes recommendations on behaviour in order to try to identify a rational design method for concrete water tanks. Fifty-one cases were analyzed in the parametric study and based on the behaviour observed in these cases the following conclusion are drawn:

1. The non-prestressed steel stress f_s recommended by ACI 350 appears to be very conservative, especially in the case of partial prestressing or an axial load with a small eccentricity. A design method based on limiting the steel stress, f_s , does not produce consistent crack or compression zone depths.
2. The residual compressive concrete stress of 1.38 MPa required by ACI 344 produces very low steel stress, f_s , for small load eccentricities. A design method based on providing a residual compressive stress in the concrete does not utilize non-prestressed reinforcement effectively.
3. Relaxing the residual compressive stress requirement permits a more efficient design. The stresses in steel are higher, but below yield so less reinforcement is used. Reasonable values of concrete stresses and considerable depths of compression zone can be achieved.
4. Load eccentricity significantly affects the behaviour of the partially prestressed concrete sections. The behaviour with a small load eccentricity, less than about half the thickness, is close to that of pure axial tension. At a load eccentricity larger than about four times the thickness, the section may be treated as a flexural member.
5. The ratio of steel in a partially prestressed concrete section has a significant effect on the member serviceability and strength. Choosing the steel ratio such that both non-prestressed and prestressed steel reach their strength simultaneously is effective in utilizing both types of steel at the ultimate limit state. Increasing the amount of prestressed steel increases the cracking load and the depth of the compression zone.

6. Increasing the wall thickness is very effective in increasing the capacity of the section and improving its serviceability by increasing the compression zone and reducing the deformations. However, according to the existing specifications this requires the use of more prestressing steel to achieve the required residual compression. The existing specifications appear to be irrational because adding concrete to the section should not require additional reinforcement.

6.4 Hydraulic Conductivity of Concrete

As presented in Chapter 3, leakage tests showed that leakage does not occur through the concrete section as long as a compression zone exists. A separate numerical study was performed to investigate the effect of the uncracked compression zone on the rate of water leakage through the concrete. In this study a 255 mm thick wall segment was subjected from one side to an 8 m head of water and leakage of water through the section was studied. These values were chosen to represent the experimental leakage test.

Laplace's equation for steady-state flow which states that:

$$\frac{\partial^2 u}{\partial x^2} + \frac{\partial^2 u}{\partial y^2} = 0 \quad (6.1)$$

was used to find the distribution of hydraulic pressure through the section, where u in this case is the hydraulic pressure. This equation was solved numerically using a finite difference technique. Darcy's law for laminar flow in porous media was used to calculate leakage through the wall thickness. Darcy's law (Cedergreen, 1989) states that:

$$Q = kiAt \quad (6.2)$$

where, Q is the quantity of seepage or leakage (m^3) through a media with a coefficient of permeability k and a cross section with an area A normal to the direction of flow, under a hydraulic gradient i , during a time period t .

A computer program was written to perform this study. The numerical solution for Laplace's equation is found in Gerald (1980). The finite difference mesh used in the analysis is shown in Fig. 6.24. The shaded area in the middle of the mesh represents a crack that varies in depth. The mesh extends horizontally to the mid-point between cracks. An additional line of nodes at each side was used to apply the boundary condition of zero flow in the horizontal direction along the vertical edges. The hydraulic pressure on the top row of nodes and on all the nodes located on the perimeter of the crack was taken equal to 8 metres. Zero pressure was considered on the lower row of nodes, located on the soffit of the section. A coefficient of permeability for concrete of 30×10^{-12} m/s was used in this study. This value was taken from Neville (1981) and is conservative since it was originally obtained from concrete with a water/cement ratio of 0.47 used in dams. The concrete coefficient of permeability can also be obtained from CEB-FIP Model Code 1990 Eq. 2.1-103 (1993), which gives significantly smaller value. The depth of the crack was changed from 0.0 to 250 mm and leakage in each case was calculated.

In Fig 6.25 the nodal vertical flow rate through the thickness, at the vertical line directly below the crack, is plotted for different depths of compression zone. It can be observed from the figure that increasing the depth of the compression zone reduces the flow rate. The horizontal distribution of flow rate for a 135 mm crack depth is plotted in Fig. 6.26 at three different horizontal layers; one just below the crack, other at the soffit and a third layer mid-way between these two layers. It can be seen that within the 120 mm compression zone, the distribution of flow becomes more uniform as one moves away from the crack. Finally, the volume of water that leaks through the thickness from one square metre of wall per week is plotted in Fig. 6.27 for different depths of compression zone. The leakage quantity Q can be calculated using a simple but conservative approach. In this approach the hydraulic gradient i is assumed to vary linearly within the compression zone which means that: $i = H/c$. Water head H is assumed to be constant on a horizontal layer located at the top of the compression zone. In other words, the section is assumed uncracked with a thickness equal to the compression zone depth c . With these assumptions Eq. 6.2 becomes:

$$Q = k H/c \quad (\text{m}^3/\text{m}^2/\text{s}) \quad (6.3)$$

The dashed curve in Fig. 6.27 gives the values obtained from this approximate method. The significant effect of increasing the depth of compression zone on reducing leakage is clear in the figure. Furthermore, it is obvious from Fig. 6.27 that the quantity of leakage in either case is negligible particularly when compared to the allowable leakage rate in various standards. ACI 344 allows about $H/300$ per week, while BS8007 allows loss of $H/500$ per week. The value of Q that corresponds with the allowable leakage rates in BS8007 is plotted in Fig. 6.27 for two rectangular tanks.

If the water fast evaporates from the wall surface than it flows through the wall, the surface will stay dry. Water evaporation can be estimated using mass-transfer method given by Ponce (1989):

$$E_a = (0.013 + 0.00016v)e_o \frac{100 - RH}{100} \quad (6.4 a)$$

$$\text{where, } e_o = 6.11 \exp\left(\frac{17.27T}{237.3 + T}\right) \quad (6.4 b)$$

where,

E_a is mass-transfer evaporation rate, in centimeters per day per square metre,

v is wind velocity, in kilometers per day,

e_o is saturation vapor pressure in millibars at the overlying air temperature T in °C,

RH is the relative humidity in percent.

For the conditions of a relative humidity, RH , of 75% and a wind velocity of 5 km/hr, the air temperature T necessary to give a dry surface are given in Table 6.2 for various points in Fig. 6.27.

This section studied the leakage through cracks with compression zone. Leakage through through-cracks is discussed in Section 2.5.1

The above analysis for the cases studied shows that virtually any compression zone depth will give adequate leakage control. While a compression zone thickness of 5 mm may be theoretically adequate, bug holes, honey combing and other small voids greater than 5mm may cause a breach of the compression zone. A practical minimum design thickness for the compression zone should account for these possible defects.

Table 6.1 Summary of the variables for the parametric study

Variable examined	h (mm)	e/h	A _s (mm ²)	A _p (mm ²)	A _s /A _p	d (mm)	d _p (mm)	Case No.
Load eccentricity (e)	250	0.00	800	800	1.0	200	150	1
		0.16						2
		0.40						3
		1.60						4
		4.40						5
		10.00						6
		∞						7
Wall thickness (h)	190	4.40	800	800	1.0	200	150	8
	250							9
	300							10
Effective depth (d) for non-prestressed steel	250	4.40	800	800	1.0	225	150	11
						200		12
						175		13
Effective depth (d _p) for prestressed steel	250	4.40	800	800	1.0	200	200	14
							150	15
							125	16
steel ratio A _s /A _p with ρ _{total} = constant	250	4.40	1600	0	∞	200	150	17
			1500	100	15.00			18
			1200	400	3.00			19
			800	800	1.00			20
			400	1200	0.33			21
			100	1500	0.07			22
			0	1600	0.00			23
steel ratio A _s /A _p with ω = constant	250	4.40	4011	0	∞	200	150	24
			3000	252	11.90			25
			2670	334	8			26
			2000	501	4.00			27
			1600	600	2.67			28
			1200	700	1.71			29
			800	800	1.00			30
			400	990	0.40			31
			0	1000	0.00			32

- The last variable, steel ratio with ω = constant, was repeated for pure moment (cases 33 to 40), for axial tension (cases 41 to 48) and for d = d_p = 200 mm (cases 49 to 56).
- The variable of each case is shaded

Table 6.2 Temperature required to equate evaporation and leakage rates

c (mm)	Q (m ³ / week) = E _a (m ³ / week)	Temperature (°C)
255	0.000579	7.2
180	0.000658	9.2
120	0.000849	13
60	0.001279	19.5

Evaporation calculations assumes: wind speed = 5 km/hr, RH = 75%
 The values of Q are those obtained from the finite difference analysis.

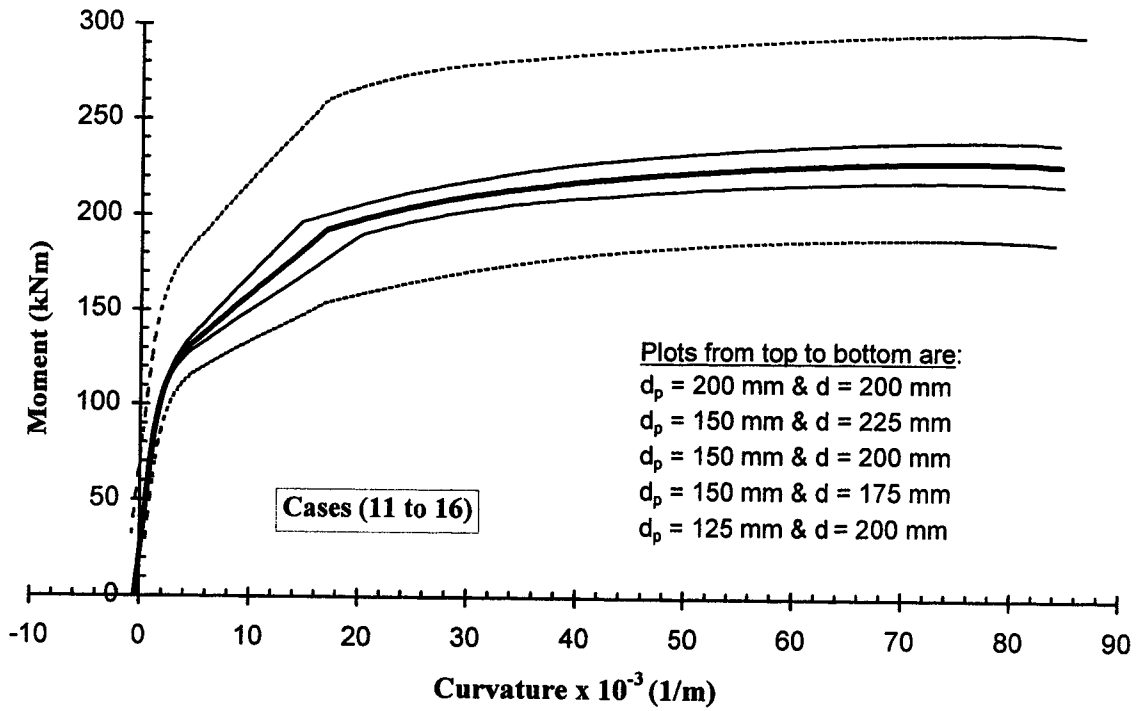


Figure 6.1 Effect of effective depth on moment versus curvature response

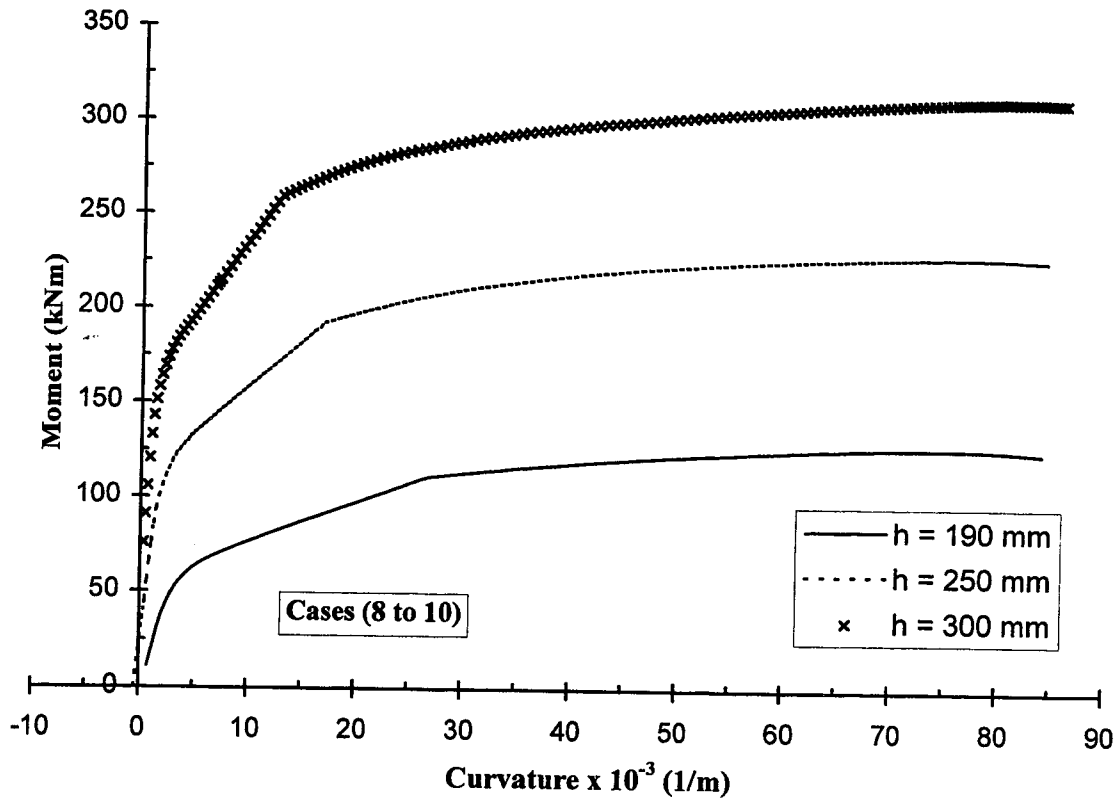


Figure 6.2 Moment versus curvature for different wall thicknesses

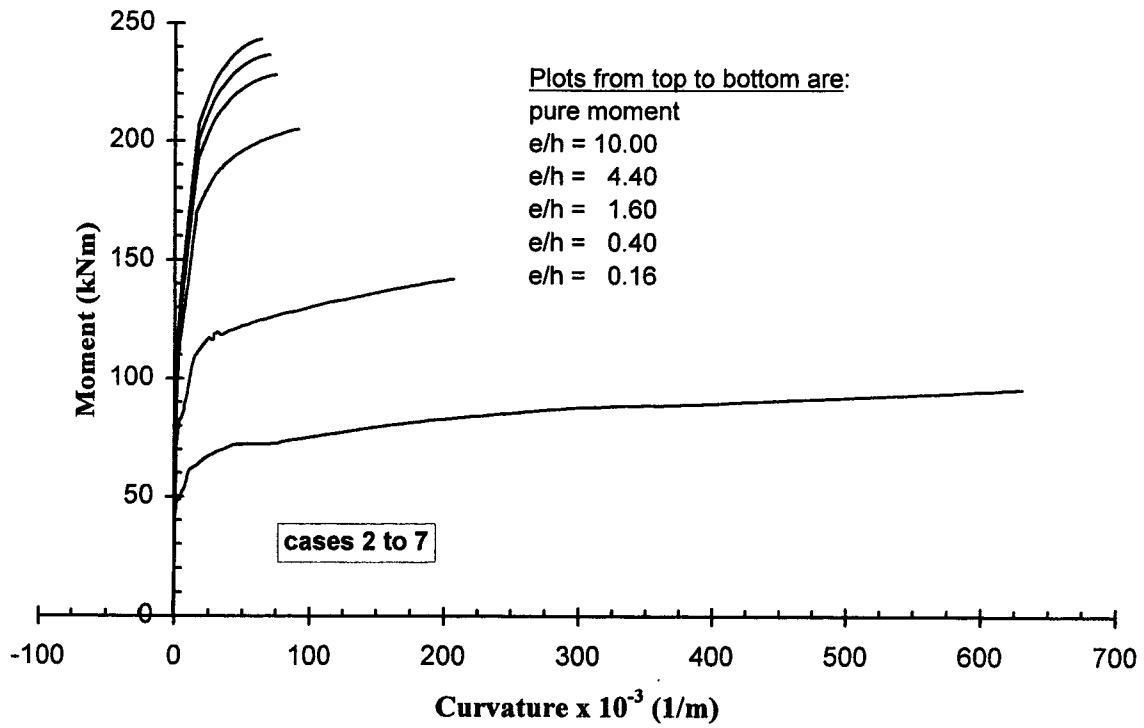


Figure 6.3 Moment versus curvature for different load eccentricities

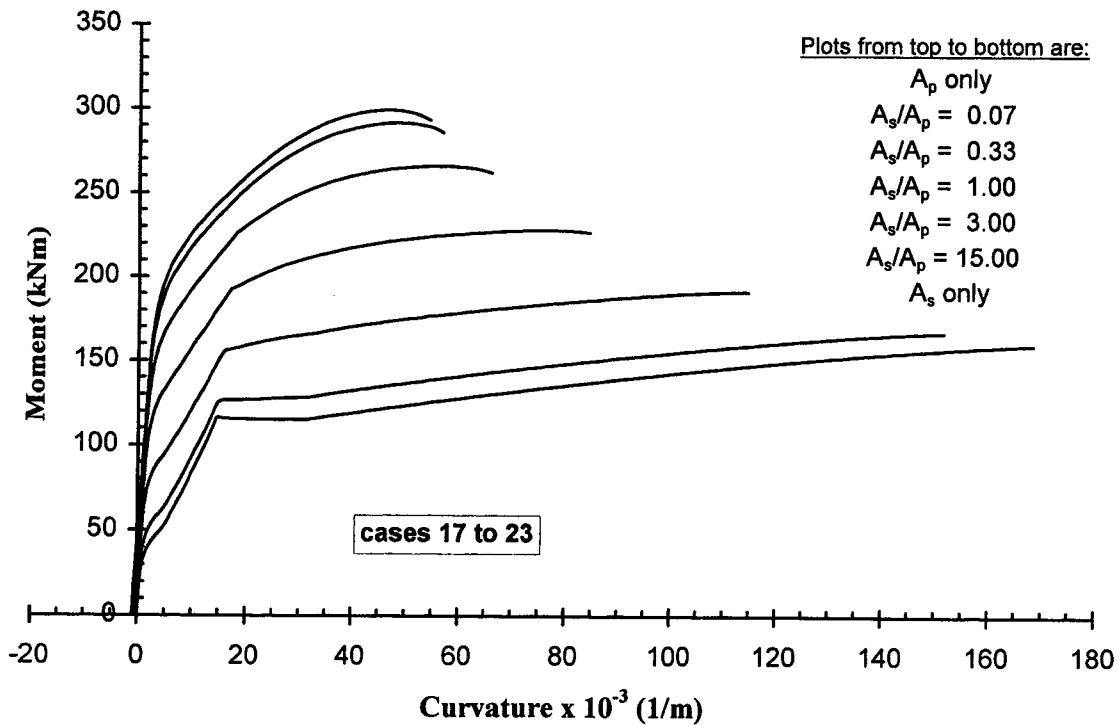
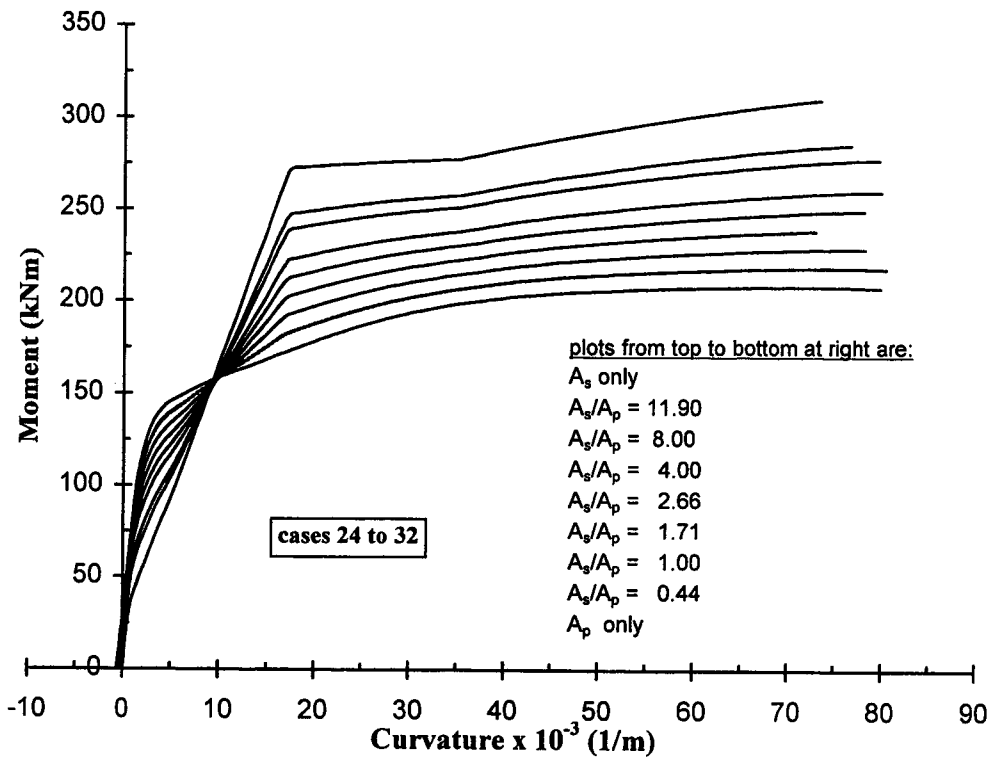
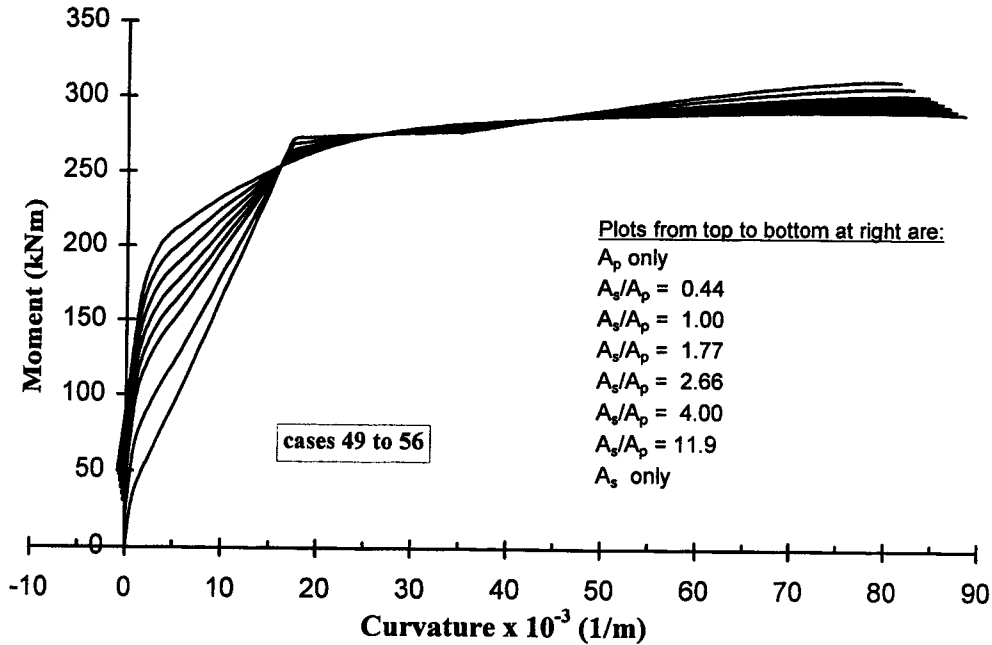


Figure 6.4 Effect of steel ratio on moment versus curvature response for constant ρ_{total}



(a) $d_p = 150$ mm & $d = 200$ mm



(b) $d = d_p = 200$ mm

Figure 6.5 Effect of steel ratio on moment versus curvature for constant ϖ

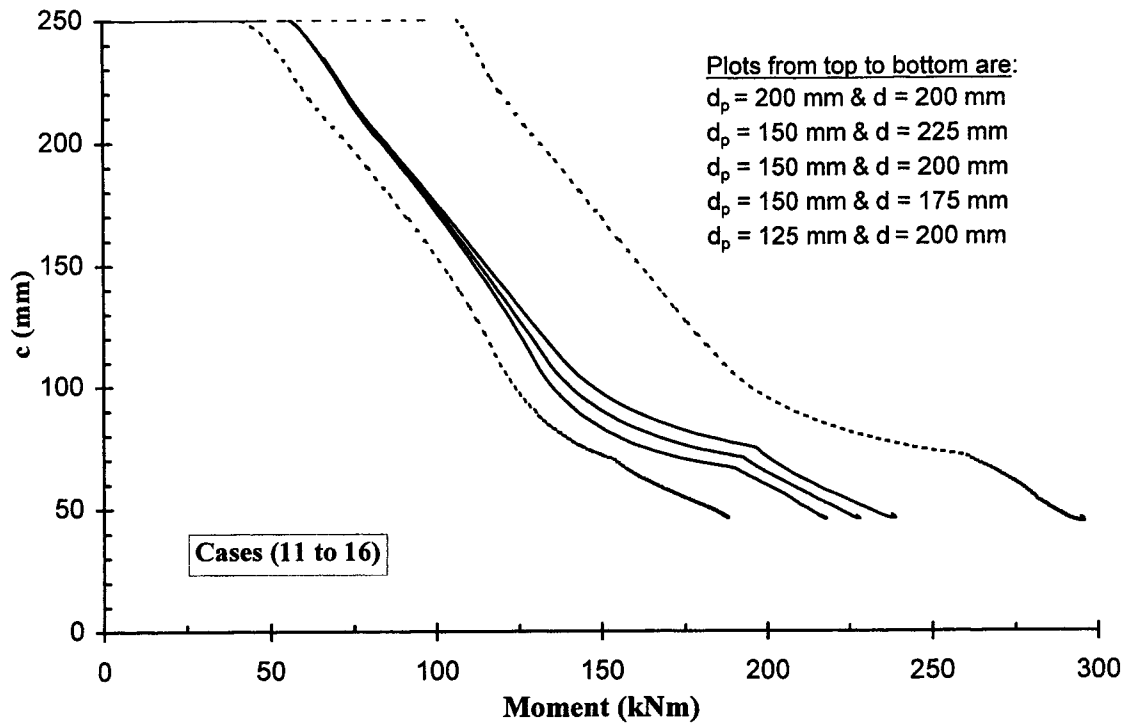


Figure 6.6 Effect of effective depth on compression zone depth

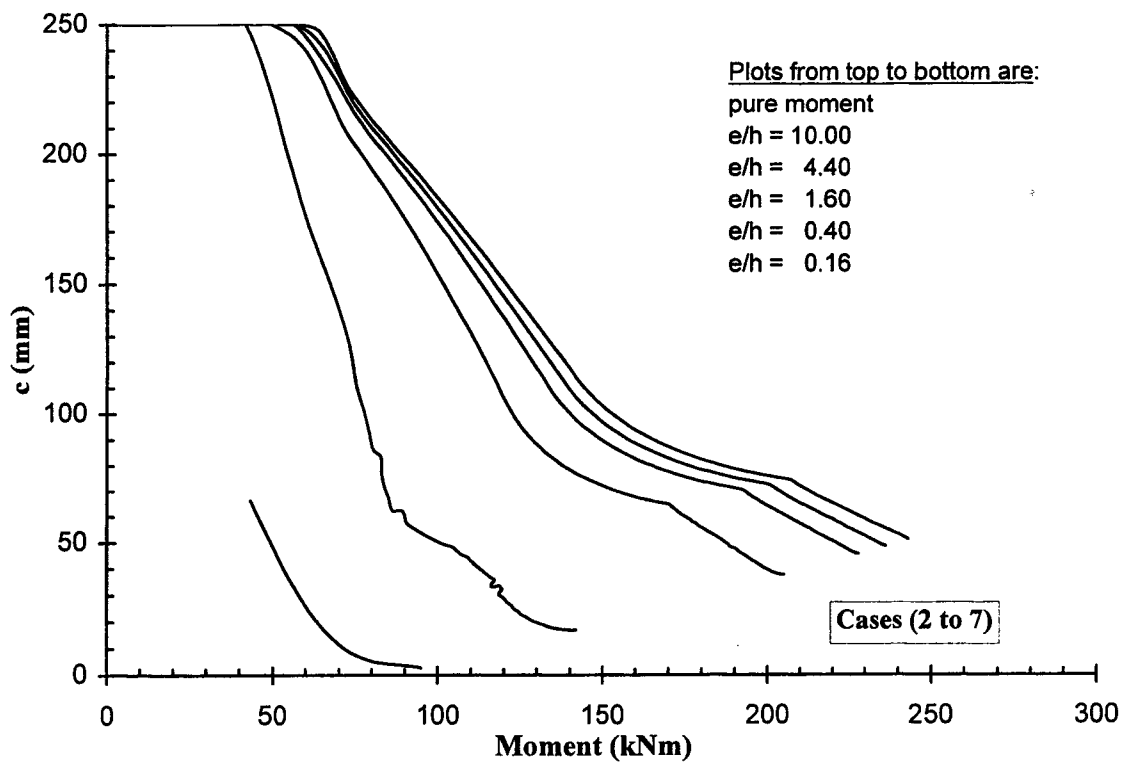


Figure 6.7 Effect of load eccentricity on compression zone depth

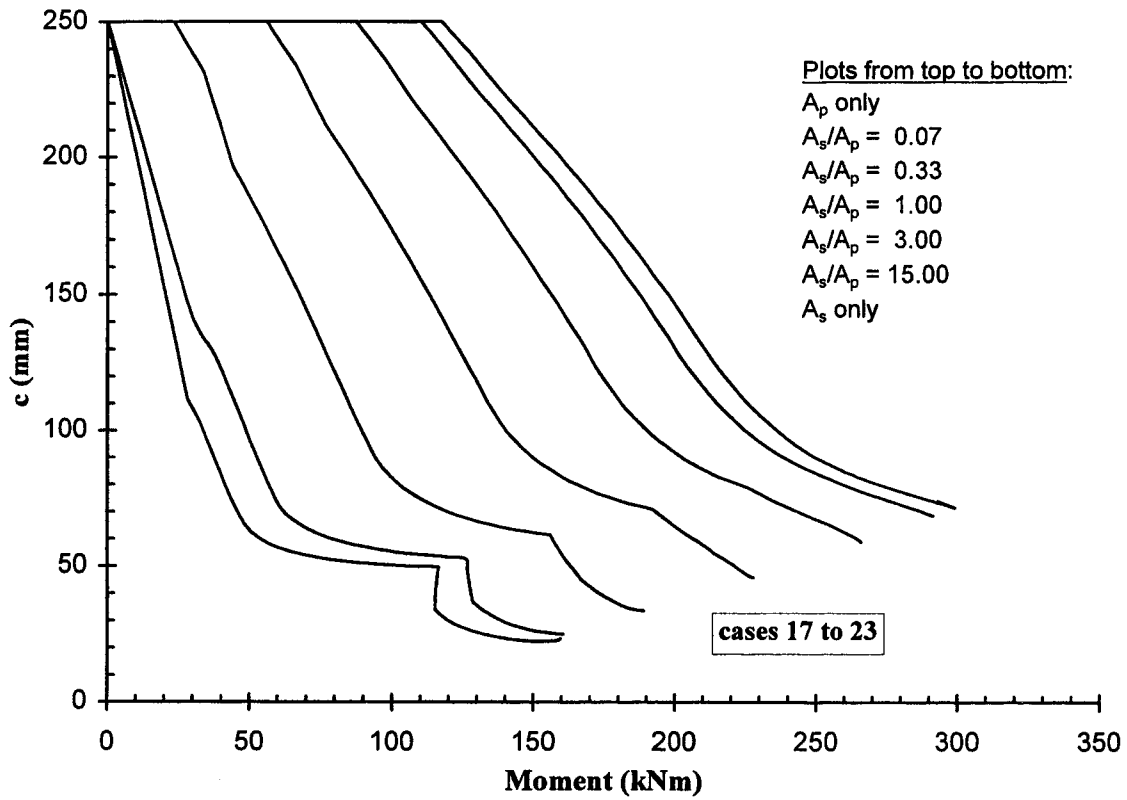


Figure 6.8 Effect of steel ratio on compression zone depth for constant ρ_{total}

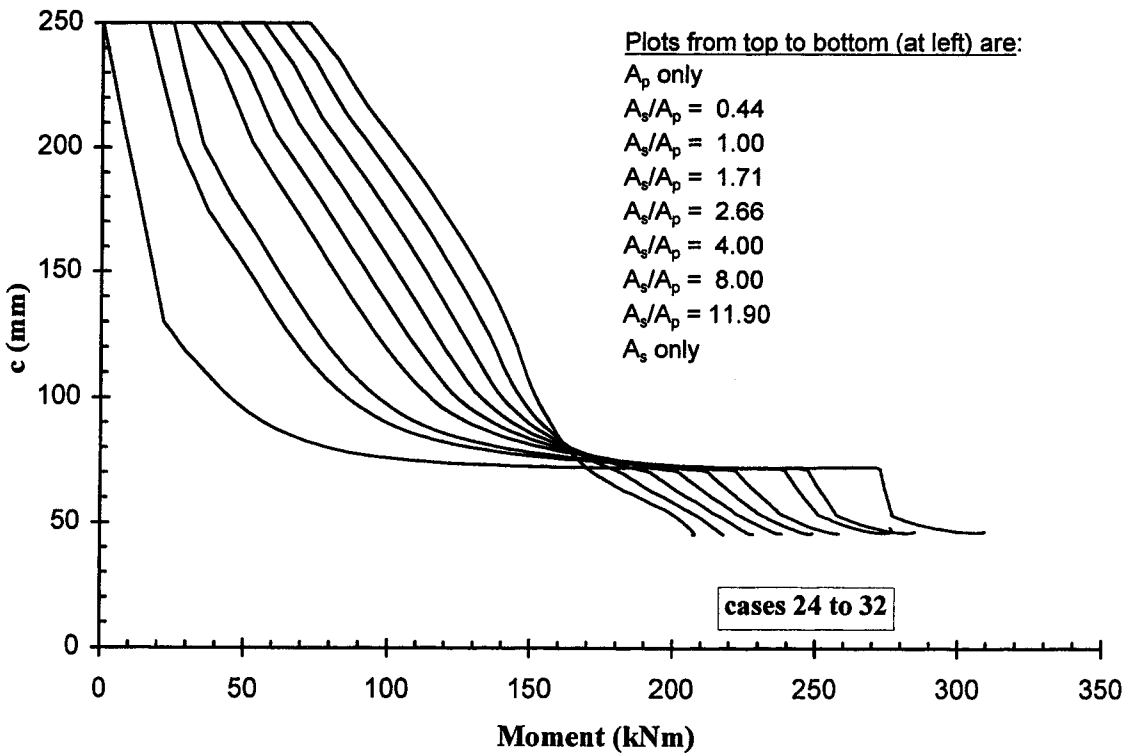


Figure 6.9 Effect of steel ratio on compression zone depth for constant ϖ

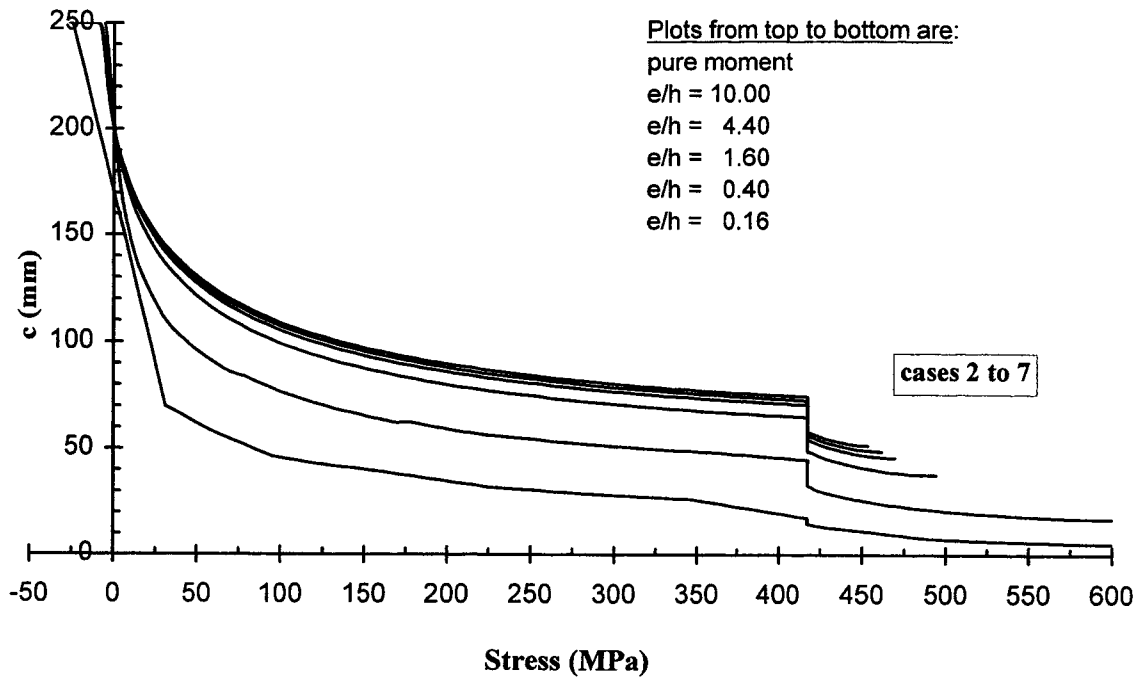


Figure 6.10 Effect of load eccentricity on compression zone depth versus non-prestressed steel stress

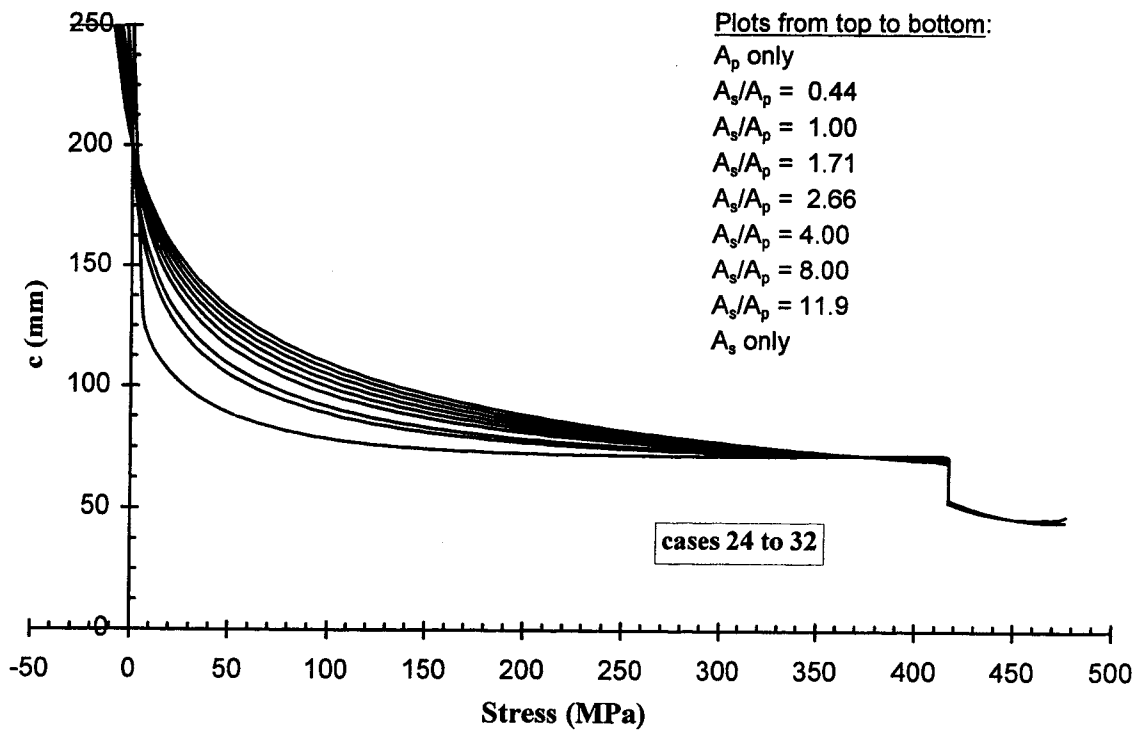


Figure 6.11 Effect of steel ratio on compression zone depth versus non-prestressed steel stress ($\varpi = \text{constant}$)

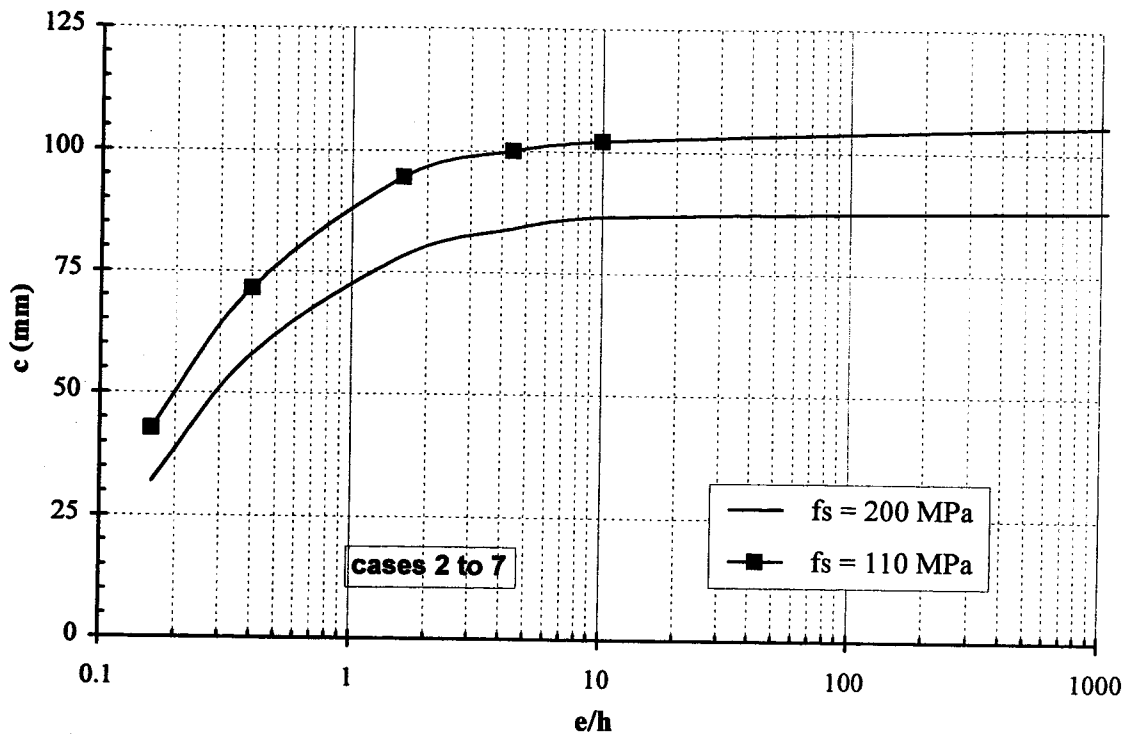


Figure 6.12 Effect of increasing steel stress on depth of compression zone for different load eccentricities

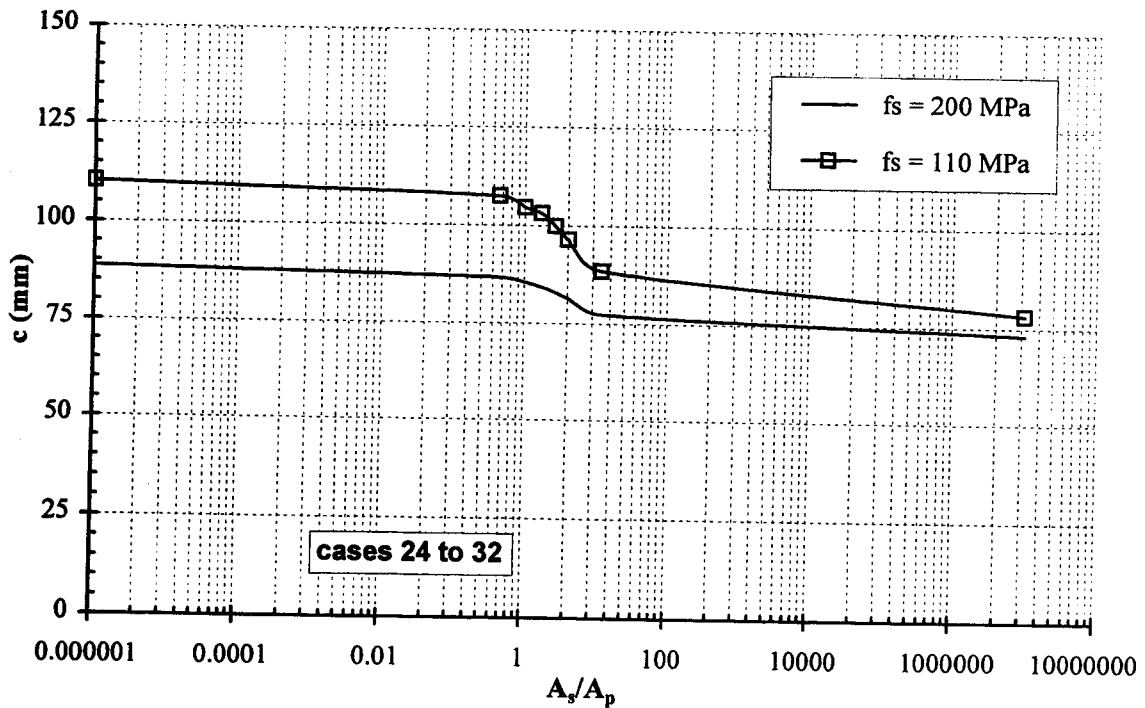


Figure 6.13 Effect of increasing steel stress on depth of compression zone for different steel ratios ($\varpi = \text{constant}$)

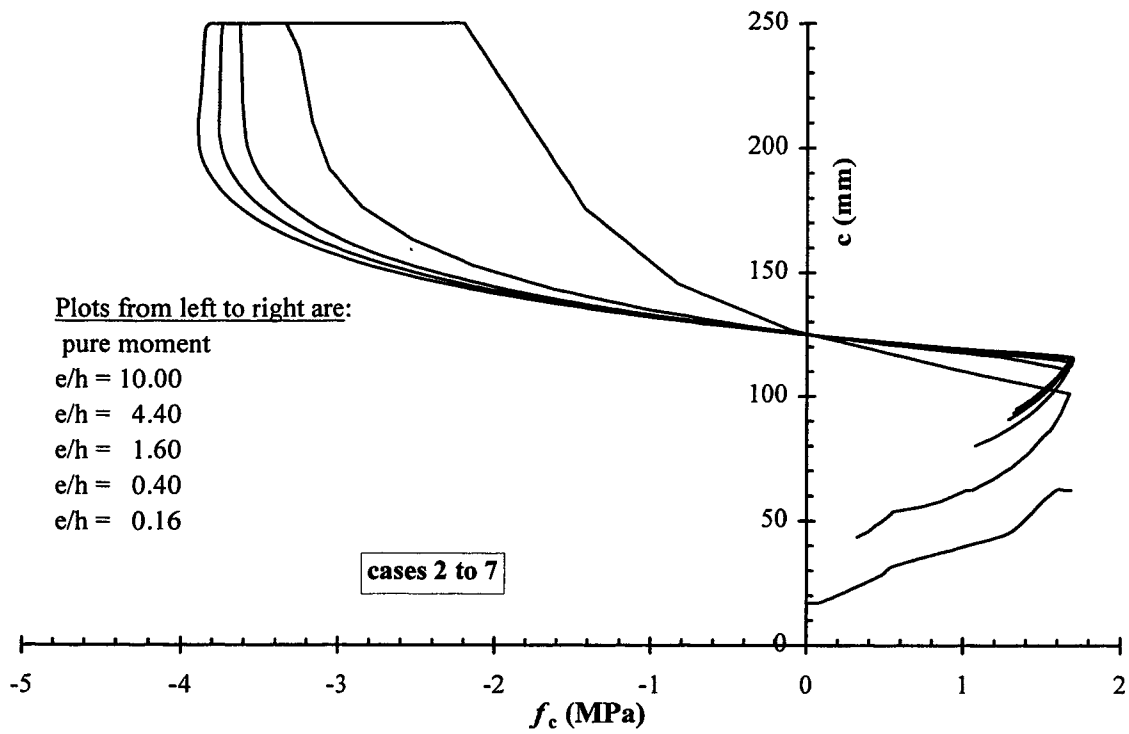


Figure 6.14 Compression zone depth versus residual stress at centroid for different load eccentricities

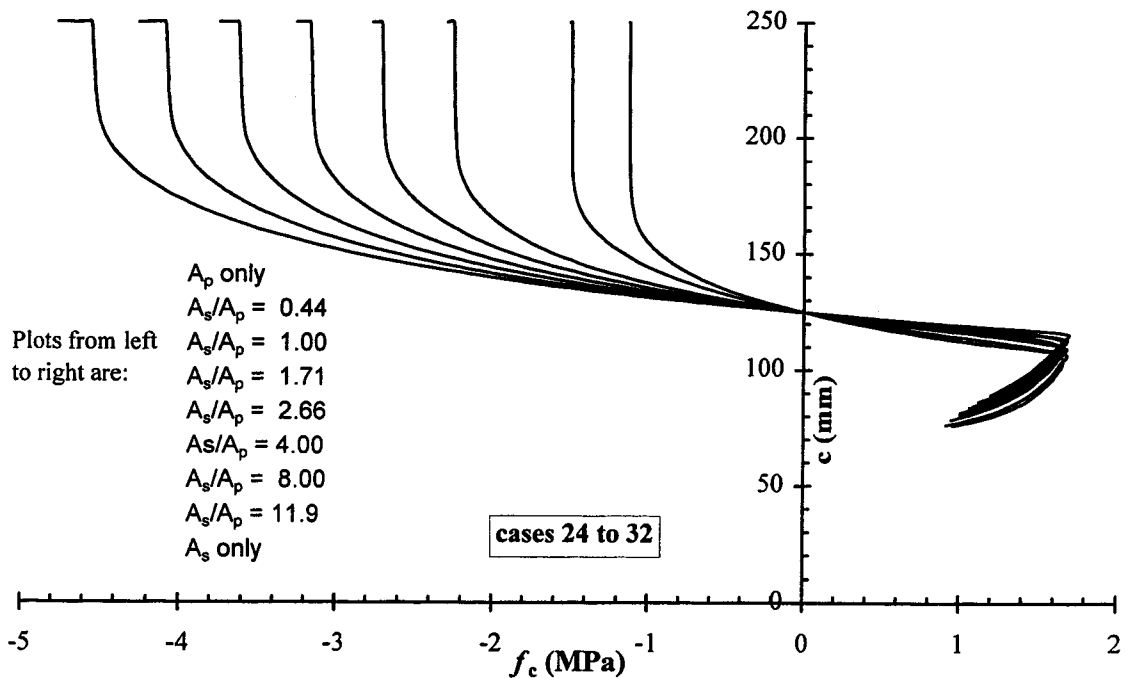


Figure 6.15 Compression zone depth versus residual stress at centroid for different steel ratios ($\varpi = \text{constant}$)

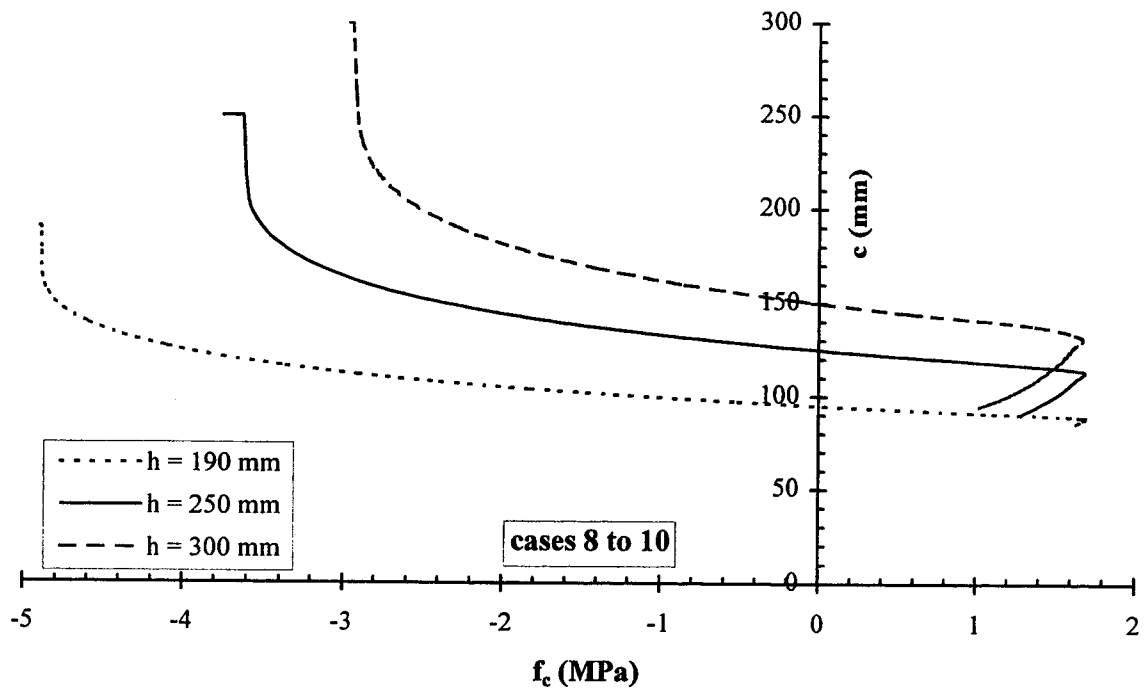


Figure 6.16 Compression zone depth versus residual stress at centroid for different wall thicknesses

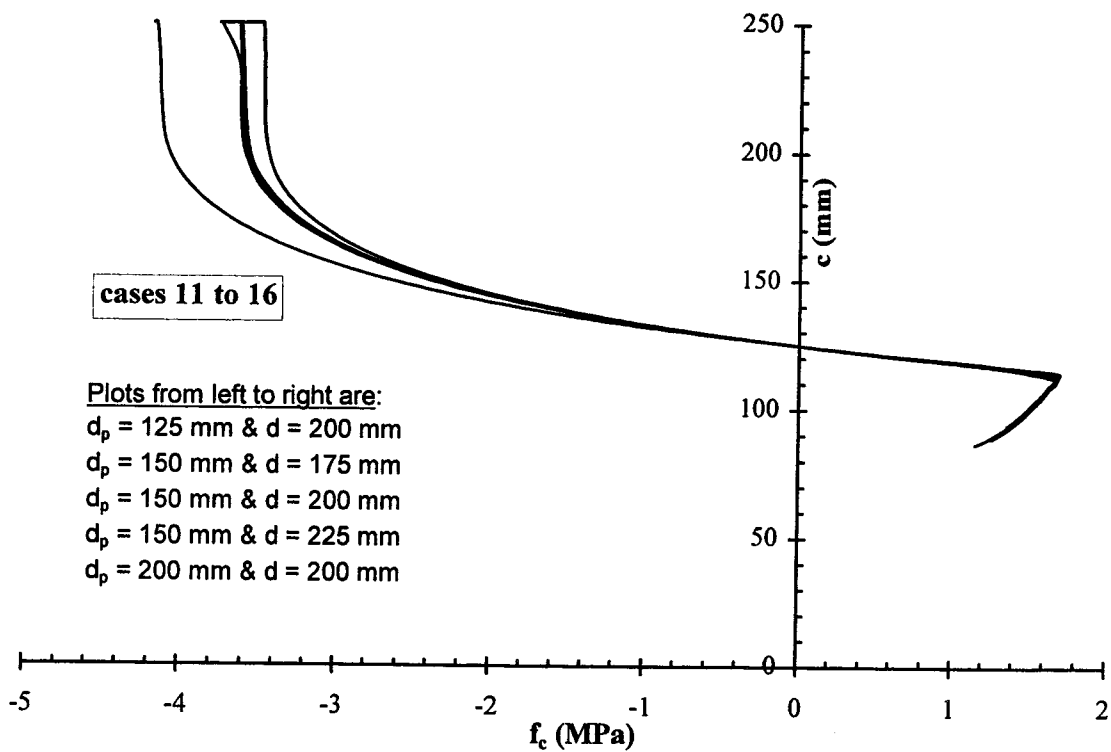
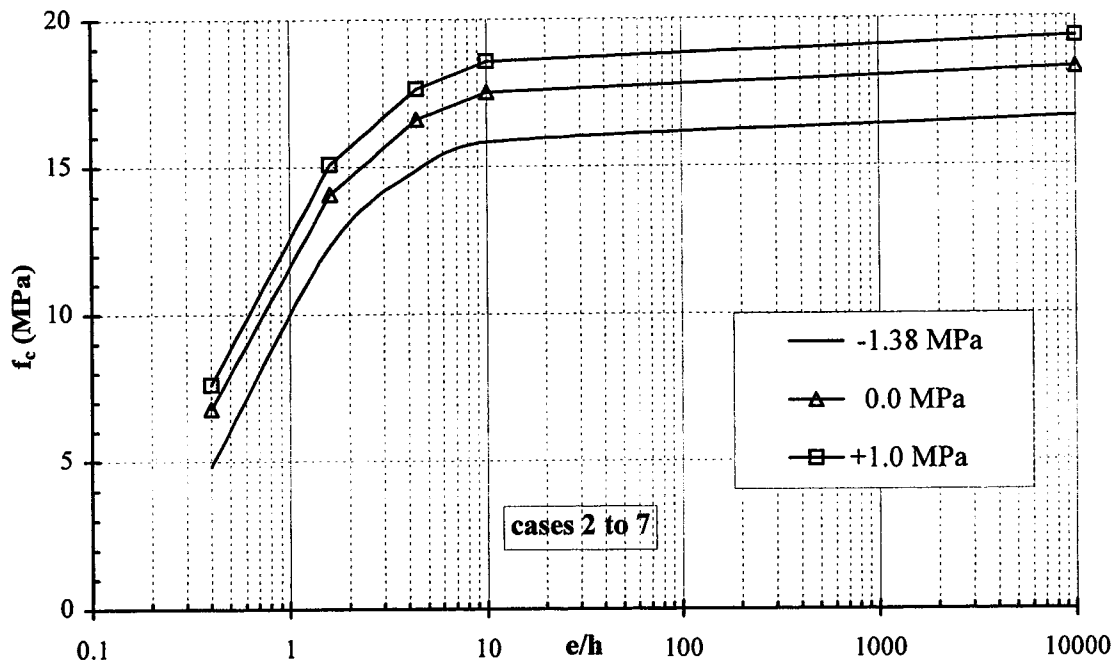
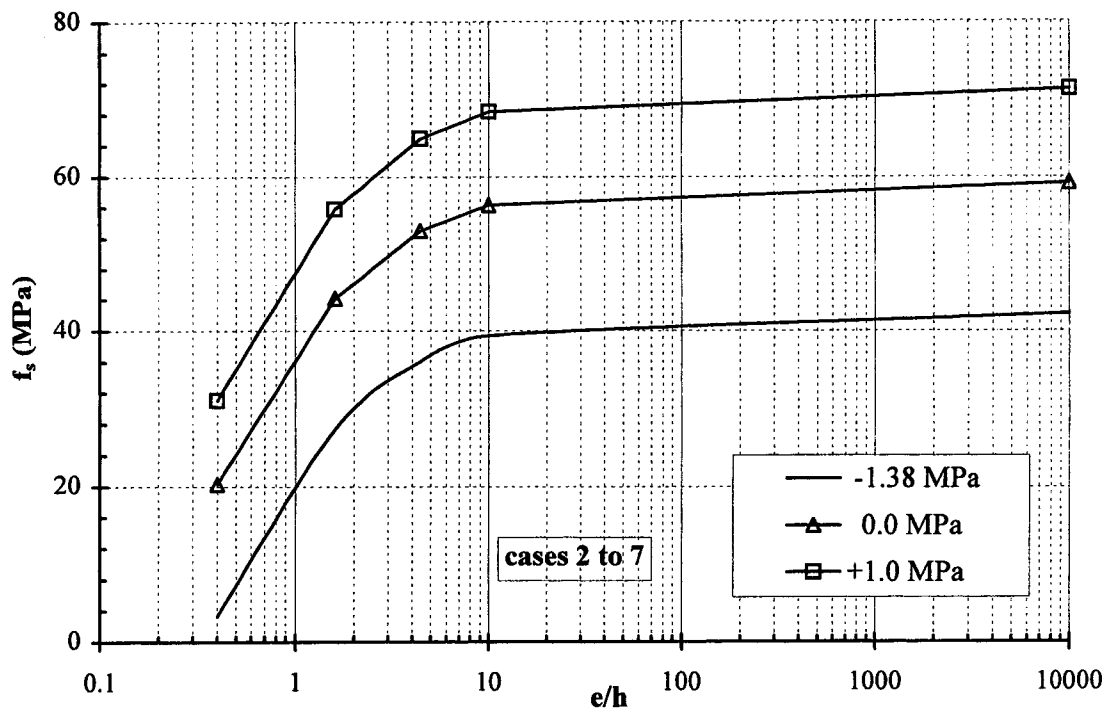


Figure 6.17 Compression zone depth versus residual stress at centroid for different effective depths

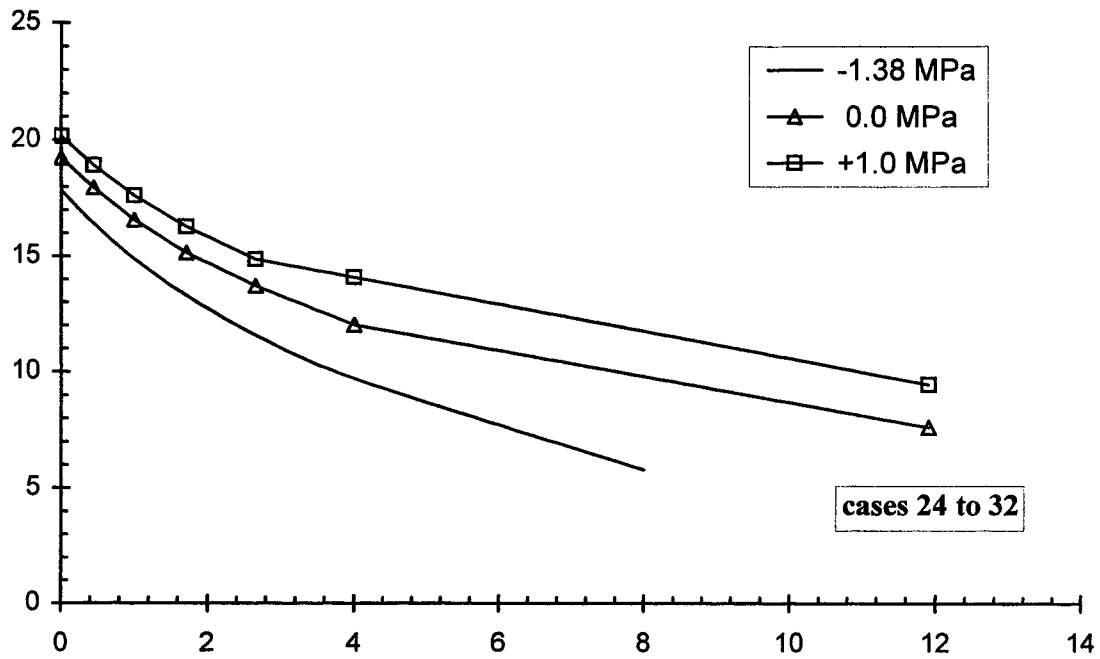


(a) Concrete extreme fibre stress

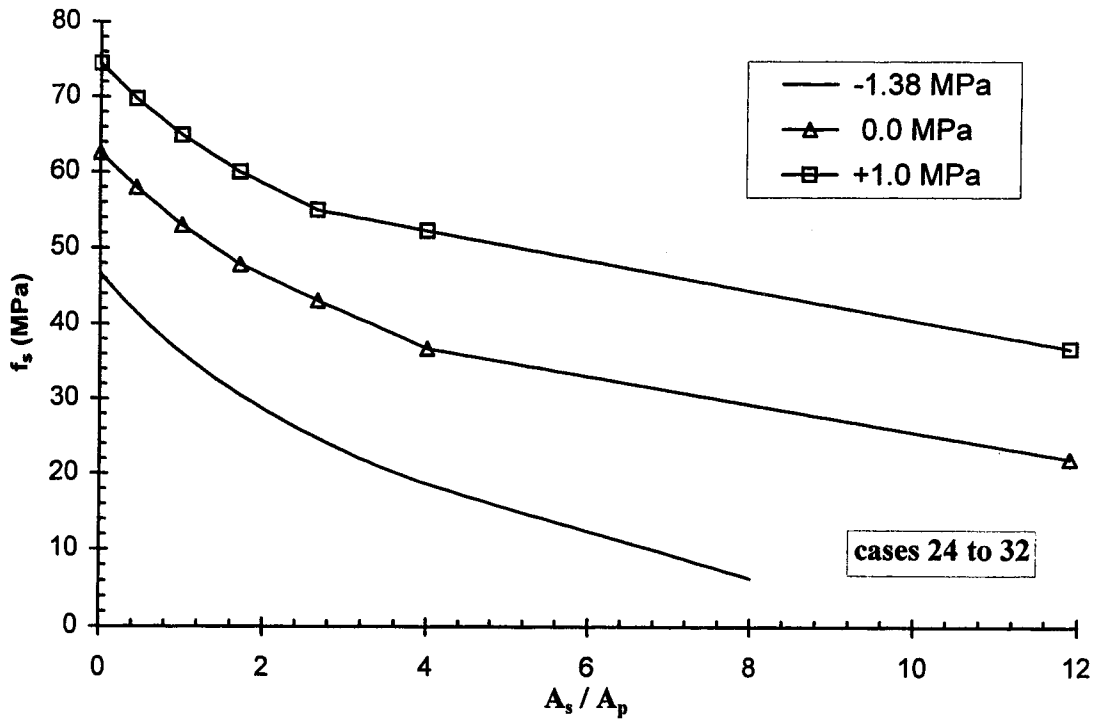


(b) Non-prestressed steel stress

Figure 6.18 Effect of changing concrete residual stress for different load eccentricities

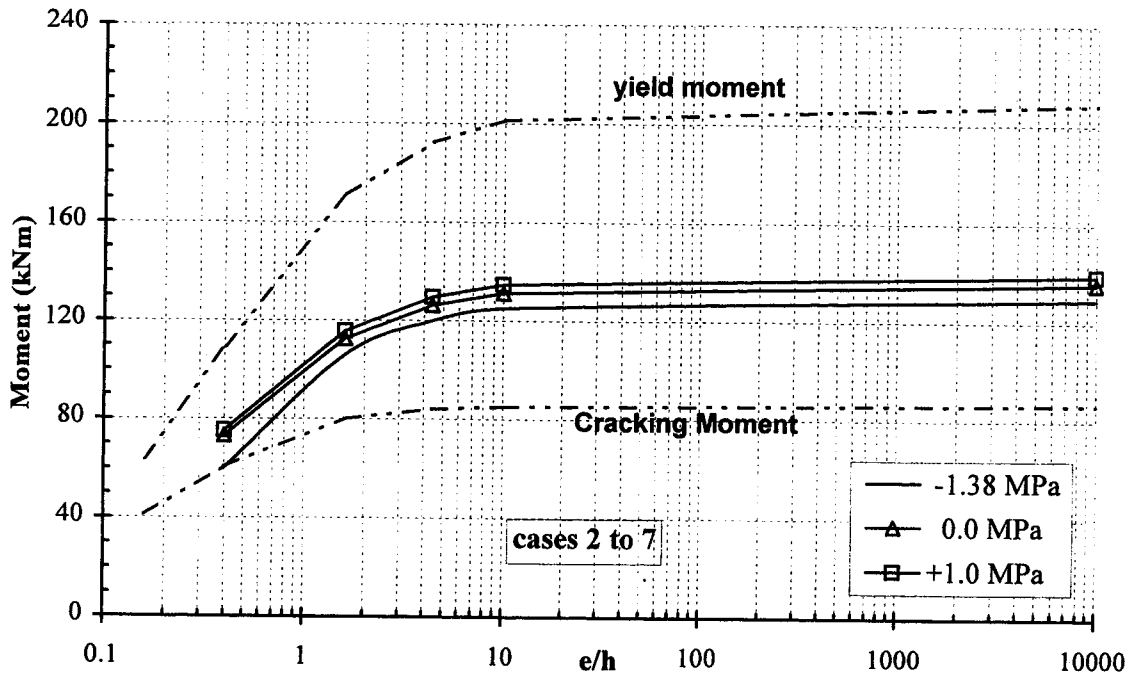


(a) Concrete extreme fibre stress

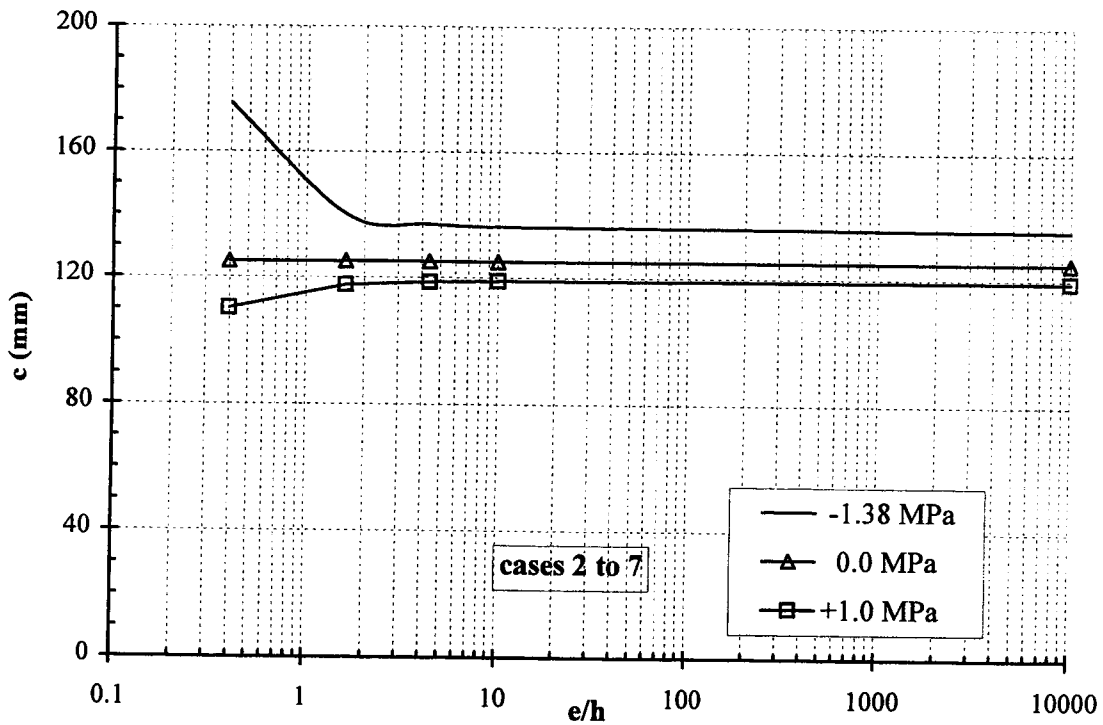


(b) Non-prestressed steel stress

Figure 6.19 Effect of changing concrete residual stress for different steel ratios ($\nu = \text{constant}$)

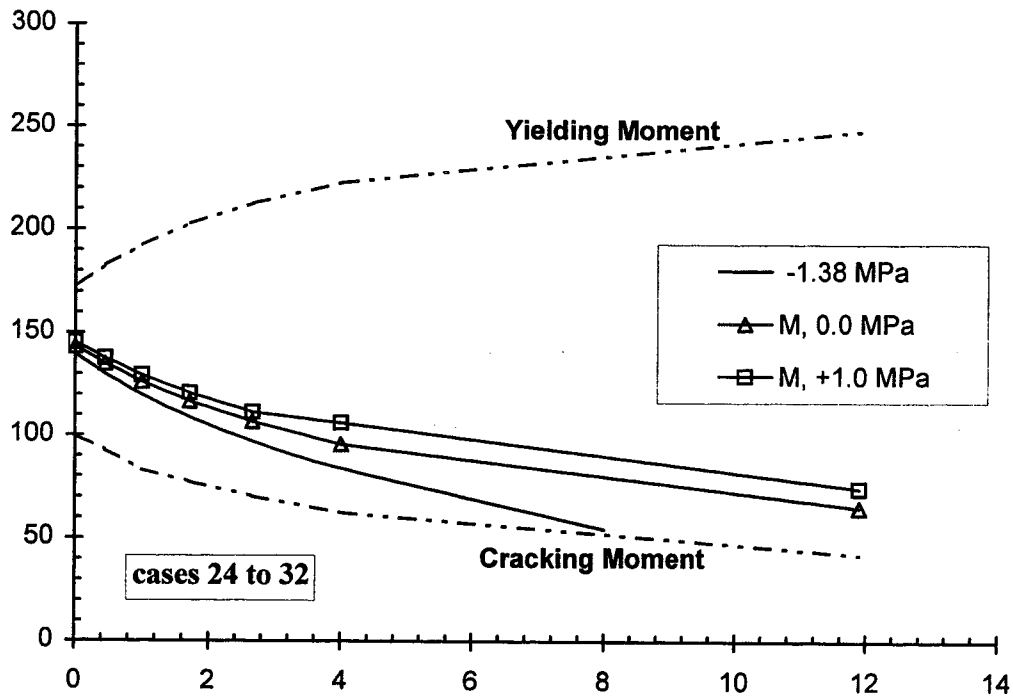


(a) Moment

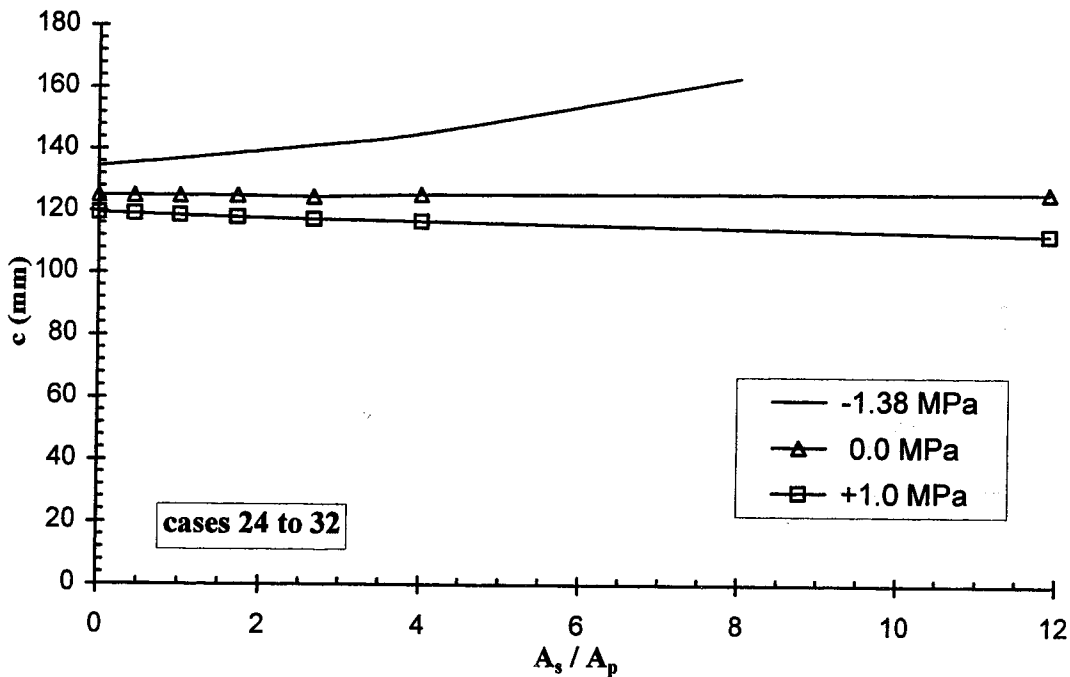


(b) depth of compression zone

Figure 6.20 Effect of changing concrete residual stress on moment and depth of compression zone for different load eccentricities



(a) Moment



(b) Depth of compression zone

Figure 6.21 Effect of changing concrete residual stress on moment and depth of compression zone for different steel ratios

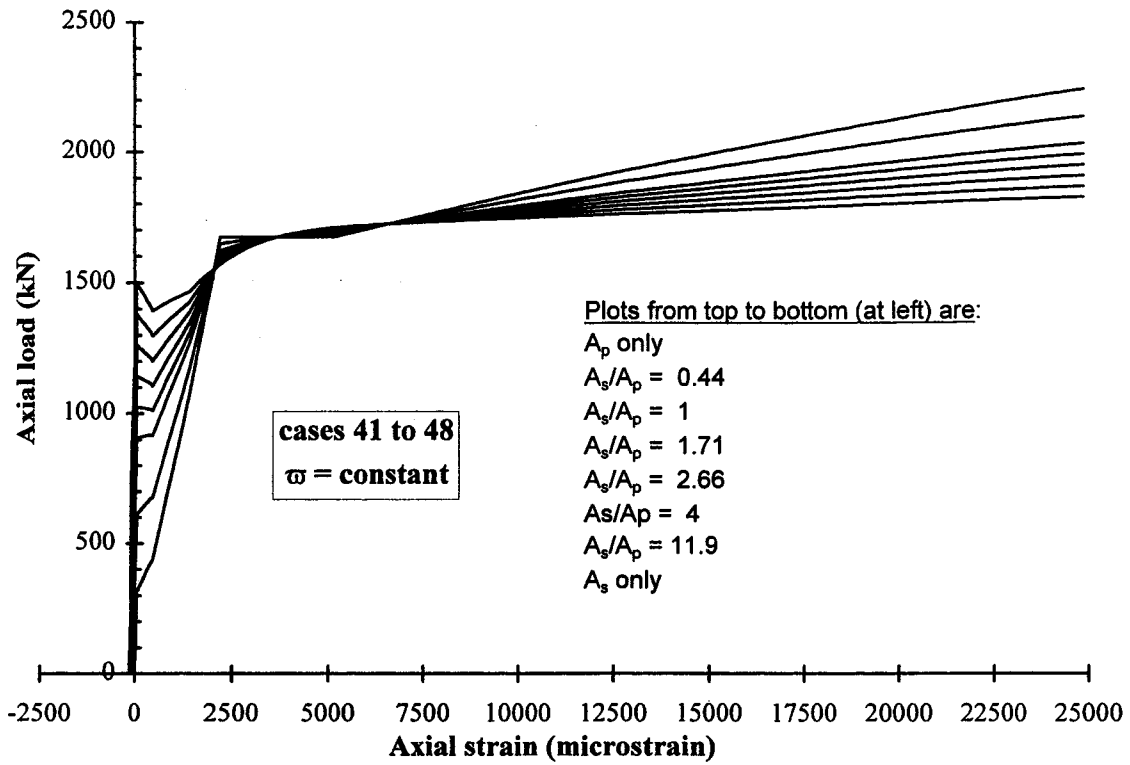


Figure 6.22 Load versus strain for axially loaded member with different steel ratios

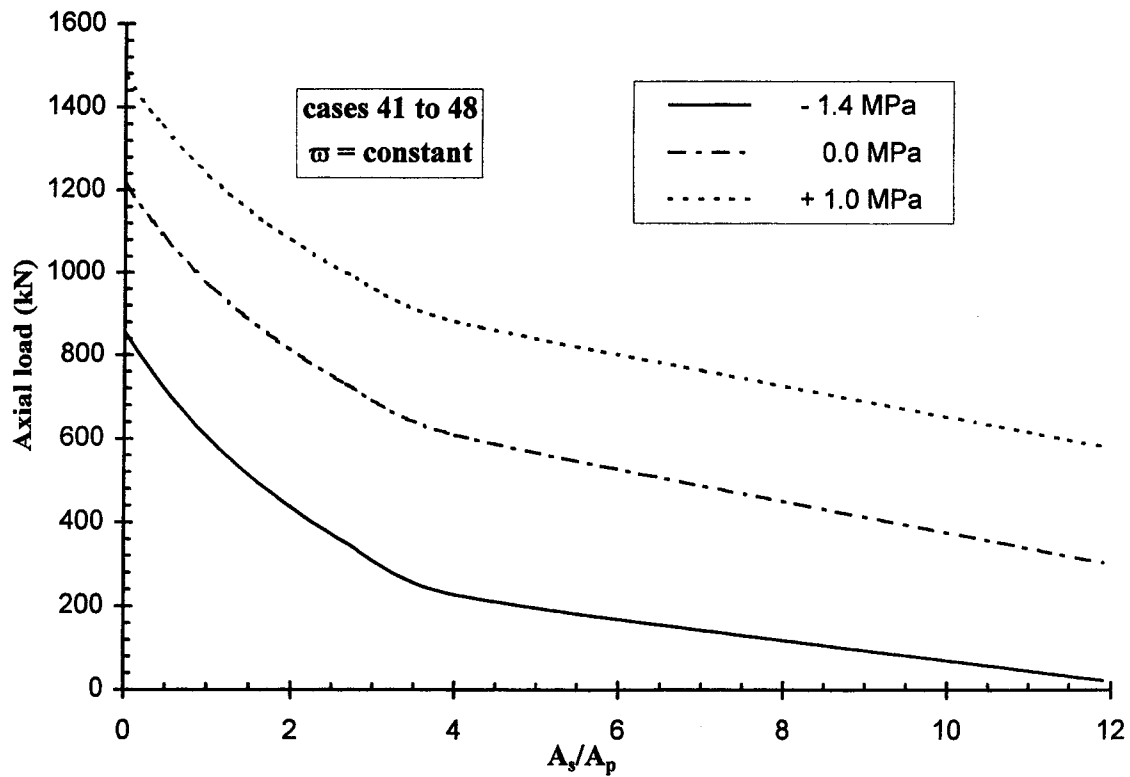


Figure 6.23 Axial tension versus steel ratio for different concrete residual stresses

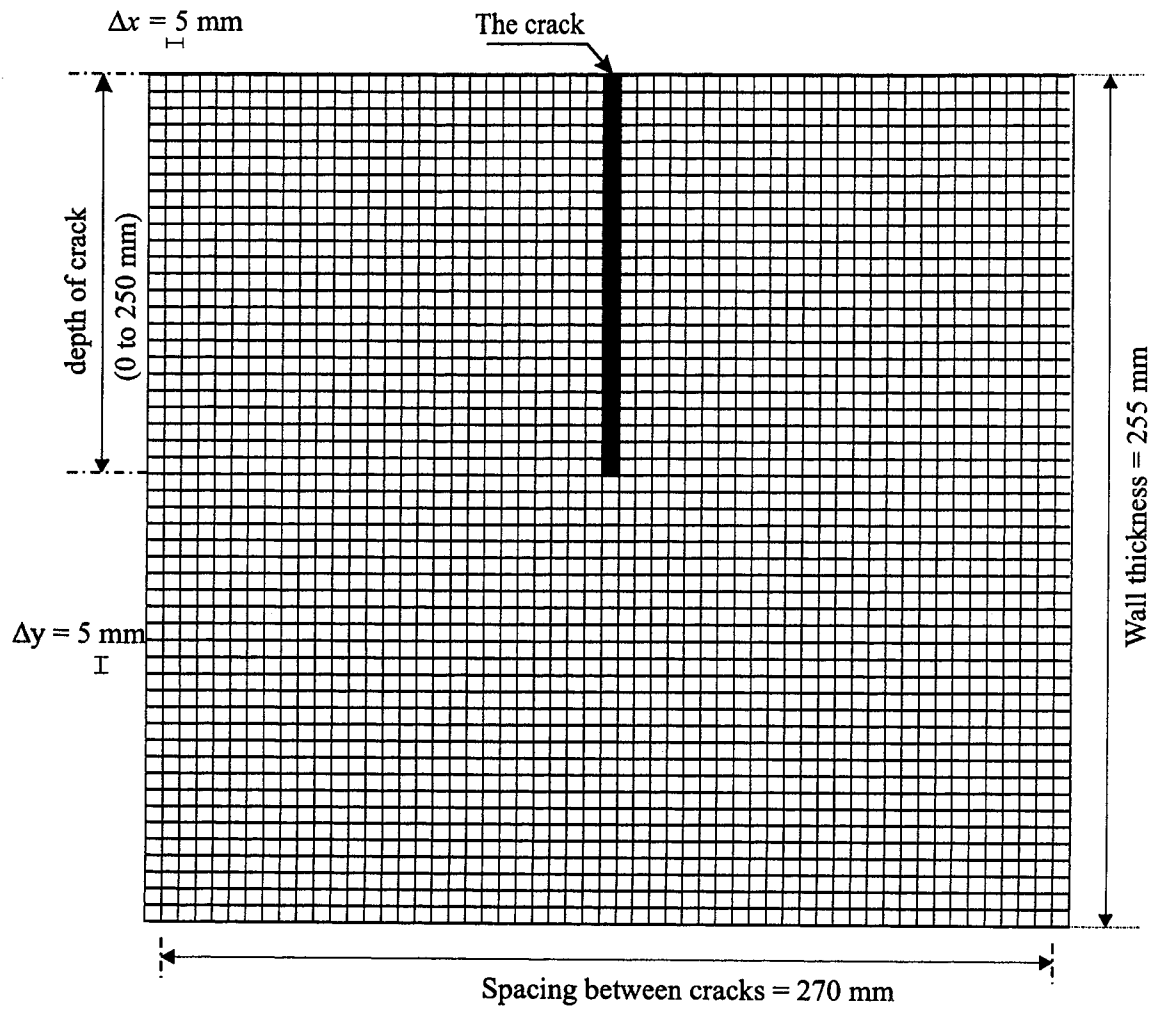


Figure 6.24 Finite difference mesh

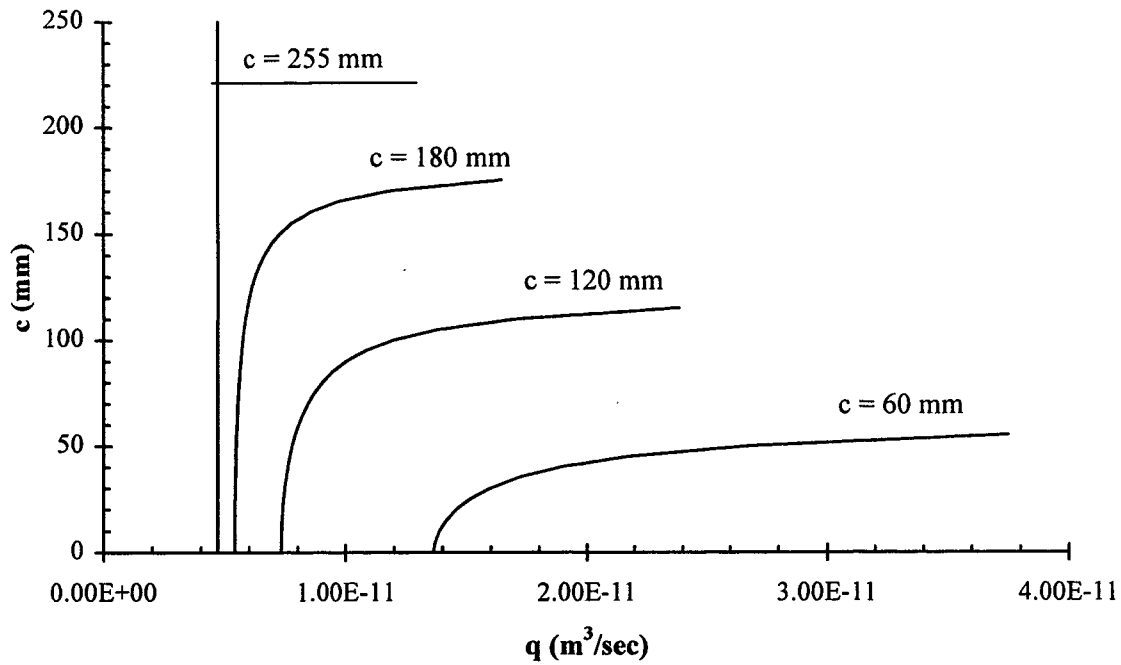


Figure 6.25 Nodal flow rate below cracks for different depths of compression zone

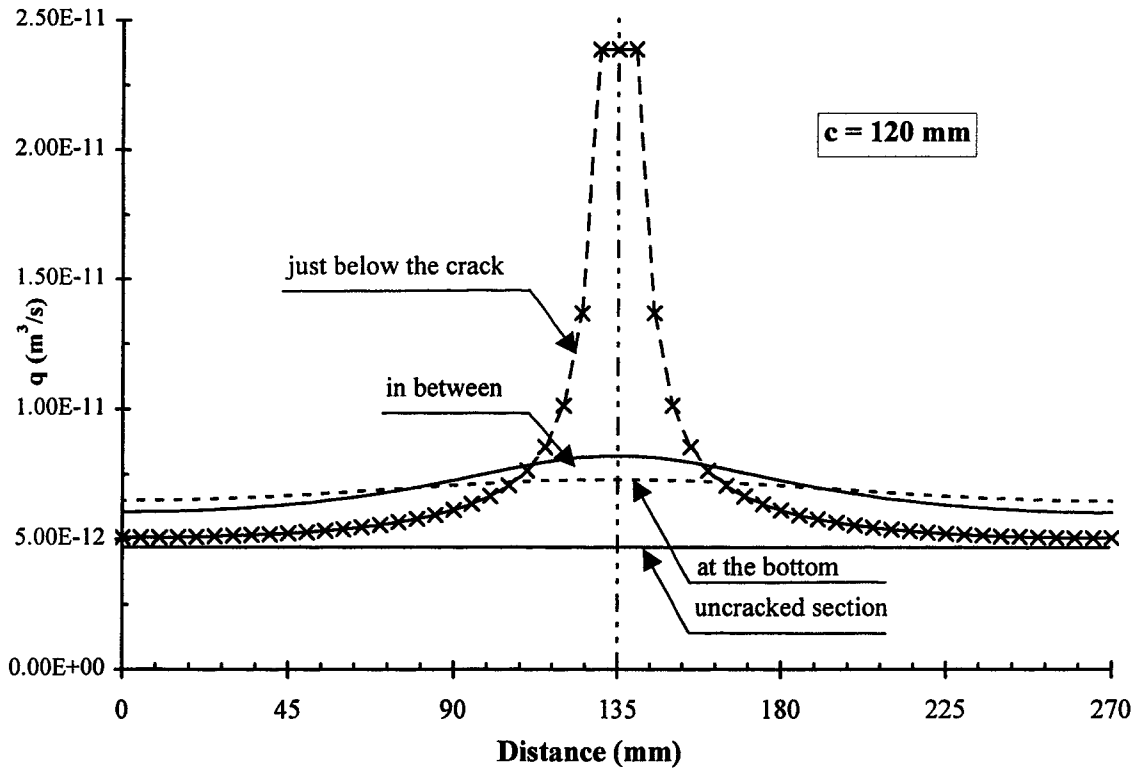


Figure 6.26 Horizontal distribution of the flow at different depths

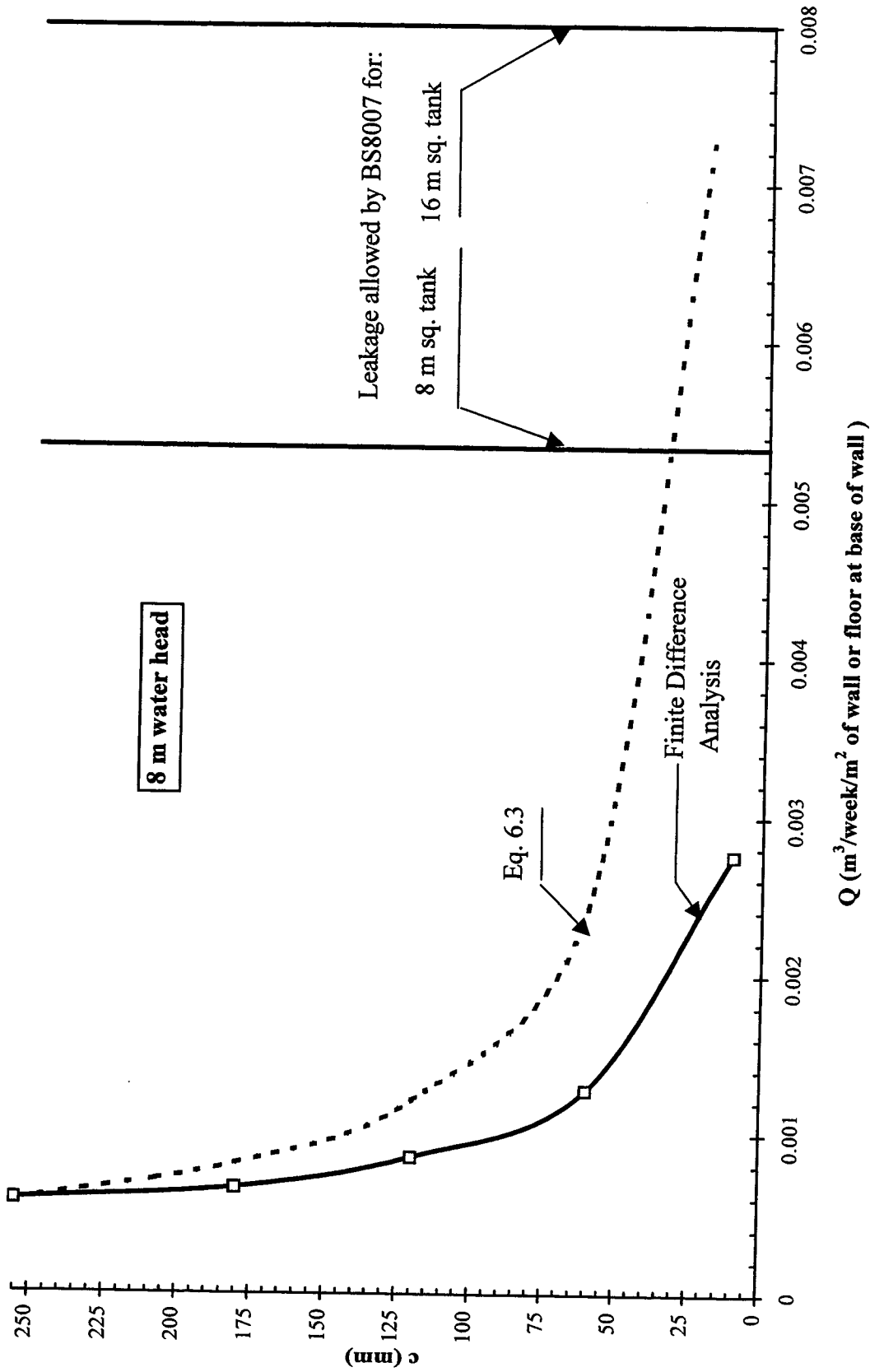


Figure 6.27 Leakage per square metre versus compression zone depth

7- Limit States Design for Liquid Containing Tanks

7.1 Introduction

Limit states design for liquid containing tanks is discussed in this chapter in the light of the results drawn in the preceding chapters. A unified limit states design approach for the design of water tanks ranging from reinforced concrete at one end of the design spectrum to fully prestressed concrete at the other is proposed.

In concrete structures, “design” is the selection of dimensions and details for concrete and reinforcement. “A limit state” is defined as the condition at which the structure or structural element becomes unfit for its intended use. “Limit states design” is defined as a process that involves identification of all potential modes of failure, determination of acceptable levels of safety against occurrence of each limit state and then consideration of the significant limit states. For normal structures, the acceptable levels of safety against limit states are determined by the building code authorities. Frequently for buildings, a limit state design is carried out by proportioning members for the ultimate limit state followed by a check of the serviceability limit states (MacGregor, 1997). The limit states for tanks are the ultimate strength limit state and serviceability limit states that include leakage, durability and deflection limit states. Cracking is not a real limit state in itself; limiting cracking is an indirect method used to control leakage and enhance durability. This report focuses only on the leakage limit state and on the resistance side of ultimate strength limit state. Within the ultimate strength limit state, this report does not cover aspects such as shear and flotation of the tank. Within the serviceability limit states, this report does not cover deflection and durability limit states.

The following sections include detailed discussions of the ultimate strength and leakage limit states with emphasis on the leakage limit state.

7.2 Ultimate Strength Limit State

The ultimate limit state involves a structural collapse of part or all of the structure. The structure should be designed such that:

$$\text{Factored resistance} \geq \text{Effect of factored loads} \quad (7.1)$$

The effect of the factored loads includes moment, axial load, shear, and torsion. The load factors for liquid containing structures are addressed in the different building codes. ACI 318-95 (1995) recommends a load factor of 1.7 (live load) for earth pressure, ground water pressure and granular materials pressure. The Code specifies a factor of 1.4 (dead load) for liquids with well-defined densities and controllable maximum heights. ACI 344 (1988) recommends a load factor of 1.5 for fluid pressure and 1.7 for earth pressure. ACI 350 (1989) recommends a load factor of 1.7 for both lateral liquid and earth pressures. Note that ACI 350 increases the load factor by the sanitary durability coefficient (1.3 for flexure and 1.65 for direct tension). The final load factors are 2.21 and 2.7 for flexure and direct tension respectively. This was done to accommodate designers who were unfamiliar with working stress design procedures as explained in Section 2.2.1. The National Building Code of Canada (NBCC 1995) recommends a load factor of 1.5 for hydrostatic and earth pressures (live load). However, it is stated in Commentary F of NBCC that a load factor of 1.25 (dead load) is appropriate for fluids in storage tanks. The load factors discussed above are not adequate for significant increases in liquid heights. The ultimate limit state should be checked with the maximum possible heights rather than with the normal operating liquid levels.

The resistance of an element subjected to bending and eccentric tension is conservatively predicted by CSA A23.3-94. Table 7.1 compares the test results with predictions based on CSA A23.3-94 (with material resistance factors set equal to 1.0), and the proposed model. The proposed model is a better predictor than the code model because it includes strain hardening and the real stress-strain curves for the materials used.

The ultimate limit state equations for American and Canadian codes will now be presented for pure tension, pure moment and combined tension and moment.

For direct tension, the basic design equation as expressed in ACI-318-95 is:

$$\phi T_n \geq T_f \quad (7.2)$$

where;

ϕ is the strength reduction factor (0.9 for direct or eccentric tension and for flexure),

T_n is the nominal strength (nominal axial tension in this case),

T_f is the factored axial tension.

For water, and for concrete section with low-relaxation tendons, Eq. 7.2 becomes:

$$0.9[A_s f_y + A_p(0.9 f_{pu})] \geq 1.4T \quad (7.3)$$

For the same conditions, CSA A23.3-94 (1994) gives:

$$A_s(0.85 f_y) + A_p(0.9 \times 0.9 f_{pu}) \geq 1.25T \quad (7.4)$$

Comparison of Eqs. 7.3 and 7.4 shows that CSA A23.3-94 is slightly less conservative than ACI 318-95. For the same concrete section, the service axial tensile load that can be carried according to Eq. 7.4 is 5 to 12% more than that given by Eq. 7.3 for reinforced and prestressed concrete respectively.

For flexure, the design equation for a rectangular section according to ACI 318-95 is:

$$0.9[A_s f_s (d - \frac{a}{2}) + A_p f_{ps} (d_p - \frac{a}{2}) + A'_s f'_s (\frac{a}{2} - d')] \geq (1.4M_D + 1.4M_w) \quad (7.5)$$

In this equation f_s and f'_s are the tension and compression non-prestressed reinforcement stresses determined from strain compatibility. The stress in tendons f_{ps} at ultimate may be obtained from strain compatibility or empirical equations contained in the code.

CSA A23.3-94 produces a similar equation:

$$0.85f_s A_s (d - \frac{a}{2}) + 0.9f_{ps} A_p (d_p - \frac{a}{2}) + 0.85f'_s A'_s (\frac{a}{2} - d') \geq (1.25M_D + 1.25M_w) \quad (7.6)$$

Again CSA A23.3-94 is less conservative than ACI-318-95.

For eccentric tension the ultimate limit state, Eq. 7.1, can not be expressed as simply as in Eqs. 7.3 through 7.6. In the case of ACI-318, the nominal strength (M_n and T_n) of the concrete section can be calculated for different load eccentricities. The nominal strength is then multiplied by $\phi = 0.9$ to produce the design strength (the factored resistance). The different values of ϕM_n and ϕT_n obtained for different load eccentricities are used to plot the interaction diagram for the concrete section. The strength ultimate limit state is satisfied when the point representing the factored moment and the factored tension is located on or inside the interaction diagram. When using CSA A23.3-94, the interaction diagram is produced with ϕ_c , ϕ_s and ϕ_p .

7.3 Leakage Limit State

7.3.1 General

Existing codes when dealing with leakage express it as watertightness (or leakage) criteria. Watertightness can be defined locally and globally. Local watertightness requires that the surface of the wall, at no point, exhibit moist or wet spots. Global watertightness requires that leakage rate must not exceed a specified leakage rate. These two definitions for watertightness can be translated into two limit states for leakage:

1. leakage rate \leq evaporation rate,
2. leakage rate \leq water loss (during certain period) expressed as a specific percentage of water volume

The above two limit states can be written in a general form as:

$$\text{Predicted leakage rate} \leq \text{Allowable leakage rate} \quad (7.7)$$

The “*allowable leakage rate*” is obtained from the leakage test criterion that is contained in the design standards for liquid containment structures. “*The predicted leakage rate*” has not been calculated explicitly and is not well defined in the literature.

The remaining portion of this section discusses the leakage limit state with emphasis on “*the predicted leakage rate*”. It should be noted that the leakage limit state is under normal operating conditions, therefore service loads and stresses are used.

The design strategies for the leakage limit state range from preventing cracking completely to limiting through-crack widths such that leakage rates are acceptable. Experimental and theoretical evidence in the preceding chapters suggest that a separate design procedure should be followed to control leakage from each of direct tension, which produces through-cracks, and eccentric tension or flexure, which produces cracks with compression zones. The two load cases are discussed individually in the following sections.

7.3.2 Direct tension

The leakage rate in sections subjected to axial tension is governed mainly by the width of the through-cracks. The tests conducted in this study showed that:

- if there was no through-crack there was no leakage,
- if the through-cracks were narrower than 0.15 mm, the cracks leaked initially but then self-sealed,
- if the through-cracks were wide, water flowed through the cracks continuously

There are three strategies for satisfying the leakage limit state.

7.3.2.1 Prevent Cracking

Prevent cracking completely gives a zero leakage rate. A conservative approach is to prohibit any tensile stresses in concrete, or even require some residual compressive stresses. This can be only done by prestressing. This approach is sufficient but excessive.

It can not be applied to reinforced concrete sections. It also ignores the presence of non-prestressed steel. The trial designs presented in Chapter 2 showed that the requirement of residual concrete compressive stress uses more prestressing, does not benefit from the thick walls require for constructability.

Preventing cracking may theoretically be done by keeping the tensile stresses in concrete below the cracking stress. This can be done in reinforced concrete by increasing the dimensions of the concrete section, which may produce thick walls. This was the basis behind the PCA reinforced concrete circular tank design as discussed in Section 2.2. In prestressed concrete, allowing low tensile stresses in the concrete has advantages that were discussed in the parametric study presented in Chapter 5. It effectively reduces the amount of prestressing and utilizes the presence of non-prestressed steel in the section. Unfortunately, if the concrete ever develops a crack due to temporary overload or shrinkage and temperature effect, this approach may not work. To examine this approach trial designs were carried out on four 1 m wide sections of 250 mm thick wall as shown in Table 7.2. The sections were subjected to an axial tension. The steel areas were chosen such that all sections have the same ultimate capacity and have a concrete tensile stress of 1.0 MPa under service loads. Although the chosen tensile stress (1.0 MPa) is small compared with the concrete cracking stress, it affects the width of any working joint or pre-opened through crack that occurred due to secondary effects such as shrinkage and creep. The widths of working (cold) joint or pre-opened crack for the four cases were calculated employing crack width calculation in CEB-FIP Model Code 1990 (1993).

The results are presented in Table 7.2 which shows that the width of the pre-opened crack varies from 0.03 mm for reinforced concrete section to 0.38 mm for fully prestressed concrete. Specifying a certain residual tensile stress produces different crack widths, and significantly different leakage rates. Thus, while specifying a minimum residual compression stress prevents through cracks, allowing a tensile stress in the concrete does not necessary guarantee satisfactory leakage behaviour.

7.3.2.2 Limiting Through Crack Widths Such That Cracks Self-Seal

In this approach through-cracks are allowed but limited such that cracks self-seal to produce a zero leakage rate. Edvardsen (1996) recommended crack widths for autogenous healing and self-sealing as indicated in Table 7.3. Such values can be used as the permissible through crack widths. This approach is applicable to reinforced and prestressed concrete. The design procedure to be followed after determining that permissible through crack widths is explained in Section 7.3.2.4.

7.3.2.2 Limiting Through Crack Widths Such That Leakage Rates are Acceptable

Through-cracks are allowed and the predicted leakage rate is explicitly calculated to satisfy Eq. 7.7. Knowing the effective crack width, water head, and the wall thickness, the leakage rate can be calculated.

Equations 2.4 through 2.6 proposed by Imhof-Zeitler can be used for the leakage rate predictions. The equations can be re-written for water as:

$$Q = \frac{9.25}{A} [1 + I] w / S \quad (\text{m}^3/\text{m}^2/\text{s}) \quad (7.8)$$

With the friction coefficient A :

$$A = \frac{6.1 \times 10^{-8}}{c w^{3.6} (14I - 20)} \quad (1/\text{m}^2) \quad \text{for } w \geq 0.0001 \quad (7.9 \text{ a})$$

$$A = \frac{2.25 \times 10^{-4}}{c w^{2.6}} \quad (1/\text{m}^2) \quad \text{for } w < 0.0001 \quad (7.9 \text{ b})$$

where,

Q is the leakage rate in $\text{m}^3/\text{m}^2/\text{s}$,

I is the hydraulic gradient = $\Delta H/h$,

ΔH is the water head in m,

h is the wall thickness in m,

S is the expected crack spacing in m (assuming parallel cracks in one direction only),
 $c = 1$ for water soluble liquids and $1/0.53$ for other liquids,
 w is the crack width in metre.

The value of Q obtained from Eq. 7.8 can be used to apply the leakage limit state as:

$$Q \times \text{wetted surface area of the tank} \leq \text{The allowable loss of water volume per second}$$

The crack width that satisfies this condition can be obtained for any tank with known dimensions. However, the effect of self-sealing is considered in the friction coefficient, A , for crack width less than 0.1 mm, Eq. 7.9 b. Therefore it was noted from applying the above equations on some numerical examples that a crack width < 0.1 mm satisfies the above condition in all the cases.

In using Eqs. 7.8 and 7.9 to determine the leakage rate through the wall, one-half and one-third of the hydraulic gradient I should be used for $w < 0.1$ mm and $w \geq 0.1$ respectively. This is because the water head varies linearly along the wall height which makes Q varies linearly along the height for $w < 0.1$ and varies quadratically for $w \geq 0.1$.

The approach presented in this section is applicable for both reinforced and prestressed concrete. The design procedure to be followed after determining the permissible through-crack widths is explained below.

7.3.2.4 Design to Satisfy Permissible Crack Widths

Having determined the permissible through-crack width, either as in Section 7.3.2.2 or 7.3.2.3, there is a direct design procedure that will produce the desired crack width. The CEB-FIP Model Code 1990 (1993) crack width approach is used. This procedure tries to obtain steel stresses that satisfy certain crack widths in reinforced, partially prestressed and fully prestressed concrete members.

The relation after cracking between non-prestressed steel stress f_s and total steel ratio in the section $\rho_{tot, eff}$ for a specific characteristic crack width w_k can be derived from CEB-FIP Model Code 1990 equations as follows:

The maximum crack spacing after cracking $l_{s, max}$ is given by CEB-FIP Eq. 7.4-11 as:

$$l_{s, max} = \frac{\Phi_s}{3.6 \rho_{tot, eff}} \quad (7.10)$$

The average steel strain within $l_{s, max}$ is given by CEB-FIP Eq. 3.2-11 as

$$\varepsilon_{s, m} = \varepsilon_{s2} - \frac{2}{3} \beta (\varepsilon_{sr2} - \varepsilon_{sr1}) \quad (7.11)$$

where, ε_{sr1} is the steel strain at the point of zero slip (mid-way between two cracks) under cracking force reaching f_{cr} . At the point of zero slip the steel strain is equal to the concrete strain, hence:

$$\varepsilon_{sr1} = \varepsilon_{c1} = \frac{f_{cr}}{E_c} \quad (7.12)$$

The reinforcement strain, ε_{sr2} , at the crack under cracking forces reaching f_{cr} is:

$$\varepsilon_{sr2} = \frac{f_{cr}}{E_s \rho_{tot, eff}} (1 + \eta \rho_{tot, eff}) \quad (7.13)$$

The concrete strain after cracking within $l_{s, max}$ varies from zero at the crack to the concrete cracking strain ε_{c1} at the point of zero slip with an average of ε_{cm} where:

$$\varepsilon_{cm} = \beta \varepsilon_{c1} \quad (7.14)$$

CEB-FIP Eq. 7.4-2 gives the characteristic crack width w_k as the crack spacing times the difference between average steel strain and average concrete strain, i.e.

$$w_k = l_{s, max} (\varepsilon_{sm} - \varepsilon_{cm}) \quad (7.15)$$

The characteristic crack width, w_k , is the 95% fractile of the crack widths could be expected on a member (CEB, 1985).

Substituting Eqs 7.10 through 7.14 into 7.15 neglecting the term $(1 + \eta\rho_{tot,eff})$ for simplicity and rearranging the equation yields:

$$f_s = 3.6w_k\rho_{tot,eff} \frac{E_s}{\Phi_s} + \frac{\beta}{3} f_{cr}\eta + \frac{\frac{2}{3}\beta}{\rho_{tot,eff}} f_{cr} \quad (7.16)$$

where,

w_k is the characteristic crack width in mm,

η is the modular ratio = E_s/E_c

E_s is the Modulus of Elasticity of non-prestressed steel (bars) in MPa,

E_c is the tangential Modulus of Elasticity of concrete in MPa

β is an integration factor for strain distribution between cracks(CEB-FIP Table 7.4.2),

f_{cr} is the cracking tensile stress in concrete in MPa,

$\rho_{tot, eff}$ is the total effective reinforcement ratio = $\rho_{s, eff} + \psi \rho_{p, eff}$

$\rho_{s, eff}$ and $\rho_{p, eff}$ are $\frac{A_s}{A_{c,eff}}$ and $\frac{A_p}{A_{c,eff}}$ respectively;

Φ_s and Φ_p are non-prestressed and prestressed reinforcement diameters respectively,

$A_{c, eff}$ is the effective area of concrete in tension as shown in Fig. 7.1 adapted from

CEB-FIP Model Code 1990;

ψ is the bond coefficient = $\frac{\tau_{bp}}{\tau_{bs}} \times \frac{\Phi_s}{\Phi_p}$;

τ_{bp} and τ_{bs} : bond stresses for tendons and bars respectively. The ratio between them is

given by CEB-FIP Model Code 1990 for different combinations as follows:

$\tau_{bp} / \tau_{bs} = 0.40$ for post-tensioned tendons, indented bars or strands

$\tau_{bp} / \tau_{bs} = 0.60$ for post-tensioned tendons, ribbed bars

$\tau_{bp} / \tau_{bs} = 0.60$ for pre-tensioned tendons, indented bars or strands

$\tau_{bp} / \tau_{bs} = 0.80$ for pre-tensioned tendons, ribbed bars

If E_s is taken equal to 200,000 MPa, $E_c = 4500\sqrt{f'_c}$ MPa, $\beta = 0.38$ for long-term or repeated load and f_{cr} is conservatively taken as $0.25\sqrt{f'_c}$ MPa, (as observed in the experimental tests) then Eq. 7.16 can be used to plot a series of curves that give the relationship between f_s and $\rho_{tot, eff}$ for different bar sizes for each design characteristic crack width w_k and concrete compressive strength f'_c . Figures 7.2 and 7.3 show two groups of curves for $f'_c = 35$ MPa and $w_k = 0.10$ and 0.15 mm respectively. Increasing the total steel ratio and reducing bar diameter allow increased steel stresses for a given crack width. CEB-FIP Model Code 1990 crack width equation is based on multiplying the crack spacing times the difference between average steel strain and average concrete strain within crack spacing. Very small steel ratios produce unrealistically large crack spacings and very small differences in strain between steel and concrete. Equation 7.16 should not be used for small steel ratios. Equation 7.16 produces sagging curves with minimum values at approximate 1% total steel ratio in Figs. 7.2 and 7.3. The values to the left of the minimum point are uncertain and therefore ignored. One of the ignored portion of the curves is shown dashed. The chosen steel areas should be checked to ensure that the steel does not yield at the onset of cracking. The following equation can be used for that purpose:

$$\phi_s A_s f_y + \left(0.9\phi_p - \frac{f_{pe}}{f_{pu}}\right) A_p f_{pu} \geq f_{cr} A_c \quad (7.17)$$

where,

ϕ_s and ϕ_p are the strength reduction factors specified by CSA A23.3-94 for non-prestressed steel and tendons respectively (0.9 and 0.85),

f_{pe} is the effective prestressing stress after all losses,

f_{pu} is the ultimate strength of prestressed tendons.

The CEB-FIP Model Code 1990 gives the width of working joints (or pre-opened through cracks). The Code uses the same equations replacing the steel stress at cracking (which does not occur yet) by the actual steel stress at the joint. The following equation, which gives f_s corresponding to working joints of width w_k , can be easily derived from Code equations:

$$f_s = \sqrt{\frac{2.7w_k E_s f_{cr}}{0.62\Phi_s}} \quad (7.18)$$

This equation is independent of the total steel ratio and gives the horizontal lines shown in Figs. 7.2 and 7.3.

Equations 7.17 and 7.18 and Figs. 7.2 and 7.3 are applicable to reinforced or prestressed concrete members. For prestressed concrete members without non-prestressed steel, a similar relationship between the allowable increment of prestressed steel stress after decompression, Δf_p , and the effective steel ratio $\rho_{p, \text{eff}}$ for a characteristic crack width w_k is given by the following equation:

$$\Delta f_p = 3.6w_k \rho_{p, \text{eff}} \frac{E_p}{\Phi_p} + \frac{2}{3} \beta \frac{f_{cr}}{\rho_{p, \text{eff}}} + \beta f_{cr} \eta \quad (7.19)$$

Equation 7.19 is plotted in Figs. 7.4 and 7.5 for $f'_c = 35$ MPa and $w_k = 0.10$ and 0.15 mm respectively. In these plots, $E_p = 195000$ MPa., $\beta = 0.38$, and $f_{cr} = 0.25\sqrt{f'_c}$.

For fully prestressed concrete with working joints and w_k of 0.10 or 0.15 mm, the equation corresponding to Eq. 7.18 is:

$$\Delta f_p = \sqrt{\frac{1.08w_k E_p f_{cr}}{0.62\Phi_s}} \quad (7.20)$$

In this equation, it is assumed that the member is post-tensioned with strand tendons. This gives a strand bond stress of:

$$\tau_{hp} = 0.4\tau_{bs} = 0.4 \times 1.35 f_{ct} \quad (7.21)$$

Equation 7.20 produces the horizontal lines in Figs. 7.4 and 7.5.

Equation 7.16 (curves plotted in Figs. 7.2 and 7.3), can be used in conjunction with the following equation (CEB-FIP Eq. 7.4-8) to calculate the required reinforcement in a reinforced concrete or partially prestressed concrete section:

$$f_s = \frac{T - A_p f_{pe}}{A_s + A_p \sqrt{\psi}} \quad (7.22)$$

where,

T is the applied axial tension under service loads in N,

f_{pe} is the effective prestress stress after losses in MPa

The procedure is to select a suitable f_s from Fig. 7.2 or 7.3 as appropriate for the design w_k obtained from the leakage limit state. Knowing f_s and either A_s or A_p solve for A_p or A_s respectively using Eq. 7.22. Once both A_s and A_p are determined, one should return to Fig. 7.2 or 7.3 to confirm that f_s is appropriate to the total steel ratio. In trial designs conducted, the convergence was achieved from two or three circles. If the design is based on pre-existing cracks, the value of f_s is independent on the total steel ratio and no iteration is required.

For a prestressed member without non-prestressed reinforcement, Eq. 7.19 (curves plotted in Figs. 7.4 and 7.5), can be used in conjunction with the following equation (CEB-FIP Eq. 7.4-9) to calculate the required prestressed steel area.

$$\Delta f_p = \frac{T - A_p f_{pe}}{A_p} \quad (7.23)$$

7.3.3 Combined Tension and Bending

This section deals with combined flexure and tension (i.e. eccentric tension) that produces cracking a compression zone. Two strategies can be followed to satisfy leakage limit state.

7.3.3.1 Prevent Cracking Completely

Cracking can be prevented by allowing zero tensile stress in concrete. The cracking may also be prevented by allowing tensile stresses in concrete below the concrete cracking stress. The first option can only be done with prestressing. Therefore, it is not applicable for reinforced concrete. It also does not recognize the benefits of non-prestressed reinforcement in the section. It requires large amounts of prestress. Allowing low tensile stresses in the concrete section can be done in reinforced concrete by increasing the dimensions of the concrete section, but this may produce very thick walls. Also, cracks due to shrinkage or temperature effect can be problematic as illustrated in Section 7.3.2.1 for the case of through-cracks.

7.3.3.2 Maintain Minimum Depth of Compression Zone

Recognizing the difficulty of the above approach, the existing specifications for the design of water containing structures allow cracking in the case of flexure. This applies to both reinforced concrete (ACI 350) and prestressed concrete (ACI 344). The 1.38 MPa average compressive stress due prestressing required by ACI 344 in the vertical direction, subjected to flexure, is not always sufficient to prevent cracking. The parametric study proved that this requirement gives very low steel stress f_s and requires more prestressing.

The tests conducted show that the presence of a compression zone prevents leakage even if cracks are present. The leakage limit state can be satisfied by maintaining an adequate compression zone under service load. The depth of the compression zone must be chosen to satisfy each of the two leakage limit states mentioned in Section 7.3.1. The minimum depth of compression zone can be determined by equating the predicted

leakage rate with the allowable loss of water volume. The minimum compression zone depth for a given leakage rate can be obtained from refined methods such as the finite difference simulation used in Section 6.5. Alternatively, Eq. 6.3 can be used.

For a circular tank of a diameter D and a water head H , the minimum depth of the compression zone c can be obtained from Eq. 6.3 as:

$$c = \frac{k(2H + D)}{\xi D} \quad (\text{m}) \quad (7.24 \text{ a})$$

and for an $L_1 \times L_2$ rectangular tank:

$$c = \frac{k\{H(L_1 + L_2) + L_1L_2\}}{\xi L_1L_2} \quad (\text{m}) \quad (7.24 \text{ b})$$

where,

k is the coefficient of permeability of concrete (m/s),

ξ is the allowed percentage of water loss per second (expressed as a decimal number).

In Eqs. 7.24 (a) and 7.24 (b), one-half the hydraulic gradient is used in calculating leakage rate through the wall to consider the average water head on the wall. Equation 7.24(a) is plotted in Fig. 7.6 for different water heads considering $\xi = 0.05$ % per day as specified by ACI 350 (1989) and $k = 3 \times 10^{-11}$ m/s. Fig. 7.6 and Eq. 7.24(a) show that for diameters greater than the height, the minimum compression zone depth is less than 15.6 millimeters.

The minimum depth of the compression zone can be also obtained by equating the predicted leakage rate with the evaporation rate. The evaporation rate, given by Eq. 6.4, depends on the weather. The water needs months (or even years) to penetrate the compression zone. Therefore, the average weather conditions (air temperature, wind speed, and relative humidity) for long periods (one year or many months) should be used in Eq. 6.4. The Q obtained from Eq. 6.3 (or the refined approach) gives the velocity of water assuming uniform flow through one squared meter of the concrete. To account for

the presence of aggregate in concrete, Q is divided by the voids ratio of the concrete. The time in which the water penetrates the compression zone is obtained by dividing the compression zone depth, c , by the water velocity. Detailed calculations are given in the second example in Appendix C.

The minimum thickness of the compression zone obtained from the leakage limit state should be increased to provide a margin of safety and to account for any possible honey combing, bug holes or other shallow surface defects in the concrete.

Having determined the minimum depth of the compression zone, the structural design of the wall section can be performed. First, the prestressed steel should be determined. Prestressed steel could be chosen to balance a portion or all of the external tensile force. The maximum spacing between tendons should be considered. The permissible compression stresses in concrete specified by the general codes immediately after prestressing transfer and after allowance for all prestressing losses should be satisfied. The working stress design method can be used to determine the area of the non-prestressed steel. The chosen non-prestressed steel area must be larger than the minimum required by the codes for shrinkage and temperature effects. It must also satisfy the constructive requirements for minimum bar sizes and maximum bar spacing. Small diameter, closely spaced bars should be used for better crack control. The concrete section can then be analyzed as a transformed cracked section to determine the actual depth of compression zone and compare it with the minimum required for the leakage limit state.

A constant allowable non-prestressed steel stress f_s gives different depths of compression zone for the different load eccentricities or steel ratios, as shown in Figs. 6.10 and 6.11. However, for eccentricities greater than ten times the wall thickness a constant f_s gives almost the same depth of compression zone. This conclusion is based on the case of $A_s/A_p = 1.0$. Figure 7.8 shows that the steel stress for the same compression zone depth insignificantly changes for high steel ratios, approximately greater than $A_s/A_p = 12$. This conclusion is based on the cases of $e/h = 4.4$ and pure flexure. The permissible

values of f_s should reflect these changes. A form of equation similar to the following can be used:

$$f_s = 4 \left(25 - \frac{A_s}{A_p} \right) \log \left(20 \times \frac{e}{h} \right) \quad \text{for } 0.4 < \frac{e}{h} < 10 \text{ and } \frac{A_s}{A_p} < 12 \quad (7.25 \text{ a})$$

$$f_s = 4 \left(25 - \frac{A_s}{A_p} \right) \log(200) \quad \text{for } \frac{e}{h} \geq 10 \text{ and } \frac{A_s}{A_p} < 12 \quad (7.25 \text{ b})$$

$$f_s = 36 \log \left(20 \times \frac{e}{h} \right) \quad \text{for } 0.4 < \frac{e}{h} < 10 \text{ and } \frac{A_s}{A_p} \geq 12 \quad (7.25 \text{ c})$$

$$f_s = 120 \text{ MPa} \quad \text{for } \frac{e}{h} \geq 10 \text{ and } \frac{A_s}{A_p} \geq 12 \quad (7.25 \text{ d})$$

Equations 7.25 (a) through 7.25 (d) are plotted in Figs 7.9 and 7.10 for different load eccentricities and partial prestressing ratios respectively. Equations 7.25 (a) through 7.25 (d) are also plotted in Figs. 7.7 and 7.8. Comparing these plots with the responses obtained from the parametric study shows that these equations produce compression zones of depth ranging from 85 to 100 mm. The purpose of these equations is to provide values for f_s to be used in the calculation of the non-prestressed reinforcement directly. Equations 7.25 (a) through 7.25 (d) do not replace the calculation of the compression zone depth and comparison with the minimum depth required for leakage control. These tentative equations are based on the limited parametric study carried out in this report.

7.4 Trial Designs

The circular and the rectangular tanks designed in Section 2.3 using the existing specifications are designed in Appendix C using the proposed approach. Some conclusions from the trial designs are discussed below.

For the case of a section subjected to an axial tension, it is shown in Section 7.2 that the ultimate limit state according to CSA A23.3-94, Eq. 7.4, is less conservative than

that according to ACI 318-95, Eq. 7.3. If the approach of preventing cracks, discussed in Section 7.3.2.1, was chosen and the prestress force is selected to give zero concrete tensile stress under service load:

$$P_e = f_{pe} A_p = T \quad (7.26)$$

where,

P_e and f_{pe} are the effective prestressing force and stress after all losses respectively.

Comparing Eqs. 7.3 and 7.26, shows that the ultimate strength limit state is satisfied if:

$$f_{pe} \leq (0.81/1.4) f_{pu} \quad (7.27a)$$

$$\text{or } f_{pe} \leq 0.58 f_{pu} \quad (7.27b)$$

There is no need to check the ultimate limit state if f_{pe} satisfies Eq. 7.27 providing that the same water height, H , is used to determine T in serviceability and ultimate limit states.

If the design is based on a 0.1 mm wide pre-existing crack, the ultimate limit state is automatically satisfied if:

$$f_{pe} \leq 0.54 f_{pu} \quad (7.28)$$

Equation 7.28 can be derived as follows:

Equation 7.22 can be rearranged as:

$$T = A_s f_s + A_p (f_s \sqrt{\psi} + f_{pe}) \quad (7.29)$$

Comparing Eqs. 7.3 and 7.29, shows that the ultimate strength limit state is satisfied if:

$$f_s \leq 0.643 f_y \quad (7.30a)$$

$$\text{and } f_{pe} \leq 0.58 f_{pu} - f_s \sqrt{\psi} \quad (7.30b)$$

Figure 7.2 shows that Eq. 7.30(a) will always be satisfied.

For Eq. 7.30(b), f_s corresponding to pre-existing crack or working joints of width w_k is given in Eq. 7.18. Hence:

$$f_s \sqrt{\psi} = \sqrt{\frac{2.7 w_k E_s f_{cr}}{\Phi_p}} \quad (7.31)$$

For the values used in plotting Figs. 7.2 and 7.3:

$f_s \sqrt{\psi} = 78.4$ and 85.2 MPa for strands sizes 13 and 11. For $f_{pu} = 1860$ MPa these values are 0.0421 and $0.0458 f_{pu}$ respectively. Hence, Eq. 7.30 b can be rewritten as:

$$f_{pe} \leq 0.536 f_{pu} \quad \text{for strand size 13} \quad (7.32a)$$

$$f_{pe} \leq 0.532 f_{pu} \quad \text{for strand size 11} \quad (7.32a)$$

Equation 7.32 can be approximated as by Eq. 7.28 which is applicable to both stand sizes. The difference due to this approximation is less than $0.8\% f_{pu}$.

Equations similar to Eqs. 7.27 and 7.28 can be obtained using CSA A23.3-94 for the two cases of zero tensile stress and 0.1 mm crack width respectively as:

$$f_{pe} \leq 0.65 f_{pu} \quad (7.33)$$

$$\text{and } f_{pe} \leq 0.60 f_{pu} \quad (7.34)$$

An equation similar to Eq. 7.28 or 7.34 can be developed for a crack width of 0.15 mm. Such equations can save the effort of checking the ultimate strength limit state providing that the same water height H is used in both ultimate and serviceability

calculations. If Eq. 7.28 or 7.34 is not satisfied, the ultimate strength limit state must be checked but this still does not mean that it will govern the design.

It is difficult to obtain an equation similar to Eq. 7.28 or 7.34 that eliminates the need for checking for flexure or eccentric tension. The ultimate strength limit state does not govern in the second example of Appendix C.

Comparing the trial designs presented in Section 2.3 with those presented in Appendix C, shows that the proposed design approach requires less reinforcement, especially less prestressed steel. The reinforcement of the circular tank designed in Appendix C is 21% less expensive than that of the tank designed using ACI 344. This presents 4.4% reduction in the total cost. The total cost of the rectangular tank designed in Appendix C is 14% less than the fully prestressed tank designed in Section 2.3. The proposed design procedure addresses the leakage limit state directly. It recognizes the benefits of increasing wall thickness and non-prestressed reinforcement. The proposed design approach offers smooth and logical transition between the design of fully prestressed and fully reinforced concrete water tanks.

Table 7.1 Comparison between failure and design (coded) ultimate load

Specimen	Ultimate Moment (kNm)			Test/model	Test/code
	A23.3-94	Predicted (model)	Observed (test)		
1C20	181	209	207	0.99	1.14
1C40	172	211	222	1.05	1.29
2A	109	152	147	0.97	1.35
2C	209	242	256	1.06	1.22
3A	184	208	217	1.04	1.18
3B	155	197	220	1.11	1.42
3C	$P_u = 1330$	$P_u = 1648$	$P_u = 1600$	0.98	1.20
mean				1.03	1.26
Coefficient of variation				0.048	0.079

Note:

For specimen 3C, P_u is the ultimate load in kN.

Table 7.2 Width of pre-opened crack for different partial prestressing ratios.

the case	A_s (mm ²)	A_p (mm ²)	Total steel ratio %	bar No.	strand size	w_k (mm)
Reinforced concrete	5000	-	2.0	20	-	0.03
$A_s/A_p = 2$	1680	840	1.0	20	13	0.10
$A_s/A_p = 1$	1010	1010	0.8	20	13	0.15
Fully prestressed	-	1265	0.5	-	13	0.38

Table 7.3 Permissible crack widths for water tanks (after Edvardsen)

Hydraulic gradient I	Permissible crack width (mm)			
	Tanks with active cracks			Tanks with stationary cracks
	$\Delta w \leq 10\%$	$\Delta w \leq 30\%$	$\Delta w \leq 50\%$	
≤ 10	0.20	0.15 ~ 0.20	0.10	0.20
10 - 20	0.15	0.10 ~ 0.15	0.05	0.15
20 - 30	0.10	0.05 ~ 0.10	0.05	0.10
30 - 40	-	-	-	0.05

Δw is the variation of crack width with time

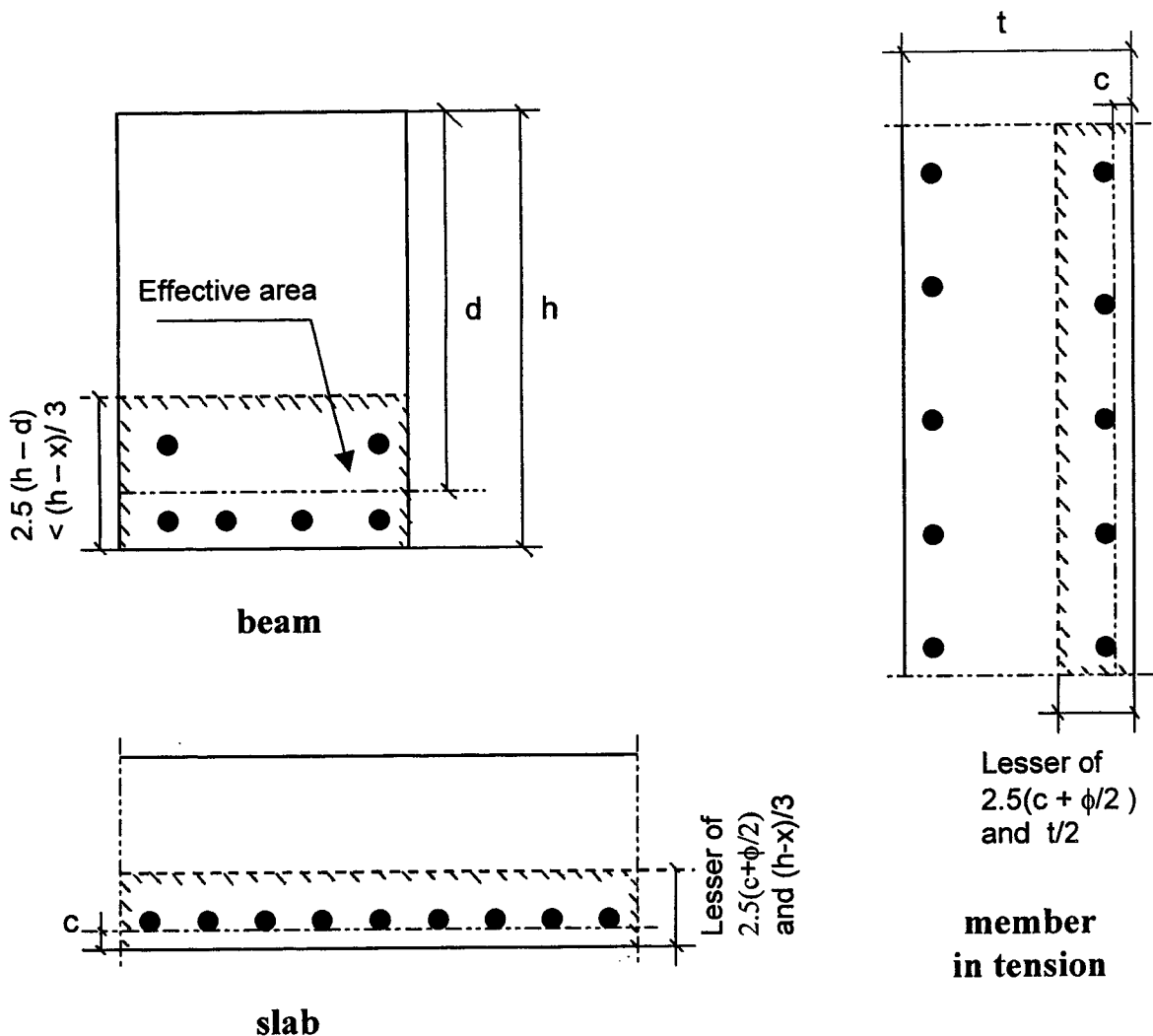


Figure 7.1 Effective tension area as defined by CEB-FIP Model 1990

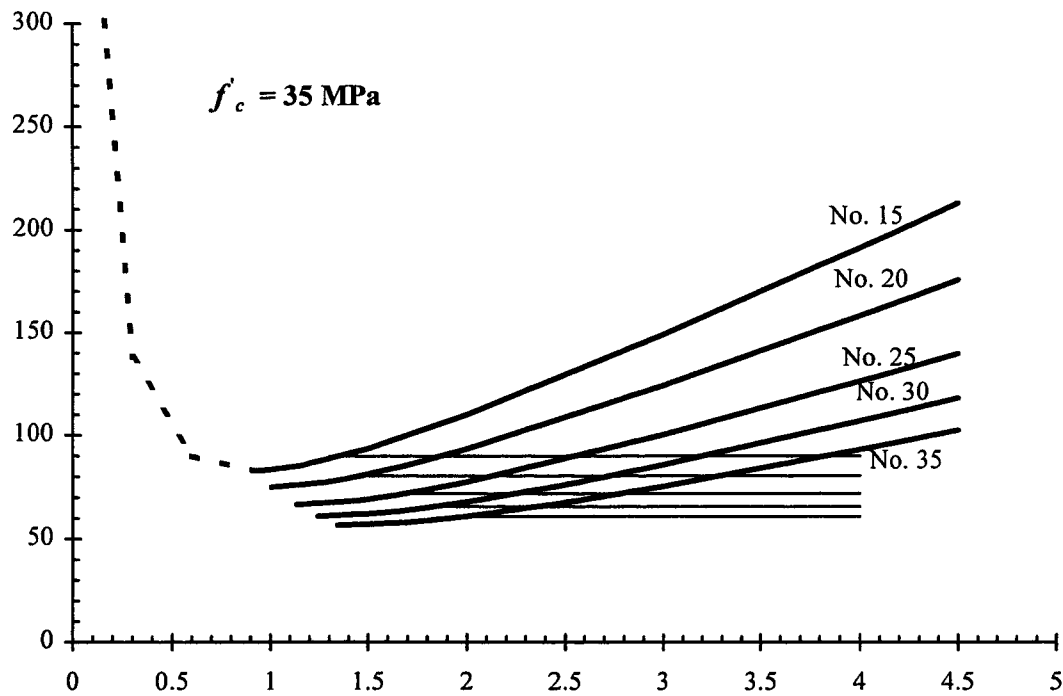


Figure 7.2 Non-prestressed steel stress versus total reinforcement ratio for a crack width of 0.10 mm

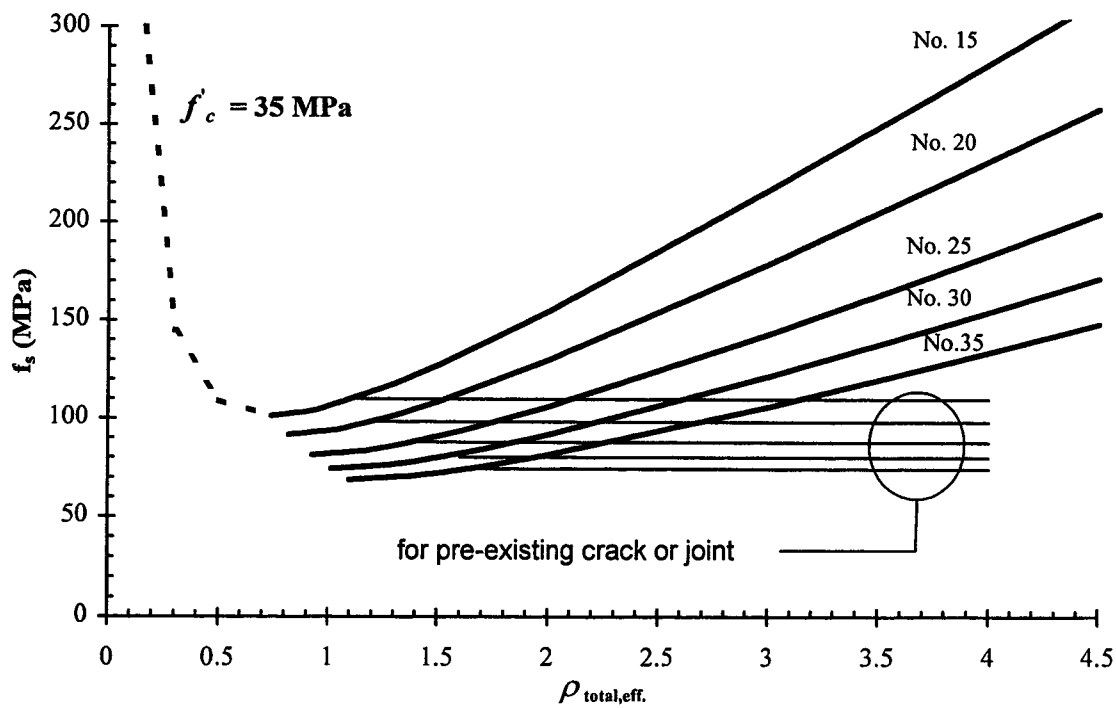


Figure 7.3 Non-prestressed steel stress versus total reinforcement ratio for a crack width of 0.15 mm

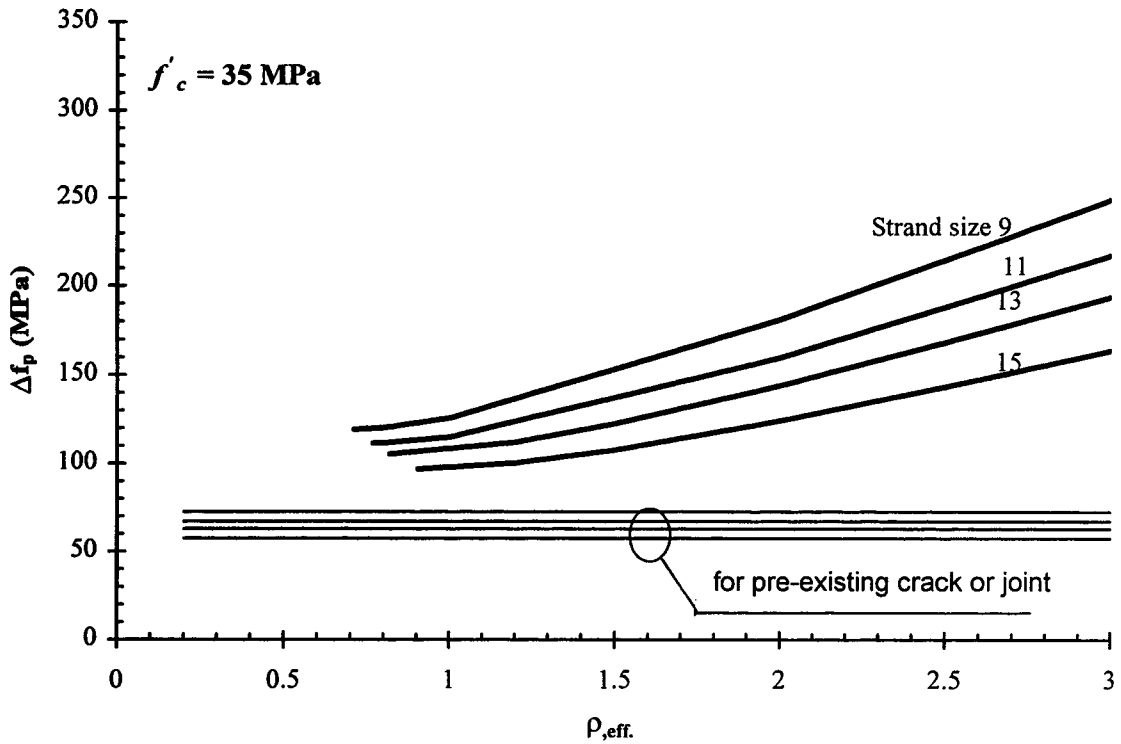


Figure 7.4 Prestressed reinforcement stress versus steel ratio for a crack width of 0.10 mm

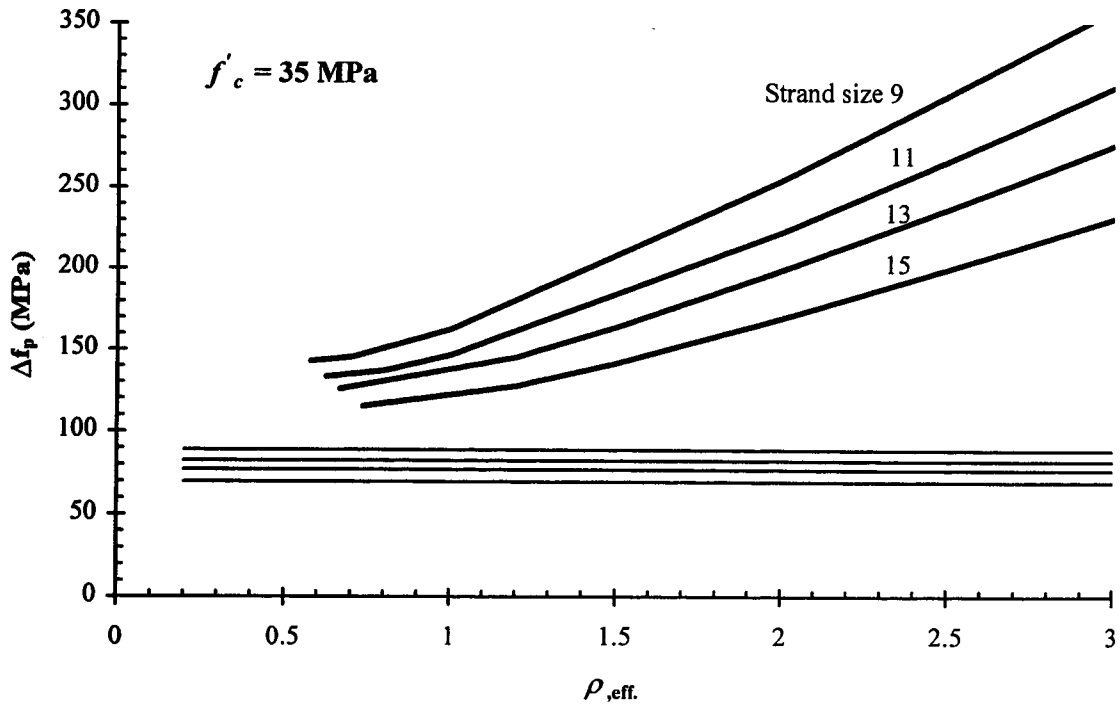


Figure 7.5 Prestressed reinforcement stress versus steel ratio for a crack width of 0.15 mm

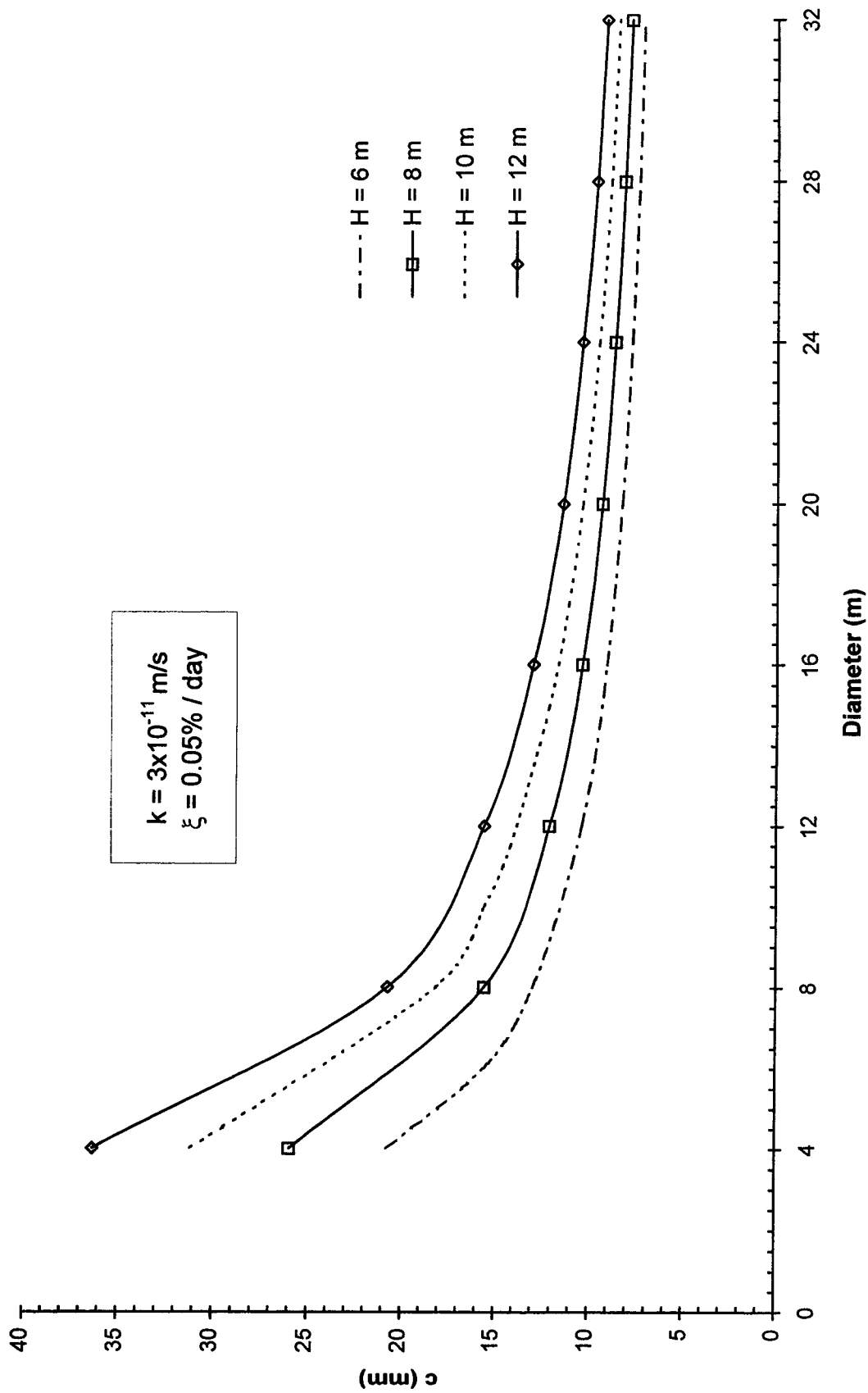


Figure 7.6 The minimum depth of compression zone required to control leakage

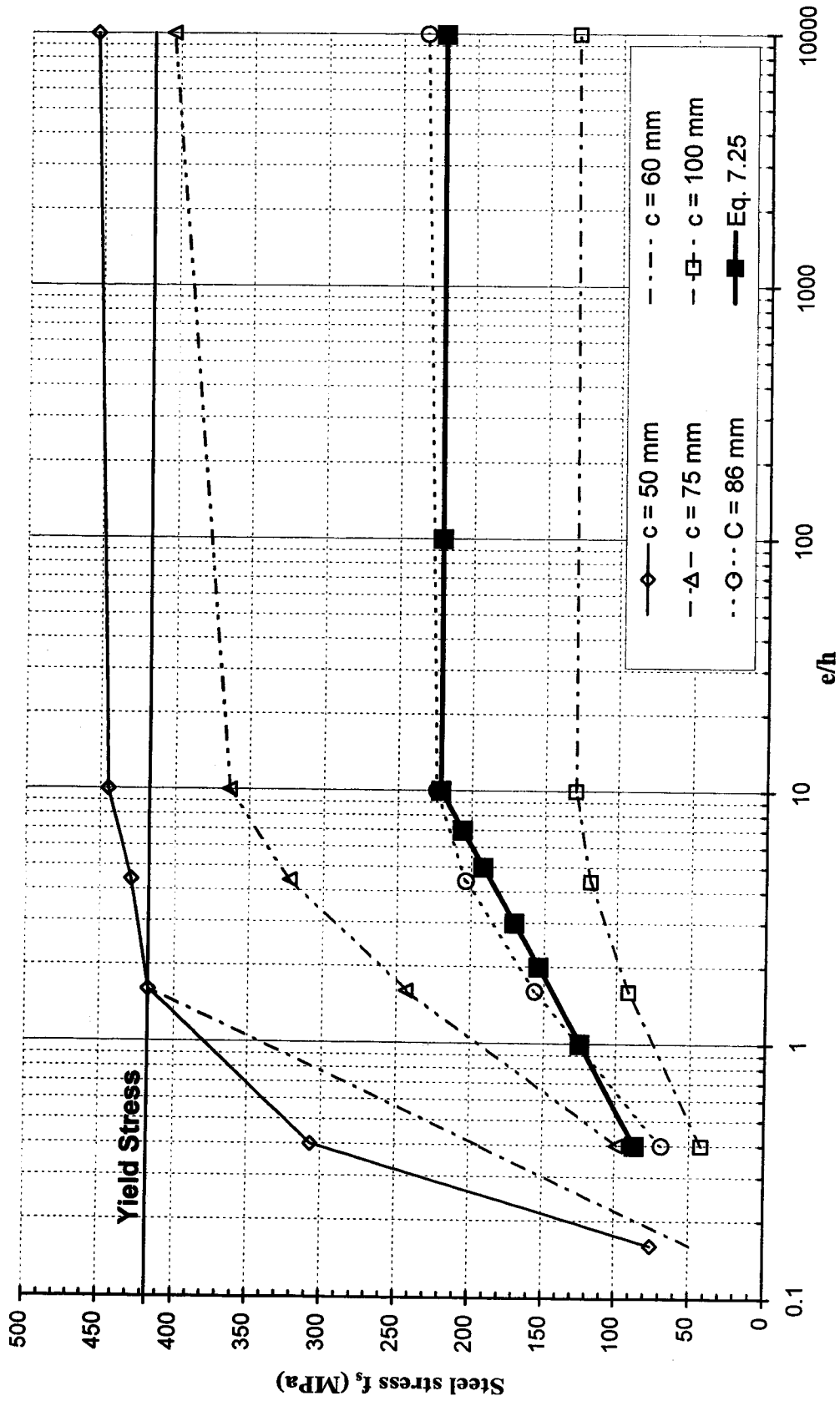


Figure 7.7 Non-prestressed steel stress versus eccentricity for different depths of compression zones

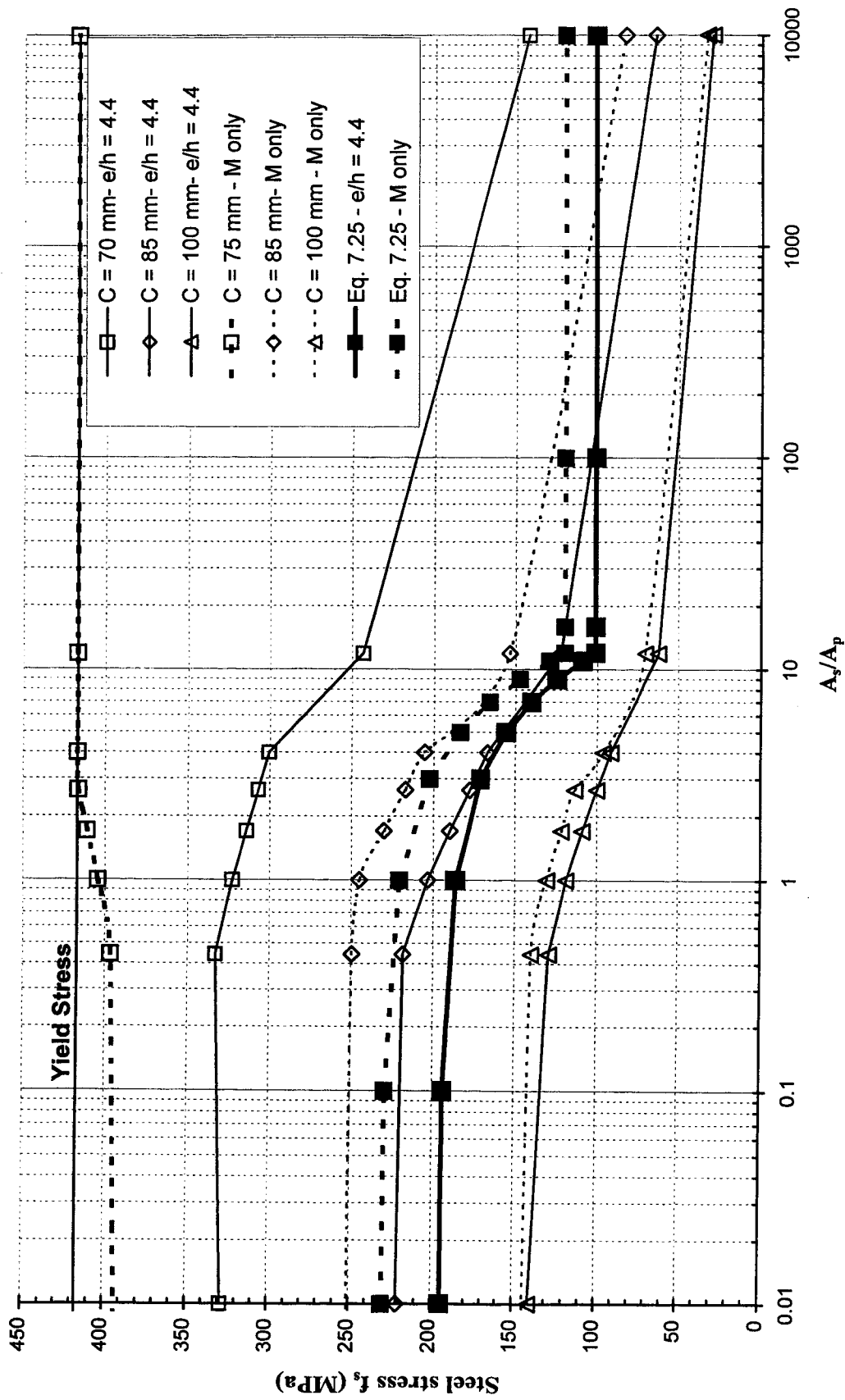


Figure 7.8 Non-prestressed steel stress versus steel ratio for different depths of compression zone

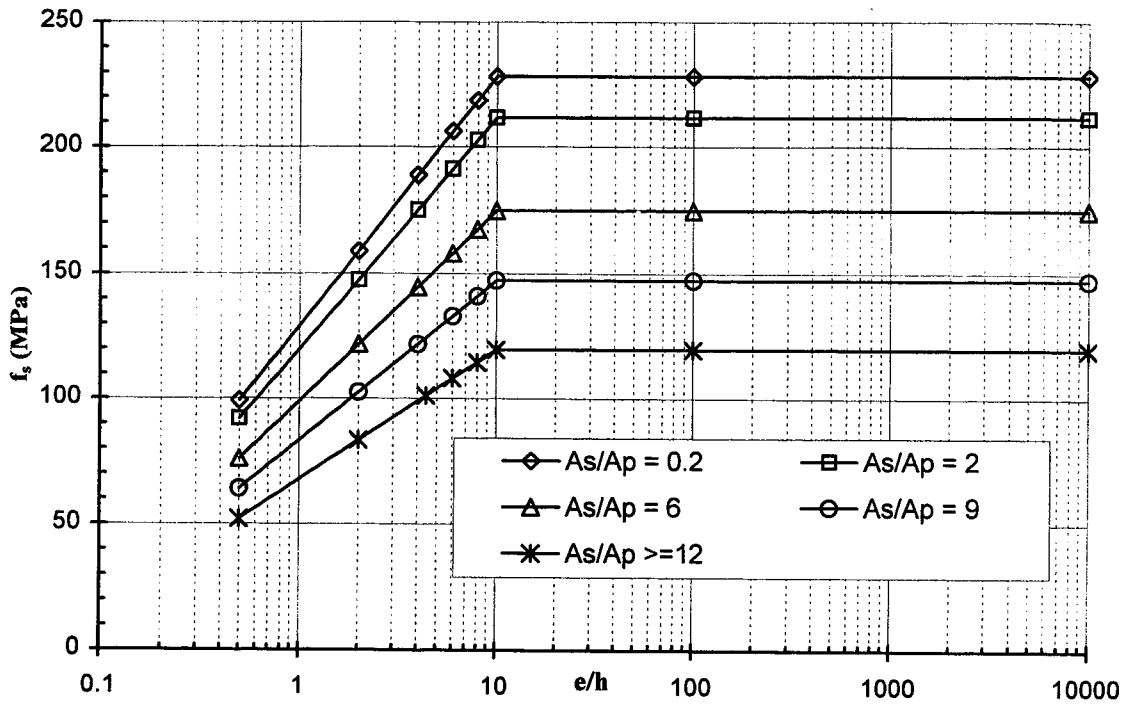


Figure 7.9 Steel stress obtained using the proposed equation for different partial prestressing degrees

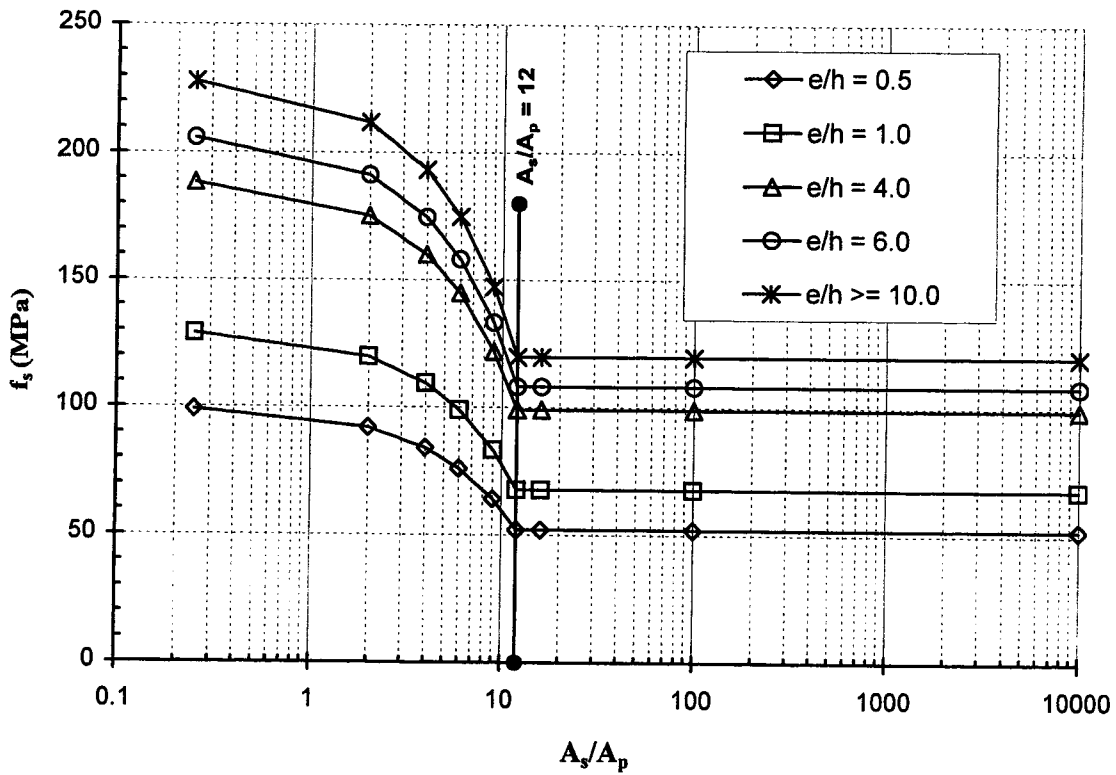


Figure 7.10 Steel stress obtained using the proposed equation for different load eccentricities

8- Summary, Conclusion, and Recommendations

8.1 Summary

The design of concrete water containment structures is studied in this report with the aim of developing a rational design procedure for both reinforced and prestressed concrete tanks that assure a safe leak resistant structure. In particular, the concepts of partial prestressing and watertightness in liquid retaining structures are investigated.

A critical review of the existing design approaches for liquid containing structures was carried out. The review together with design trials illustrated the differences between the existing approaches especially those between the design of reinforced concrete and prestressed concrete tanks. The review and the design trials highlighted the advantages of partial prestressing in the design of water tanks. The literature review also revealed a growing understanding of the phenomena of watertightness and self-sealing of cracks.

The experimental program consisted of two phases. The first phase addressed the structural response of wall panels representing a typical wall segment from a tank with varying reinforcement patterns, prestressing ratios and loading. The second phase addressed leakage rates through cracked wall panels. Eight full-scale specimens, which had three different configurations, were tested. Six specimens were subjected to leakage tests concurrently with structural load application. The goal of the experimental program was to provide new data that was used to develop and calibrate an analytical model.

An analytical model was written to analyze partially prestressed concrete sections. The model considers the actual measured stress-strain relationships for the different materials. The analytical model uses a tension stiffening description based on the test results. The analytical model was used to simulate the test specimens. The response predictions were satisfactory. The analytical model was then used to carry out a

parametric study on structural behaviour. The aim of this parametric study was to provide further insight into the behaviour of partially prestressed sections subjected to combinations of axial load and moments. A further objective was to examine the existing code recommendations in order to identify a rational method for the design of concrete water tanks. Another limited parametric study was conducted to investigate hydraulic conductivity through cracks and the compression zone of a cracked concrete section.

Various design strategies for the leakage limit state are next discussed. These strategies range from preventing cracking completely to limiting through-crack widths such that leakage rates are acceptable. Based on the results of physical and numerical experiments, a unified limit states design approach for the design of water tanks is proposed. The proposed approach covers water tank designs ranging from reinforced concrete at one end of the design spectrum to fully prestressed concrete at the other. Two design examples that illustrate the practical implementation of this proposed approach are provided.

8.2 Conclusions

8.2.1 Conclusions from Comparison of Existing Specifications

The broad general conclusions that can be drawn from the experience of doing 23 different designs based on the existing specifications for the design of water containment structures are:

1. Ultimate strength never governs the design based on existing specifications.
2. Choosing the reinforcement to meet specific crack width limits requires the least reinforcement but requires the most design calculations.
3. Working stress design is the easiest and produced structures only slightly more expensive than structures designed on the basis of explicit crack width calculations.
4. Existing design standards are based on either fully prestressed or fully non-prestressed concepts.

5. The existing specifications for prestressed tanks require the use of more prestressing steel for thicker walls to achieve the required residual compression. The existing specifications appear to be irrational because adding concrete to the section should not require additional reinforcement. The existing specifications also do not provide a recognized benefit for additional non-prestressed reinforcement.
6. There appears to be merit in a design based on partial prestressing concepts since it would recognize the benefits of additional wall thickness and additional non-prestressed reinforcement

8.2.2 Findings from Tests

8.2.2.1 Structural Response of Wall Panels

1. Non-prestressed steel improves the cracking behaviour and increases the ductility of the prestressed member.
2. Unbonded tendons produced the same cracking and ultimate moments as bonded tendons in the specimens tested. The cracks in the specimen with unbonded tendons were significantly wider and had an irregular crack pattern. The large in-plane tension was such that the tendons yielded at ultimate.
3. In the case of eccentric tension or flexure the cracks formed at a low load level but did not progress quickly. Under pure axial tension through-cracks occurred at higher load level but once they occurred they become wide and progressed through the section rapidly.

8.2.2.2 Leakage Tests

1. In the absence of through-cracks there was no leakage. The presence of the compression zone prevented leakage regardless of the crack widths.
2. If the effective width of a through-crack was narrower than 0.15 mm, the cracks would leak initially and then self-seal.
3. If the through-cracks were wide, water flowed through the cracks continuously
4. The pre-opened cracks self-sealed within a few hours.

8.2.3 Conclusions from the Parametric Studies

1. A design method based on limiting the steel stress, f_s , does not produce consistent crack or compression zone depths under the application of partial prestressing nor under a combination of axial load and moment.
2. A design method based on providing a residual compressive stress in the concrete does not utilize non-prestressed reinforcement effectively.
3. Relaxing the residual compressive stress requirement permits a more efficient design. The stresses in the non-prestressed steel are higher, but remain below yield under service load. Therefore, less reinforcement is required.
4. Load eccentricity significantly affects the behaviour of the partially prestressed concrete sections. The behaviour with a small load eccentricity, less than about half the thickness, is close to that of pure axial tension. At a load eccentricity larger than about four times the thickness, the section may be treated as a flexural member.
5. The ratio of non-prestressed steel to prestressed steel in a partially prestressed concrete section has a significant effect on the member serviceability and strength. Choosing the ratio such that both non-prestressed and prestressed steel reach their strength simultaneously utilizes both types of steel at the ultimate limit state effectively.
6. Increasing the wall thickness is very effective in increasing the capacity of the section and improving its serviceability by increasing the compression zone depth and reducing the deformations.
7. Virtually any compression zone depth will give adequate leakage control. While a compression zone thickness of 5 mm may be theoretically adequate, a practical minimum design thickness for the compression zone should account for the possible defects in concrete surface.

8.2.4 Conclusions from the Proposed Design Approach

Design trials show that the proposed design approach has the following features:

1. Less reinforcement, especially less prestressed steel, is required.
2. The leakage limit state is addressed directly.
3. The benefits of increasing wall thickness and non-prestressed reinforcement are recognized.
4. The proposed approach also offers a smooth and logical transition between the design of fully prestressed and fully reinforced concrete water tanks.

8.3 Recommendations for Future Research

The study of partially prestressed water tanks is relatively a new research field. Many experimental and analytical research topics can be suggested such as:

1. Additional experimental investigation of full-scale specimens subjected to axial tension is needed. The investigation should include parameters such as partial prestressing ratios, crack widths, and elongation. Non-prestressed reinforcement stress should be also obtained to validate a design equation which gives f_s depending on the partial prestressing level and the crack width, which in turn depends on leakage limit state. Leakage rate through the cracks formed in these specimens should also be investigated. This load case governs the design of the circular tanks. Only one specimen subjected to an axial tension was tested in the current study.
2. Leakage tests should be conducted on small specimens to investigate aspects such as cracks that change their width with time (active cracks), variable water head, and closed pre-existing cracks. These aspects may have effect on the leakage and the self-sealing behaviour of through cracks.
3. A design aid, such as tables, should be generated to give the minimum compression zone depth for a given leakage rate using an accurate approach, e.g. the finite difference simulation. The variables in these tables are the wall thickness and the

water pressure. These tables can be prepared for a specific location for a given allowable loss of water volume and the average annual weather conditions. The designer can obtain the minimum depth of compression zone directly from these tables.

4. Deflection of partially prestressed tanks should be investigated. This can be done on two levels. On the simple level, shell and plate theory equations can be used to prepare tables, similar to the PCA tables, that give deformations. The equations given by the building codes for the effective moment of inertia can be used to calculate the deflection. At an advanced level, a computer program which considers cracking and non-linearity in concrete sections and has the ability to model both types of reinforcement, can be used in a parametric study to investigate the deformation of partially prestressed water tanks. Deflection is critical in situations such as walls that support roofs or are attached to any mechanical or structural element which might be affected by the large deflection.

References

- Abeles, P. W., 1945. Fully and Partially Prestressed Reinforced Concrete. *ACI Journal*, Vol. 41, No. 3, January 1945, pp. 181-214.
- ACI Committee 350, 1989. Environmental Engineering Concrete Structures (ACI 350R-89). American Concrete Institute, Detroit, 24 pp.
- ACI Committee 344, 1989. Design and Construction of Circular Prestressed Concrete Structures (ACI 344). American Concrete Institute, Detroit, 38 pp.
- ACI 350.1R-93/AWWA 400-93, 1993. Testing Reinforced Concrete Structures for Watertightness. American Concrete Institute, Detroit. October 1993.
- ACI Committee 318, 1995. Building Code Requirements for Structural Concrete (ACI 318-95) and Commentary (ACI318R-95). American Concrete Institute, Detroit, 369 pp.
- Al-Manaseer, A.A. and Philips, D.V., 1987. Numerical Study of Some Post-Cracking Material Parameters Affecting Nonlinear Solutions in RC Deep Beam. *Canadian Journal of Civil Engineering*, Vol. 14, pp. 655-666.
- Alvarez, M. and Marti, P., 1996. Versuche zum Verbundverhalten von Bewehrungsstahl Bei plastischen Verformungen. IBK Bericht Nr. 222, Sept. 1996. 135 pp.
- Beeby, A.W., 1983. Cracking, Cover, and Corrosion of Reinforcement. *Concrete International*, Vol. 5, No. 2, Feb. 1983. pp 35-40
- Bennett, E.W. and Veerasubramanian, N., 1972. Behaviour of Nonrectangular Beams with Limited Prestress after Flexural Cracking. *ACI Journal* Sept. 1972. pp. 533-542.

- Bick, D., Cordes, H., and Trost, H., 1997. Eindring- und Durchströmungsvorgänge umweltgefährdender Stoffe an feinen Trennrissen in Beton. Deutscher Ausschuss Für Stahlbeton. Heft 475. Berlin, pp. 101-171.
- Bomhard, H., 1986. Concrete Tanks for Water Storage – a Conceptual Approach. Proceedings of the Tenth International Congress of the FIP. New Delhi, India. pp 55-77.
- Brøndum-Nielsen, T., 1984. On the Problems of Partial Prestressing. The Proceedings of NATO Advanced Research Workshop. Paris, France. June 18-22. Vol. 2. pp. 3-13.
- BS 8110:Part 1:1985. Structural Use of Concrete. British Standard Institute, London.
- BS 8007: 1987. Code of Practice for the Design of Concrete Structures for Retaining Aqueous Liquids. British Standard Institute, London.
- CAN A23.3-M77, 1977. Code for the Design of Concrete Structure for Buildings. Canadian Standard Association, CSA. Rexdale, Ontario, 131 pp.
- CEB, 1985. CEB Manual on Cracking and Deformations, Bulletin D'Information No 158-E. Comite Euro-International du Beton, EPF Lausanne, Swizerland, 65 pp.
- CEB-FIP Model Code 1990, 1993. Comite' Euro-International du Beton, EPF Lausanne, Swizerland.
- Cedergreen, H. R., 1989. Seepage, Drainage, and Flow Nets. Third Edition. John Wiley & Sons, New York, 465 pp.
- Clear, C.A., 1985. The Effect of Autogenous Healing upon the Leakage of Water through Cracks in Concrete. Cement and Concrete Association. Report No. 559. May 1985. 31 pp.
- Collins, M.P. and Mitchell, M., 1987. Prestressed Concrete Basics. Canadian Prestressed Concrete Institute. 614 pp.

- Collins, M.P. and Mitchell, M., 1991. Prestressed Concrete Structures. Prentice Hall.
- CSA A23.3-94, 1994. Design of Concrete Structures. Canadian Standard Association, Rexdale, Ontario.
- Dunne, T. and Leopold, L.B., 1978. Water in Environmental Planning. W. H. Freeman and Company. San Francisco. 818 pp.
- Edvardsen, C.K., 1996. Wasserdurchlässigkeit und Selbstheilung von Trennrissen in Beton. Deutscher Ausschuss Für Stahlbeton. Heft 455. Berlin, 134 pp.
- Elwi, A. E., 1992. FEPARCS 92- A Finite Element Program for the Analysis of Axisymmetric Reinforced Concrete Structures. Department of Civil Engineering, University of Alberta.
- Foster, S. J., 1992. The Structural Behaviour of Reinforced Concrete Deep Beams. Ph.D. thesis. University of New South Wales. Australia.
- Gerald, C. F., 1980. Applied Numerical Analysis. Second Edition. Addison-wesley Publishing Company. Massachusetts. 518 pp.
- Gergely, P. and Lutz, L. A., 1968. Maximum Crack Width in Reinforced Concrete Flexural Members, Causes, Mechanism, and Control of Cracking in Concrete. SP-20, American Concrete Institute, Detroit, pp. 87-117.
- Ghali, A. and Favre, R., 1986. Concrete Structures: Stresses and Deformations. Chapman and Hall, London. 352 pp.
- Gilbert, R. I. and Warner, R. F., 1978. Tension Stiffening in Reinforced Concrete Slabs. Journal of the Structural Division, ASCE, Vol. 104, No. ST12, pp. 1885-1900.
- Gogate, A.B., 1981. Structural Design of Reinforced Concrete Sanitary Structures- Past, Present, and Future. Concrete International, Vol. 3, No. 4, April 1981. pp. 24-28.

- Gray, W. S., 1948. Reinforced Concrete Reservoirs and Tanks. Concrete Publications Limited, London, 189 pp.
- Habib-Allah, A., and Wilson, E.L., 1984. SAP80- A Computer Program for the Finite Element Analysis of Structures," Berkeley, California.
- Harajli, M.H. and Naaman, A.E., 1984. Deformation and Cracking of Partially Prestressed Concrete Beams under Static and Cyclic Fatigue Loading. Report No. UMEE 84R1. Department of Civil Engineering. The University of Michigan, Ann Arbor. Aug. 1984. 177 pp.
- Harajli, M.H. and Naaman, A.E., 1989. Cracking in Partially Prestressed Beams under Static and Fatigue Loading. ACI Publication SP-113, Detroit, Michigan pp. 29-56.
- Hassoun, M.N. and Sahebjam, K., 1989. Cracking of Partially Prestressed Concrete Beams. ACI Publication SP-113, Detroit, Michigan. pp. 57-78.
- Imhof-Zeitler, C., 1996. Fließverhalten von Flüssigkeiten in durchgehend gerissenen Betonkonstruktionen. Deutscher Ausschuss Für Stahlbeton. Heft 460. Berlin, 199 pp.
- Krishna Mohan Rao, S.V. and Dilger, W.H., 1992. Control of Flexural Crack Width in Cracked Prestressed Concrete Members," ACI Structural Journal, V. 89, No. 2, pp. 127-138.
- MacGregor, J.G., 1997. Reinforced Concrete Mechanics and Design. Third edition, Prentice Hall. 939 pp.
- Massicotte, B., Elwi, A.E., and MacGregor, J.G., 1990. Tension-Stiffening Model for Planar Reinforced Concrete Members. ASCE. Journal of Structural Engineering. Vol. 116, No. 11, Nov. 1990. pp 3039- 3057.
- Mathieu, H., 1984. Importance of Serviceability. Reexamination of Cracking Criteria. The Proceedings of NATO Advanced Research Workshop. Paris, France. June 18-22. Vol. 2. pp. 15-28.

- Mattock, A.H., 1979. Flexural Strength of Prestressed Concrete Section by Programmable Calculator. Journal of Prestressed Concrete Institute, Vol. 24, No. 1, Jan-Feb., pp. 32-54.
- Murray, M.H., 1981. Crack Widths in Water Retaining Structures. The 10th Biennial Conference. Concrete Institute of Australia, Adelaide, Australia.
- Naaman, A.E., 1982. Fatigue in Partially Prestressed Concrete Beams. ACI Publication SP-75, Detroit, Michigan. pp. 25-46.
- Naaman, A.E., 1984. Partially Prestressed Concrete Members under Static Loading: American Perspective. The Proceedings of NATO Advanced Research Workshop. Paris, France. June 18-22. Vol. 1. pp. 79-124.
- Nawy, E.G. and Huang, P.T., 1977. Crack and Deflection Control of Pretensioned Prestressed Beams. PCI Journal may/June 1977. Pp. 30-47.
- Nawy, E.G., 1984. Flexural Cracking of Pre- and Post-Tensioned Flanged Beams. The Proceedings of NATO Advanced Research Workshop. Paris, France. June 18-22. Vol. 2. pp. 137-156.
- Nawy, E.G., 1989. Cracking Behaviour of Partially Prestressed Pretensioned and Post tensioned Beams – state of the Art. ACI Publication SP-113, Detroit, Michigan, pp. 1-28.
- NBCC, 1995. National Building Code of Canada 1995. National Research Council of Canada, Ottawa .
- Neville, A.M., 1981. Properties of Concrete. Third edition. PITMAN Publication Limited. London. 779 pp.
- PCA, 1942. Circular Concrete Tanks without Prestressing. Portland Cement Association, Skokie, (revised 1993).

- PCA, 1963. Rectangular Concrete Tanks. Portland Cement Association, Skokie, (revised 1981).
- PCI Committee on Precast Prestressed Concrete Storage Tanks. 1987. Recommended practice for precast concrete circular storage tanks. PCI journal, pp. 80-125.
- Ponce, V.M., 1989. Engineering Hydrology Principles and Practices. Prentice Hall.
- Raju, N. K., Basavarajaiah, B. S., and Kutty, U. C., 1973. Flexural Behaviour of Pretensioned Concrete Beams with Limited Prestress. Building Science, Progamon Press, Vol. 8, pp. 179-185.
- Simmonds, S. H., Rizkalla, S. H., and MacGregor, J. G., 1979. Tests of Walls Segments from Reactor Containment. Structural Engineering Report No. 81, Vol.1, Department of Civil Engineering, University of Alberta, 207 pp.
- Stevens, R.F., 1969. Tests on Prestressed Concrete Beams. Concrete November 1969. pp. 457-462.
- Tadros, M. K., 1982. Expedient Service Load Analysis of Cracked Prestressed Concrete Sections. PCI Journal. V. 27, No. 6, Dec. 1982, pp. 50-63.
- Vecchio, F.J. and Collins, M.P., 1986. The Modified Compression-Field theory for Reinforced Concrete Elements Subjected to Shear. ACI Journal March/April 1986. Pp. 219-231.
- Wilby, A.C., 1977. Structural Analysis of Reinforced Concrete Tanks. Journal of the Structural Division, ASCE, V. 103, No. ST5, May 1977, pp. 989-1004.

Appendix A: Listing of the Computer Program

The computer program was written using Visual Basic. The program consists of main subroutine, MAIN1, and six subroutines. The main subroutine reads the data and calls the other subroutines then writes the output. Subroutine MACRO2 calculates the strain distribution resulting from the prestressing force only before applying the external loads, FIRSTVALUE calculates stresses and deformations corresponding to that strain distribution. MACRO1 calculates stress resultants, stresses and deformations for each strain increment until failure. Subroutine SHRINK calculates the effect of creep and shrinkage. Subroutine PLOTTING automatically prepares moment versus curvature plots. Subroutine MYDATA opens and prepares new spreadsheet to enter the data and print the results in it. The different material models were expressed as functions grouped in a separate subroutine. Only one subroutine was written for the case of axial load, MAIN2.

Listing of the complete program is below. An example for a spreadsheet that contains the input data and a part of the output results is given in Fig. A.1.

```
' This is the main subroutine, which calls the other subroutines.
,
Public cs As Double, Ntot1, Mtot1, cforce1, cmom1 As Double
Public ecc, ecco, bottstrain, phi, cstre, topstrain, y, H As Double
Public bottp, eccp, bott7, psfo, pA As Double
Public topinitial, botinitial, psinitial, ds, dps As Double
Public sstrain, pstrain, sstre, pstre, sforce As Double
Public sarea, pforce, parea, spforce, smoment As Double
Public l, K1, K2, layerN As Integer
Public a, bl1, bl2, bto, dl1, dl2, dto, ro1, ro2, comp1 As Double
Public tcon, ts, tps, fcon, phiun, phicr As Double
Public creep, shstrain, zertop, zerbot, deltop, delbot As Double
Public delMtot1, delNtot1, delsstra, delsstre, delsforc As Double
Public delsmome, delcforc, delcmom1, delcs, zerccs, redcmom As Double
Public delcstre, Mtot2, Ntot2, cstre2, sstre2 As Double
,

Sub main1()
topinitial = [d2].Value: botinitial = [D3].Value
psinitial = [D4].Value: parea = [B4].Value: sarea = [B5].Value
ds = [F2].Value: dps = [F1].Value: H = [b1].Value
B = [b2].Value: Bt = [B3].Value
fcc = [J2].Value: cso = [J3].Value
```

```

ccrack = [J4].Value: cmod = [J5].Value
ecco = [F5].Value: creep = [m1].Value
shstrain = [m2].Value: zertop = [m3].Value
zerbot = [m4].Value: deltop = [m5].Value
delbot = [m6].Value
pA = psinitial / 1000000
psfo = 200000 * pA * (0.026 + 0.974 / (1 + (117.3 * pA) ^ 10) ^ 0.1) * parea
  For K1 = 1 To 350
    topstrain = -0.005 * (K1 + 4300)
    Macro2
    Cells(8, 2).Value = K1
    If Ntot1 < -psfo Then Exit For
  Next K1
  Cells(8, 3).Value = ecc
  Cells(8, 4).Value = Ntot1 / 1000          'initial normal force
  Cells(8, 5).Value = Mtot1 / 1000000     'initial moment
  Cells(8, 6).Value = (bottp - topstrain) / H  'phi
  Cells(8, 7).Value = topstrain: Cells(8, 8).Value = bottp
  Cells(8, 9).Value = (-Ntot1 - psfo) / psfo * 100
  ecco = [F5].Value
,
' Subroutine to calculate the first values of moment and N
firstvalue
,
topstrain = 0
  For K2 = 1 To 200
    topstrain = -25 * K2
    Macro1
    Cells(11 + K2, 2).Value = K2
  Next K2
  plotting
  End Sub
,
' Subroutine calculates strain distribution equivalent to zero external moment
Sub Macro2()
  I = 1
  H = [b1].Value
  ecc = 0: bottp = 0
  Do
    Ntot1 = 0
    Mtot1 = 0
    Cells(8, 1).Value = I
    If I = 1 Then ' first estimate of bottom strain
      bottstrain = 3 * topstrain
    Else
      End If
    sstrain = (bottstrain + (topstrain - bottstrain) * ds / H) / 1000000 'rebar strain
    pstrain = (bottstrain + (topstrain - bottstrain) * dps / H) / 1000000 'p/s strain
    sstre = sstress(sstrain) 'rebar stress
  ' P/S stress using Osgood func. w/ ultimate stress of 1860 MPa
  pstre = 200000 * pstrain * (0.026 + 0.974 / (1 + (117.3 * pstrain) ^ 10) ^ 0.1)
  If pstre > 1860 Then Exit Sub
  sforce = sstre * sarea ' rebar force

```

```

pforce = pstre * parea ' p/s force
spforce = sforce + pforce ' total steel force
' total steel moment @ the mid-height of the section
smoment = sforce * (H / 2 - ds) + pforce * (H / 2 - dps)
cforce1 = 0
cmom1 = 0
For layerN = 1 To 100
'concrete strain at the centroid of the layer
cs = (bottstrain - (layerN - 0.5) / 100 * (bottstrain - topstrain)) / 1000000
' If cs < -0.0033 Then Exit Sub
'Distance between layer's centroid and section mid-height
y = (H / 2) - (layerN - 0.5) * H / 100
'Concrete stress
cstre = cstres1(fcc, cs, cso, ccrack, cmod)
' cstres & cstre are concrete stress formula and value respectively
cforce1 = cforce(cs, cstre, ccrack, H, B, Bt) ' concrete force/layer
cmom1 = cforce1 * y ' concrete moment/layer
Ntot1 = Ntot1 + cforce1
Mtot1 = Mtot1 + cmom1
cforce1 = 0
cmom1 = 0
Next layerN
cforce1 = 0
cmom1 = 0
Ntot1 = spforce + Ntot1 ' total steel & concrete tension
Mtot1 = smoment + Mtot1 ' total steel & concrete moment
ecc = Mtot1 / Ntot1
ecco = H / 2 - dps
I = I + 1
If I = 2 Then
bottp = bottstrain
eccp = ecc
bottstrain = bottstrain + Mtot1 * 2 / (25 * 389) * (1 / ecco - 1 / ecc)
End If
If I > 2 And eccp = ecc Then
bott7 = bottstrain + 200 * (I + 1)
bottp = bottstrain
bottstrain = bott7
eccp = ecc
End If
If I > 2 And eccp <> ecc Then
bott7 = bottstrain + (1 / ecco - 1 / ecc) / (1 / ecc - 1 / eccp) * (bottstrain - bottp)
bottp = bottstrain
bottstrain = bott7
eccp = ecc
End If
Loop Until (Abs(ecc - ecco)) < 0.07
End Sub

```

' This module contains the different material models

```

Public ss As Double, cs As Double, cstre As Double, ecc As Double
Public fcc As Double, cso As Double, ccrack As Double, cmod As Double
Public H As Double, B As Double, Bt As Double, cforc1 As Double, y As Double
Public cmom1 As Double, Mtot1 As Double

```

```

' The following function calculates steel stress (sstress) knowing steel strain (ss)
' yield stress = 417 MPa, Es = 190000 MPa, strain hardening strain = 0.00512
' stress after strain hardening found by best fitting of the actual stress-strain curve

```

```

Public Function sstress(ss) As Double
If ss <= (417 / 190000) And ss >= (-417 / 190000) Then
sstress = ss * 190000
ElseIf ss > (417 / 190000) And ss <= 0.00512 Then
sstress = 417
ElseIf ss > 0.00512 And ss <= 0.125 Then
sstress = ss ^ 3 * 369604 - 105391 * ss ^ 2 + 10015 * ss + 368
ElseIf ss < (-417 / 190000) And ss >= -0.00512 Then
sstress = -417
ElseIf ss < -0.00512 And ss >= -0.125 Then
sstress = 369604 * ss ^ 3 + 105391 * ss ^ 2 + 10015 * ss - 368
End If
End Function

```

```

' The following function calculates concrete stress (cstress) knowing concrete strain (cs)
' two parabolic eqns. fit the stress-strain curve of specimen 1C40

```

```

' Public Function cstres1(fcc, cs, cso, ccrack, cmod) As Double
ft1 = 0.22 * Sqr(-fcc)
ccrack = ft1 / cmod
If 0 >= cs And cs > cso Then ' concrete in compression
cstres1 = 0.0135 + 27450 * cs + 3221420# * cs ^ 2
ElseIf cso >= cs And cs >= -0.0033 Then
cstres1 = 59.04 + 97530 * cs + 22644000# * cs ^ 2
ElseIf cs > 0 And cs <= (ft1 / cmod) Then
cstres1 = cs * cmod ' cmod is the concrete modules of elasticity
ElseIf cs > (ft1 / cmod) And cs <= (3 * ft1 / cmod) Then
cstres1 = (0.4 + 0.25 / 4 * (3 - cs / ccrack) ^ 2) * ft1
Else
cstres1 = 0.4 * ft1
End If
End Function

```

```

' The following function calculates concrete force (cforce) knowing concrete stress

```

```

Public Function cforce(cs, cstre, ccrack, H, B, Bt) As Double
If cs < ccrack Then
cforce = cstre * B * H / 100
Else
cforce = cstre * Bt * H / 100
End If
End Function

```

" In the case of axial tension the section was divided only into 4 layers

```
Public Function cforceX(cs, cstre, ccrack, H, B, Bt) As Double
If cs < ccrack Then
cforceX = cstre * B * H / 4
Else
cforce X= cstre * Bt * H / 4
End If
End Function
```

```
Public cs As Double, Ntot1, Mtot1, cforce1, cmom1 As Double
Public ecc, ecco, bott1strain, phi, cstre, top1strain, y, H As Double
Public l, layerN As Integer
Public bottp, eccp, bott7 As Double
Sub firstvalue()
H = [b1].Value
ecc = 0: bottp = 0
Ntot1 = 0: Mtot1 = 0
top1strain = [g8].Value: bott1strain = [h8].Value
sstrain = (bott1strain + (top1strain - bott1strain) * ds / H) / 1000000 'rebar strain
pstrain = (psinitial + (bott1strain + (top1strain - bott1strain) * dps / H)) / 1000000 'p/s strain
sstre = sstress(sstrain) 'rebar stress
' P/S stress using Osgood func. w/ ultimate stress of 1860 MPa
pstre = 200000 * pstrain * (0.026 + 0.974 / (1 + (117.3 * pstrain) ^ 10) ^ 0.1)
If pstre > 1860 Then Exit Sub
sforce = sstre * sarea ' rebar force
pforce = pstre * parea ' p/s force
spforce = sforce + pforce ' total steel force
' total steel moment @ the mid-height of the section
smoment = sforce * (H / 2 - ds) + pforce * (H / 2 - dps)
cforce1 = 0: cmom1 = 0
For layerN = 1 To 100
'concrete strain at the centroid of the layer
cs = (bott1strain - (layerN - 0.5) / 100 * (bott1strain - top1strain)) / 1000000
' If cs < -0.0033 Then Exit Sub
' distance between layer's centroid and section mid-height
y = (H / 2) - (layerN - 0.5) * H / 100
cstre = cstres1(fcc, cs, cso, ccrack, cmod) 'concrete stress
' cstress & cstre are concrete stress formula and value respectively
cforce1 = cforce(cs, cstre, ccrack, H, B, Bt) ' concrete force/layer
cmom1 = cforce1 * y ' concrete moment/layer
Ntot1 = Ntot1 + cforce1
Mtot1 = Mtot1 + cmom1
cforce1 = 0: cmom1 = 0
Next layerN
Ntot1 = spforce + Ntot1 ' total steel & concrete tension
Mtot1 = smoment + Mtot1 ' total steel & concrete moment
ecc = Mtot1 / Ntot1
'
' shrinkage and creep effect
'
H = [b1].Value
Shrink
```

```

Ntot2 = Ntot1 + delNtot1
Mtot2 = Mtot1 + delMtot1
cstre2 = cstre + delcstre
sstre2 = sstre + delsstre
Cells(11, 3).Value = ecc 'final eccentricity
Cells(11, 4).Value = Ntot1 / 1000 'final normal force
Cells(11, 5).Value = Mtot1 / 1000000 'final moment
Cells(11, 6).Value = (bott1strain - top1strain) / H 'phi
Cells(11, 7).Value = top1strain
Cells(11, 8).Value = bott1strain
compzone = -top1strain * H / (bott1strain - top1strain)
If Abs(compzone) > H Then compzone = H
Cells(11, 9).Value = compzone
Cells(11, 10).Value = sstre
Cells(11, 11).Value = pstre
Cells(11, 16).Value = Ntot2 / 1000 'final normal force
Cells(11, 17).Value = Mtot2 / 1000000 'final moment
Cells(11, 18).Value = ((bott1strain + delbot) - (top1strain + deltop)) / H
Cells(11, 19).Value = (top1strain + deltop)
Cells(11, 20).Value = (bott1strain + delbot)
compzone = -(top1strain + deltop) * H / (bott1strain + delbot - top1strain - deltop)
If Abs(compzone) > H Then compzone = H
Cells(11, 21).Value = compzone
Cells(11, 22).Value = sstre2
Cells(11, 23).Value = cstre2
End Sub

```

```

' Macro1 Macro
' This macro conducts structural analysis for the concrete section
,
Public cs As Double, Ntot1, Mtot1, cforce1, cmom1 As Double
Public ecc, ecco, bottstrain, phi, cstre, y, H, compzone As Double
Public l, layerN As Integer
Public bottp, eccp, bott7 As Double
Public a, bl1, bl2, bto, dl1, dl2, dto, ro1, ro2, comp1 As Double
Public tcon, ts, tps, fcon, phiun, phicr As Double
Sub Macro1()
    l = 1
    H = [b1].Value
'Shrinkage and crrep effect
    Shrink
    ,
    ecc = 0: bottp = 0
    Do
    Ntot1 = 0
    Mtot1 = 0
    Cells(K2 + 11, 1).Value = l
    If l = 1 Then ' first estimate of bottom strain
    topstrain = topstrain 'top strain
    bottstrain = -3 * topstrain
    Else
    End If
    sstrain = (bottstrain + (topstrain - bottstrain) * ds / H) / 1000000 'rebar strain

```

```

pstrain = (psinitial + (bottstrain + (topstrain - bottstrain) * dps / H)) / 1000000 'p/s strain
sstre = sstress(sstrain) 'rebar stress
' P/S stress using Osgood func. w/ ultimate stress of 1860 MPa
pstre = 200000 * pstrain * (0.026 + 0.974 / (1 + (117.3 * pstrain) ^ 10) ^ 0.1)
If pstre > 1860 And topstrain < -3000 Then Exit Sub
sforce = sstre * sarea ' rebar force
pforce = pstre * parea ' p/s force
spforce = sforce + pforce ' total steel force
' total steel moment @ the mid-height of the section
smoment = sforce * (H / 2 - ds) + pforce * (H / 2 - dps)
cforce1 = 0
cmom1 = 0
For layerN = 1 To 100
' concrete strain at the centroid of the layer
cs = (bottstrain - (layerN - 0.5) / 100 * (bottstrain - topstrain)) / 1000000
If cs < -0.006 Then Exit Sub
' Distance between layer's centroid and section mid-height
y = (H / 2) - (layerN - 0.5) * H / 100
' Concrete stress
cstre = cstres1(fcc, cs, cso, ccrack, cmod)
' cstres & cstre are concrete stress formula and value respectively
cforce1 = cforce(cs, cstre, ccrack, H, B, Bt) ' concrete force/layer
cmom1 = cforce1 * y ' concrete moment/layer
Ntot1 = Ntot1 + cforce1
Mtot1 = Mtot1 + cmom1
cforce1 = 0
cmom1 = 0
Next layerN
cforce1 = 0
cmom1 = 0
Ntot1 = spforce + Ntot1 ' total steel & concrete tension
Mtot1 = smoment + Mtot1 ' total steel & concrete moment
ecc = Mtot1 / Ntot1
ecco = [F5].Value
If (ecco/H) > 200 GoTo line1
l = l + 1
If l = 2 Then
bottp = bottstrain
eccp = ecc
bottstrain = bottstrain + Mtot1 * 2 / (25 * 389) * (1 / ecco - 1 / ecc)
End If
If l > 2 And eccp = ecc Then
bott7 = bottstrain + 200 * (l + 1)
bottp = bottstrain
bottstrain = bott7
eccp = ecc
End If
If l > 2 And eccp <> ecc Then
bott7 = bottstrain + (1 / ecco - 1 / ecc) / (1 / ecc - 1 / eccp) * (bottstrain - bottp)
bottp = bottstrain
bottstrain = bott7
eccp = ecc
End If

```

```

Loop Until (Abs(ecc - ecco)) < 4
GoTo line2
,
Line1:
I = I + 1
  If I > 600 Then Exit Sub
  If I = 2 Then
    bottp = bottstrain
    bottstrain = bottstrain - 2 / (25 * 389) * Ntot1
    Ntotp = Ntot1
  End If
  If I > 2 And Ntotp = Ntot1 Then
    bott7 = bottstrain + 100 * (I + 1)
    bottp = bottstrain
    bottstrain = bott7
    Ntotp = Ntot1
  End If
  If I > 2 And Ntotp <> Ntot1 Then
    bott7 = bottstrain + Ntot1 / (Ntotp - Ntot1) * (bottstrain - bottp)
    bottp = bottstrain
    bottstrain = bott7
    Ntotp = Ntot1
  End If
  Loop Until (Abs(Ntot1)) < 5
  'the loop ends
  GoTo line2
Line2:
  Ntot2 = Ntot1 + delNtot1
  Mtot2 = Mtot1 + delMtot1
  cstre2 = cstre + delcstre
  sstre2 = sstress(sstrain + delssstra)
,
'Printing the calculated values
,
If (ecco/H) > 200 GoTo line3
Cells(11 + K2, 3).Value = ecc                'final eccentricity
Line3:
Cells(11 + K2, 4).Value = Ntot1 / 1000      'final normal force
Cells(11 + K2, 5).Value = Mtot1 / 1000000  'final moment
Cells(11 + K2, 6).Value = (bottp - topstrain) / H 'phi
phicr = Cells(11 + K2, 6).Value
Cells(11 + K2, 7).Value = topstrain
Cells(11 + K2, 8).Value = bottp
compzone = -topstrain * H / (bottp - topstrain)
If Abs(compzone) > H Then compzone = H
Cells(11 + K2, 9).Value = compzone
Cells(11 + K2, 10).Value = sstre
Cells(11 + K2, 11).Value = pstre
'The following are values after considering creep and shrinkage effect
,
Cells(11 + K2, 12).Value = Ntot2 / 1000      'final normal force
Cells(11 + K2, 13).Value = Mtot2 / 1000000  'final moment
Cells(11 + K2, 14).Value = ((bottp + delbot) - (topstrain + deltop)) / H

```



```

Cells(11 + K2, 15).Value = (topstrain + deltop)
Cells(11 + K2, 16).Value = (bottp + delbot)
compzone = -(topstrain + deltop) * H / (bottp + delbot - topstrain - deltop)
If Abs(compzone) > H Then compzone = H
Cells(11 + K2, 17).Value = compzone
Cells(11 + K2, 18).Value = sstre2
Cells(11 + K2, 19).Value = cstre2
End Sub

```

```

' Subroutine to calculate the change in concrete stress, steel stress, total moment
' and total axial force due to shrinkage and creep strains

```

```

Sub Shrink()
  H = [b1].Value
  delNtot1 = 0: delMtot1 = 0
  delsstra = (delbot + (deltop - delbot) * ds / H) / 1000000 'rebar strain
  delsstre = delsstra * 190000 'rebar stress
  delsforc = delsstre * sarea ' rebar force
  ' total steel moment @ the mid-height of the section
  delsmome = delsforc * (H / 2 - ds)
  delcforc = 0
  delcmom1 = 0
  For layerN = 1 To 100
    ' Concrete strain at the centroid of the layer
    delcs = (delbot - (layerN - 0.5) / 100 * (delbot - deltop)) / 1000000
    zercs = (zerbot - (layerN - 0.5) / 100 * (zerbot - zertop)) / 1000000
    ' distance between layer's centroid and section mid-height
    y = (H / 2) - (layerN - 0.5) * H / 100
    ' Concrete stress
    redcmod = cmod / (1 + 0.8 * creep)
    delcstre = redcmod * (-creep * zercs - shstrain / 1000000 + delcs)
    delcforc = delcstre * H / 100 * B ' concrete force/layer
    delcmom1 = delcforc * y ' concrete moment/layer
    delNtot1 = delNtot1 + delcforc
    delMtot1 = delMtot1 + delcmom1
    delcforc = 0
    delcmom1 = 0
  Next layerN
  delcforc = 0
  delcmom1 = 0
  delNtot1 = delsforc + delNtot1 ' total steel & concrete tension
  delMtot1 = delsmome + delMtot1 ' total steel & concrete moment
End Sub

```

```

' Mydata Macro
' this macro prepare the input to start new problem in new sheet

```

```

Sub Mydata()
  Windows("MOD-1c40.XLS").Activate
  Sheets("Sheet3").Select
  Range("A1:w10").Select
  Selection.Copy
  Workbooks.Add

```

```
ActiveSheet.Paste
Range("K12").Select
End Sub
```

```
' plotting Macro
' Macro plots moment-curvature diagram
```

```
Sub plotting()
Range("E11:F260").Select
Charts.Add
ActiveChart.ChartWizard Source:=Sheets("Sheet1").Range("E11:F260"), _
    Gallery:=xlXYScatter, Format:=6, PlotBy:=xlColumns, _
    CategoryLabels:=1, SeriesLabels:=0, HasLegend:=2, Title:= _
    "Moment vs Curvature", CategoryTitle:="curvature", ValueTitle:= _
    "moment (kN.m)", ExtraTitle:=""
ActiveChart.PlotArea.Select
With Selection.Border
    .Weight = xlThin
    .LineStyle = xlNone
End With
Selection.Interior.ColorIndex = xlNone
ActiveChart.SeriesCollection(1).Select
ActiveChart.SeriesCollection(1).XValues = "=Sheet1!R11C6:R260C6"
With ActiveChart.SeriesCollection(1)
    .Name = ""
    .Values = "=Sheet1!R11C5:R260C5"
End With
ActiveChart.PlotArea.Select
With ActiveChart.Axes(xlCategory)
    .HasMajorGridlines = True
End With
With ActiveChart.Axes(xlValue)
    .HasMajorGridlines = True
End With
ActiveChart.Axes(xlValue).MajorGridlines.Select
With Selection.Border
    .ColorIndex = 4
    .Weight = xlHairline
    .LineStyle = xlDot
End With
ActiveChart.Axes(xlCategory).MajorGridlines.Select
With Selection.Border
    .ColorIndex = 4
    .Weight = xlHairline
    .LineStyle = xlDot
End With
End Sub
```

```
'This is the main subroutine used for axial loading
```

```
Public cs As Double, Ntot1, cforce1 As Double
Public bottstrain, cstre, topstrain, H As Double
Public topinitial, botinitial, psinitial, ds, dps As Double
```

```

Public sstrain, pstrain, sstre, pstre, sforce As Double
Public sarea, pforce, parea, spforce As Double
Public creep, shstrain, zertop, zerbot, deltop, delbot As Double
Public delNtot1, delsstra, delsstre, delsforc As Double
Public delcforc, delcs, zercs, redcmo As Double
Public delcstre, Ntot2, cstre2, sstre2 As Double
Public K, layerN As Integer
Sub main2()
topinitial = [D2].Value: botinitial = [D3].Value
psinitial = [D4].Value
parea = [B4].Value: sarea = [B5].Value
ds = [F2].Value: dps = [F1].Value
H = [B1].Value
B = [B2].Value: Bt = [B3].Value
fcc = [J2].Value: cso = [J3].Value
ccrack = [J4].Value: cmod = [J5].Value
    creep = [m1].Value: shstrain = [m2].Value
    zertop = [m3].Value: zerbot = [m4].Value
    deltop = [m5].Value: delbot = [m6].Value
'
' Determine the strain corresponding to zero external load
H = [B1].Value
topstrain = -149.69
Do
    Ntot1 = 0
    bottstrain = topstrain
    sstrain = (bottstrain + (topstrain - bottstrain) * ds / H) / 1000000 'rebar strain
    pstrain = (psinitial + (bottstrain + (topstrain - bottstrain) * dps / H)) / 1000000 'p/s strain
    sstre = sstress(sstrain) 'rebar stress
' P/S stress using Osgood func. w/ ultimate stress of 1860 MPa
    pstre = 200000 * pstrain * (0.026 + 0.974 / (1 + (117.3 * pstrain) ^ 10) ^ 0.1)
' If pstre > 1860 Then Exit Sub
    sforce = sstre * sarea ' rebar force
    pforce = pstre * parea ' p/s force
    spforce = sforce + pforce ' total steel force
    cforce1 = 0
    For layerN = 1 To 4 ' the section is divided into four layers
' concrete strain at the centroid of the layer
        cs = (bottstrain - (layerN - 0.5) / 4 * (bottstrain - topstrain)) / 1000000
        If cs < -0.0045 Then Exit Sub
        If cs > -0.00009 Then Exit Do
' concrete stress
        cstre = cstres1(fcc, cs, cso, ccrack, cmod)
' cstres & cstre are concrete stress formula and value respectively
        cforce1 = cforce(cs, cstre, ccrack, H, B, Bt) ' concrete force/layer
        Ntot1 = Ntot1 + cforce1
    cforce1 = 0
    Next layerN
    cforce1 = 0
    Ntot1 = spforce + Ntot1 ' total steel & concrete tension
    If Abs(Ntot1) > 20# Then
        topstrain = topstrain + 0.005
    Else

```

```

End If
Loop Until Abs(Ntot1) <= 20#
'effect of shrinkage and creep
,
Shrink
,
Cells(11, 2).Value = Ntot1 / 1000          'final normal force
Cells(11, 3).Value = topstrain
Cells(11, 4).Value = bottstrain
Cells(11, 5).Value = sstre
Cells(11, 6).Value = pstre
Cells(11, 7).Value = (Ntot1 + delNtot1) / 1000      'final normal force
Cells(11, 8).Value = (topstrain + deltop)
Cells(11, 9).Value = (bottstrain + delbot)
Cells(11, 10).Value = sstress(sstrain + delsstra)
Cells(11, 11).Value = (cstre + delcstre)
,
,
topstrain = 0
For K = 1 To 700
topstrain = -50 * (3 - K)
' For K = 200 To 320
'topstrain = K / 2
Macro1
Cells(11 + K, 1).Value = K
Next K
End Sub
,
,
' Macro1 Macro
,
Sub Macro1()
H = [B1].Value
Ntot1 = 0
topstrain = topstrain 'top strain
bottstrain = topstrain
sstrain = (bottstrain + (topstrain - bottstrain) * ds / H) / 1000000 'rebar strain
pstrain = (psinitial + (bottstrain + (topstrain - bottstrain) * dps / H)) / 1000000 'p/s strain
sstre = sstress(sstrain) 'rebar stress
' P/S stress using Osgood func. w/ ultimate stress of 1860 MPa
pstre = 200000 * pstrain * (0.026 + 0.974 / (1 + (117.3 * pstrain) ^ 10) ^ 0.1)
If pstre > 1860 Then Exit Sub
sforce = sstre * sarea ' rebar force
pforce = pstre * parea ' p/s force
spforce = sforce + pforce ' total steel force
cforce1 = 0
For layerN = 1 To 4
' concrete strain at the centroid of the layer
cs = (bottstrain - (layerN - 0.5) / 4 * (bottstrain - topstrain)) / 1000000
If cs < -0.0045 Then Exit Sub
' Concrete stress
cstre = cstres1(fcc, cs, cso, ccrack, cmod)
' cstres & cstre are concrete stress formula and value respectively

```

```

cforce1 = cforce(cs, cstre, ccrack, H, B, Bt) ' concrete force/layer
Ntot1 = Ntot1 + cforce1
cforce1 = 0
Next layerN
cforce1 = 0
Ntot1 = spforce + Ntot1 ' total steel & concrete tension
Ntot2 = Ntot1 - delNtot1
cstre2 = cstre + delcstre
sstre2 = sstre + delsstre
Cells(11 + K, 2).Value = Ntot1 / 1000           'final normal force
Cells(11 + K, 3).Value = topstrain
Cells(11 + K, 4).Value = bottstrain
Cells(11 + K, 5).Value = sstre
Cells(11 + K, 6).Value = pstre
Cells(11 + K, 7).Value = Ntot2 / 1000         'final normal force
Cells(11 + K, 8).Value = (topstrain + deltop)
Cells(11 + K, 9).Value = (bottstrain + delbot)
Cells(11 + K, 10).Value = sstress(sstrain + delsstra)
Cells(11 + K, 11).Value = cstre2
End Sub

```

	A	B	C	D	E	F	G	H	I	J	K	L
1	h =	248	Initial strains ($\mu\epsilon$)						concrete ($\sigma-\epsilon$)			
2	B =	1000	$\epsilon_{top} =$	0	$d_p =$	90	mm (from bottom)		$f_{co} =$	-51.85	MPa	
3	$B_t =$	960	$\epsilon_{bottom} =$	0	d =	48	mm (from bottom)		$\epsilon_{co} =$	-0.002626	ϵ	
4	$A_p =$	198	P/S =	6064					$\epsilon_{cr} =$	8.754E-05	ϵ	
5	$A_s =$	1000			e_o (mm) =	520	mm		$E_c =$	27143.552	MPa	
6												
7	strain corresponding		ecc	N	M	ϕ	ϵ_{top}	ϵ_{bottom}	% of differ.			
8	to zero external load		33.958828	-239.378	-8.12898	-0.211321	-7.535	-59.94264	0.0020483			
9	# of Iter.	Counter	eccen.	total force	total mom.	ϕ	ϵ_{top}	ϵ_{bottom}	comp. zone	f_s	f_{ps}	f_c
10	I	K	mm	kN	kNm	$\mu\epsilon/mm$	$\mu\epsilon$	$\mu\epsilon$	mm	MPa	MPa	MPa
11			235.34717	0.048948	0.01152	-0.211321	-7.535	-59.94264	248	-9.461854	1201.04	-0.20887
12	8	1	518.228	25.43847	13.18293	0.1537869	-50	-11.86085	248	-3.656098	1203.986	-1.36053
13	10	2	519.86242	40.18063	20.8884	0.3684723	-75	16.381123	203.54313	-0.248054	1205.711	-2.03376
14	10	3	523.90782	54.49405	28.54986	0.5828228	-100	44.540063	171.57873	3.1472676	1207.424	-2.70344
15	9	4	522.40221	68.60814	35.84105	0.8020261	-125	73.902469	155.85528	6.7269911	1209.285	-3.3694
16	9	5	517.61803	79.30069	41.04746	1.0526597	-150	111.05961	142.49619	11.501069	1212.104	-4.03077
17	8	6	520.00618	86.21875	44.83428	1.3350415	-175	156.09029	131.08207	17.481576	1215.887	-4.68755
18	8	7	519.55174	92.02994	47.81431	1.6498648	-200	209.16647	121.22206	24.694862	1220.652	-5.33974

Figure A.1 A spreadsheet contains the input data and part of the output results

	M	N	O	P	Q	R	S	T	U
1	$\phi_{creep} =$	0.665							
2	$\epsilon_{cs} =$	-147.47							
3	$\epsilon_{o\ top} =$	-8.1							
4	$\epsilon_{o\ bot} =$	-59							
5	$\Delta \epsilon_{top} =$	-145							
6	$\Delta \epsilon_{bot} =$	-178							
7									
8	including creep & shrinkage effect								
9	total force	total mom.	ϕ	ϵ_{top}	ϵ_{bottom}	comp. zone	f_s	f_c	c/h
10	kN	kNm	$\mu\epsilon/mm$	$\mu\epsilon$	$\mu\epsilon$	mm	MPa	MPa	
11	3.8280737	-2.389527	-0.344386	-152.535	-237.9426	248	-42.06831	-0.069591	1
12	29.217598	10.781882	0.0207224	-195	-189.8608	248	-36.26255	-1.221259	1
13	43.959757	18.487354	0.2354078	-220	-161.6189	248	-32.85451	-1.894482	1
14	58.273177	26.148814	0.4497583	-245	-133.4599	248	-29.45918	-2.564162	1
15	72.387268	33.439999	0.6689616	-270	-104.0975	248	-25.87946	-3.230126	1
16	83.079811	38.646418	0.9195952	-295	-66.94039	248	-21.10538	-3.891496	1
17	89.997876	42.433236	1.201977	-320	-21.90971	248	-15.12488	-4.548278	1
18	95.809062	45.413267	1.5168003	-345	31.166467	227.45249	-7.91159	-5.200467	0.4887986

Figure A.1 (cont.)

Appendix B: Time-dependent Stress and Strain

The concrete strain at the centroid ε_o and the curvature ψ due to the specimen stressing and the change in these two quantities between casting and testing the specimen due to time effects $\Delta\varepsilon_o$ and $\Delta\psi$ were obtained from Demecs readings as described in Section 3.10. These actual values were first used to obtain the corresponding values of the creep coefficient ϕ and the free shrinkage strain ε_{cs} that are usually obtained from empirical equations. Ghali and Favre (1986) approach for calculating time-dependent stress and strain was used as follows:

The relation between the changes in strain and curvature and the restraining force is given by Ghali and Favre's Equation 2.35 as :

$$\begin{Bmatrix} \Delta\varepsilon_o \\ \Delta\Psi \end{Bmatrix} = \frac{1}{\bar{E}_c} \begin{Bmatrix} -\Delta N / \bar{A} \\ -\Delta M / \bar{I} \end{Bmatrix} \quad (\text{B-1})$$

The restraining axial force ΔN and the restraining moment ΔM are those due to creep and shrinkage that their values are given by Ghali and Favre Equations 2.37 and 2.38 respectively. Hence, the restraining force can be expressed as:

$$\begin{Bmatrix} \Delta N \\ \Delta M \end{Bmatrix} = -\bar{E}_c \begin{Bmatrix} (\phi\varepsilon_o + \varepsilon_{cs})A_c \\ \phi\Psi I_c \end{Bmatrix} \quad (\text{B-2})$$

Substituting in Eq. B-1 yields:

$$\begin{Bmatrix} \Delta\varepsilon_o \\ \Delta\Psi \end{Bmatrix} = \begin{Bmatrix} (\phi\varepsilon_o + \varepsilon_{cs})A_c / \bar{A} \\ \phi\Psi I_c / \bar{I} \end{Bmatrix} \quad (\text{B-3})$$

Rearranging Equation B-3 yields:

$$\phi = \frac{\Delta\Psi \bar{I}}{\Psi I_c} \quad (\text{B4 a})$$

$$\text{and } \varepsilon_{cs} = \frac{\Delta\varepsilon_o \bar{A}}{A_c} - \varphi\varepsilon_o \quad (\text{B-4b})$$

where,

ε_o , $\Delta\varepsilon_o$, ψ and $\Delta\psi$ are the initial and the change in concrete axial strain at the centroid and the initial and the change in the curvature respectively. They are obtained from Demecs readings,

A_c and I_c are the area and moment of inertia of uncracked concrete section,

\bar{A} and \bar{I} are the area and the moment of inertia of the uncracked transformed section.

In the above equations the section was considered symmetric, i.e. the small shift in the centroid of the transformed section than the centroid of the concrete section due to the presence of the reinforcement was neglected. This small shift slightly affects \bar{I} .

The stress increment that develops during the period between casting and testing at any fibre in concrete at a distance y from the centroid is given by Ghali and Favre Equation 2.41 as:

$$\Delta\sigma_c = \sigma_{restrained} + E_c(\Delta\varepsilon_o + y\Delta\Psi) \quad (\text{B-5})$$

$$\text{with } \sigma_{restrained} = -\bar{E}_c(\varphi\varepsilon_c + \varepsilon_{cs})$$

Hence,

$$\Delta\sigma_c = \bar{E}_c(-\varphi\varepsilon_c - \varepsilon_{cs} + \Delta\varepsilon_o) \quad (\text{B-6 a})$$

$$\text{and } \Delta\sigma_{ns} = E_s(\Delta\varepsilon_s) \quad (\text{B-6 b})$$

where,

ε_c and $\Delta\varepsilon_c$ are the initial and the change in concrete strain at any fibre at a distance y from the centroid,

$\Delta\sigma_s$ and $\Delta\varepsilon_s$ are the change in non-prestressed steel stress and strain respectively,

$\Delta\varepsilon_s$ and $\Delta\varepsilon_c$ can be obtained from the strain distribution defined by $\Delta\varepsilon_o$ and $\Delta\psi$.

After calculating $\Delta\varepsilon_o$ and $\Delta\psi$ using Equation B-4 the changes in non-prestressed steel and concrete stresses and the changes in the axial force and the bending moment were calculated. This was done in the computer program in the subroutine called “Shrink”, in which the concrete section was divided into 100 layer. These changes were calculated for each layer then numerically integrated for the whole section.

Appendix C: Solved Examples

This appendix contains two solved examples. The aim of these two examples is to illustrate the application of the water containment structures design approach proposed in Chapter 7. The complete design of the tank is beyond of the scope of these solved examples. The first example presents the design of the wall of a 7900 m³ open topped circular tank of 36 m diameter and 8 m height. The tank rests on soil and has a membrane floor thickened beneath the wall. The thickness of the wall is taken as 250 mm. PCA (1942) tables for circular tanks are used for the structural analysis.

The second example presents the design of the wall of a 920 m³ open topped rectangular tank. The length of the short wall = 8 m, the length of the long wall = 20 m and the wall height = 6 m. The wall thickness is taken as 300 mm. The tank rests on soil and has a membrane floor thickened beneath the wall. The structural analysis was performed with SAP80 (Habib-Allah and Wilson 1984).

Zero free board was used for each design. Therefore, the water height is considered the same in both the ultimate strength and the serviceability design. Normally, the water height with a free board of approximately 0.3 m is considered for the serviceability limit states while the maximum possible height of the water is considered for the ultimate strength.

When applicable A23.3-94 is used. Some of ACI 350 recommendations (e.g. the allowable water loss in leakage test and temperature reinforcement) are followed in the examples.

Example 1: Open Topped Circular Tank

water pressure

from PCA Table A-5 $T = \text{coeff. } (9.81 \times 8 \times 18) = 1412.64 \text{ coeff.}$

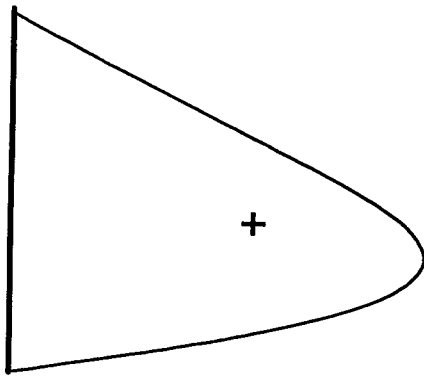
from PCA Table A-7 $M = \text{coeff. } (9.81 \times 8^3) = 5022.72 \text{ coeff.}$

$$H^2 / Dt = 7.1111111 \cong 7$$

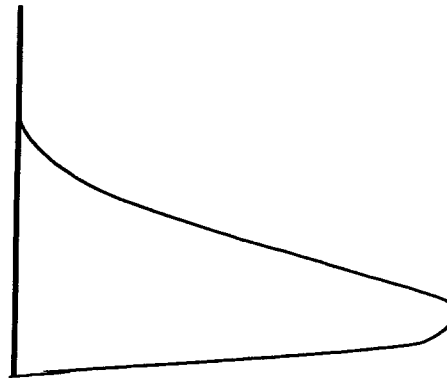
	height	coeff. for T	Coeff. for M	T (kN/m)	M (kNm/m)
top	0	-0.013	0	-18.4	0
	0.8	0.1	0	141.3	0
	1.6	0.216	0	305.1	0
	2.4	0.334	0	471.8	0
	3.2	0.453	0.0004	639.9	2.0
	4	0.565	0.0013	798.1	6.5
	4.8	0.65	0.003	918.2	15.1
	5.6	0.67	0.005	946.5	25.1
	6.4	0.584	0.00675	825.0	33.9
	7.2	0.3565	0.0061	503.6	30.6
bottom	8	0	0	0	0

Maximum water pressure = 946.5 kN

Maximum vertical moment = 33.9 kNm



T - distribution



M - distribution

Prestressing

Consider the average initial stress in the strand (after initial losses) = $0.6 f_{pu}$

and that the long term losses are 8% of that stress. Hence:

$$P_i = 0.6 \times 1860 \times A_p = 1116 A_p$$

$$P_e = 0.92 \times 0.6 \times 1860 \times A_p = 1026.7 A_p$$

During prestressing the wall is free to slide. The friction with the wall pad is considered.

Wall base friction only affects the region near the base of the wall.

Therefore the ring compression due to prestressing is approximately = the prestressing force.

Choosing A_s

A_s should not be less than No 15 @ 300 mm each way each face ($A_s = 1333.33 \text{ mm}^2 / \text{m} = 0.0053 A_c$)
[$A_{s \text{ min}}$ for temperature effects required by ACI 350 varies from 0.0028 to 0.006 A_c]

Try using No. 15 @ 200 mm each face ($A_s = 2000 \text{ mm}^2 / \text{m} = 0.008 A_c$)

Design for leakage limit state

For direct tension

Consider the allowed water loss as 0.05 % of water volume / day as specified by ACI 350

Therefore, $Q_{\text{allowable}} = 0.0005 \pi r^2 H / (24 \times 60 \times 60) = 4.71 \times 10^{-5} \text{ m}^3/\text{s}$

The predicted leakage rate from a through crack can be calculated using Eqs 7.8 and 7.9.
In these equations, crack spacing can be calculated using CEB-FIP Model Code 1990 as
 $S = \Phi_s / 3.6 \rho_{\text{eff, total}} = 509 \text{ mm} = 0.509 \text{ m}$

(it was noted from experiments that cracks occurred at the location of transverse steel which means that crack spacing is likely to be 300 mm. However, S is taken = 0.509 m because this crack spacing equation was used to obtain the equations and the curves that are used to get steel stress.

for $w = 0.1 \text{ mm}$

$$A = 2.25 \times 10^{-4} / (1 \times 0.0001^{2.6}) = 5651744.5 \text{ m}^{-2}$$

for wall: $Q = \{9.25 \times [1 + I/2] w / (S A)\} \times (2\pi r H) = 4.95 \times 10^{-6} \text{ m}^3/\text{s}$

for floor: $Q = \{9.25 \times [1 + I] w / (S A)\} \times (\pi r^2) = \frac{10.8 \times 10^{-6}}{1.57 \times 10^{-5}} \text{ m}^3/\text{s} = 33\% Q_{\text{allowed}}$

for $w = 0.15 \text{ mm}$

for wall $A = 6.1 \times 10^{-8} / (1 \times 0.0001^{3.6} \times (14 I/3 - 20)) = 11847 \text{ m}^{-2}$

$$Q = \{9.25 \times [1 + I/3] w / (S A)\} \times (2\pi r H) = 16.2 \times 10^{-5} \text{ m}^3/\text{s}$$

for floor $A = 6.1 \times 10^{-8} / (1 \times 0.0001^{3.6} \times (14 I - 20)) = 35800.2 \text{ m}^{-2}$

$$Q = \{9.25 \times [1 + I] w / (S A)\} \times (\pi r^2) = \frac{70.6 \times 10^{-5}}{86.8 \times 10^{-5}} \text{ m}^3/\text{s}$$

not acceptable

Hence, w is taken 0.1 mm

In the above equations, $I = 8/0.25 = 32$. For the wall, 0.5 and 0.33 I are considered for $w = 0.1$ and 0.15 mm respectively, as explained in Section 7.3.2.2.

Alternative approach to determine the permissible crack width w , is to obtain w directly from Table 7.3 for the case of self-healing.

For $w = 0.10$ mm, and considering the probability of having preopened cracks, Fig. 7.2 gives the permissible steel stress f_s for No. 15 bars as 90 MPa.

The maximum ring tension in the wall (service load) is approximately
 $= 946469 - P_e = 946469 - 1026.7 A_p$

This force is considered as the net axial tension acting on the section and is resisted at the crack locations by both prestressed and non-prestressed steel.

The non-prestressed steel stress f_s given by Eq. 7.22 is: $f_s = T / (A_s + \sqrt{\psi} A_p)$

$$90 = (946469 - 1026.7 A_p) / (2000 + \sqrt{0.4 \times 15 / 11} A_p)$$

from which, $A_p = \mathbf{643.20 \text{ mm}^2}$

Use 10 size 11 strands per metre grouped into multi-strand tendons (ducts) as desired for constructability.

$$A_{p \text{ used}} = 10 \times 74 = 740 \text{ mm}^2 / \text{m}$$

Check the ultimate strength limit state

$$T_f = 1.25 \times 946.5 = 1183.125 \text{ kN}$$

$$T_r = \phi_s A_s f_y + \phi_p A_p (0.9 f_{pu})$$

$$= 0.85 \times 2000 \times 400 + 0.9 \times 740 \times (0.9 \times 1860) = 1794884 \text{ N}$$

$$= 1794.9 \text{ kN} > T_f$$

There was no need to check the ultimate limit state because $f_{pe} = 0.552 f_{pu}$
 i.e. $f_{pe} < 0.60 f_{pu}$ as explained in Section 7.4.

Internal forces due to prestressing force

for 10 strands : $P_i = 825.8 \text{ kN}$ & $P_e = 759.8.0 \text{ kN}$

The wall weight = $0.25 \times 24 \times 8 = 48 \text{ kN/ m}$ of perimeter

Assuming coefficient of friction for the pad = 0.15

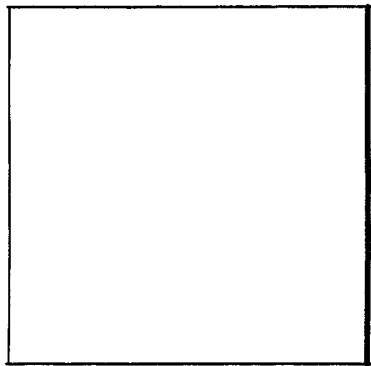
$$\text{Friction force } V = 0.15 \times 48 = 7.2 \text{ kN/m}$$

The number of strands should be reduced towards the top and the bottom. CPA tables can not be used in this case. In this example, A_p is taken constant along the wall. It is also more accurate to consider the effect of creep and relaxation on the stress resultants for the chosen structural system. This effect is beyond the scope of this example.

Axial force

The axial force in the horizontal direction is the resultant of the prestressing force (for free base) and force resulting from the friction force which can be obtained from PCA Table A-8

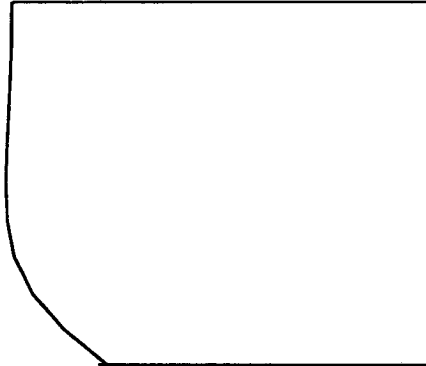
	prestress force (kN)		friction = coeff. (-V) r / H coefficient force		total force (kN)
top	0	-760	0	0	-760
	0.8	-760	0.01	-0.162	-760.16
	1.6	-760	0.13	-2.106	-762.11
	2.4	-760	0.3	-4.86	-764.86
	3	-760	0.48	-7.776	-767.78
	3	-760	0.48	-7.776	-767.78
	3.2	-760	0.5	-8.1	-768.1
	4	-760	0.63	-10.206	-770.21 = max. C
	4.8	-760	0.48	-7.776	-767.78
	5.6	-760	-0.26	4.212	-755.79
	6.4	-760	-2.06	33.372	-726.63
	7	-760	-4.4	71.28	-688.72
	7	-760	-4.4	71.28	-688.72
	7.2	-760	-5.27	85.374	-674.63
bottom	8	-760	-9.72	157.464	-602.54



free base
(compression)



friction



total
(compression)

Vertical moments are due to the friction force only

Moment due to friction = coeff.(Table A-9) x (-V) H

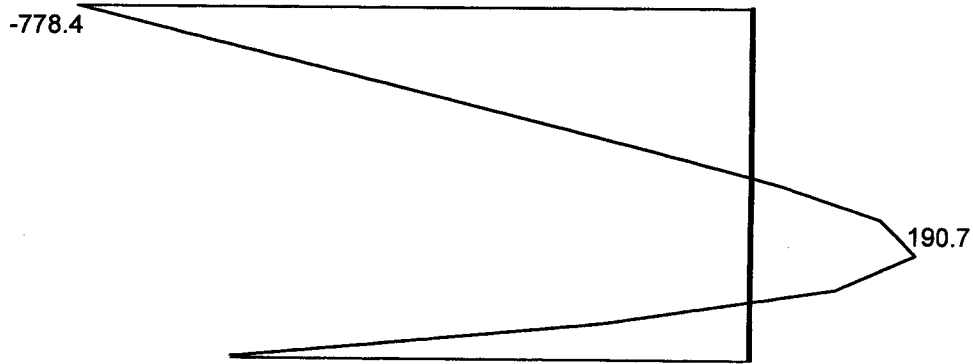
	coefficient	moment (kNm)
top	0	-0.003
	0.8	-0.003
	1.6	-0.003
	2.4	-0.001
	3.2	0.003
	4	0.0125
	4.8	0.028
	5.6	0.048
	6.4	0.064
	7.2	0.06
bottom	8	0

Case of full tank

consider water pressure and the effective prestressing force (after all losses)

Horizontal axial force

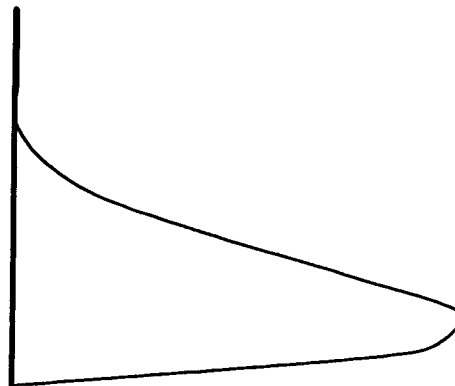
height	water pressure	prestressing	total (kN)
0	-18.4	-760.0	-778.4
0.8	141.3	-760.2	-618.9
1.6	305.1	-762.1	-457.0
2.4	471.8	-764.9	-293.0
3	598.0	-767.8	-169.8
3	598.0	-767.8	-169.8
3.2	639.9	-768.1	-128.2
4	798.1	-770.2	27.9
4.8	918.2	-767.8	150.4
5.6	946.5	-755.8	190.7 max. N
6.4	825.0	-726.6	98.4
7	583.0	-688.7	-105.7
7	583.0	-688.7	-105.7
7.2	503.6	-674.6	-171.0
8	0	-602.536	-602.5



Ring Tension in the case of full tank

Vertical bending moment

height	water	prestressing	total (kNm)
0	0	0.173	0.173
0.8	0	0.173	0.173
1.6	0	0.173	0.173
2.4	0.000	0.058	0.058
3.2	2.009	-0.173	1.836
4	6.530	-0.720	5.810
4.8	15.068	-1.613	13.455
5.6	25.114	-2.765	22.349
6.4	33.903	-3.686	30.217
7.2	30.639	-3.456	27.183
8	0	0	0



Check of stresses

$$\text{max } T = 190.7 \text{ kN}$$

$$f_s = 190700 / (2000 + \sqrt{0.4 \times 15 / 11}) \times 740 = 74.9 \text{ MPa} \\ < 90 \text{ MPa}$$

$$\text{max compression} = 778.4 \times 759.8 / 825.8 = 846.09 \text{ kN (before losses)}$$

$$f_c = 846090 / (250 \times 1000 \times 0.97) = 3.49 \text{ MPa} \\ \text{very small}$$

(concrete area is reduced by 3% for ducts area)

Check that reinforcement will not yield at cracking (Eq. 7.17)

$$\text{Cracking force} = 0.25 \sqrt{35} \times (250000) = 369.755 \text{ kN}$$

$$\phi_s A_s f_y + (0.9 \phi_p - f_{pe}/f_{pu}) A_p f_{pu} = 0.85 \times 2000 \times 400 + (0.9 \times 0.9 - 0.552) \times 1860 \times 740 = \\ = 1051.628 \text{ kN} > \text{cracking force}$$

Vertical Direction

$$\text{Maximum Moment} = 30.2 \text{ kNm (from the case of full tank)}$$

This moment is small and produces compression on water side of the wall. Hence the wall will be non-prestressed. Ultimate strength design may be used to calculate A_s required

$$M_f = 1.25 \times 30.2 = 37.75$$

$$A_s \text{ required} = 617 \text{ mm}^2 / \text{m (use No. 15 bar @ 300 mm / m, } A_s = 667 \text{ mm}^2)$$

Example 2 - Open Topped Rectangular Tank

$$L_1 = 20 \text{ m}$$

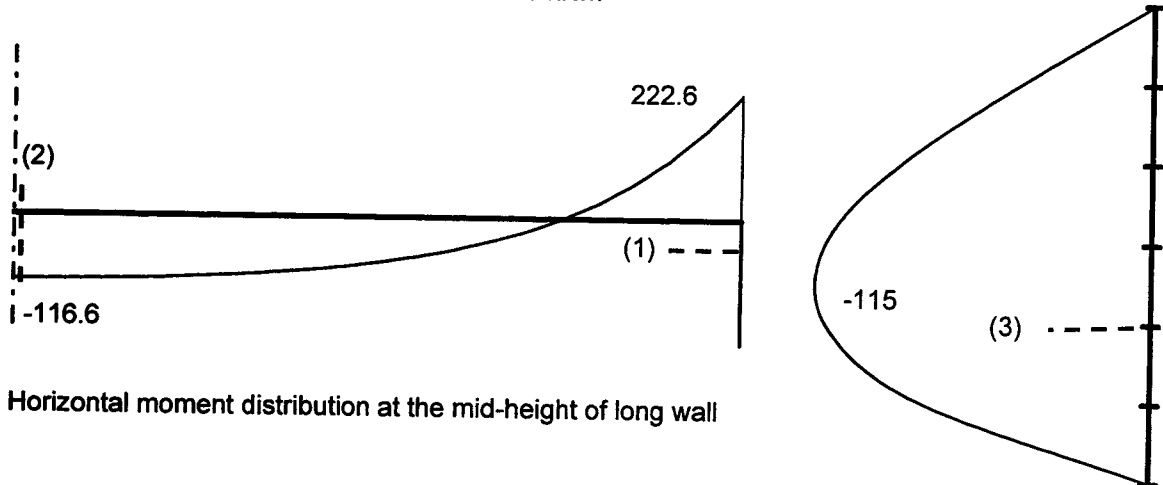
$$L_2 = 8 \text{ m}$$

$$H = 6 \text{ m}$$

$$\text{wall thickness} = 300 \text{ mm}$$

Water pressure The stress resultants at the critical sections :

- Horizontal direction at the mid-height of the wall
 - sec. 1-1** connecting moment = 220 kNm & T = 129 kN
 - sec. 2-2** mid-span moment = 116 kNm & T = 120 kN
- Vertical direction at the mid-length of long wall
 - sec. 3-3** maximum vertical moment = 115 kNm



Horizontal moment distribution at the mid-height of long wall

Vertical moments at the mid-length of long wall

Prestressing force

Due to the high bending moments, prestressing is used in both vertical and horizontal directions use 7-wire size 11 low relaxation strands, for which $A_p = 74 \text{ mm}^2$

$$\text{effective prestressing force, } P_e = 0.92 (0.6 \times 1860) (74) = 75.98 \text{ kN / strand}$$

Vertical prestressing

Try using 8 straight strands/m with a constant eccentricity of 45 mm (outward)

$$P_e = 8 \times 76 = 608 \text{ kN} \quad \text{and} \quad M_p = 608 \times 0.045 = 27.4 \text{ kNm}$$

The number of strands were reduced away from the long wall mid-span because the vertical moments become smaller toward wall ends. The vertical prestressing for short wall was also less

Horizontal prestressing

Try using 8 deflected strands/m with an eccentricity of 25 mm (outward) at mid-span and 50 mm (inward) at ends.

The number of strands was reduced toward the top and the bottom where moments are smaller

The tank was analyzed for both full and empty conditions.

Full Tank

Stress resultants are:

- sec. 1-1 connecting moment = 145 kNm & N = -416 kN
- sec. 2-2 mid-span moment = 73 kNm & N = -145 kN
- sec. 3-3 maximum vertical moment = 103 kNm & N = -624 kN

Empty tank

- sec. 1-1 connecting moment = -75 kNm & N = -545 kN
- sec. 2-2 mid-span moment = -43 kNm & N = -256 kN
- sec. 3-3 maximum vertical moment = -12 kNm & N = -624 kN

The minimum depth of compression zone which satisfies leakage limit state

(1) Allowable Leakage rate = Loss of water volume permitted by ACI 350

Take the allowed water loss as 0.05 % of water volume per day as specified by ACI 350

$$\xi = 0.0005 / (24 \times 3600) = 5.79 \times 10^{-9} \quad 1/s$$
$$k = 3 \times 10^{-11} \text{ m/s}$$

The minimum depth of the compression zone can be obtained using Eq. 7.24 (b) as:

$$c = 3 \times 10^{-11} \{ 6 (20 + 8) + 20 \times 8 \} / (\xi 20 \times 8) = 10.63 \text{ mm}$$

(2) Allowable Leakage rate = Evaporation Rate

Assuming that the weather conditions on a given day are:

$$\text{Air temperature, } T = 5 \text{ }^\circ\text{C} \quad \text{Wind velocity} = 5 \text{ km/h} \quad \text{Relative humidity, } RH = 70\%$$

The evaporation rate can be calculated using Eq. 6.4 as:

$$e_o = 6.11 \exp (17.27 T / (237.3 + T)) = 8.726$$
$$E_o = e_o (0.013 + 0.00016 \times 5 \times 24) (100 - RH)/100 = 0.0843 \text{ cm/day}$$
$$= 9.76 \times 10^{-10} \text{ m/s}$$

At the wall base, the leakage rate through the compression zone = $3 \times 10^{-11} (6 / c) \text{ m/s}$

$$\text{Therefore, } c = 18 \times 10^{-11} / (9.76 \times 10^{-10}) = 184 \text{ mm}$$

However, the critical section (Section 1-1) is located at the mid-height ($\Delta H = 3 \text{ m}$)

$$\text{Therefore, } c = 9 \times 10^{-11} / (9.76 \times 10^{-10}) = 92 \text{ mm}$$

The velocity of the water through the compression zone at Section 1-1 =

$$(3 \times 10^{-11}) \times (3 / 0.092) / 0.3 = 3.26 \times 10^{-9} \text{ m/s}$$

The 0.3 in this equation is the assumed void ratio of the concrete

The time required for the water to pass through the compression zone =

$$0.092 / (3.26 \times 10^{-9}) / (3600 / 24 / 365) = 0.895 \text{ year} = 10.7 \text{ months}$$

Hence, it is more appropriate to consider the annual weather conditions to calculate the evaporation rate. For instance, if the average annual conditions are:

$$\text{Air temperature, } T = 14 \text{ }^\circ\text{C} \quad \text{Wind velocity} = 13 \text{ km/h} \quad \text{Relative humidity, } RH = 70\%$$

The minimum c required at Section 1-1 = **51.5 mm** (103 mm at the wall base)

In this example, the evaporation rate governs the minimum depth of compression zone.

This depth should be increased to provide a margin of safety against any defects in concrete

Analyze the critical sections

For section 1-1 & full tank: $M = 145 \text{ kNm}$ & $N = -416 \text{ kN}$

Estimation of A_s

$h = 300 \text{ mm}$, $d = 250 \text{ mm}$, $d_p = 200 \text{ mm}$

use Eq. 7.18, to estimate non-prestressed steel stress f_s

Assuming that A_s/A_p is approximately 2. For $M/T = 220/129 = 1.7$, $e/h = 5.7$

$f_s = 192 \text{ MPa}$

Consider equilibrium equations:

$$C = N + T = N + A_s f_s \quad (A)$$

$$M = C (jd) - N (d_s - h/2) \quad (B)$$

(in Eq. B, the moments are taken at the location of A_s . The contribution of prestressed steel after decompression is neglected for simplicity since it is just a primary estimation)

Substitute Eq. A into B

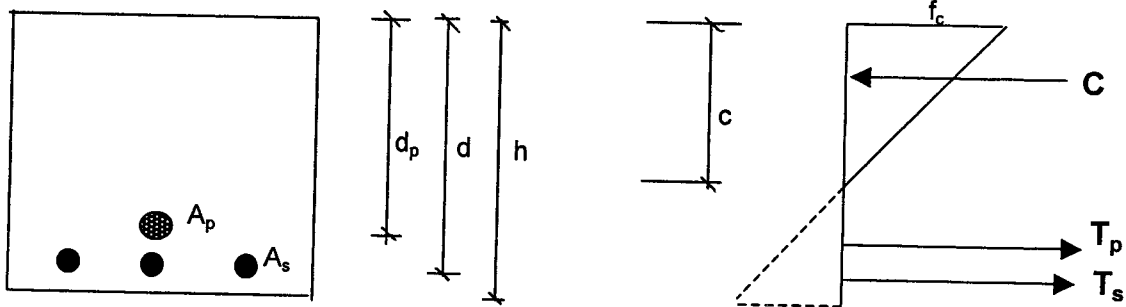
$$A_s = [M + N (d_s - h/2)] / f_s jd_s - N/f_s$$

and assume $jd = 0.85 d$

$$A_s = [145 + 416 (0.25 - 0.3/2)] \times 10^6 / (192 \times 0.85 \times 250) - 416000 / 192 = 2407 \text{ mm}^2$$

use 8 - No. 20 /m (2400 mm²)

Analysis of the cracked transformed section under the effect of $M = 145 \text{ kNm}$ & $N = -416 \text{ kN}$



Consider $E_s = E_p = 200000 \text{ MPa}$, hence $\eta = E_s / E_c = 7$

$$N = C - T_p - T_s$$

$$416000 = 0.5 f_c c (1000) - 7 \times 592 f_c (200-c)/c - 7 \times 2400 f_c (250-c)/c$$

$$f_c = 832 c / [c^2 - 8.29 (200 - c) - 33.6 (250 - c)]$$

moments about A_s location:

$$[M + N (d_s - h/2)] 10^6 = C (d_s - c/3) - A_p \times 7 f_c (200-c)/c \quad (50)$$

$$186600000 = 0.5 f_c \times c (1000) (250 - c/3) - 592 \times 7 f_c (200-c)/c (50) \quad \text{----- (d)}$$

Solving the two equations gives:

$$c = 103.93 \text{ mm} \quad f_c = 16.96 \text{ MPa} = 0.42 f'_c$$

Hence, $f_s = 7 (16.96) (250 - 103.93)/103.93 = 167 \text{ MPa} = 0.41 f_y$
 and, $\Delta f_p = 7 (16.96) (200 - 103.93)/103.93 = 109.7 \text{ MPa} = 0.06 f_{pu}$

Therefore the actual depth of compression zone satisfies leakage limit state.

For the same section & empty tank: M = - 75 kNm & N = - 545 kN

Stresses distribution assuming uncracked section and considering only the concrete section for simplicity:

$$f_1 = N/A + M/I \quad y = -545000/300000 - 75000000 / (1000 \cdot 300^2/6) = -6.8 \text{ MPa} = 0.17 f'_c$$

$$f_2 = N/A - M/I \quad y = -545000/300000 + 75000000 / (1000 \cdot 300^2/6) = 3.18 \text{ MPa} = 0.5 \text{ sqrt}(f'_c)$$

- Considering the transformed section yields smaller stresses. However any reduction in concrete area (e.g. at water stops) should also be considered.
- The stresses before long-term losses are 8% higher (8% is the percentage of long-term losses with respect to the initial prestressing force after lock-off)
- Although the section is uncracked, it is preferable to add non-prestressed steel in tension side, the area of this steel can be calculated to resist tensile force = area under tension in stresses distribution on the section. Steel stress may be taken around $0.5 f_y$

$$\text{depth of tension zone} = 300 \times 3.18 / (3.18 + 6.8) = 95.6 \text{ mm}$$

$$T = 0.5 \times 95.6 \times 3.18 \times 1000 = 151990 \text{ N}$$

$$A_s = 151990 / (0.5 \times 400) = 759.9499 \text{ mm}^2$$

use 4 - No. 15 /m

Check the strength of the section (ultimate limit state)

Factored forces resulting from water pressure:

$$M_f = 1.25 M = 1.25 \times 220 = 275 \text{ kNm}$$

$$T_f = 1.25 T = 1.25 \times 129 = 161 \text{ kN}$$

$$e = 275 / 161.25 = 1.7 \text{ m}$$

The given cross section was analyzed using CSA A23.3-94 equations and gives:

$$M_r = 300.5 \text{ kNm} > M_f$$

$$T_r = 176.7 \text{ kN} > T_f$$

For section 3-3 & full tank: M = 103 kNm & N = - 624 kN

This section is not as critical as section 1-1 because the stress resultants are smaller.

The same procedure followed in section 1-1 can be used here to calculate the required A_s

Estimation of A_s

$h = 300 \text{ mm}, d_s = 250 \text{ mm}, d_p = 195 \text{ mm}$

use Eq. 7.18, to estimate non-prestressed steel stress f_s

and assume that A_s/A_p will be approximately 2, and for flexure

$f_s = 210 \text{ MPa}$

consider equilibrium equations:

$A_s = [103 + 624 (0.25 - 0.3/2)] \times 10^6 / (210 \times 0.85 \times 250) - 624000 / 210 = 735 \text{ mm}^2$

use 4 - No. 15 /m (800 mm²)

Analysis of the cracked transformed section under the effect of $M = 103 \text{ kNm}$ & $N = - 624 \text{ kN}$

$N = C - T_p - T_s$

$624000 = 0.5 f_c c (1000) - 7 \times 592 f_c (195-c)/c - 7 \times 800 f_c (250-c)/c$

$f_c = 1248 c / [c^2 - 8.29 (195 - c) - 11.2 (250 - c)]$

moments at A_s location:

$[M + N (d_s - h/2)] 10^6 = C (d_s - c/3) - A_p \times 7 f_c (195-c)/c (50)$

$165400000 = 0.5 f_c c (1000) (250 - c/3) - 592 \times 7 f_c (200-c)/c (50)$

solving the two equations by trial and error yields:

$c = 106.6 \text{ mm}$

$f_c = 14.74 \text{ MPa} = 0.37 f'_c$

Hence, $f_s = 138.8 \text{ MPa} = 0.347 f_y$

For the same section & empty tank: $M = - 12 \text{ kNm}$ & $N = - 624 \text{ kN}$

stresses distribution assuming uncracked section and consider only the concrete section for simplicity:

$f_1 = N/A + M/I \quad y = -624000/300000 - 12000000 / (1000 \cdot 300^2/ 6) = -2.88 \text{ MPa} = 0.07 f'_c$

$f_2 = N/A - M/I \quad y = -624000/300000 + 12000000 / (1000 \cdot 300^2/ 6) = -1.28 \text{ MPa}$

A_s for section 2-2, and for the critical sections of the short wall should also be calculated.

Summary:

The wall is 300 mm thick

reinforced at the critical section 1-1 with:
eight 7-wire size 11 strands and
8 No. 20 / m from inside and 4 No. 15/m from outside

206. *Shrinkage and Flexural Tests of a Full-Scale Composite Truss* by Michael B. Maurer and D.J. Laurie Kennedy, December 1994.
207. *Analytical Investigation of the Compressive Behavior and Strength of Steel Gusset Plate Connections* by Michael C.H. Yam and J.J. Roger Cheng, December 1994.
208. *The Effect of Tension Flange Movement on the Strength of Point Loaded I-Beams* by Dean Mullin and J.J. Roger Cheng, January 1995.
209. *Experimental Study of Transversely Loaded Continuous Steel Plates* by Kurt P. Ratzlaff and D.J. Laurie Kennedy, May 1995.
210. *Fatigue Tests of Riveted Bridge Girders* by Daniel Adamson and Geoffrey L. Kulak, July 1995.
211. *Fatigue of Riveted Tension Members* by Jeffery DiBattista and Geoffrey L. Kulak, November 1995.
212. *Behaviour of Masonry Cavity Walls Subjected to Vertical Eccentric Loads* by Ru Wang, Alaa E. Elwi, Michael A. Hatzinikolas and Joseph Warwaruk, February 1996.
213. *Thermal Ice Loads on Structures* by Azita Azarnejad and Terry M. Hrudey, November 1996.
214. *Transmission of High Strength Concrete Column Loads Through Concrete Slabs* by Carlos E. Ospina and Scott D.B. Alexander, January 1997.
215. *Seismic Behaviour of Steel Plate Shear Walls* by Robert G. Driver, Geoffrey L. Kulak, D.J. Laurie Kennedy and Alaa E. Elwi, February 1997.
216. *Extended End Plate Moment Connections under Cyclic Loading* by Bryan T. Adey, Gilbert Y. Grondin and J.J. Roger Cheng, June 1997.
217. *Connection on Infill Panels in Steel Plate Shear Walls* by A. Schumacher, Gilbert Y. Grondin and Geoffrey L. Kulak, August 1997.
218. *Shear Rehabilitation of G-Girder Bridges using CFRP Sheets* by John G.S. Alexander and J.J. Roger Cheng, October 1997.
219. *Seismic Evaluation of Steel Buildings with Concentrically Braced Frames* by Manoj S. Medhekar and D.J. Laurie Kennedy, October 1997.
220. *Rational Design of Prestressed and Reinforced Concrete Tanks* by Abdelaziz A. Rashed, David M. Rogowsky and Alaa E. Elwi, December 1997.